KATHOLIEKE UNIVERSITEIT LEUVEN

Faculteit Wetenschappen

Radiative Processes in Astronomy

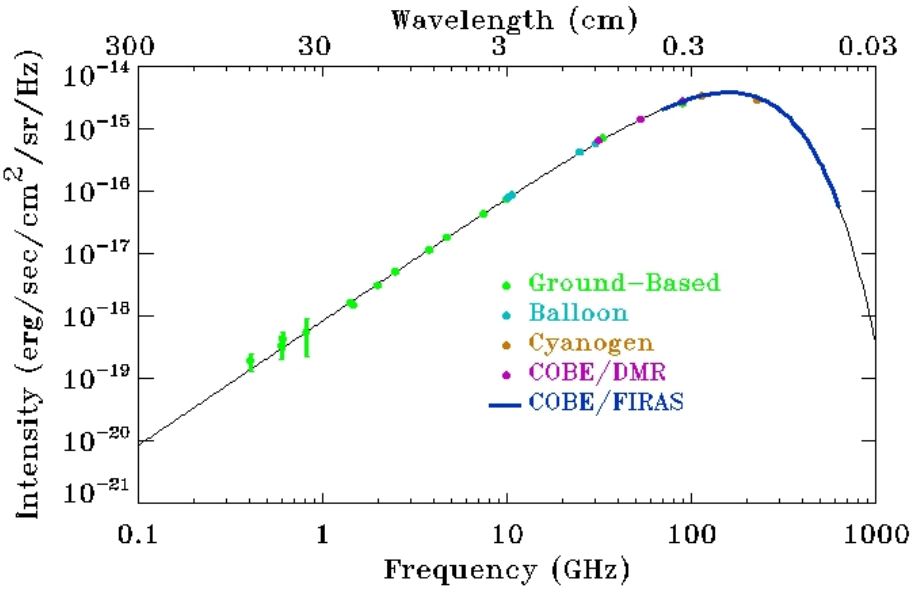

The measured Cosmic Background Radiation (CMB) with a colour temperature of $2.725^o \pm 0.001$ K. The full line represents the Planck curve with the same temperature (reference: Nasa).

Prof. dr. H. Van Winckel
Teaching assistant: dr. Devika Kamath
Departement Natuurkunde en Sterrenkunde
Faculteit Wetenschappen
Katholieke Universiteit Leuven
Hans.VanWinckel@ster.kuleuven.be
Devika.Kamath@ster.kuleuven.be
www.ster.kuleuven.be

Contents

1 Introduction **1**

1.1 Introduction 1

1.2 Solar Abundances 7

1.3 Basic Quantities in the study radiative processes 14

1.3 .1 Specific intensity 14

1.3 .2 Moments of the specific intensity 17

1.4 Radiative Transfer 20

1.5 Simple solutions of the transfer equation 25

1.5 .1 Homogeneous slab 25

1.5 .2 Plane parallel atmosphere in the Eddington-Barbier relation 28

1.6 Thermal Radiation 31

1.6 .1 Energy density 33

1.6 .2 Radiation Pressure 34

1.6 .3 Wiens displacement law 36

1.6 .4 Rayleigh-Jeans tail of BB radiation 37

1.6 .5 Wienn approximation: high frequencies 38

1.7 Problems 38

2 Fundamental concepts to describe radiative processes **43**

2.1 Introduction 43

2.2 Excitation law of Bolzmann 46

2.3 Ionisation law of Saha 47

2.4 Bound-bound transitions of the hydrogen atom 49

2.4 .1 The strength of the Ca II lines versus the Balmer lines in the sun 50

2.5 Evaluation: the spectral classification of stars 53

2.6 Einstein coefficients 60

2.6 .1 Spontaneous emission 60

2.6 .2 Radiative Absorption 61

2.6 .3 Stimulated emission 62

2.6 .4 Collisional transitions 63

2.6.5 Relation between the Einstein coefficients 63
2.7 Absorption and Emission coefficients using the Einstein coefficients 64
2.7.1 Transfer equation for b-b transitions 64
2.7.2 Thermal b-b treatment 66
2.7.3 Non-thermal b-b treatment 67
2.7.4 Inverted Population: maser emission 67
2.8 Broadening of Spectral Lines 68
2.8.1 Microscopic velocities in (L)TE 68
2.8.2 Microturbulent velocity 71
2.8.3 Pressure broadening 71
2.9 Voigt Profile 72
2.10 Problems 74

3 Transitions of H **77**
3.1 Introduction 77
3.2 Solutions of the Schrödinger equation 79
3.3 Energy Levels and Quantum Numbers 81
3.4 Angular Momentum Coupling 86
3.4.1 Fine Structure Lines of H 87
3.4.2 Hyper Fine Structure line of H 87
3.5 Transition Rules 89
3.5.1 Two-Photon process 89
3.6 H-like atoms 90
3.7 Problems 91

4 Lines of more complex systems **93**
4.1 Indistinguishable Particles 94
4.2 Russell-Saunders Coupling scheme 95
4.2.1 Hund's rules 97
4.2.2 Parity and the Laporte Rule 98
4.3 Selection Rules 98
4.4 Nebular spectra 101
4.4.1 Electron collisions 102
4.4.2 Bowen (1898-1973) lines: Resonance-Fluorescence . . . 104
4.5 Molecules 106
4.5.1 Nomenclature 108
4.5.2 Born-Oppenheimer approximation 109
4.5.3 Schrödinger equation 110
4.5.4 Tri-atomic molecules 113
4.6 Molecular spectroscopy 113
4.6.1 Pure rotational lines 114

4.6.2 Ro-Vibrational transitions 115
4.7 Problems 119

5 The Strength of Spectral Lines 121
5.1 Introduction 121
5.1.1 Rotational Diagrams 125
5.2 Curve of Growth in an isothermal slab 127
5.3 Two layer atmosphere model in LTE 129
5.3.1 Weak lines 130
5.3.2 Saturated lines 131
5.3.3 Very Strong Lines 131
5.4 The Curve of Growth following the approach of Milne & Eddington 132
5.4.1 Curve of Growth 134
5.4.2 Theoretical Curve of Growth 137
5.4.3 Observable Curve of Growth 138
5.5 Abundance Determinations 142
5.5.1 Spectroscopic determination of the stellar atmosphere parameters 145

6 Continuum processes 149
6.1 Classical Theory 149
6.1.1 Poynting's Theorem 152
6.2 Free-Free radiation or thermal bremsstrahlung 153
6.2.1 Free-free radiation of a single electron-ion collision 155
6.2.2 ν of the emitted radiation 158
6.2.3 Many thermal electrons and a single ion 159
6.2.4 Volume emissivity 161
6.2.5 Integrated volume emissivity 162
6.2.6 Specific Intensity 163
6.2.7 Free-Free extinction 164
6.3 The Dipole approximation 165
6.4 Scattering processes 166
6.4.1 Thomson scattering 166
6.4.2 Rayleigh scattering 168
6.5 Bound-Free processes 169
6.5.1 Photo-Ionisation 170
6.5.2 Spontaneous recombination 174
6.5.3 Induced photo-recombination 175
6.5.4 Collisional Ionisation 175
6.5.5 Collisional Recombination 176

6.6 Special Case: H^- extinction 176
6.7 Dominant continuum process in the Sun 177
6.8 Notions of high-energy processes 180
6.8 .1 Synchrotron emission 182
6.8 .2 Compton Scattering 185
6.9 Evaluation 187
6.10 Concluding Remarks 189

A Astronomical and Physical constants. 191

B Stellar properties in function of Spectral Type 195

C Literature: Books 199

Index 214

Chapter 1

Introduction

1.1 Introduction

The history of spectral investigations of celestial bodies goes back to Wollaston (1766-1828) who passed solar light through a prism to investigate the dark lines which appeared at discrete colours. Fraunhofer (1787-1826) catalogued somewhat less than 500 lines in the solar spectrum. The identification of one of the lines followed the experiment in which salt was thrown in a flame: the line coincided in wavelength with one of the strong lines in the solar spectrum. The Sodium lines at 5889.950 and 5895.924 Å are still called Sodium D lines following the nomination of Fraunhofer. The Fraunhofer H and K lines, are produced by CaII and are at 3933.7 and 3968.5 Å : these are the strongest lines in the spectrum of the Sun.

The basis of spectroscopy was further elaborated by Bunsen (1811-1899) and Kirchoff (1824-1887) who found e.g. that 70 dark lines in the spectrum of the sun, corresponded in wavelength to 70 bright lines emitted by iron vapor. Kirchoff formulated fundamental laws:

- A hot, dense or hot solid object produces a continuous spectrum without dark lines.
- A hot, diffuse gas produces bright emission lines.
- A diffuse gas in front of a source of a continuous spectrum, produces absorption lines in the spectrum.

Since then, deciphering of the observed spectral information of all celestial bodies has become a mature science and the quantified interpretation of the (spectral) observations in terms of local physical and chemical conditions are possible with models of growing sophistication. In this course we will give an overview of the physical basis of the radiative processes which are involved in astronomical research.

While the radiative processes in astronomical environments are by no means limited to stellar processes, it is still a good idea to glance through the library of high-quality optical stellar spectra obtained with one of the best optical spectrographs of the world UVES attached to one of the 8-meter VLT-telescopes of ESO, the European Southern Observatory. The spectra are on-line available at the "uvespop" page. A sample of spectra is given in Fig. 1.1 and Fig. 1.2. The reduced spectra are presented but some artifacts of the reduction process are still visible.

The variety of points can be addressed when browsing through the spectra:

- In the stellar spectra, absorption lines prevail irrespective of the spectral type of the object. Following Kirchoffs laws, this obviously means that the stellar photospheres are cooler than the stellar interiors which are not visible by direct light.
- Most lines can be related to bound-bound transitions of free atoms, while only in the cooler stars spectral bands, typical of molecules, are detected.
- Astronomers make a division in continuous processes, which are processes relevant for a wide continuous range of wavelengths, and discrete processes, which are only relevant to a very limited wavelength range. Absorption lines, coming from electronic bound-bound transitions of a given atom (molecule) is an example of a discrete process. The strong Hydrogen lines are apparent in almost all spectral classes and are strongest in A-type stars. The Balmer jump at about 360 nm forms a discrete jump in which the blueward wavelengths show a much smaller flux level than the redward wavelengths.
- After the early detection by Fraunhofer that different stars had different spectra, the first very systematic spectral classification was developed at Harvard by Edward Pickering and Williamina Fleming and performed by a whole set of female assistants. The first classification was based on the strength of the hydrogen lines, but it was Annie Cannon who rearranged the sequence of spectra by placing O and B before A and adding a finer grid

which she labeled e.g. F0–F9. The Harvard classification is still in used and can be remembered using the famous "Oh Be A Fine Girl Kiss Me". Despite the very wide range of spectral signatures, the most fundamental quantity discriminating the different spectral types is the temperature and not the chemical content. It was Cecilia Payne-Gaposchkin, who discovered that the chemical composition of stars can indeed be quantified. She discovered that all stars have very similar relative chemical abundances with hydrogen and helium comprising 99% by number.

- One of the characteristics of the spectral line is its central wavelength. In the rest-frame, this often enough to uniquely identify the transition responsible for the spectral line of an atomic transition (the chemical element, the ionisation stage and the electron transition) (see Fig. 1.3). In cooler stars, and/or more to the blue, the line density may become so large that all lines are blended. The observed wavelength (λ) is in the nearby universe and in normal condictions, directly related to the wavelength in the rest-frame (λ_0) by the velocity of the object with respect to the telescope (Doppler-shift). Blue-shifted lines come from objects with a velocity towards us, redshifted lines from receding objects. At cosmological distances, the shift is dominated by the expansion of the Universe and wavelength shift is called "the redshift". The search for the highest redshift equals the search for light which was emitted when the Universe was at its infancy. Redshifts around about 7 are now being detected with the Hubble Space Telescope as well as with the biggest ground-based telescopes. With a redshift of 7, emitted H_α (656.3nm) photons, are received at 5.25 μm...

$$\frac{\lambda - \lambda_0}{\lambda_0} = \frac{v_{\text{object}}}{c} \tag{1.1}$$

$$z = \frac{\lambda - \lambda_0}{\lambda_0} \tag{1.2}$$

$$\tag{1.3}$$

- Some lines and/or spectral bands appear to be present in all spectra, irrespective of the spectral type of the star being observed. These are telluric of origin and are formed in the earth atmosphere (see Fig. 1.4).

- The profiles of most lines in a given star are rather similar but the hydrogen lines form an exception: they tend to be much broader.

- ...

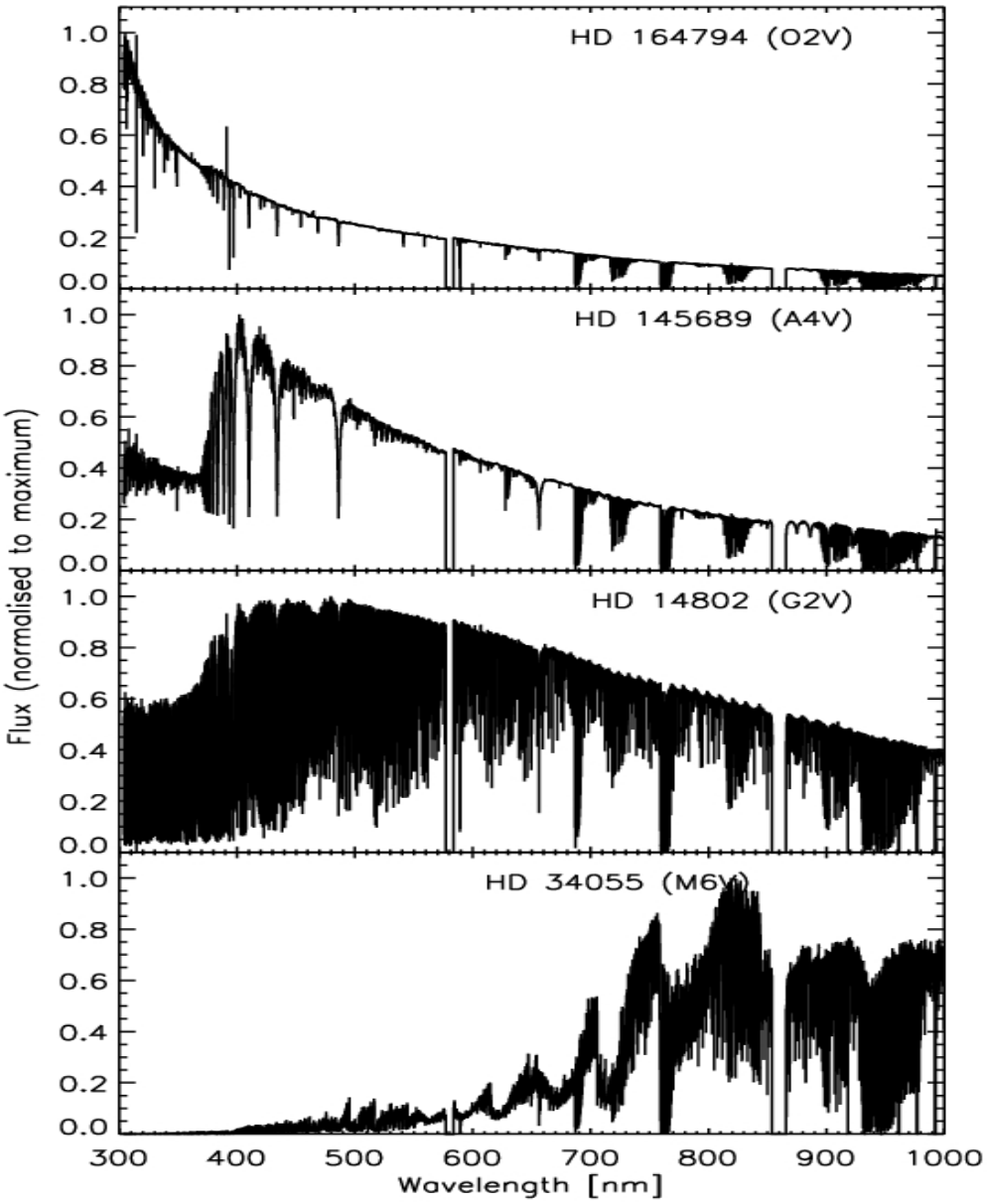

Figure 1.1: A sample of spectra of main sequence stars spanning the spectral range from O to M. The spectral window covers the UV up to the near-IR.

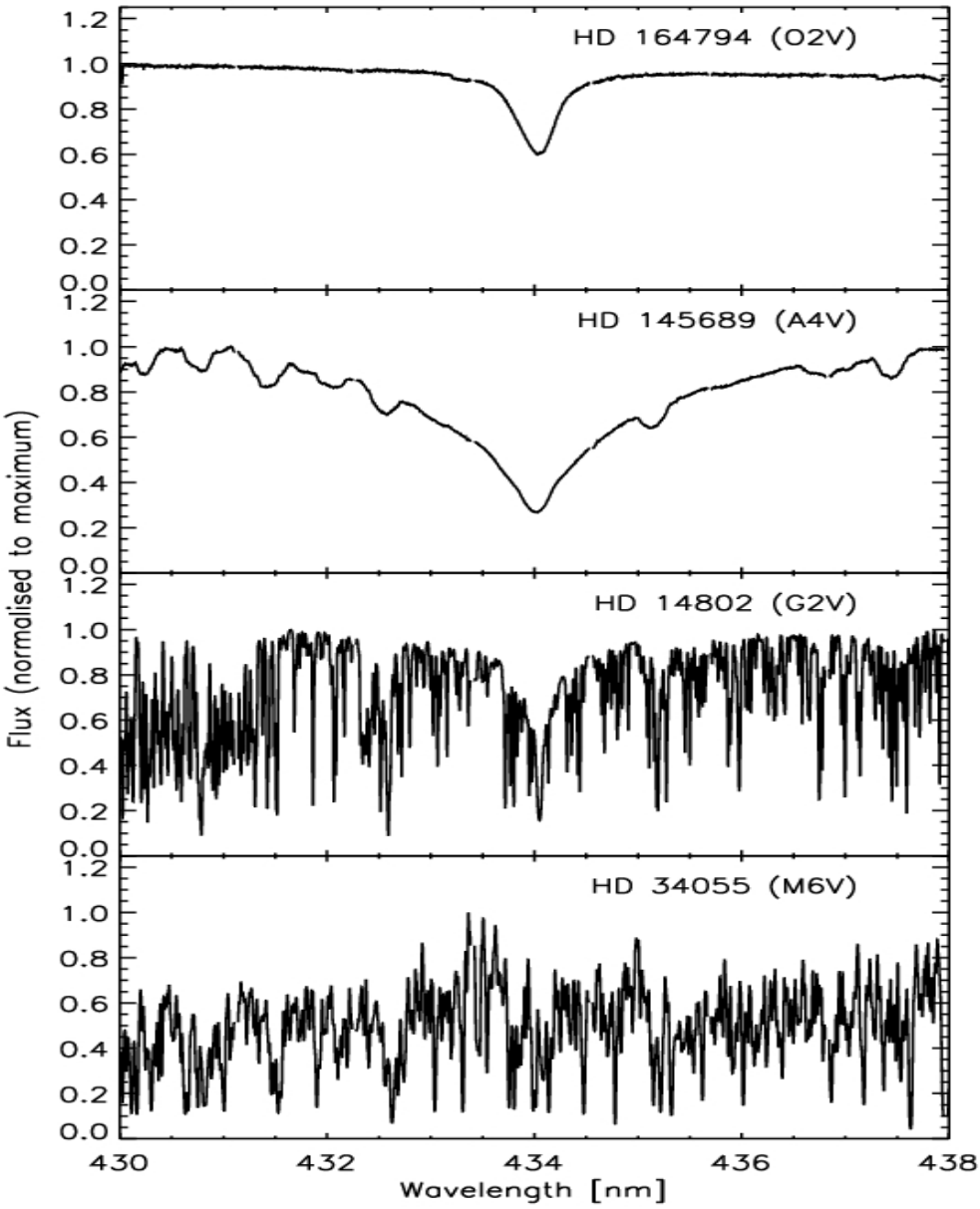

Figure 1.2: A sample of spectra of main sequence stars spanning the spectral range from O to M. The spectral zoom is around the Balmer-γ transition of Hydrogen.

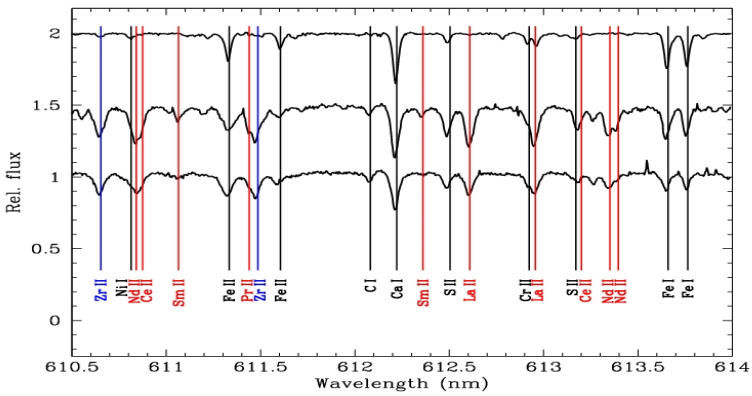

Figure 1.3: A spectral detail of several stars with very similar temperatures and gravities. Only in this case is the difference in strength of a spectral line, directly related to a difference in the abundance of the carrier. High-resolution spectra are very powerful to quantify trace elements: e.g. for every Pr atom in the sun, there are 2×10^{11} particles of H.

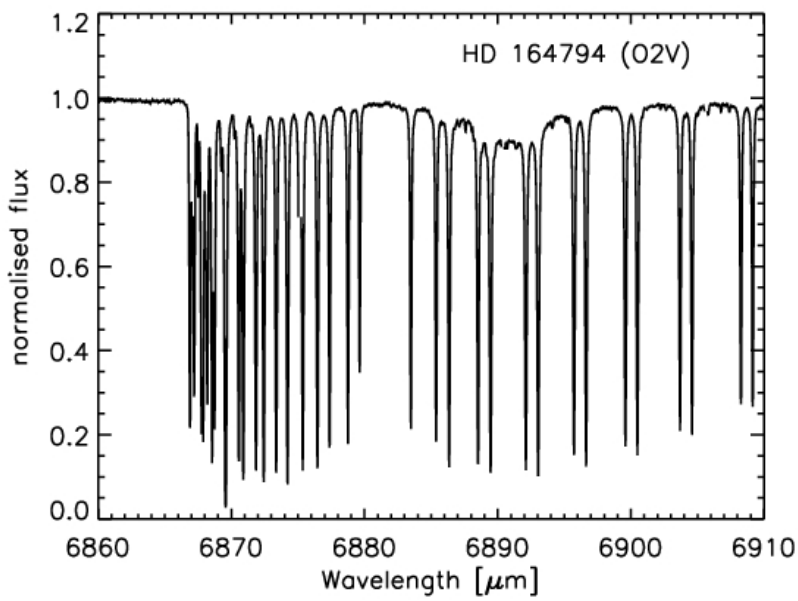

Figure 1.4: A spectral detail of the telluric contamination. This band is mainly due to O_2 absorptions in the earth atmosphere.

1.2 Solar Abundances

It is now clear that H and He are indeed everywhere in the universe so abundant, because these are the only elements made in significant number in the very early Universe. Before the first generation of stars appeared, the universe consisted of H, He and trace amounts of Li, Be and B. The chemical content of the Interstellar Medium (ISM), a star or a planet is the result of this Big-Bang nucleosynthesis enriched by the yields of all earlier generations of stars which contributed to the enrichment of the ISM in which the star was formed.

The abundance of a chemical element ($A_{\rm el}$) is the number density of that given element compared to the number density of H. This is usually given in a logarithmic scale with the abundance of H defined as A(H) = 12.

$$A_{\rm el} \equiv \log\ N_{\rm el} - \log\ N_{\rm H} + 12 \tag{1.4}$$

The abundance pattern is the distribution of the abundances of all chemical species given in the periodic table of Mendeljev. If you want a good mnemonic for all elements you can use this link.

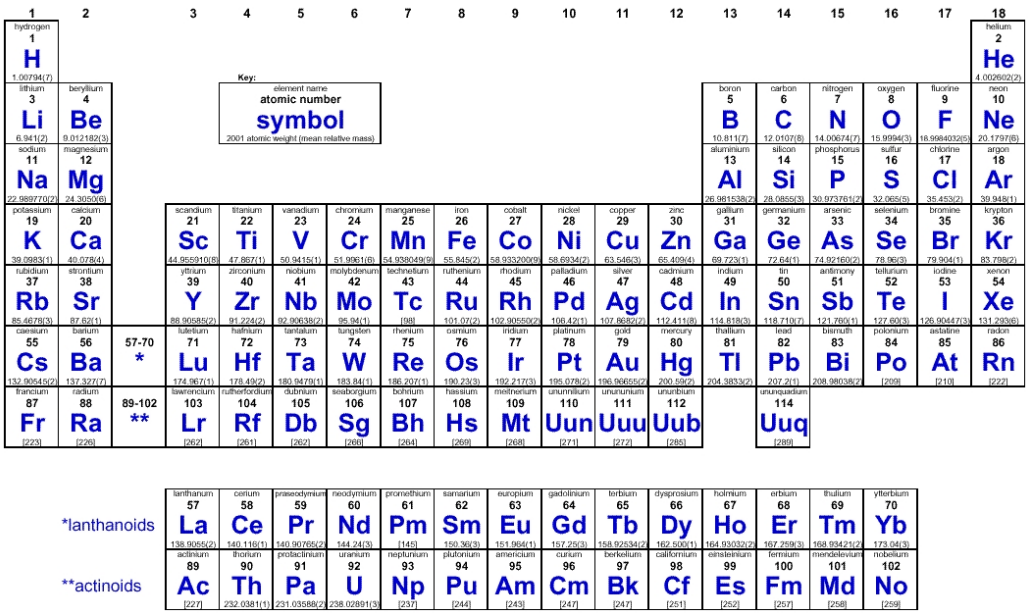

Figure 1.5: The period table of chemical elements known as the table of Mendeljev.

Spectroscopists usually relate the abundance of a given species to the solar abundance and indicate with square brackets the log of the abundance of the celestial object minus the log of the solar abundance of that species:

$$[el/H] = \log \frac{N_{\rm el}}{N_{\rm H}} - \left(\log \frac{N_{\rm el}}{N_{\rm H}}\right)_{\odot} \tag{1.5}$$

The Fe relative abundances is then:

$$[\mathrm{Fe/H}] = \log\,(\mathrm{N_{Fe}/N_H})_{\mathrm{object}} - (\log\ \mathrm{N_{Fe}/N_H})_{\odot} \tag{1.6}$$

Intuitively it is clear that the strength of a spectral line of a stellar spectrum is related to the photospheric abundance of the carrier, but this relation is by no means straightforward. The determination of chemical abundances requires an accurate knowledge of the physical conditions (e.g. temperature, density, radiation field) in the line forming region as well as a good knowledge of the atomic (molecular) data of the given transition (e.g. transition probability, ionisation stages) and the radiative transfer through the medium towards the observer. Only by using spectra of stars with very similar temperature and gravity, the relative strength of a line is a good tracer for the possible difference in the abundances of the element.

In Table 1.1 we list the Solar photospheric abundances up to Ni and a useful link for the whole set.

It may come to a surprise that even the solar photospheric abundances are still a matter of active debate within the astronomical literature (Fig. 1.6). The main reason is that the photospheric abundance of key elements like C, N and O are not only based on free atomic transitions, but also on temperature sensitive molecular CN, OH, NH transitions. Not all tracers of the C and O abundance of the Sun yield similar results. Recently, complex multi-dimensional computations, which are only now becoming available, suggest a very significant decrease in the solar C and O abundances (see Table 1.2). This decrease is, however, not undisputed and especially the helioseismologists fail to reproduce the solar oscillation patterns with models of such a low overall metallicity.

In table 1.3 we give the impact of the recent changes, which are quite significant for O and even Fe.

In contrast to the number abundances, we can also describe the relative abundances in terms of the contribution to the total mass. The fraction of mass which resides in a given element is called the mass fraction. Given the abundance pattern, it is custom to group together all elements heavier than He and the terms X

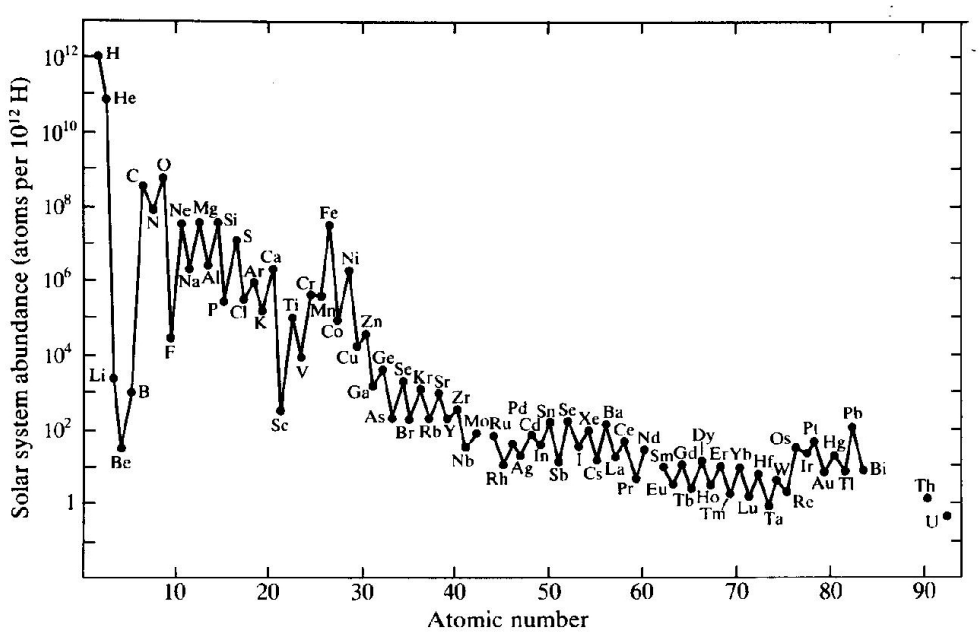

Figure 1.6: The abundance pattern of the solar photosphere. Note the strong general decline of the abundance in function of atomic mass, but with a few significant exceptions: the Fe-peak elements make up a local maximum. This is directly related to the stability of these nuclei, with ^{56}Fe, the most stable of all nuclei (See Fig. 1.7). Note as well that O is more abundant than C thanks to the vigorous O-production of massive stars. The odd-even effect is very well detected and is the result of the nuclear stability of odd versus even nucleon numbers. Some elements do not have a stable isotope (e.g. Tc). *Fig. from Cox (1998)*

(Hydrogen mass fraction), Y (Helium mass fraction) and Z (all the other elements) are given. Since these fractions include all mass (excluding dark matter), the sum must be unity. In the astronomical literature, Z is often called "the metals" but note that C,N and O and Ne are major contributors.

$$X + Y + Z = 1 \tag{1.7}$$

From the data in Table 1.1 you can compute the relative mass fractions with M_{A} the total mass of atoms of atomic weight A in some volume of gas. Also here, the once canonical value of Z = 0.02, still found in many textbooks turns out to be quite different from the more recent estimates.

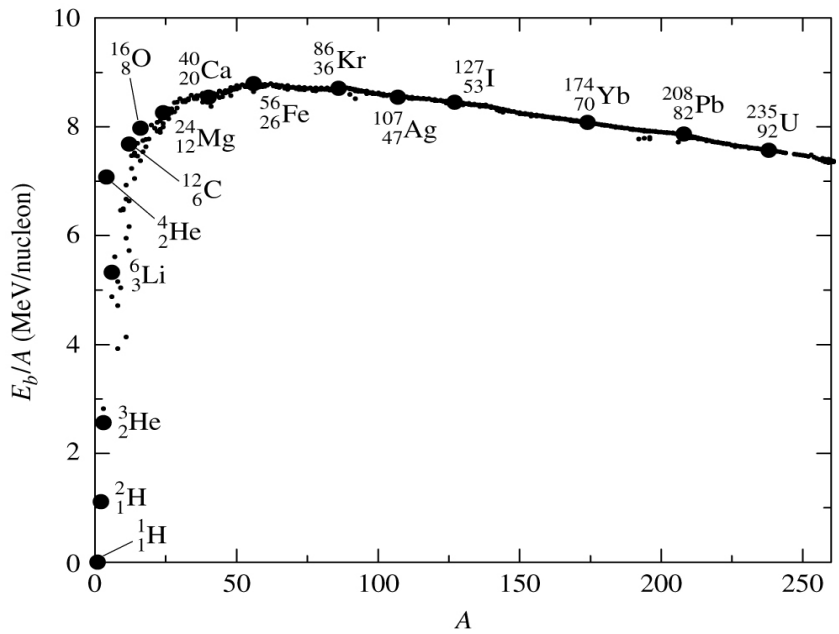

Figure 1.7: The binding energy per nucleon (E_b/A) as a function of the mass number A. *Fig. taken from Carroll & Ostlie (1996)*

$$X = \frac{M_{\rm H}}{\sum_A M_{\rm A}} = 0.7383 \tag{1.8}$$

$$Y = \frac{M_{\rm He}}{\sum_A M_{\rm A}} = 0.2495 \tag{1.9}$$

$$Z = 1 - X - Y = 0.0122 \tag{1.10}$$

Isotopes and the division of the number abundances over the different isotopes give a wealth of information on the physical conditions of possible production sides as well as on the intrinsic nuclear physics involved. The table of nuclides is sometimes called " the table of Mendeljev for adults" and contains the division of the abundances over the different stable isotopes of a given species. For the solar system, isotope abundances come almost exclusively from the study of carbonaceous chondrites (primitive meteorites) and the most famous ones are Murchison meteorite found in Australia, and the Allende meteorite found in Mexico. A review on the different tracers for the solar abundances can be found here.

Despite the uncertainties involved, it is clear that the Universe is chemically rather simple. The high abundance of both H and He makes that the (radiative) processes involving both species are in many environments the dominant

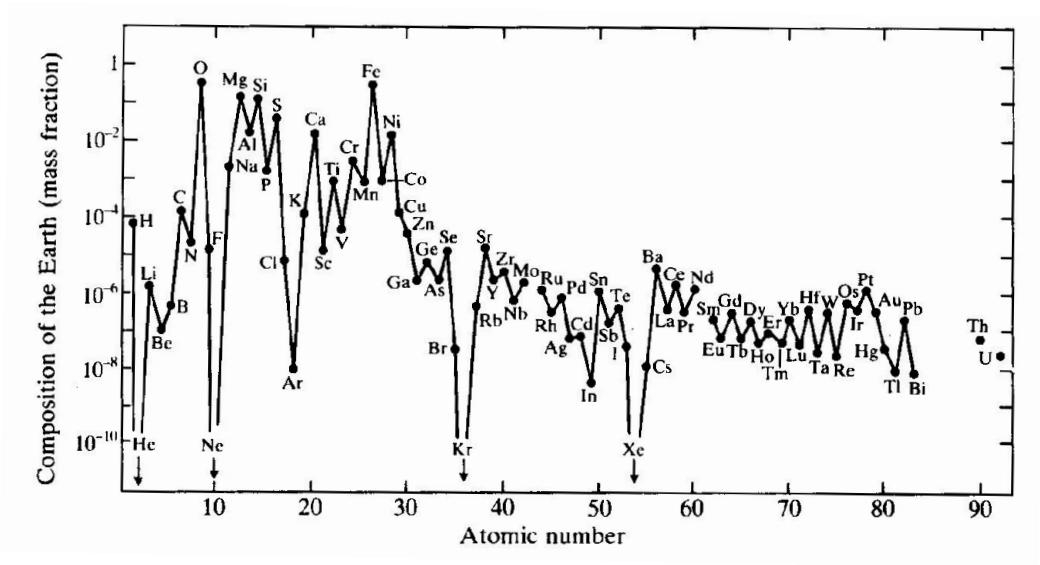

Figure 1.8: The abundance pattern of the whole earth. Compared to the sun, the most apparent difference is that the volatile elements (like H and He) are lacking. The main abundance trend is also determined by the chemical properties of the species. Note that only 4 elements have an abundance of more than 10% Fe, O, Mg and Si and together they make up some 90% of the total mass of the earth. S, Ni, Ca and Al occur with more than 1 %. All other elements together constitute only about 1%.*Fig. from Cox (1989)*

ones. The relative abundances of the sun, reflect the abundances of the Interstellar Medium (ISM) and they may as well be taken as characteristics of the ISM elsewhere in the Galaxy. Hence, the terms “Cosmic Abundances” or “Universal abundances” are used.

Table 1.1: The Solar photospheric abundances up to Ni as given in Asplund et al., 2005, ASPC 336, 25. A is the proton number, ATW the atomic weight, both abundance by number as by mass are given.

Atom (X)	A	ATW	log n by number	n(X)/n(H) by number	n(X)/n(He) fraction	mass
H	1	1.0080	12.00	1.000E+00	1.175E+01	7.347E-01
He	2	4.0026	10.93	8.511E-02	1.000E+00	2.483E-01
Li	3	6.9390	1.05	1.122E-11	1.318E-10	5.675E-11
Be	4	9.0120	1.38	2.399E-11	2.818E-10	1.576E-10
B	5	10.8100	2.70	5.012E-10	5.888E-09	3.949E-09
C	6	12.0100	8.39	2.455E-04	2.884E-03	2.149E-03
N	7	14.0100	7.78	6.026E-05	7.079E-04	6.153E-04
O	8	16.0000	8.66	4.571E-04	5.370E-03	5.331E-03
F	9	19.0000	4.56	3.631E-08	4.266E-07	5.028E-07
Ne	10	20.1800	7.84	6.918E-05	8.128E-04	1.018E-03
Na	11	23.0000	6.17	1.479E-06	1.738E-05	2.480E-05
Mg	12	24.3100	7.53	3.388E-05	3.981E-04	6.004E-04
Al	13	26.9800	6.37	2.344E-06	2.754E-05	4.610E-05
Si	14	28.0900	7.51	3.236E-05	3.802E-04	6.625E-04
P	15	30.9700	5.36	2.291E-07	2.692E-06	5.171E-06
S	16	32.0600	7.14	1.380E-05	1.622E-04	3.226E-04
Cl	17	35.4500	5.50	3.162E-07	3.715E-06	8.171E-06
Ar	18	39.9500	6.18	1.514E-06	1.778E-05	4.407E-05
K	19	39.1000	5.08	1.202E-07	1.413E-06	3.426E-06
Ca	20	40.0800	6.31	2.042E-06	2.399E-05	5.965E-05
Sc	21	44.9600	3.05	1.122E-09	1.318E-08	3.677E-08
Ti	22	47.9000	4.90	7.943E-08	9.333E-07	2.773E-06
V	23	50.9400	4.00	1.000E-08	1.175E-07	3.713E-07
Cr	24	52.0000	5.64	4.365E-07	5.129E-06	1.655E-05
Mn	25	54.9400	5.39	2.455E-07	2.884E-06	9.830E-06
Fe	26	55.8500	7.45	2.818E-05	3.311E-04	1.147E-03
Co	27	58.9300	4.92	8.318E-08	9.772E-07	3.573E-06
Ni	28	58.7100	6.23	1.698E-06	1.995E-05	7.267E-05

Table 1.2: The estimated solar photospheric abundances based on different tracers and different models. It is remarkable to note that the abundance of key elements like C, N are still a matter of debate. For a detailed review the interested reader is referred to Asplund, M., 2005, ARA&A 43, 481-530

		A(el)	
Lines	3D-model	1D-model Holweger&Müller	1D-model MARCS
C I	8.36 ± 0.03	8.39 ± 0.03	8.35 ± 0.03
CH $\Delta\nu = 1$	8.38 ± 0.04	8.53 ± 0.04	8.42 ± 0.04
N I	7.85 ± 0.08	7.97 ± 0.08	7.94 ± 0.08
NH $\Delta\nu = 1$	7.73 ± 0.05	7.95 ± 0.05	7.82 ± 0.05
O I	8.64 ± 0.02	8.64 ± 0.08	8.72 ± 0.03
OH $\Delta\nu = 1$	8.61 ± 0.03	8.87 ± 0.03	8.74 ± 0.03

Table 1.3: The recent history in the estimated solar photospheric abundances. The older values are from Anders & Grevesse, 1989, Geochimica et Cosmochimica Acta, Vol. 53,, the recent ones from Asplund et al., 2005, ASPC 336, 25.

Element	1989	2005
H	12.00	12.00
He	10.99	10.93
C	8.56	8.39
N	8.05	7.78
O	8.93	8.66
Ne	8.09	7.84
Mg	7.58	7.53
Si	7.55	7.51
S	7.21	7.14
Fe	7.67	7.45

1.3 Basic Quantities in the study radiative processes

1.3.1 Specific intensity

The most natural coordinate system in the study of celestial bodies are spherical coordinates and a basic concept is the solid angle (most often written as Ω). It is an angular area on the celestial sphere (see Fig. 1.9). The solid angle, is written in terms of two angular displacements dθ, dϕ. An unresolved object on the sky is smaller than the spatial resolution of your instrument and is called a point-source. Resolved objects cover a solid angle on the sky which is larger than the resolution and are therefore extended. In almost all frequency bands, from radio to gamma-rays, the sky exhibits both extended or diffuse emission in addition to point sources (see Fig. 1.10). A solid angle can be expressed in square degrees, square arcsec but the natural unit is sr.

$$d\Omega = \sin\theta \; d\theta \, d\phi \tag{1.11}$$

$$\Omega_{full\,sphere} = \int_{sphere} d\Omega = \int_0^{2\pi} d\phi \int_0^{\pi} \sin\theta d\theta = 2\pi \int_{-1}^{+1} d\mu \tag{1.12}$$

$$\Omega_{full\,sphere} = 2\pi \left(-\cos\theta\right)|_0^{\pi} = 4\pi \; (\mathrm{sr}) \tag{1.13}$$

In the astronomical literature the transformation $\cos\theta = \mu$ can often be found.

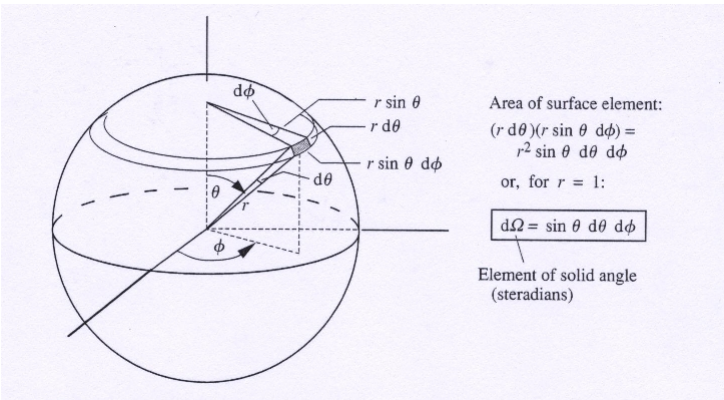

Figure 1.9: The solid angle Ω is the angular area on a sphere (gray area on the figure). The units is in "steradians" (square radians) or sr. Integration over a total sphere yields a total solid angle of 4π steradians. *Fig. from Bradt (2004)*

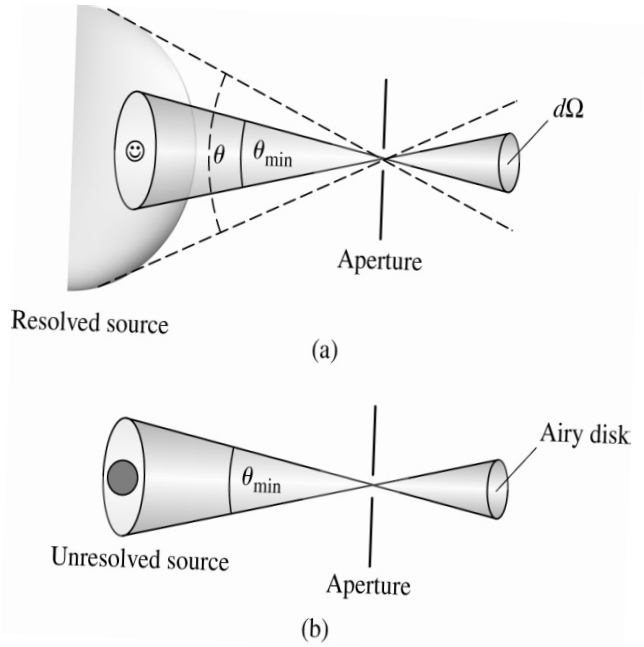

Figure 1.10: The solid angle of your device (eye, optical telescope, X-ray telescope etc.) and the solid angle of the source will determine whether the object is unresolved or resolved. *Fig. taken from Carroll & Ostlie (1996)*

$$1.0\,\mathrm{sr} \equiv \frac{360}{2\pi}\,\frac{360}{2\pi} = (57.2958)^2 = 3282.806\,\mathrm{deg}^2 \tag{1.14}$$

The specific energy I_ν is a fundamental concept (see Fig. 1.11) and gives the amount of energy per unit time and frequency which passes through a surface area dA at an angle θ into a cone of unit solid angle $\mathrm{d}\Omega$. $dA\,\cos\theta$ is the area dA projected onto a plane perpendicular to the direction in which the energy is traveling. The units of specific intensity are:

$$I_\nu(\theta,\phi) \propto \mathrm{J\,s^{-1}\,m^{-2}\,sr^{-1}\,Hz^{-1}} \tag{1.15}$$
$$\propto \mathrm{Watt\ m^{-2}\,sr^{-1}\,Hz^{-1}} \tag{1.16}$$
$$\propto \mathrm{Jansky\ sr^{-1}} \tag{1.17}$$
$$I_\lambda(\theta,\phi) \propto \mathrm{J\,s^{-1}\,m^{-2}\,sr^{-1}\,nm^{-1}} \tag{1.18}$$
$$\propto \mathrm{Watt\ m^{-2}\,sr^{-1}\,nm^{-1}} \tag{1.19}$$

The specific intensity is distance independent ! To see this, take a ray and at

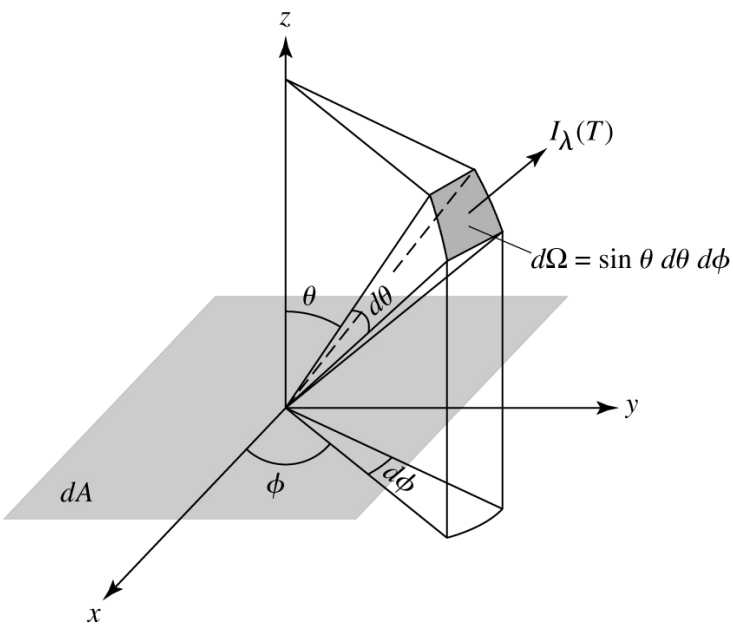

Figure 1.11: The specific intensity. *Fig. taken from Carroll & Ostlie (1996)*

any points along the ray we can have two infinitesimal surface areas, normal to the ray at distance R from each other. Since energy is conserved this translates to:

$$dE_1 = I_{\nu_1}\, dA_1\, dt\, d\Omega_1\, d\nu_1 = I_{\nu_2}\, dA_2\, dt\, d\Omega_2\, d\nu_2 = dE_2 \tag{1.20}$$

Here $d\Omega_1$ is the solid angle covered by dA_2 seen at dA_1 which is $\frac{dA_2}{R^2}$ and vice versa. It immediately follows that $I_{\nu_1} = I_{\nu_2}$ and we can conclude that indeed:

$$\frac{dI_\nu}{ds} = 0 \tag{1.21}$$

A spectral band is between ν and $\nu + \Delta\nu$ in frequency and between $\lambda + \Delta\lambda$ and λ in wavelength. The description of the intensity over wavelength band or frequency band is numerically not equal since $\nu\,\lambda = c$ and $d\nu = -\frac{c}{\lambda^2}\, d\lambda$. Requiring $d\nu$ and $d\lambda$ both positive we get:

$$I_\nu\, d\nu = I_\lambda\, d\lambda \tag{1.22}$$

$$I_\nu = \frac{c}{\nu^2}\, I_\lambda \tag{1.23}$$

$$I_\lambda = \frac{c}{\lambda^2}\, I_\nu \tag{1.24}$$

The total energy which passes through the surface is than the integral over time, frequency, solid angle and area which is:

$$E = \int dt \int d\nu \int d\Omega \int dA \, \cos\theta \, I_\nu(\theta, \phi). \tag{1.25}$$

1.3 .2 Moments of the specific intensity

In a radiation field we can have a small area dA with an arbitrary orientation. The radiative flux from the solid angle $d\Omega$ is then equal to:

$$dF_\nu = \cos\theta \, dI_\nu \, d\Omega = \text{with units } (Watt \, m^{-2} \, Hz^{-1}) \tag{1.26}$$

Integrating over all solid angles gives the net transport of energy which is called the radiant flux (often just called: flux):

$$F_\nu = \int I_\nu \, \cos\theta \, d\Omega \tag{1.27}$$

If the radiation field is isotropic, the net flux is zero since there will be as much energy transferred in the direction of n as in the opposite direction.

The momentum of a photon is $\frac{E}{c}$ so the momentum along a ray at angle θ is dF_ν/c. The component normal to dA is found by multiplying by $\cos\,\theta$:

$$p_\nu = \frac{1}{c} \int I_\nu \, \cos^2\theta \, d\Omega \tag{1.28}$$

Integration over frequency will yield the total momentum.

We can define than the moments of intensity and attach the physical meaning to them:

$$M_n = \frac{\int d\Omega \, I_\nu(\theta, \phi) \, \cos^n\theta}{\int d\Omega}. \tag{1.29}$$

The 0-rd moment is the mean intensity over the solid angle. It has the same units as specific intensity but, contrary to the specific intensity, it is distance dependent ! In an isotropic radiation field, $J_\nu = I_\nu$

$$J_\nu = \frac{1}{4\pi} \int d\Omega \, I_\nu(\theta, \phi) \tag{1.30}$$

The energy density u_ν in a given frequency band has units of $J\,m^{-3}\,Hz^{-1}$ and is related to the specific intensity. The surface in the direction of I_ν is $dS = dA\,\cos\theta$. The total energy can thus be written as:

$$E = \int dt \int d\nu \int d\Omega \int dS \, I_\nu(\theta, \phi), \tag{1.31}$$

Per unit of time, the radiation travels a distance c so per unit of time, a volume $dV = c\,dS$ is covered:

$$c\,E = \int dt \int d\nu \int dV \int d\Omega \, I_\nu(\theta, \phi). \tag{1.32}$$

The energy density per spectral band is related to the mean intensity using:

$$u_\nu = \frac{1}{c} \int d\Omega \, I_\nu(\theta, \phi) \tag{1.33}$$

such that $u_\nu = (4\pi/c) J_\nu$.

The total energy density ($J\,m^{-3}$) is than found by integrating over the whole spectrum:

$$u = \int d\nu \, u_\nu. \tag{1.34}$$

The first moment is related to the net flux in the direction of the $\vec{n}$. In an isotropic radiation field, $H_\nu = 0$ and the fact that we observe stars (galaxies etc.) means that the intensity cannot be isotropic everywhere. $F_\nu = 4\,\pi\,H_\nu$.

$$H_\nu = \frac{1}{4\pi} \int d\Omega \, I_\nu(\theta, \phi) \, \cos\theta \tag{1.35}$$

$$F_\nu = \int d\Omega \, I_\nu(\theta, \phi) \, \cos\theta \tag{1.36}$$

If we assume a sphere of uniform brightness B_ν (see Fig. 1.12), we can compute the flux obtained from this sphere at distance r:

$$F_\nu = \int I_\nu \cos\theta \, d\Omega = B_\nu \int_0^{2\pi} d\phi \int_0^{\theta_c} \sin\,\theta \,\cos\,\theta \, d\theta \tag{1.37}$$

The result becomes ($\sin\theta_c \,=\, R/r$):

$$F_\nu \;=\; \pi\, B_\nu\,(1-\cos^2\,\theta_c) \;=\; \pi\, B\,\sin^2\theta_c \tag{1.38}$$

$$F_\nu \;=\; \pi\, B_\nu \left(\frac{R}{r}\right)^2 \tag{1.39}$$

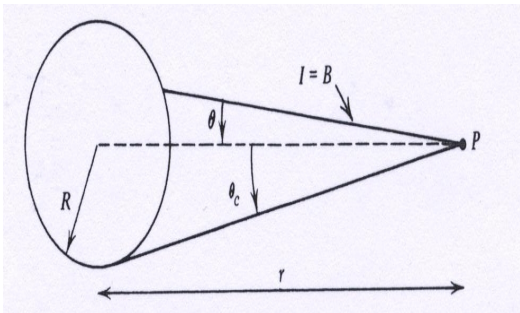

Figure 1.12: The sphere has uniform brightness B and is seen in point P at a distance of r. *Fig. from Rybicki & Lightmann (1979)*

So while the specific intensity is constant over distance, it is the solid angle covered by the object, which makes that the flux received is dependent on the inverse square of the distance. On the surface of the sphere with uniform brightness, we obtain: $F_\nu = \pi\, B_\nu$.

If we assume now a star with radius R at a given distance d with a surface flux of F_ν. On our detector on earth, we measure a flux of f_ν coming from this star than, assuming that there is no loss in radiation we can write:

$$4\pi\, R^2\, F_\nu \;=\; 4\pi\, d^2\, f_\nu \tag{1.40}$$

$$f_\nu \;=\; F_\nu \left(\frac{R}{d}\right)^2 \tag{1.41}$$

For the sun, the amount of flux we receive on earth is called the solar constant and is the integral of f_{nu} over frequency. The mean solar constant (solar irradiance) is about 1365 $Watt\, m^{-2}$.

The second moment of intensity is related to the radiation pressure. The amount of energy per unit frequency, time, solid angle and surface in the direction of $\vec{n}$, is $I_\nu \cos\theta$. The momentum associated with this energy again in the direction of $\vec{n}$ is obtained by devision with c and multiplication by $\cos\theta$ by the equation:

$$K_\nu = \frac{1}{4\pi}\int d\Omega\, I_\nu(\theta,\phi)\cos^2\theta \tag{1.42}$$

$$P_\nu = \int d\Omega\, \frac{1}{c}\, I_\nu(\theta,\phi)\, \cos^2\theta \tag{1.43}$$

So K_ν relates to the radiation pressure by $K_\nu = c\, P_\nu/4\pi$.

1.4 Radiative Transfer

When radiation travels through a medium, it will interact and energy may be added or subtracted from the beam. The specific intensity will not remain constant: the global reducing effect is called extinction which can be either absorption of photons (so photon destruction), or scattering of photons (the photons are not absorbed but scattered outside the beam). The global intensity increasing effect is called emission.

To describe the emission we define the emission coefficient j_ν as a volume emissivity. j_ν has the units of $\mathrm{Watt\,m^{-3}\ Hz^{-1}}$ and is the radiated power per unit volume per unit frequency per unit solid angle as:

$$dI_\nu = \frac{j_\nu}{4\pi}\, ds \tag{1.44}$$

The amount of extinction per unit distance is dependent on the strength of the incoming radiation as well as on the amount of material which is capable of photon extinction:

$$dI_\nu = -\,\alpha_\nu\, I_\nu\, ds \tag{1.45}$$

$$= -\,\kappa_\nu\, \rho\, I_\nu\, ds \tag{1.46}$$

$$= -\,\sigma_\nu\, n\, I_\nu\, ds \tag{1.47}$$

With ρ the mass density and n the number density. So the extinction coefficient can have different forms, depending on how the description of the extinction

is formulated: α_ν has units m^{-1}; κ_ν has units of m^2/kg and is the monochromatic cross-section per unit mass. σ_ν is the cross-section with units m^2 and gives the monochromatic cross-section and can be seen as an effective surface of a particle which is a measure for its efficiency in photon extinction. It is sometimes confusing that α_ν as well as κ_ν or σ_ν are called 'opacity' coefficient or just 'the opacity'.

Another variable is optical thickness which, assuming we describe it following the radiation, can be written as:

$$d\tau_\nu = \alpha_\nu \, ds \tag{1.48}$$

The total optical thickness along the ray after having traveled a distance D is than the integral over the path:

$$\tau_\nu(D) = \int_0^D \alpha_\nu \, ds \tag{1.49}$$

The cross-section of a particle can be seen as the effective area of a particle at that given wavelength or frequency. Assume that a beam impinges on a thin slab of area A (m^2) material in which the number density of particles is n (particles m^{-3}). The number of particles in the slab is then $n\,A\,ds$ and the effective area blocked by all particles is $\sigma_\nu \, n \, A \, ds$. We assume that this quantity is much less then A. The fractional area is then $\sigma_\nu \, n \, ds$ which gives the fractional deminishing of the radiation. Expressed in number of photons N_ν of a given frequency this yields:

$$\frac{dN_\nu}{N_\nu} = -\,\sigma_\nu \, n \, ds \tag{1.50}$$

Integrating over ds gives than the exponential decay of the radiation (number of photons). At a distance of $s = (\sigma_\nu \, n)^{-1}$ the number of photons has been reduced to 1/e of the initial value. The computation of the mean-free path shows that this is where the average destruction has this 1/e value so the local mean free path in a homogeneous material is equal to $(\sigma_\nu \, n)^{-1}$. This gives the average geometrical length of a path of a photon, before it gets destroyed. The * supperscript is often used to designate that the expression is valid when following the ray. The "mean optical depth" traveled by a photon is unity :

$$< \tau_\nu^*(z) > \equiv \frac{\int_0^\infty \tau_\nu^*(z) e^{-\tau_\nu^*(z)} d\tau_\nu^*(z)}{\int_0^\infty e^{-\tau_\nu^*(z)} d\tau_\nu^*(z)} = 1. \tag{1.51}$$

The "mean free path" l_ν is the physical distance traveled in a homogeneous medium and is determined by:

$$l_\nu = \frac{< \tau_\nu^*(z) >}{\alpha_\nu} = \frac{1}{\alpha_\nu}. \tag{1.52}$$

In a inhomogeneous medium, it gives a good approximation and is called the "local mean path". In stellar interiors, the local mean photon path is in the order of cm; while in the atmosphere it is in the order of thousands of km.

If a medium absorbs radiation, the radiation will exert a force on the medium, because it carries momentum. The radiation flux vector, aligned with the direction of the radiation $\vec{n'}$

$$\vec{F_\nu} = \int I_\nu \, \vec{n'} \, d\Omega \tag{1.53}$$

Every photon carries momentum E/c so the momentum vector per unit area, per unit time, per unit path length absorbed by the medium is the integral over frequency of the fraction of the radiation flux vector which is absorbed. Assuming the absorption coefficient is isotropic and there is no momentum imparted by emission (isotropic emission coefficient):

$$\vec{\mathcal{F}} = \frac{1}{c} \int \alpha_\nu \, \vec{F_\nu} \, d\nu \tag{1.54}$$

The force per unit mass of material in the direction of the radiation is

$$\vec{f} = \frac{1}{c} \int \kappa_\nu \, \vec{F_\nu} \, d\nu \tag{1.55}$$

In order to be able to describe the change of the radiation field we have to find a good description of all relevant processes in the interaction of the radiation with the material, and this over the whole frequency spectrum. In many cases the emission and extinction coefficient share a very similar frequency dependency and the source function, defined as:

$$S_\nu = \frac{j_\nu}{4\pi\,\alpha_\nu} \tag{1.56}$$

gives often a much smoother frequency dependence.

The physical meaning of optical thickness is illustrated solving the equation for the change of intensity when only allowing for extinction:

$$dI_\nu = -\,\alpha_\nu\, I_\nu\, ds \tag{1.57}$$
$$dI_\nu = -I_\nu d\tau_\nu \tag{1.58}$$

The integral over length D gives:

$$I_\nu(\tau_\nu(D)) = I_\nu(\tau_\nu(0))\,\exp(-\tau_\nu(D)) \tag{1.59}$$

so the total optical thickness gives the exponential decay of the incoming radiation. When the optical thickness is 1, the intensity is diminished by a factor e (2.7182....). A slab of material is called optically thick when the optical thickness is > 1 and optically thin when the total optical depth remains < 1. The optical depth gives the thickness in units of mean free path of photons and is a dimensionless quantity.

The integral is often described from the viewpoint of the observer and not following the rays themselves. Optical thickness 0 is at the surface of the object, and increases inwards. The optical thickness from the observers point of view is called "optical depth". In a plane-parallel medium, the optical depth is often described in the vertical direction, normal to the slab (See Fig. 1.13). A factor $\cos\theta$ will then appear in the equation:

$$\tau_\nu = \frac{\tau_{\nu,vert.}}{\cos\theta} = \tau_{\nu,vert.}\,\sec\theta \tag{1.60}$$

Unfortunately, the term "optical depth" is found in the literature both from the observers viewpoint, or following the radiation...

The transfer equation now gives the change of specific intensity by incorporating both emission and absorption into one equation:

$$\frac{dI_\nu}{ds} = -\,\alpha_\nu\, I_\nu + \frac{j_\nu}{4\pi} \tag{1.61}$$

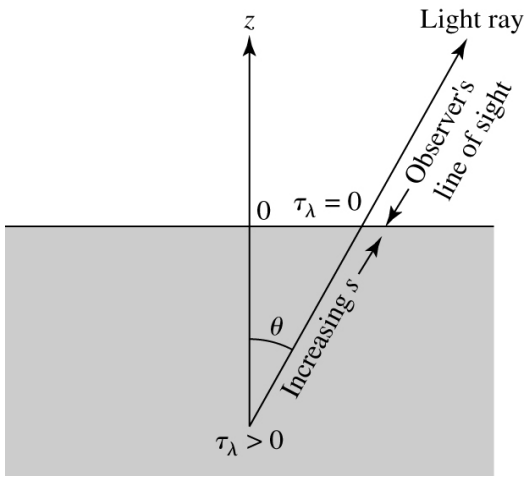

Figure 1.13: The orientation vectors to describe the optical thickness of a material. *Fig. taken from Carroll & Ostlie (1996)*

using now the definition of the source function and assuming that we follow the ray (we change the direction of view so we flip the sign):

$$\frac{dI_\nu}{d\tau_\nu} = -\,I_\nu + S_\nu \tag{1.62}$$

The formal solution can be found by multiplying both terms by e^{τ_ν} and integrating along the optical thickness. The solution is then:

$$I_\nu(\tau_\nu) = I_\nu(0)\, e^{-\tau_\nu} \; + \int_0^{\tau_\nu} S_\nu(t_\nu)\, e^{-(\tau_\nu - t_\nu)}\, dt_\nu \tag{1.63}$$

This can be understood as the resulting intensity is the original intensity diminished by the exponential of the total optical thickness, plus the integral of the source function diminished by absorption along the way.

While the formal solution of the transfer equation is simple, the practical solution is rather complex : the frequency dependence of all processes involved in the interaction between material and radiation field needs to be described. Moreover, the relevant processes rely on a detailed knowledge of the state of the intervening material (e.g. electron density, ionisation fraction, excitation fraction etc. etc.) while this on its turn, is dependent on the radiation field.

1.5 Simple solutions of the transfer equation

1.5 .1 Homogeneous slab

It is very instructive to look in a bit more detail on a simple solution when incident radiation falls on a slab of material which is homogeneous. The slab has a total optical thickness of $\tau_\nu(D)$. Equation 1.63 can than be solved easily because we can bring S_ν outside the integral (the slab has a constant source function). The solution is than:

$$I_\nu(\tau_\nu(D)) = I_\nu(\tau_\nu(0))\, e^{-\tau_\nu(D)} + S_\nu(1 - e^{-\tau_\nu(D)}). \tag{1.64}$$

So the observed radiation is the sum of the incident radiation diminished with the exponential decay due to the total optical thickness of the layer plus the factor which expresses the source function addition.

Special cases include:

- **The layer is optically thick:** $\tau_\nu(D) \gg 1$

  All incident radiation will be extinguished and what we will observe equals the source function:

  $$I_\nu(\tau_\nu(D)) \simeq S_\nu \tag{1.65}$$

- **The layer is optically extremely thin:** $\tau_\nu(D) \ll 1$

  We will have no contribution from the source function and all we see is the incident radiation.

- **The layer is optically thin:** $\tau_\nu(D) < 1$

  In this case we can use the Taylor expansion of the exponential

  $$\exp x = 1 + x + \frac{x^2}{2!} + \frac{x^3}{3!} + \frac{x^4}{4!} + ... \tag{1.66}$$

  and use only the linear term.

  $$I_\nu(\tau_\nu(D)) \simeq I_\nu(\tau_\nu(0)) + \tau_\nu(D)\,(S_\nu - I_\nu(\tau_\nu(0)) \tag{1.67}$$

When the slab of material has a source function which is larger than the incident intensity, we will get out-coming radiation which is larger than the incoming radiation and the slab will introduce net emission. When the source function is smaller, the slab will introduce net absorption. Without incident radiation, the equation becomes:

$$I_\nu(\tau_\nu(D)) = \tau_\nu(D)\, S_\nu \tag{1.68}$$

and what we see is a fraction of the source function and that fraction ($\tau_\nu(D) < 1$) scales with the total optical thickness of the slab.

In Fig. 1.14 we illustrate the different cases assuming a homogeneous slab of material with a source function which includes a spectral line.

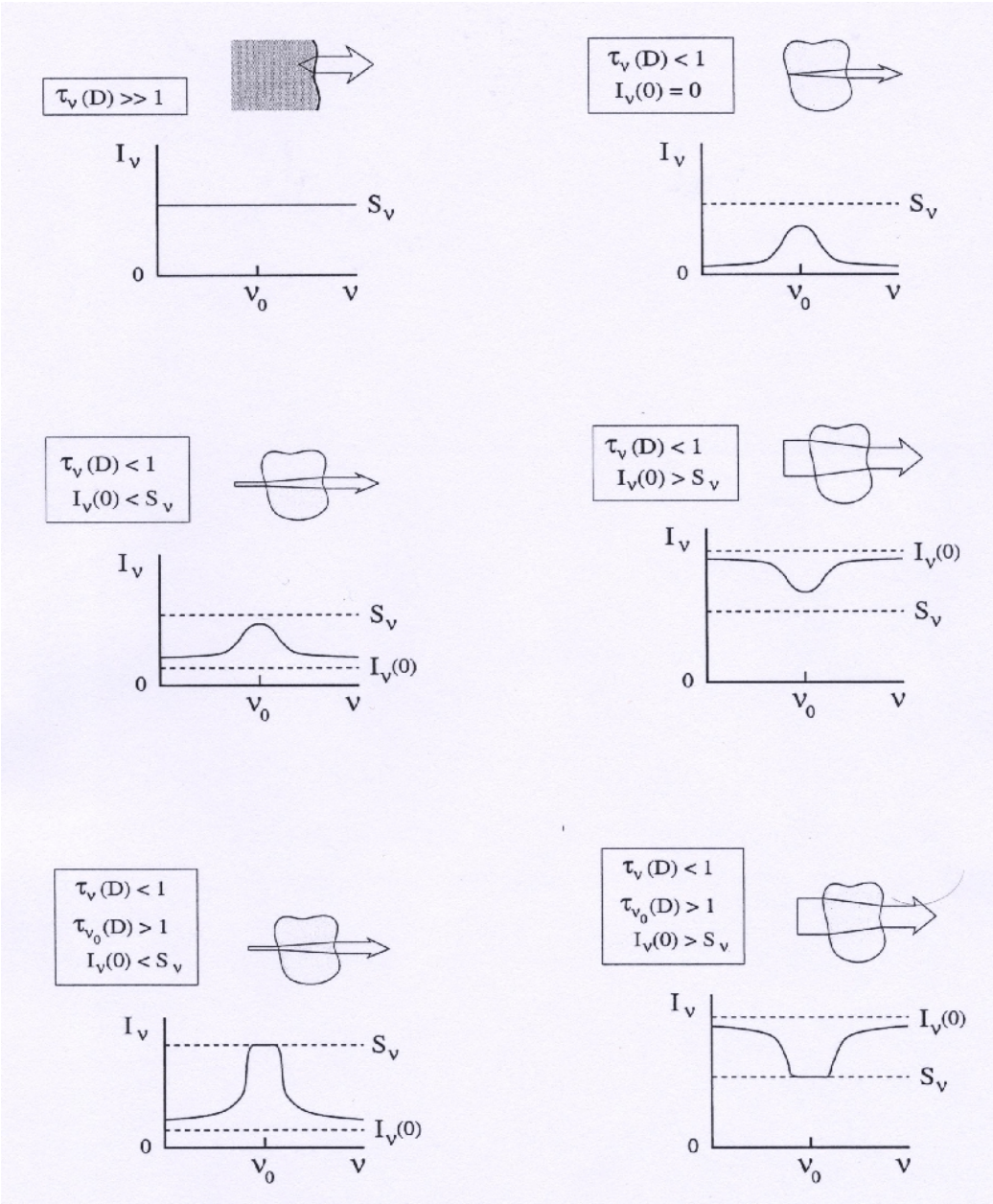

Figure 1.14: This figure illustrates the solution of the transfer equation assuming a homogeneous spectral slab, with a source function which includes a spectral line.*Fig. from Rutten (2000).*

1.5 .2 Plane parallel atmosphere in the Eddington-Barbier relation

To describe the radiation transfer in a star or very optically thick body, the observers viewpoint is taken and the optical depth is 0 at the surface and increases inwards and is defined along the radial direction (see Fig. 1.15).

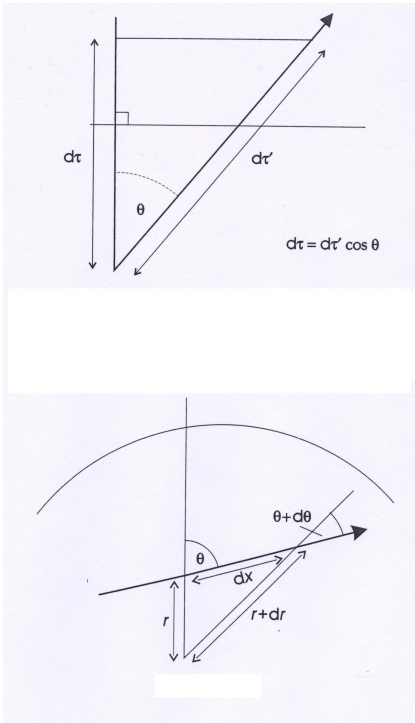

Figure 1.15: This figure illustrates the difference between a plane-parallel approximation and a spherical case. In the latter case, a ray will intersect with different layers at another angle from the radial direction. In the plane-parallel approximation, the ray intersects with all the different layers at the same angle θ. *Fig. from Gray (1992)*

To describe the transfer of radiation through a photosphere of a star, a significant simplication comes from the fact that we assume the photospere to be thin relative to the curvature of the star. We also define place the τ=0 point outside the star, the sign therefore changes with respect to the situation where we follow the radiation itself. This approximation is called the 'plane-parellel' approximation and the radiative transfer equation becomes.

$$\cos\theta \, \frac{dI_\nu}{d\tau_\nu} = \mu \, \frac{dI_\nu}{d\tau_\nu} = I_\nu - S_\nu \tag{1.69}$$

This appriximation is quite good in main sequence stars: the optical thickness of 1 is in our Sun reached in a geometrical depth of about 700 km (compared to its radius of about 7 10^5km). In a red giant, the geometrical depth where an optical depth of 1 is found is about 500000 km. In a white dwarf this is only about 1 km. Needless to say that the geometrical depth where the optical depth is 1 is dependent on the frequency of the radiation being considered. When the opacity is small, the optical depth = 1 will be at larger geometrical depth.

For spherical geometry, the transfer equation becomes:

$$\mu \, \frac{\partial I_\nu}{\partial \tau_\nu} + \frac{(1-\mu^2)}{\tau_\nu} \, \frac{\partial I_\nu}{\partial \mu} = I_\nu - S_\nu \tag{1.70}$$

The formal solution for the outcoming intensity along a given direction in the plane-parallel approximation is ($d\tau_\nu = \alpha_\nu \, dz$):

$$I_\nu^+(0,\theta) = \int_0^\infty \mathrm{d}\tau_\nu \, \sec\theta \, S_\nu(\tau_\nu) \, e^{-\tau_\nu \, \sec\theta} \tag{1.71}$$

The Eddington-Barbier relation now assumes for the photosphere of a star, a polynomial dependency of the source function in function of the optical depth.

$$S_\nu(\tau_\nu) = \sum_{n=0}^{\infty} a_n \tau_\nu^n = a_0 + a_1\tau_\nu + a_2\tau_\nu^2 + \ldots \tag{1.72}$$

The transfer equation can now be solved using the integral equation $\int_0^\infty x^n \, exp(-x) \, dx = n!$:

$$I_\nu^+(0,\theta) = a_0 \, + \, a_1 \, \mu + 2 \, a_2 \, \mu^2 \, + \, \ldots \, + \, n! \, a_n \, \mu^n \tag{1.73}$$

Or only the linear term:

$$I_\nu^+(0,\theta) \approx S_\nu(\tau_\nu = \mu) \tag{1.74}$$

So the intensity at the surface in a given direction θ equals the source function at radial optical depth of $\cos\theta$. When looking in the radial direction, the intensity

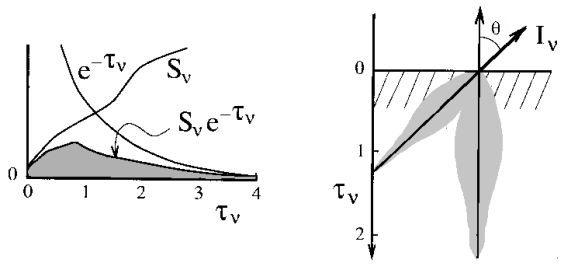

Figure 1.16: This figure illustrates the solution of the transfer equation to determine the outcoming radiation in function of the viewing angle θ. The left panel shows the evaluation of the integral $S_\nu \exp(-\tau_\nu)$ and the relative contribution of the different layers at different optical depth. The panel on the right, shows the limb-darkening: under a given angle θ on the normal, the layer which contribute most, is at shallower optical depth when θ becomes larger. *Fig. from Rutten (2000)*

equals the source function at optical depth 1, while looking at an inclination, the intensity will be smaller. This is called 'limb-darkening' (see Fig. 1.16, Fig. 1.17).

When we measure the solar limb-darkening at different wavelengths, we can fit the measurements rather well using the following fit to the intensity profile:

$$I_\nu(0,\theta) \;=\; I_{\theta=0}\,[(1 \,-\, u_\nu) \,+\, u_\nu \,\cos\theta] \tag{1.75}$$

with $u_\nu \;=\; 0.7$ in the UV, $u_\nu \;=\; 0.6$ in het blue and $u_\nu \;=\; 0.55$ in the red.

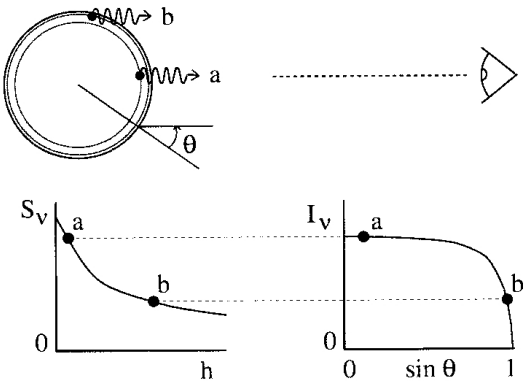

Figure 1.17: This figure illustrates the limb darkening. Only the sun is close enough, so that the measured limbdarkening gives a direct probe on how the source function behaves in function of optical depth. *Fig. from Rutten (2000)*

1.6 Thermal Radiation

This course will focus on the relation between the physical state of the matter and the radiation field.

Blackbody radiation will be a good approximation when the material is optically thick and photons scatter many times before being detected and it is in perfect thermal equilibrium (TE). Photons and particles share their kinetic energies. This is only possible when there are no gradients in the system. In astrophysics the assumption of TE can be a good approximation but only on a local scale. When applied in the description of an astrophysical object and its radiation field, we call it LTE for Local Thermodynamic Equilibrium.

The total overall energy output of an object (e.g. a star) can be approximated, in 0rd order, by assuming the object radiates as a black-body.

The shape of the emitted spectrum of a body of constant temperature (see Kirchoff's first law) was deduced experimentally before Planck (1858-1947) could prove that the constants involved can be expressed by fundamental constants (see Fig. 1.18).

$$B_\nu(T) \;=\; I_\nu(T) \;=\; \frac{2h\nu^3}{c^2}\,\frac{1}{e^{h\nu/kT}-1} \tag{1.76}$$

$$B_\lambda(T) \;=\; I_\lambda(T) \;=\; \frac{2\,h\,c^2}{\lambda^5}\,\frac{1}{e^{hc/\lambda\,kT}-1}. \tag{1.77}$$

The unit of B_ν is typically Watt m^{-2} Hz^{-1} sr^{-1} and B_λ is e.g. Watt m^{-2} nm^{-1} sr^{-1} which is the specific intensity of the blackbody. Both curves are only equivalent, if we take care of the difference between spectral bandwidth and frequency bandwidth: $\lambda\,B_\lambda \;=\; \nu\,B_\nu$.

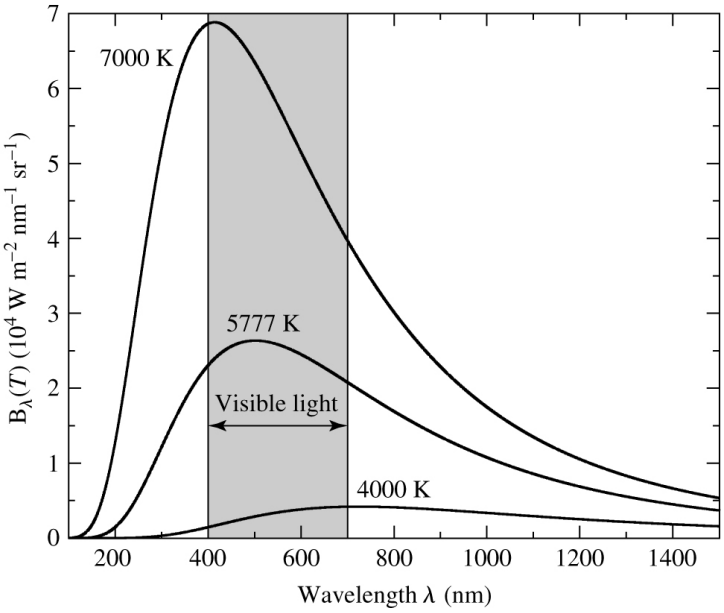

Figure 1.18: The Black-Body spectrum (B_λ) for different temperatures. For hot resp. cool stars, the peak of the energy distribution falls outside the visible range. *Fig. taken from Carroll & Ostlie (1996)*

Since the radiation is isotropic the flux, which is an integral over the whole solid angle, will be zero. The outward flux at the surface of e.g. a star, can be computed by integration only over half the sphere (between $\theta = 0$) and ($\theta = \pi/2$). And in this case we write:

$$\mathcal{F}_\nu^+ = \pi\,I_\nu = \pi\,B_\nu \tag{1.78}$$

The total power leaving 1 m^2 of the surface (flux density in Watt m^{-2}) is:

$$Flux = \int_0^\infty \int_{\theta=0}^{\pi/2} \int_{\phi=0}^{2\pi} B_\nu \frac{dA\,\cos\theta}{dA} \sin\theta d\theta d\phi d\nu \tag{1.79}$$

So this becomes:

$$Flux = \pi \int_0^\infty B_\nu d\nu \tag{1.80}$$

When we integrate the curve over the whole frequency range we obtain expressions for a and σ (the Stefan-Bolzmann constant) in terms of fundamental constants:

$$\int_0^\infty B_\nu(T)\,d\nu = \frac{2h}{c^2}\left(\frac{k\,T}{h}\right)^4 \int_0^\infty \frac{x^3\,dx}{(e^x - 1} \tag{1.81}$$

The integral is a Riemann ζ-function (see Table 1.4) has a value of $\pi^4/15$ so we have the result:

$$\int_0^\infty B_\nu(T)\,d\nu = \frac{\sigma\,T^4}{\pi} \tag{1.82}$$

$$\sigma = \frac{2\,\pi^5\,k^4}{15\,c^2\,h^3} \tag{1.83}$$

$$a = \frac{8\,\pi^5\,k^4}{15\,c^3\,h^3} \tag{1.84}$$

$$\tag{1.85}$$

1.6.1 Energy density

The energy density of BB radiation is the sum of all energies hν of photons contained in e.g. m^{-3} and as photons travel at speed c we get:

$$\frac{4\,\pi\,I_\nu}{c} = u_\nu(\nu, T) \tag{1.86}$$

So for BB radiation we get:

$$u_\nu(\nu, T) = \frac{8\pi h\nu^3}{c^3}\,\frac{1}{e^{h\nu/kT} - 1} \tag{1.87}$$

Table 1.4: The Riemann ζ-functions and their numerical value for different z values.

$\zeta(z) = \frac{1}{(z-1)!}\int_0^\infty \frac{x^{z-1}}{e^x-1}\,dx$	
z	ζ(z)
1	diverges
2	$\frac{\pi^2}{6}$
3	1.202057...
4	$\frac{\pi^4}{90}$

So for the total energy density (intergral over de frequency) we get:

$$u(T) = \int_0^\infty u_\nu(\nu, T)\,d\nu = \frac{4}{c}\,\sigma\,T^4 = a\,T^4 \tag{1.88}$$

The total energy density is:

$$u = \frac{4\pi}{c}\int_0^\infty B_\nu(T)\,d\nu = \frac{4\sigma\,T^4}{c} = a\,T^4 \tag{1.89}$$

The associated number density of photons is equal to:

$$n_\nu = \frac{u_\nu(\nu, T)d\nu}{h\,\nu} = \frac{8\pi h\nu^2}{c^3}\,\frac{1}{e^{h\nu/kT}-1} \tag{1.90}$$

The total number density:

$$n(T) = \int_0^\infty n_\nu(\nu, T)d\nu = 16\pi\left(\frac{kT}{hc}\right)^3 \times 1.202 = 2.029 \times 10^7 T^3 m^{-3} \tag{1.91}$$

The average photon energy is:

$$h\nu_{aver} = \frac{u(T)}{n(T)} = 2.70\,k\,T \tag{1.92}$$

1.6 .2 Radiation Pressure

Energy per unit volume moving towards a surface A and angle θ per sr:

$$\frac{u(T)}{4\pi} \tag{1.93}$$

Total momentum (p = E/c):

$$\frac{u(T)}{4\pi\, c} \tag{1.94}$$

The momentum directed towards θ,ϕ in solid angle $d\Omega$ is then u $d\Omega$/(4πc). The photons travel with velocity c and the photonc present in the volume is c Δt will trike in that timeinterval the unit surface. The cross-section is A $\cos\theta$. Momentum carried to the surface in time $\Delta\, t$ by particles in the solid angle:

$$\Delta p_A = \frac{u}{4\pi\, c}\, d\Omega\ c\, \Delta t\, A \cos\theta \tag{1.95}$$

The momentum transferred to the surface depends on whether the photons are absorbed or reflected. When the surface is in thermal equilibrium, the net effect is the same as if each incoming photon underwent a specular reflection from the surface (like a mirror) with the same magnitude of momentum with which it arrived. The component of the momentumvector which is normal to the surface, will contribute to the pressure.

The momentum transfer is then:

$$\Delta p_{ph} = -2\Delta p_A \cos\theta\ \vec{n} \tag{1.96}$$

This becomes:

$$\Delta p_{ph} = \frac{2\, u}{4\pi\, c}\, d\Omega\ c\, \Delta t\ A \cos^2\theta\ \vec{n} \tag{1.97}$$

The photon pressure (momentum transfer per unit time, per unit area

$$dP = \frac{2\, u}{4\pi\, c} \frac{d\Omega\ c\, \Delta t A \cos^2\theta}{A\Delta t} = \frac{u}{2\pi} \cos^2 d\Omega \tag{1.98}$$

This gives for the total pressure (integration over half a hemisphere):

$$P = \int_{\theta=0}^{\pi/2} \int_{\phi=0}^{2\pi} \frac{aT^4}{2\,\pi} \cos^2\theta \sin\theta d\theta d\pi \tag{1.99}$$

Or with the integration solved:

$$P = \frac{aT^4}{3} \tag{1.100}$$

The pressure is 1/3rd of the energy density.

The evaluation of the curve of Planck is interesting since it gives a first order approximation on the radiation properties of objects in the sky. Remember as well that the effective temperature of a source T_{eff}, is defined as the temperature of a black-body radiator with the same total integrated flux (integrated over all frequencies) at the location of the source. For stars this relates to:

$$L = 4\,\pi\,R_*^2\,\sigma\,T_{eff}^4 \tag{1.101}$$

1.6 .3 Wiens displacement law

The frequency at which the peak of the energy distribution occurs, can be found by solving for

$$\frac{\partial B_\nu}{\partial \nu} = 0 \tag{1.102}$$

$$\frac{\partial B_\lambda}{\partial \lambda} = 0 \tag{1.103}$$

When solving the first equation we get:

$$h\nu_{max} = 2.82kT \tag{1.104}$$

$$\frac{\nu_{max}}{T} = 5.8789 \times 10^{10}\mathrm{Hz\,K} \tag{1.105}$$

So the frequency of the peak of B_ν shifts linearly with temperature and this peak determined the full spectral energy distribution of the object.

Wiens displacement law is more known in solving for the peak of B_λ which gives:

$$\lambda_{max}\,T = 2897.8\,\mu\mathrm{m\,K} \tag{1.106}$$

Note that the B_λ and B_ν are fundamentally different: for a given T will the peak of the distribution of B_ν fall on a different wavelength as the peak of the distribution of B_λ. For the Sun (T_{eff} = 5777 K) the peak of B_ν falls at 883 nm, while the peak of B_λ is at 502 nm

1.6 .4 Rayleigh-Jeans tail of BB radiation

When the frequency is small compared to the frequency of the peak of the distribution ($h\,\nu \ll kT$) we can stop the exponential expansion at the linear term:

$$\exp\left(\frac{h\nu}{kT}\right) = 1 + \frac{h\nu}{kT} + ... \tag{1.107}$$

The Rayleigh-Jeans tail of the distribution gives a quadratic slope of the distribution in frequency units, to the 4rth power in wavelength units :

$$B_\nu(T) = \frac{2\,\nu^2}{c^2}\,k\,T \tag{1.108}$$

$$B_\lambda(T) = \frac{2\,c\,k\,T}{\lambda^4} \tag{1.109}$$

At radio wavelengths, this is in almost all cases a valid approximation. In log-log (intensity versus frequency) plots, the Rayleigh-Jeans tail shows up as a straight line.

1.6 .4.1 Brightness Temperature

The brightness temperature is a concept which is used mainly in radio astronomy and it is the temperature of a hypothetical object which fills the beam completely, radiates as a black-body and gives the same intensity as the measured object:

$$I_\nu = B_\nu(T_b) \tag{1.110}$$

In radio astronomy (small frequencies) the Rayleigh-Jeans approximation can be used and we get:

$$I_\nu = \frac{2\,\nu^2}{c^2}\,k\,T_b \tag{1.111}$$

$$T_b = \frac{c^2}{2\,\nu^2\,k}\,I_\nu \tag{1.112}$$

and instead of the intensity units, we can express the radio intensity just by the Temperature. Even the radiative transfer equation (see eq 1.113) can now be expressed in function of the temperature:

$$\frac{dT_b}{d\tau_\nu} = -T_b + T \quad (h\,\nu \ll kT) \tag{1.113}$$

And for a slab of constant temperature (see eq. 1.64), the expression becomes:

$$T_b = T_b(0)\, e^{-\tau_\nu(D)} + T\ (1 - e^{-\tau_\nu(D)}) \quad (h\,\nu \ll kT) \tag{1.114}$$

So at large optical depths, we directly observe on radio frequencies, the temperature of the object. Note that the brightness temperature is dependent on the frequency being observed (!) and only if indeed the object does emit like a blackbody, the brightness temperature will be the same over all frequencies.

1.6 .5 Wienn approximation: high frequencies

When h$\nu \gg$ k,T, we that the exponential is much larger than 1:

$$I_\nu \sim \frac{2h\nu^3}{c^2}\, e^{-h\nu/kT} \tag{1.115}$$

In this regime, the Intensity drops fast with increasing frequency. (ν^3 increases more slowly than the exponential). In a log-log plot of frequency versus I(ν,T), the high energy slope is very steep.

In next chapters of this course we will focus more on spectral lines and how we can use spectral lines to decipher astrophysical properties of the emitting objects.

1.7 Problems

1. An active research domain in modern astrophysics is the structure and evolution of the first generation of stars. The only elements available to produce them, were the yields of the Big-Bang nucleosynthesis. In a first approximation this was only H, He and Li (Be, B had even lower abundances). Although the exact Big-Bang production of Li is still very much in debate, you can assume it is about 1.6×10^{-10} of the total number of atoms. The fraction of He produces was about 0.075 of the total number of nuclei. Can you compute the Z-value (“the metallicity”) of the first generation of stars ? These are the so called Population III stars.

2. Assume that the sun radiates without limb-darkening and with specific intensity I_0. What is the intensity, mean intensity and flux measured on Earth and on Neptune which rotates at about 30 A.U.

3. The solar constant is the amount of energy we receive on top of the earth atmosphere per area perpendicular to the line-of-sight and per second. The solar constant is 1366.1 $Watt\, m^{-2}$. Determine the effective temperature of the sun.

4. A pinhole camera is a square box with a dimension $L \times L \times L$. In one of the sides there is a circular aperture with diameter d. Assume $L \gg d$. Can you find the expression of the flux which is measured on the other side in function of the incoming intensity $I_\nu(\theta, \phi)$? The camera layout is given in the Fig. 1.19

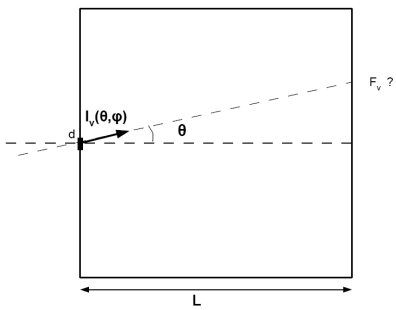

Figure 1.19: Illustration of the geometry of a pin-hole camera. *Fig. from Rybicki & Lightmann (1979)*

5. A spherically symmetric cloud of gas as an emissivity of P_ν which is the emission per second per volume per frequency band ($Watt\, m^{-3}\, Hz^{-1}$). The cloud is optically thin, has a radius R, a temperature T and distance d from the observer. Compute:

   - What is the measured intensity following a ray parallel to the line of sight and with a projected distance d from the central point.
   - Can you compute the effective temperature of the cloud ?
   - What is the flux of this cloud measured by the observer ?
   - Can you solve all the questions above but for an optically thick cloud ?

6. Assume that the extinction coefficient at two different frequencies ν_1 and ν_2 is a factor of 10 different, but that the source function at those frequency bands is the same. Compute the surface intensities at those two frequencies when

   - we have an optically thin layer without incident radiation
   - we have an optically thick layer with a source function $S_\nu(\tau_\nu) = S_\nu(0) + \tau_\nu$.

7. Why is it dark at night ? The most impressive images of the sky ever taken are without doubt the Hubble Space Telescope deep-field sequence (see Fig. 1.20). The HST was pointed for not less than 400 orbits on a small piece of the sky, accumulating as such 800 exposures with a total integration time of about 1 million seconds. The faintest objects on the image are about magnitude 30. The total field covered is about the same as what you cover with a grain of barley on an armlength distance. The image uncovered also galaxies that existed 800 million years after the big bang (at a redshift of 7). The photons from the faintest sources in this image arrived at a rate of about 1 photon per minute... On the whole image there are about 10000 galaxies but the image itself is mostly dark. Can you explain this ? A good site to find other HST results is here.

8. Assume an optically thin cloud of gas close to a star with luminosity L. Prove that the cloud will be blown away by radiation pressure when the mass-luminosity ratio of the star is below:

$$\frac{\kappa}{4\,\pi\,G\,c} \tag{1.116}$$

   With G the Gravity constant, κ the mass absorption coefficient and c the velocity of light.

   Assume then that the cloud only contains Hydrogen and we only take the scattering on free electrons as opacity source (see later in the course). The cross-section is $\sigma_T = 6.65 \times 10^{-25}\,cm^2$. Give an expression for the maximal luminosity a star of mass M can have so that it will not blow away the Hydrogen atmosphere by radiation pressure. This luminosity is called the Eddington luminosity.

9. Give the expression of the mean intensity and the flux on the surface of a star assuming the Eddington-Barbier relation holds.

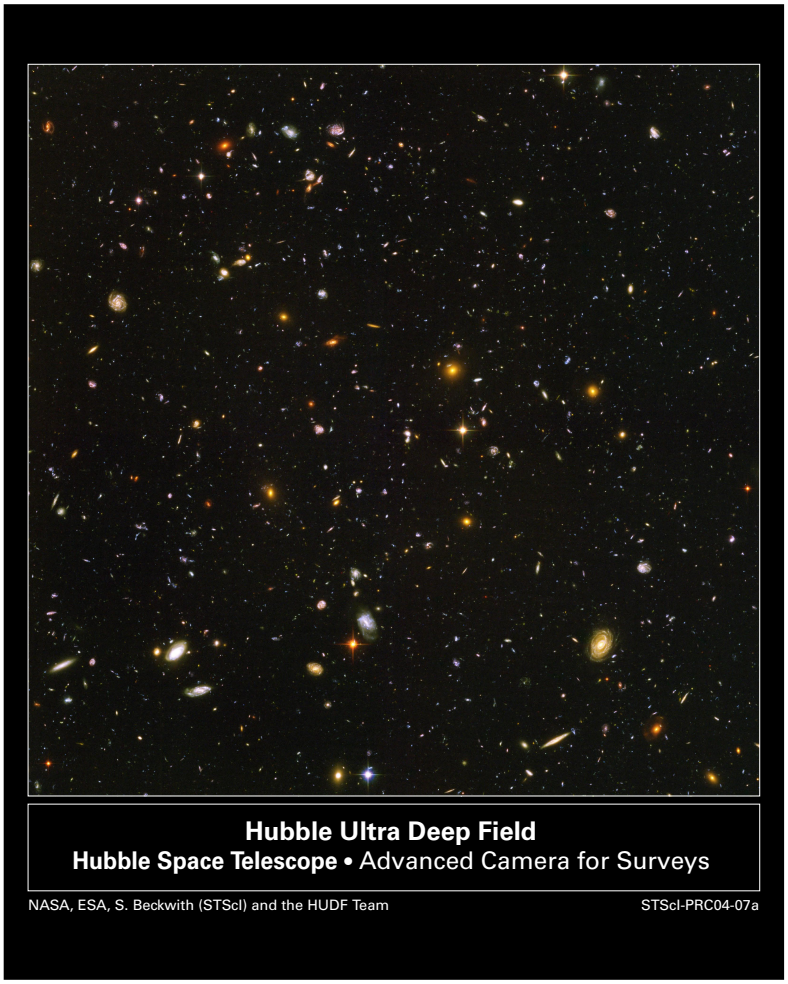

Figure 1.20: The Hubble ultra deep field press release image.

Chapter 2

Fundamental concepts to describe radiative processes

2.1 Introduction

In Fig. 2.1 two spectral regions are shown of a star which can be seen as a solar analog (the spectral class is G2 V). One plot samples the Fraunhofer Ca II lines, which are resonance lines of the Ca II isotope, and the other the Hydrogen H_α line. The latter is a transition from the 1st excited state of H, towards the second excited state.

We can see that the Ca lines are much stronger than the H line, despite the fact that in the sun, the abundance of Ca is A(Ca) = 6.31, so there are about half a million H-atom for every Ca atom. In order to understand this, and hence to understand the basis of the Spectral classification, we will introduce in this chapter a few concepts which will allow us to quantify the microscopic state of the material.

An absorption line in a spectrum appears when radiation of a given specific wavelength disappears from the beam and this in contrast to the radiation of slightly different wavelength (see e.g. Fig 2.1). We can associate specific bound-bound transitions (electron transitions from one bound state to another) of an atom or ion with the observed central wavelength of the spectral lines. Luckily, in most cases, the association is unique although when different transitions appear close to each other, blends of the spectral line profile will appear.

Electrons around atoms (ions) occupy discrete energy states. The energy of a given state is a solution of the time independent Schrödinger equation which can be written as:

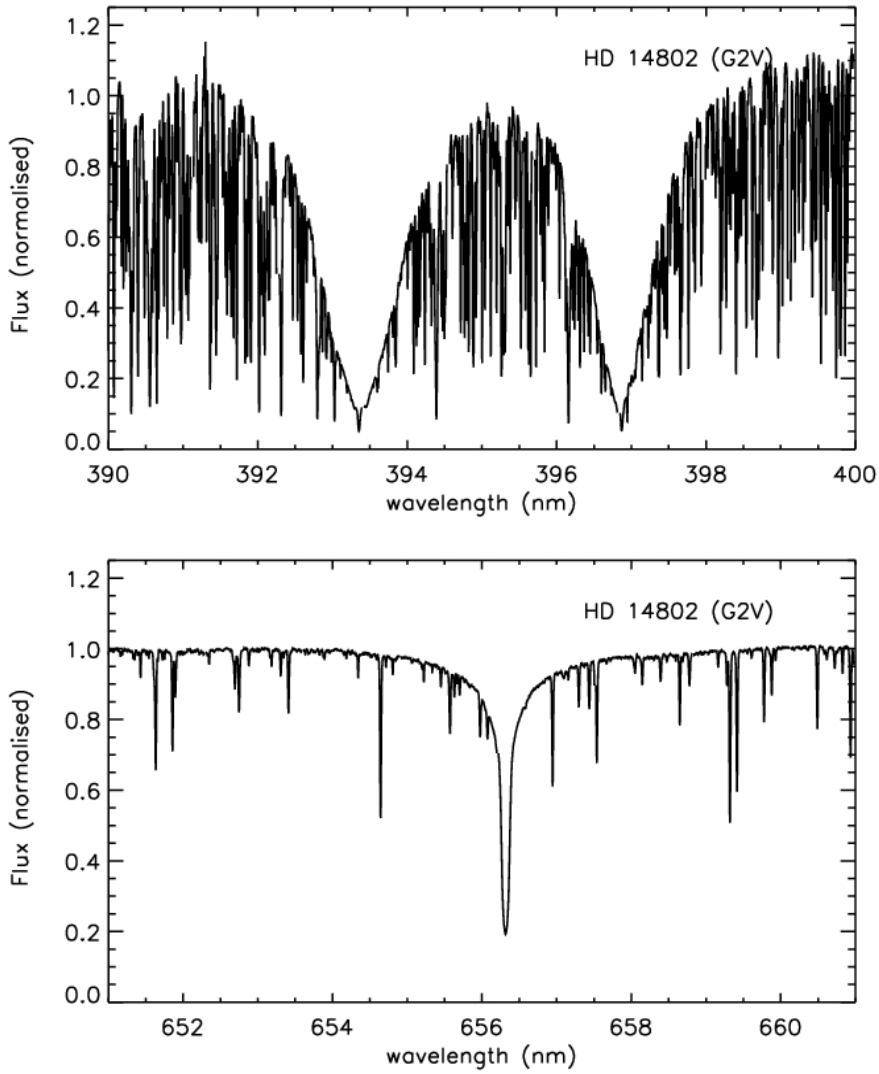

Figure 2.1: Normalised spectra of a G2 V star. The upper panel shows the strong Ca II doubled known as the Fraunhofer H and K lines. The lower panel shows the Hydrogen Balmer H_α line.

$$\mathbf{H}\psi = \mathbf{E}\psi \tag{2.1}$$

With ψ the wave function, $\mathbf{H}$ the Hamiltonian and $\mathbf{E}$ the energy related to the state. In the case of electrons with a nuclear charge of Ze, and neglecting spin, relativistic effects and nuclear effects, the Hamiltonian covers the kinetic energy,

the Coulomb interaction between the nucleus and the electrons as well as between the electrons themselves.

$$\mathbf{H} = -\frac{\hbar^2}{2\,m} \sum_j \nabla_j^2 \; - \; Z\,e^2 \sum_j \frac{1}{r_j} + \sum_{i>j} \frac{e^2}{r_{ij}} \tag{2.2}$$

Solutions of these wave equations are only possible for discrete energy levels $E(n, l, m, s)$ and for the characterisation of these energies, the quantum number n,l,m are used. n is the principle quantum number, l the angular momentum quantum number, m the magnetic quantum number and s the spin. In most atoms, the energy related to a given level without external influence is dependent only on n and l.

When we concentrate on a given l-level ('lower') and u-level ('upper'), the energy difference relates to the frequency and wavelength of the spectral line as:

$$\Delta(E) \; = \; E_{lu} = h\,\nu_{lu} = h\,\frac{c}{\lambda_{lu}} \tag{2.3}$$

In the physical processes responsible for the electron transition (see Fig. 2.2), we differentiate between radiative excitation ($l \;\rightarrow\; u$) and spontaneous de-excitation (emission) ($u \;\rightarrow\; l$) ; collisional excitation and collisional de-excitation. Moreover, a process of stimulated emission can also be important. In this process a photon of very similar characteristics as ν_{lu}, will stimulate the de-excitation process. This process of stimulated emission is of course dependent on the strength of the radiation field which is inducing the transition.

The strength of a spectral line in a given star is obviously also dependent of the relative number of atoms in the correct excited state from which the electron transition takes place.

Solving all the state equations for all these processes is by no means straightforward since it requires a detailed knowledge of all processes by which any level becomes populated or de-populated.

A significant reduction in the complexity appears when we can assume that the material is in complete thermal equilibrium (TE). Every microscopic process is in balance with its reverse process. For every frequency there is detailed balance. In such condition, the material state will be in thermal equilibrium which means that the relative populations are completely determined by the thermodynamic quantities: the temperature and the pressure. Note that in thermal equilibrium, the net flux will be zero since there is no transport of energy.

To gain insight in the spectral classification of stars, we will assume that the relative population of the various atomic levels in the photospheres of stars, can be

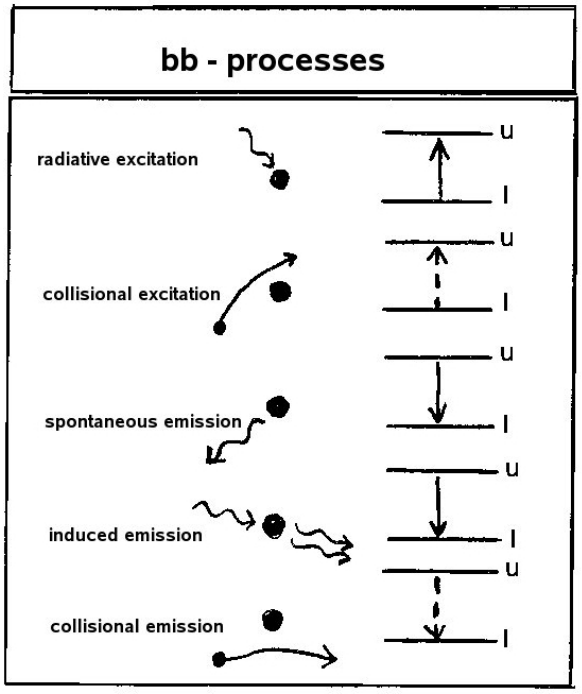

Figure 2.2: Electron transitions inbetween two bound electron states. *Fig. from Rutten (2000)*

well described by the laws of thermal equilibrium, which we apply locally. The relative number of atoms in a given ionisation and excitation state is then only dependent on the local temperature and pressure.

2.2 Excitation law of Bolzmann

In TE, the distribution of the electrons over all the excited states is described by the excitation law of Bolzmann (1844-1906). Many consider Ludwig Bolzmann the founder of statistical mechanics. The law states that the number density of a given atom or ion in an excited state s compared to the number density of the same atom or ion in an excited state t is only dependent on the temperature and obeys:

$$\left[\frac{n_{r,s}}{n_{r,t}}\right]^{\mathrm{TE}} = \frac{g_{r,s}}{g_{r,t}} \mathrm{e}^{-(\chi_{r,s}-\chi_{r,t})/kT} \tag{2.4}$$

The symbols are:

$n_{r,s}$	=	number density in excitation level s of ionisation level r;
$g_{r,s}$	=	statistical weight (degeneracy) of level s of ionisation state r; In L-S couplings, the g-factors are (2J+1) with J the total angular momentum quantum number;
$\chi_{r,s}$	=	the excitation energy of level s of the ionisation state r as measured from the ground state (r,0). So $\chi_{r,s} \equiv E_{r,s} - E_{r,0}$ and $\chi_{r,s} - \chi_{r,t} = h\nu$ for a transition between state (r,s) and (r,t), with the s-state having a higher internal energy than level t.

Another form of the same equation relates the number density of atoms/ions of a given excited state to the total number density of that atom/ion.

$$\left[\frac{n_{r,s}}{N_r}\right]^{\mathrm{TE}} = \frac{g_{r,s}}{U_r}\mathrm{e}^{-\chi_{r,s}/kT}\,, \tag{2.5}$$

with $N_r = \sum_s n_{r,s}$ the number density of all atoms in ionisation state r. The sum runs over all possible excitation states of ionisation state r. The U_r term is the *partition function* of ionisation state r which is given by

$$U_r \equiv \sum_s g_{r,s}\mathrm{e}^{-\chi_{r,s}/kT}\,. \tag{2.6}$$

The partition function is the weighted sum of the number of ways the atom (ion) can arrange its electrons with the same energy. The more energetic configurations receive in the total sum less weight by the Boltzmann factor in the exponential.

The distribution over the excited states is only temperature sensitive.

2.3 Ionisation law of Saha

In TE the distribution over different ionisation stages is given by the Saha (1893-1956) equation, named after the Indian astrophysicist Maghnad Saha. The ratio of the number density between atoms in the ground state of two successive ionisation stages is given by:

$$\left[\frac{n_{r+1,0}}{n_{r,0}}\right]^{\mathrm{TE}} = \frac{1}{N_e}\frac{2g_{r+1,0}}{g_{r,0}}\left(\frac{2\pi m_e kT}{h^2}\right)^{3/2}\mathrm{e}^{-\chi_r/kT}\,, \tag{2.7}$$

with the following symbols:

N_e	=	the electron number density
m_e	=	the electron mass
$n_{r+1,0}$, $n_{r,0}$	=	the population (number per unit volume) in the ground state of two successive ionisation stages of a given atom
$g_{r+1,0}$, $g_{r,0}$	=	the statistical weight of both levels
χ_r	=	the ionisation energy of the ionisation state r
	=	this is the minimal energy needed to ionise the state r to reach the r+1 ionisation level
k	=	the Boltzmann constant

The factor 2 just before $g_{r+1,0}$ is the statistical weight of a free electron (the double spin orientation possibilities). When we transform the equation by not considering the ground excitation stage only, but the number density of the ion itself we get:

$$\left[\frac{N_{r+1}}{N_r}\right]^{\mathrm{TE}} = \frac{1}{N_e}\frac{2U_{r+1}}{U_r}\left(\frac{2\pi m_e kT}{h^2}\right)^{3/2} \mathrm{e}^{-\chi_r/kT} \tag{2.8}$$

or

$$\left[\frac{N_{r+1}}{N_r}\right]^{\mathrm{TE}} = \frac{1}{P_e}\frac{2U_{r+1}}{U_r}\left(\frac{2\pi m_e}{h^2}\right)^{3/2} (kT)^{5/2}\mathrm{e}^{-\chi_r/kT} \tag{2.9}$$

In the last equation, the electron pressure $P_e = N_e kT$ is included. In the literature the equation is written often in the form:

$$\left[\frac{N_{r+1}}{N_r}\right]^{\mathrm{TE}} = \frac{\Phi(T)}{P_e} \tag{2.10}$$

in which

$$\Phi(T) = 0.665\frac{U_{r+1}}{U_r}T^{5/2}10^{-5040\chi/kT}\,. \tag{2.11}$$

In the ionisation equation, it is both the temperature and the pressure which are important. At higher pressure and with the same temperature, it will be more difficult to liberate electrons from the atoms.

In Fig. 2.3, the ionisation fraction of a more complex atom is shown : Fe has a very rich spectrum and millions of transitions in the optical and UV.

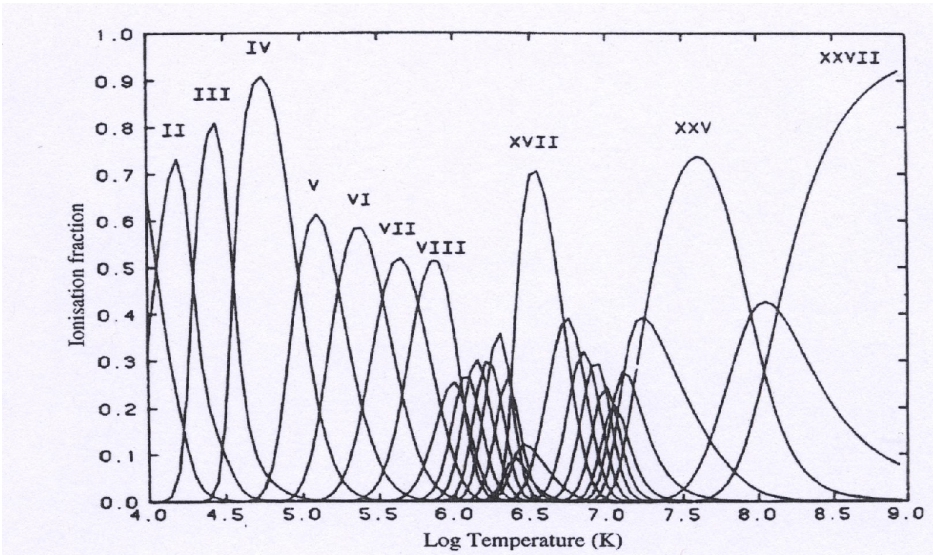

Figure 2.3: The ionisation fraction of Fe in function of the temperature. The density is kept constant.

2.4 Bound-bound transitions of the hydrogen atom

Since H is so abundant in space it is no surprise that H-lines are visible in almost all stellar spectra. The Schrödinger equation can be solved analytically and the energy levels of the single electron obey a simple rule which is only dependent on the principle quantum number n. In the Bohr model approach of the H atom this gives:

$$E_n = -\Re/n^2\,, \tag{2.12}$$

with

$$\Re = (2\pi^2\mu_H e^4/h^2) \tag{2.13}$$

the Rydberg constant named after the Swedish spectroscopist Johannes Rydberg (1854-1919). μ is the formula is the reduced mass of H which is

$$\frac{1}{\mu_H} = \frac{1}{m_p} + \frac{1}{m_e} \tag{2.14}$$

The Rydberg constant is nothing else than the ionisation potential of H which is 13.6 eV. The first excitation stage higher than the ground state is at $E =$

$-3.4eV$. The first excited state of H is already rather high in energy and relatively close to the ionisation border. It is from this level that the Balmer lines are generated. The Balmer lines are named after the Swiss teacher who discovered the phenomenological formula relating the different Balmer lines. The successive balmer lines are formed with ever increasing energy (shorter wavelength) which are related to electron transitions from the Balmer lines to ever increasing quantum number. The wavelengths are easily computed. For the Balmer α line this is:

$$\frac{h\,c}{\lambda} = \frac{-13.6\,\mathrm{eV}}{n_u^2} + \frac{13.6\,\mathrm{eV}}{n_l^2} \tag{2.15}$$

$$\frac{12398.4..\,\mathrm{eV\,\AA}}{\lambda} = -13.6\,\mathrm{eV}\left(\frac{1}{3^2} - \frac{1}{2^2}\right) \tag{2.16}$$

This gives 6563.9 Å . The Hydrogen bound-bound spectrum is given in Fig. 2.4. The different levels are called Lyman (n=1), Balmer (n=2), Paschen (n=3), Brackett (n=4), Pfund (n=5) and Humphreys (n=6) series. The Balmer-jump is related to the energy level of the n=2 level and at higher frequencies (shorter wavelengths) the photons are energetic enough to ionise the Balmer electron. Lower energy photons are not able to ionise. This jump is in many stars visible as a strong jump in the absorption coefficient.

$$\lambda\ (\mathrm{\AA}\,) \approx \frac{12400}{\mathrm{E}\ (\mathrm{eV})} \tag{2.17}$$

2.4 .1 The strength of the Ca II lines versus the Balmer lines in the sun

We can now investigate why, in the sun, the lines of a trace element like Ca, can be stronger than lines from the bulk element H.

The fraction of H-atoms in the first excited state compared to all the H atoms available can be computed assuming that the neutral H-atoms will be either in the ground state, or in the first excited state. This can be done because the first excited state is at 10.2 eV above the ground level, and for the temperature being considered, 10.2 eV $\gg$ than $k\,T$ which makes the Boltzmann factor $exp(-10.2/kT) \ll 1$. For the effective temperature of the sun, (5777 K), the Bolzmann factor is $1.2\,10^{-9}$. This also means that a good estimate for the partition function of H at temperatures of the sun, limits the total sum to the first term.

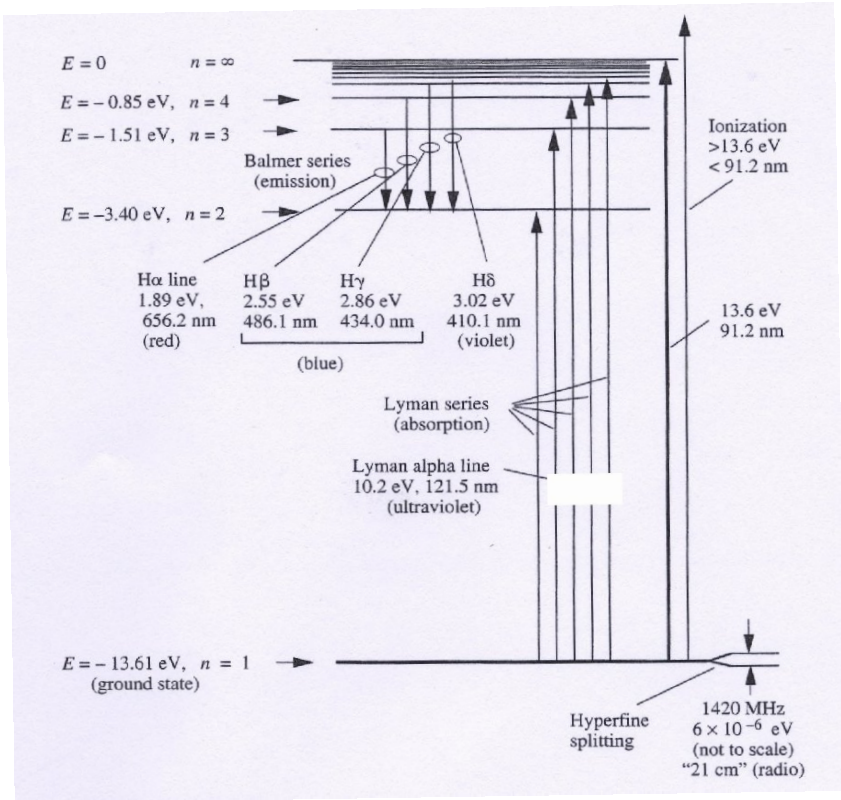

Figure 2.4: Bound-bound transition for hydrogen. *Fig. from Bradt (2005)*

$$\frac{N_{I,2}}{N_{total}} = \left(\frac{N_{I,2}}{N_{I,1}+N_{I,2}}\right)\left(\frac{N_I}{N_{total}}\right) = \left(\frac{N_{I,2}/N_{I,1}}{1+N_{I,2}/N_{I,1}}\right)\left(\frac{1}{1+N_{II}/N_I}\right) \tag{2.18}$$

We can use now the Saha and Boltzmann equations for the appropriate ratios. In the sun, the electron pressure is about $15\,dyne\,cm^{-2}$ which is in SI units $1.5\,Pa\ = 1.5\ N\,m^{-2}\ = 1.5\ kg\,s^{-2}\,m^{-1}$. The Joule is equal to $1N\,m$ which is $1kg\,m^2\,s^{-2}$

$$\left[\frac{N_{II}}{N_I}\right] = \frac{1}{P_e}\frac{2U_{r+1}}{U_r}\left(\frac{2\pi\, m_e}{h^2}\right)^{3/2}(kT)^{5/2}\,\mathrm{e}^{-\chi_r/kT} \tag{2.19}$$

$$= \frac{1}{1.5\,(kg\,s^{-2}\,m^{-1})}\,\frac{2}{2} \tag{2.20}$$

$$\times \left(\frac{2\,\pi\,9.11\,\times\,10^{-31}\,kg}{(6.6262\,\times\,10^{-34}\,kg\,m^2\,s^{-2}\,s)^2}\right)^{3/2} \tag{2.21}$$

$$\times\ (1.3807\,\times\,10^{-23}\,kg\,m^2\,s^{-2}\,K^{-1}\ 5777\,K)^{5/2} \tag{2.22}$$

$$\times\ \mathrm{e}^{-13.6(eV)/(8.6174\times10^{-5}\ eV\,K^{-1}\ \ 5777\,K)} \tag{2.23}$$

$$= 7.7\,\times\,10^{-5}\ \approx\ 1/13000 \tag{2.24}$$

Which means that there is only 1 ionised H for every 13000 neutral atoms.

The Boltzmann equation gives now how many neutral atoms there are in the first excited state. For H states, the statistical weight is $2\,n^2$

$$[N_{I,2}/N_{I,1}] = \frac{2\,2^2}{2\,1^2}\ e^{-(10.2\,eV)/(8.62\times10^{-5}\,eV\,K^{-1}\,5777\,K)} \tag{2.25}$$

$$\approx\ 4.96\,\times\,10^{-9}\ \approx\ \frac{1}{202\,000\,000} \tag{2.26}$$

So the first excited state of H is barely populated in the atmospheric conditions of the sun. Filling the appropriate terms into equation 2.18 we get:

$$\frac{N_{I,2}}{N_{total}}\ \approx\ 4.96\,\times\,10^{-9} \tag{2.27}$$

We can now compute the same for Ca. The ionisation potentials of lower ionisation stages of atoms can be found e.g. here. For Ca more specifically we find that the ionisation potential is 6.11 eV for Ca I. This is about half the ionisation energy of H. The partition functions are more difficult to compute and often polynomial approximations are used to compute them in environments similar to photospheres of stars. In `Aller, ``astrophysical quantities''` and in `Gray, ``Observations and analysis of stellar Photospheres'', appendix D` those polynomial coefficients are given. U(CaI) = 1.32 and for U(CaII) = 2.30. We can now fill in the appropriate numbers

$$\left[\frac{N_{II}}{N_I}\right]_{Ca} \approx 903 \tag{2.28}$$

The H and K lines of CaII are resonance lines which means their lower level is the ground state. The first excited state where the electron in the ground state can excite to is given in here and is at 25191.51 cm^{-1} which is

$$E\ (eV) = 1.240\,10^{-4}\,E\,(cm^{-1}) \tag{2.29}$$

at 3.12 eV. The degeneracies of the levels are g_1 = 2 and g_2 = 4. The ratio of the number of atoms in the excited versus ground state are then:

$$\left[\frac{N_{II,1}}{N_{II,0}}\right] \approx \frac{1}{264} \tag{2.30}$$

To compute now the fraction of the atoms in the ground state of the first ionisation stage of Ca, to the total Ca atoms we get:

$$\begin{aligned}
\left[\frac{N_{II,0}}{N_{total}}\right] &\approx \left[\frac{N_{II,0}}{(N_{II,0}+N_{II,1})}\right]\left[\frac{N_{II}}{N_{total}}\right] && (2.31)\\
&= \left(\frac{1}{1+[N_{II,1}/N_{II,0}]}\right)\left(\frac{[N_{II}/N_I]}{1+[N_{II}/N_I]}\right) && (2.32)\\
&= \left(\frac{1}{1\ +\ 1/264}\right)\left(\frac{903}{1+903}\right) && (2.33)\\
&= 0.995 && (2.34)
\end{aligned}$$

So in the solar photosphere almost all Ca atoms are in the first ionised ground state...

Although Ca is a trace element in absolute abundance, the fact that a fraction of 0.995 will be in the correct level to produce the Ca K line makes that there are about 400 times more CaII atoms in the ground state, than that there are neutral H atoms in the first excitation state...

2.5 Evaluation: the spectral classification of stars

The exponential forms in the population predictions in TE make that the ionisation/excitation fractions of any given element are very temperature sensitive. This is illustrated in Fig 2.5 and Fig 2.6.

In Fig. 2.5, the steep rise of the ionisation fraction of H is shown in function of the temperature of the gas. This behaviour is valid for all atoms/ions. Within

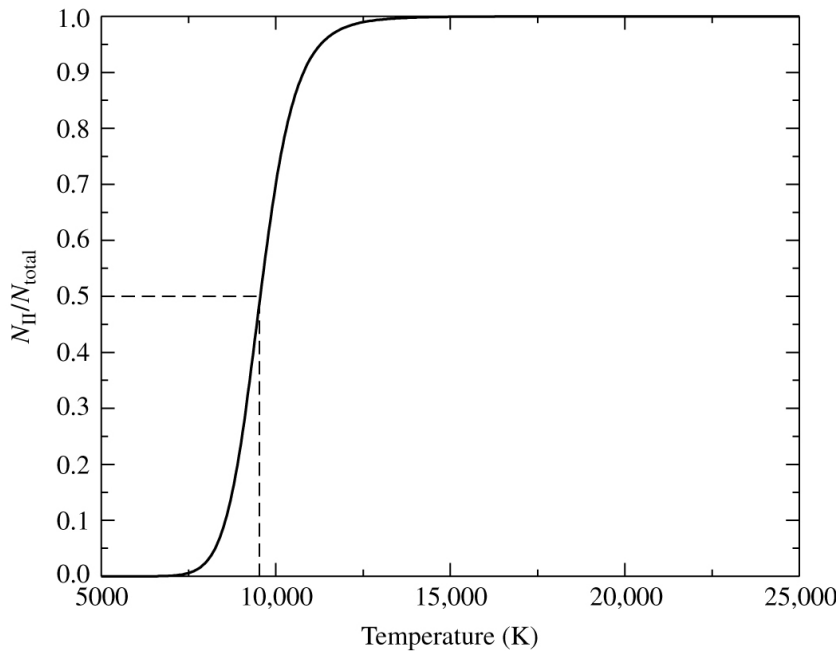

Figure 2.5: The exponential in the ionisation law of Saha, makes that the ionisation fraction (here the one of H is shown) is a steep function of temperature. *Fig. taken from Carroll & Ostlie (1996)* .

an stellar atmosphere we can conclude that the temperature range in which ions of a different ionisation stages can be present is very limited.

In Fig. 2.6 we show the combined effect of excitation and ionisation of H in function of the temperature. Since the first excited state of H is close to the ionisation border, H-ionisation will set it as soon as the n=2 level will get populated in significant numbers. The combined effect is therefore that the fraction of neutral H-atoms in the first excited state to the total H-atoms available, does reach a maximum near 10000K. This is the reason why the Balmer lines as well as the Balmer jump is maximal in strength for stars of spectral type A.

Of course, stars do not exist of H alone and all atoms/ions for which bound-bound transitions exist can produce lines. Although the strength of a given spectral line, is by no means only dependent on the fraction of atoms/ions in the correct excitation/ionisation state as computed in TE for the relevant temperatures and pressures, the evaluation of the Saha and Boltzmann equations do give a good quantified description of the spectral classification of stars.

In Fig 2.7, the estimated line strength of different ions is given in function of the temperature and the associated stellar spectral types. Note that there is no

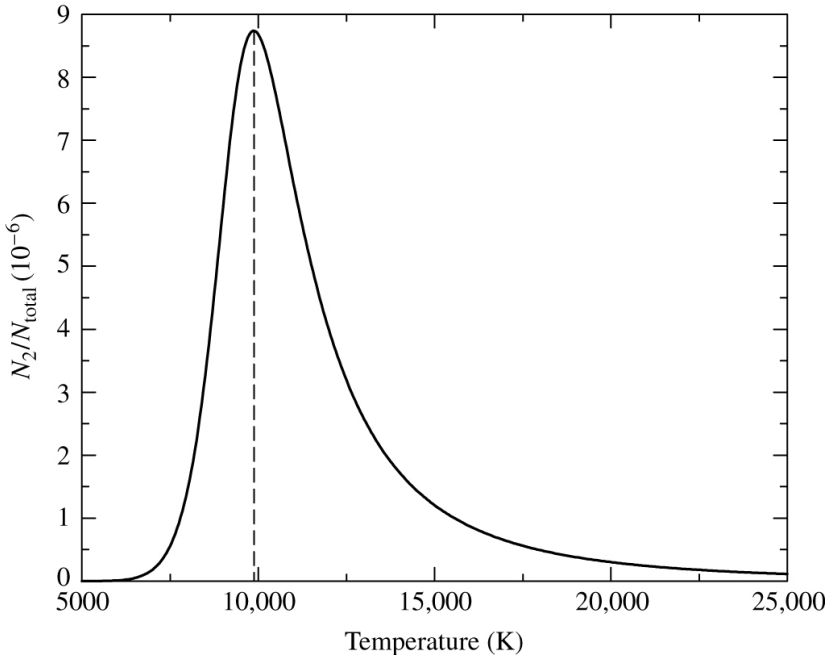

Figure 2.6: The fraction of H atoms with electrons in the Balmer level to the total number of H particles. *Fig. taken from Carroll & Ostlie (1996)* .

temperature given at which lines will appear coming from three different ionisation stages. In stellar atmospheres, the partial ionisation layers of H and He play an important role in the driving mechanisms of stellar pulsations (see e.g. course on asteroseismology). Because the high excitation and ionisation energy (see Fig. 2.8) of He, it is only in the hottest objects that He lines will be visible.

The spectral classification system, was pioneered by the Jesuit Italian priest Secchi (1818-1878). The spectral classification system was further refined in Harvard and published in the Hendry Draper catalogue (Draper was a former Harvard astronomer whose widow sponsored the classification work). It was at the time still a one dimensional classification and mainly based on the hydrogen line strength. The detectors at the time were photographic plates : glass plates with blue sensitive emulsion. The spectral classification is therefore historically based in the blue sensitive domain. The basic tremendous work at the Harvard institute (headed by Edward C. Pickering) was mostly done by female assistants (some eighty were hired in total to help with the classification work). Some of them became famous astronomers themselves like Annie Jump Cannon, Henrietta Swan Leavitt and Antonia Maury. The Harvard astronomer Cecilia Helena Payne (later to become Cecilia Payne-Gaposchkin) demonstrated that the OBAFGKM spectral

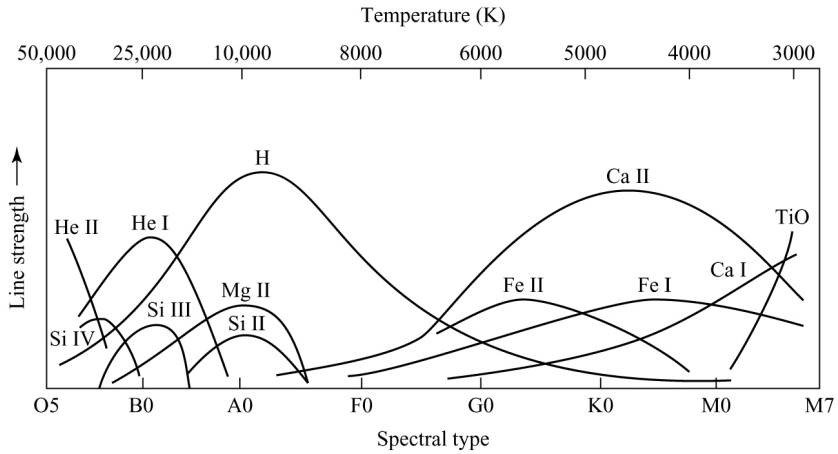

Figure 2.7: The relative strengths of lines coming from a given ion in function of the effective temperature of the central star. *Fig. taken from Carroll & Ostlie (1996)* .

sequence is actually a sequence in temperature. Spectral classes are further subdivided by a number. For example, F0 denotes the hottest stars in the F class and A9 denotes the coolest ones.

The temperature of the vast number of stars could be traced by studying the colours (for a more detailed discussion: see the course on Observational Techniques in Astronomy). A widely used system of broad-band filters and associated colours is the Johnson UBVRI system where the observed radiation of a given object is quantified after the telescope beam passing through a filter with a specific bandpass. The spectral classification pioneers, studied the relation between the broad-band colours and the spectral appearance (see Fig. 2.9)

The second dimension of the classification was added in Yerkes and is known as the MKK classification (named after William Wilson Morgan, Phillip C. Keenan and Edith Kellmann) or the later revisions made it known as the MK-classification. The second parameter was based on the characteristics of lines sensitive to gravity (local pressure). A giant and dwarf can have roughly the same mass and temperature, but the local gravity (and thus luminosity) may be very different.

The ionisation law of Saha assumes equilibrium and is valid when the ionisation and recombination are mainly determined by collisions. At lower densities, the photon induced ionisation may become important while recombination obviously is a collisional process. At lower densities, it is easier to ionise.

Another important effect is pressure broadening of the energy states. (see later in the course). This is especially effective for H and you can see this on the UVES

IONIZATION POTENTIALS[a]

Z	Element	Spectrum I	II	III	IV	V	VI	VII	VIII	IX	X	XI	XII	XIII	XIV	XV	XVI	XVII	XVIII	XIX	XX	XXI
1	H	13.598																				
2	He	24.587	54.416																			
3	Li	5.392	75.638	122.451																		
4	Be	9.322	18.211	153.893	217.713																	
5	B	8.298	25.154	37.930	259.368	340.217																
6	C	11.260	24.383	47.887	64.492	392.077	489.981															
7	N	14.534	29.601	47.448	77.472	97.888	552.057	667.029														
8	O	13.618	35.116	54.934	77.412	113.896	138.116	739.315	871.387													
9	F	17.422	34.970	62.707	87.138	114.240	157.161	185.182	953.886	1103.089												
10	Ne	21.564	40.962	63.45	97.11	126.21	157.93	207.27	239.09	1195.797	1362.164											
11	Na	5.139	47.286	71.64	98.91	138.39	172.15	208.47	264.18	299.87	1465.091	1648.659										
12	Mg	7.646	15.035	80.143	109.24	141.26	186.50	224.94	265.90	327.95	367.53	1761.802	1962.613									
13	Al	5.986	18.828	28.447	119.99	153.71	190.47	241.43	284.59	330.21	398.57	442.07	2085.983	2304.080								
14	Si	8.151	16.345	33.492	45.141	166.77	205.05	246.52	303.17	351.10	401.43	476.06	523.50	2437.676	2673.108							
15	P	10.486	19.725	30.18	51.37	65.023	230.43	263.22	309.41	371.73	424.50	479.57	560.41	611.85	2816.943	3069.762						
16	S	10.360	23.33	34.83	47.30	72.68	88.049	280.93	328.23	379.10	447.09	504.78	564.65	651.63	707.14	3223.836	3494.099					
17	Cl	12.967	23.81	39.61	53.46	67.8	98.03	114.193	348.28	400.05	455.62	529.26	591.97	656.69	749.74	809.39	3658.425	3946.193				
18	Ar	15.759	27.629	40.74	59.81	75.02	91.007	124.319	143.456	422.44	478.68	538.95	618.24	686.09	755.73	854.75	918	4120.778	4426.114			
19	K	4.341	31.625	45.72	60.91	82.66	100.0	117.56	154.86	175.814	503.44	564.13	629.09	714.02	787.13	861.77	968	1034	4610.955	4933.931		
20	Ca	6.113	11.871	50.908	67.10	84.41	108.78	127.7	147.24	188.54	211.270	591.25	656.39	726.03	816.61	895.12	974	1087	1157	5129.045	5469.738	
21	Sc	6.54	12.80	24.76	73.47	91.66	111.1	138.0	158.7	180.02	225.32	249.832	685.89	755.47	829.79	926.00						
22	Ti	6.82	13.58	27.491	43.266	99.22	119.36	140.8	168.5	193.2	215.91	265.23	291.497	787.33	861.33	940.36						
23	V	6.74	14.65	29.310	46.707	65.23	128.12	150.17	173.7	205.8	230.5	255.04	308.25	336.267	895.58	974.02						
24	Cr	6.766	16.50	30.96	49.1	69.3	90.56	161.1	184.7	209.3	244.4	270.8	298.0	355	384.30	1010.64						
25	Mn	7.435	15.640	33.667	51.2	72.4	95	119.27	196.46	221.8	248.3	286.0	314.4	343.6	404	435.3	1136.2					
26	Fe	7.870	16.18	30.651	54.8	75.0	99	125	151.06	235.04	262.1	290.4	330.8	361.0	392.2	457	489.5	1266.1				
27	Co	7.86	17.06	33.50	51.3	79.5	102	129	157	186.13	276	305	336	379	411	444	512	546.8	1403.0			
28	Ni	7.635	18.168	35.17	54.9	75.5	108	133	162	193	224.5	321.2	352	384	430	464	499	571	607.2	1547		
29	Cu	7.726	20.292	36.83	55.2	79.9	103	139	166	199	232	266	368.8	401	435	484	520	557	633	671	1698	
30	Zn	9.394	17.964	39.722	59.4	82.6	108	134	174	203	238	274	310.8	419.7	454	490	542	579	619	698	738	1856
31	Ga	5.999	20.51	30.71	64																	
32	Ge	7.899	15.934	34.22	45.71	93.5																
33	As	9.81	18.633	28.351	50.13	62.63	127.6															
34	Se	9.752	21.19	30.820	42.944	68.3	81.70	155.4														
35	Br	11.814	21.8	36	47.3	59.7	88.6	103.0	192.8													
36	Kr	13.999	24.359	36.95	52.5	64.7	78.5	111.0	126	230.39												
37	Rb	4.177	27.28	40	52.6	71.0	84.4	99.2	136	150	277.1											
38	Sr	5.695	11.030	43.6	57	71.6	90.8	106	122.3	162	177	324.1										
39	Y	6.38	12.24	20.52	61.8	77.0	93.0	116	129	146.52	191	206	374.0									
40	Zr	6.84	13.13	22.99	34.34	81.5																
41	Nb	6.88	14.32	25.04	38.3	50.55	102.6	125														
42	Mo	7.099	16.15	27.16	46.4	61.2	68	126.8	153													
43	Te	7.28	15.26	29.54																		
44	Ru	7.37	16.76	28.47																		
45	Rh	7.46	18.08	31.06																		
46	Pd	8.34	19.43	32.93																		
47	Ag	7.576	21.49	34.83																		

Figure 2.8: The ionisation potentials (eV) of the different ions. The ionisation will determine which lines of which atom-ion will be visible in the spectrum of a star.

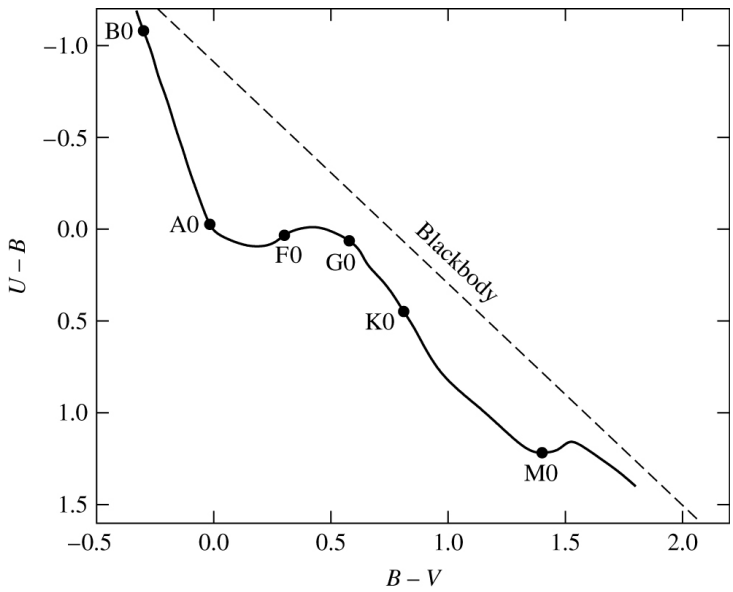

Figure 2.9: The colour-colour diagram with the Black-Body slope and the position of Main Sequence stars. *Fig. taken from Carroll & Ostlie (1996)*

spectra within a given temperature class. The effect is induced by collisions of H by charged particles and make that the energy levels are broadened. The effect on the line profiles are well visible.

Moreover, at high n, the energy levels are so close to each other in energy that any broadening effect will make that the levels overlap and the discrete levels will merge to run through to the continuum. The ionisation potential is effectively lowered. For H, the broadening by ions and electrons is the linear Stark effect which is proportional to n^2, so it is stronger for higher levels. The electron density can be estimated by use of the Inglis-Teller formula which states that the quantum number of the upper level of the last distinguishable Balmer line is related to the electron density by:

$$\log\ N_e = 29.0\ -\ 7.5\ \log(n) \tag{2.35}$$

The number of discrete Balmer lines which are visible in the spectrum, is therefore also a gravity tracer (see Fig. 2.10).

An excellent web-page showing in detail the subsequent refinements on the spectral classification is presented by Richard Gray and can be found here. The pdf version of the original MKK atlas is included as well. (here).

Table 2.1: The classification of stellar spectra was originally 1-dimensional. It turned out later that the main discrimination parameter was the Effective Temperature

SpT	Spectral appearance	colour	Temperature
O	ionized and neutral helium, weakened hydrogen	bluish	31,500-49,000 K
B	neutral helium, stronger hydrogen	blue-white	10,000-31,500 K
A	strong hydrogen, ionized metals	white	7500-10,000 K
F	weaker hydrogen, ionized metals	yellowish white	6000-7500 K
G	still weaker hydrogen, ionized and neutral metals	yellowish	5300-6000 K
K	weak hydrogen, neutral metals	orange	3800-5300 K
M	little or no hydrogen, neutral metals, molecules	reddish	2100-3800 K
L	no hydrogen, metallic hydrides, alkali metals	red-infrared	1200-2100 K

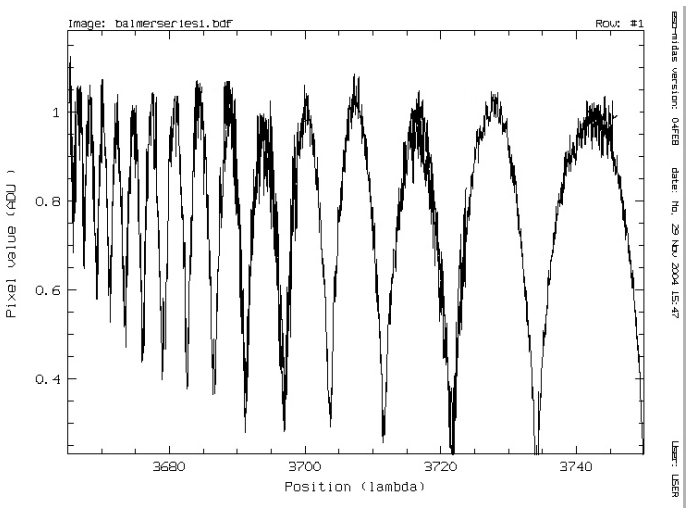

Figure 2.10: The number of discrete Balmer lines in the spectrum is a tracer of the local density. Compare the spectrum of this post-AGB star HR 4049 (supergiant of 7000K) to the spectra of similar stars in "UVESPOP"

2.6 Einstein coefficients

The Boltzmann and Saha equations assume that the level populations of atoms are only dependent on the thermodynamic quantities: the temperature and the electron pressure. Abandoning this assumption, introduces a great deal of additional complexity in which microphysics and accurate atomic data are needed as well as the need for detailed computations of the level populations.

To compute level populations, statistical equilibrium is assumed so that the net level population is not changed.

$$\frac{\mathrm{d}n_i(\vec{r})}{\mathrm{d}t} = \sum_{j\neq i}^{N} n_j(\vec{r})\, P_{ji}(\vec{r}) \; - \; n_i(\vec{r}) \sum_{j\neq i}^{N} P_{ij}(\vec{r}) = 0\,, \tag{2.36}$$

where n_i is the population in level i of interest, N is the total number of possible states of a given particle which can influence the population n_i. P_{ij} is the transition rate which is the probability of a transition from level i to level j. The equation states that all processes which lead to an increase of the population n_i, are balanced with the net effect of all processes which depopulate the level. The microscopic processes do not need to be in balance but the net level population does not change.

The main difficulty for these non-LTE calculations is that the vast number of equations are coupled and that they depend on the radiation field, which on its turn depends on the populations. These rate equations must therefore be solved simultaneously with the radiative transfer equation for all relevant frequencies. Needless to say that this is a complex problem... The state-of-the art 1D non-LTE codes do exist and 3D codes are now in full development.

The detailed transition rate P_{ij} can be decomposed into the different processes which are involved: radiative emission, radiative absorption and stimulated emission and collisional excitation/de-excitation. These processes are described using the Einstein coefficients.

2.6 .1 Spontaneous emission

Assume that an electron in level u will decay spontaneously to a lower level l by emitting a photon. The probability of this transition is called the Einstein coefficient of spontaneous emission which is the transition probability per unit time (unit is s^{-1}) per particle. The Einstein coefficient is part of the fundamental atomic data related to a given state of an atom. It is independent on the local

Table 2.2: The Einstein coefficients for transitions between u and l states.

Name	Meaning
A_{ul}	transition probability per unit time and per particle for the spontaneous emission ($u \rightarrow l$)
$B_{lu}\,\overline{J_{\nu_0}}$	transition probability per unit time and per particle for radiative absorption
$B_{ul}\,\overline{J_{\nu_0}}$	transition probability per unit time and per particle for stimulated emission
C_{lu}	transition probability for a collisional excitation per particle in state l and per second
C_{ul}	transition probability for a collisional de-excitation per particle in state u and per second

thermodynamical and/or chemical conditions. Allowed transitions have typical values of $A_{ul} \approx 10^4 - 10^8\,\mathrm{s}^{-1}$, while forbidden transitions (which violate the quantum mechanical transition rules) have much smaller values of $A_{ul} \approx 1 - 10^2\,\mathrm{s}^{-1}$. The number of transitions per unit volume is then the Einstein coefficient multiplied by the number density of the atoms in state u:

$$R_{u\rightarrow l} = N_u A_{ul} \tag{2.37}$$

If there are now decays possible to different levels, the transition probabilities just add:

$$\Gamma_u \equiv \sum_l A_{ul}\,. \tag{2.38}$$

The excitation stability of the level u, the average time of the electron to stay in state u is expressed by Γ_u^{-1} number of seconds. This is related to the Heisenberg uncertainty principle which states that:

$$\Delta E = \hbar/\Delta t \approx \hbar\Gamma_u\,, \tag{2.39}$$

We call this uncertainty in the energy state, the natural broadening of the line. This is only a part of the total broadening in-setu physics. Moreover, the observed line profile is not only dependent on the in-setu broadening effects, also the macroscopic broadening effects (macro-turbulence; object rotation etc.) as well as instrumental effects (instrumental point-spread function etc.) are important.

2.6.2 Radiative Absorption

The rate of radiative transition $l \rightarrow u$ is, obviously, dependent on the radiation field and the number of photons which are available with the correct energy. Since

it is the number of photons which is important, and not the direction from which they are coming, it is the mean intensity of the radiation which is relevant. Moreover, the energy levels are not infinitely sharp and this is described by the line profile function $\varphi(\nu - \nu_0)$ for extinction. This profile is normalised such that $\int_0^\infty \varphi(\nu - \nu_0)\, d\nu = 1$ and has dimension Hz^{-1}. The number of photons that can be used for the transition is then weighted over the profile such that:

$$\overline{J_{\nu_0}} \equiv \frac{\int_0^\infty J_\nu\, \varphi(\nu - \nu_0)\, d\nu}{\int_0^\infty \varphi(\nu - \nu_0)\, d\nu} = \int_0^\infty J_\nu\, \varphi(\nu - \nu_0)\, d\nu\,, \tag{2.40}$$

So compared to the mean intensity, $\overline{J_{\nu_0}}$ is also the mean over the extinction profile. It has the dimension of $Watt\ m^{-2}\ Hz^{-1}\ sr^{-1}$. The index ν_0 means that the mean intensity is weighted over the extinction profile of the $l \rightarrow u$ transition with frequency ν_0.

The associated Einstein coefficient for radiative absorption is B_{lu} (see Table 2.2). The rate of absorption per unit volume (number of transitions per unit volume) is then, again, the multiplication with the number density of particles in state l.

$$R_{l\rightarrow u} = N_l B_{lu} \overline{J_{\nu_0}} \tag{2.41}$$

2.6 .3 Stimulated emission

Emission of photons (transitions of $u \rightarrow l$) is not only a spontaneous process. It can also be induced by the radiation field but only by photons of the same energy as the transition. This process is called stimulated emission and, obviously, also depend on the radiation field. Another coefficient (B_{lu}) was introduced by Einstein which is very similar as in the case of absorption. The profile function need not be the same so again, the weighting is needed over the profile function:

$$\overline{J_{\nu_0}} \equiv \int_0^\infty J_\nu\, \chi(\nu - \nu_0)\, d\nu\,, \tag{2.42}$$

in which $\chi(\nu - \nu_0)$ is the normalised profile for stimulated extinction.

Remember that stimulated emission will trigger emission in which the emitted photon has exactly the same state (direction, frequency) as the stimulating photon. The emitted photon is precisely coherent with the photon of the original radiation field which stimulated the emission.

2.6.4 Collisional transitions

Collisional transitions depend on the number densities, not only of the particles in state u or l but also of the collider. The rate of transitions per unit volume for excitation is proportional to $N_l\, C_{lu}$ and for de-excitation $N_u\, C_{ul}$. The cross-sections are dependent on the kind of collider (electron, ion, neutral particle) and or better known for electron collisions than for neutral colliders.

2.6.5 Relation between the Einstein coefficients

The Einstein coefficients are fundamental atomic data which depend on the structure of the atom or molecule. They are independent on the local conditions in which the particle resides.

Using a two level atom, Einstein derived interrelations between A_{ul}, B_{ul} and B_{lu} by assuming the particle is in thermal equilibrium. The detailed processes are in equilibrium so as many absorptions as emissions occur:

$$\begin{aligned} N_l B_{lu} \overline{J_{\nu_0}} &= N_u A_{ul} + N_u B_{ul} \overline{J_{\nu_0}} \\ \overline{J_{\nu_0}} &= \frac{N_u A_{ul}}{N_l B_{lu} - N_u B_{ul}} \\ &= \frac{A_{ul}/B_{ul}}{\frac{N_l}{N_u}\frac{B_{lu}}{B_{ul}} - 1} \\ &= \frac{A_{ul}/B_{ul}}{\frac{g_l}{g_u}\frac{B_{lu}}{B_{ul}} \exp(h\nu_0/kT) - 1} \,. \end{aligned}$$

In the last step, we used the Boltzmann equation for the two-level atom:

$$\frac{N_u}{N_l} = \frac{g_u}{g_l} e^{-\frac{h\nu_{lu}}{kT}} = \frac{g_u}{g_l} e^{-\frac{h\nu_0}{kT}} \tag{2.43}$$

In TE, we know that $J_\nu = B_\nu = I_\nu$. As B_ν in only smoothly variable over the extinction profile $\varphi(\nu - \nu_0)$, we also can state that $\overline{J_{\nu_0}} = B_\nu$.

$$B_\nu = \frac{A_{ul}/B_{ul}}{\frac{g_l}{g_u}\frac{B_{lu}}{B_{ul}} \exp(h\nu/kT) - 1} \tag{2.44}$$

Equalising this to the formula of the radiation law of Planck we get the Einstein relations:

$$\frac{B_{lu}}{B_{ul}} = \frac{g_u}{g_l} \quad \text{en} \quad \frac{A_{ul}}{B_{ul}} = \frac{2h\nu^3}{c^2} \,. \tag{2.45}$$

These are two equations with three unknowns so you only have to constrain one of the Einstein coefficients to known them all three. Since the Einstein coefficients are atomic data, the Einstein relations are universal and independent on the local chemical and physical conditions.

For collisional processes we can use the same reasoning:

$$N_l C_{lu} = N_u C_{ul} \,, \tag{2.46}$$

so we can relate both coefficients by

$$\frac{C_{ul}}{C_{lu}} = \frac{g_l}{g_u} \exp(E_{lu}/kT) \,. \tag{2.47}$$

and if we know one of the coefficients, the other can be computed as well independent of the local conditions.

2.7 Absorption and Emission coefficients using the Einstein coefficients

2.7 .1 Transfer equation for b-b transitions

We can expand the treatment of bound-bound transitions in terms of the Einstein coefficients to the description in terms of the absorption and emission coefficients for the given transition.

The spontaneous de-excitation of electrons is isotropic so the number of photons, radiated per unit volume is (See Table 2.3):

$$j_\nu^{\text{spont}} = h\nu_0 \, N_u A_{ul} \, \psi(\nu - \nu_0) \,. \tag{2.48}$$

For the absorption coefficient, we compute the energy lost by radiative excitation per unit volume per unit time:

Table 2.3: From A_{ul} to the associated emission coefficient

$N_u\, A_{ul}$	number of transitions $u \to l$ per unit volume per second
$h\nu_0\, N_u A_{ul}$	total energy output per unit volume per second
$h\nu_0\, N_u A_{ul}\, \psi(\nu - \nu_0)$	total energy output per unit volume per second and per Hz
$h\nu_0\, N_u A_{ul}\, \psi(\nu - \nu_0)/4\pi$	total energy output per unit volume, per second, per Hz and per sr

$$\begin{aligned} dE^{\rm tot} &= h\nu_0\, N_l\, B_{lu}\, \overline{J_{\nu_0}}\, dV\, dt \\ &= h\nu_0\, N_l\, B_{lu}\, dV\, dt \int J_\nu\, \varphi(\nu - \nu_0) d\nu \\ &= \frac{h\nu_0}{4\pi}\, N_l\, B_{lu}\, dV\, dt \int\int I_\nu\, \varphi(\nu - \nu_0) d\Omega d\nu\,, \end{aligned}$$

This is the total energy which is absorbed. If we now only take into account, the amount of energy which is absorbed out of the beam in frequency range $d\nu$ and in solid angle $d\Omega$ during time dt we get:

$$dE^{\rm beam} = \frac{h\nu_0}{4\pi}\, N_l\, B_{lu}\, I_\nu\, \varphi(\nu - \nu_0)\, dV\, dt\, d\Omega\, d\nu\,, \tag{2.49}$$

Since the volume is $dV = dA\, ds$, the extinction coefficient is:

$$\alpha_\nu^{\rm rad.\,excitation} = \frac{h\nu_0}{4\pi}\, N_l\, B_{lu}\, \varphi(\nu - \nu_0) \tag{2.50}$$

Stimulated emission is also dependent on the local radiation field so it is much more related to extinction than to spontaneous emission. It is more convenient to incorporate the stimulated emission as negative contribution to the extinction coefficient. The total line extinction coefficient (hence the superscript l), corrected for stimulated emission can be expressed like:

$$\alpha_\nu^l = \frac{h\nu_0}{4\pi}[N_l\, B_{lu}\, \varphi(\nu - \nu_0) - N_u\, B_{ul} \chi(\nu - \nu_0)] \tag{2.51}$$

the bound-bound emission coefficient j_ν^l remains:

$$j_\nu^l = h\nu_0\, N_u A_{ul}\, \psi(\nu - \nu_0) \tag{2.52}$$

In TE the profile functions are the same and $\psi(\nu-\nu_0) = \varphi(\nu-\nu_0) = \chi(\nu-\nu_0)$.

The transfer equation in terms of the Einstein coefficients for b-b transitions can be written as:

$$\frac{dI_\nu}{ds} = -\frac{h\nu_0}{4\pi}\,[N_l\, B_{lu} - N_u\, B_{ul}]\,\psi(\nu - \nu_0) I_\nu + h\nu_0\, N_u A_{ul}\, \psi(\nu - \nu_0) \tag{2.53}$$

Where we assumed the profile functions to be the same.

The source function for b-b transitions is then:

$$S_\nu^l = \frac{N_u A_{ul}}{N_l\, B_{lu} - N_u\, B_{ul}} \tag{2.54}$$

If we now insert the Einstein relations we get :

$$\alpha_\nu^l = \frac{h\nu_0}{4\pi}\, N_l B_{lu}\, (1 - g_l\, N_u/g_u\, N_l)\, \psi(\nu - \nu_0) \tag{2.55}$$

$$S_\nu^l = \frac{2\, h\, \nu^3}{c^2} \left(\frac{g_u\, N_l}{g_l\, N_u} - 1\right)^{-1} \tag{2.56}$$

2.7 .2 Thermal b-b treatment

When we can describe the local population distribution with the equations of thermal equilibrium, we can insert the Boltzmann equation into the description of the source function and the extinction coefficient and we get:

$$\alpha_\nu^l = \frac{h\nu_0}{4\pi}\, N_l B_{lu} \left[1 - \exp\left(\frac{-h\nu}{k\, T}\right)\right] \psi(\nu - \nu_0) \tag{2.57}$$

$$S_\nu^l = B_\nu \tag{2.58}$$

So the thermal value of the source function of the b-b process is the Planck function.

2.7 .3 Non-thermal b-b treatment

This case covers all situations in which

$$\frac{N_u}{N_l} \neq \frac{g_u}{g_l} \exp\left(\frac{-h\,\nu}{k\,T}\right) \tag{2.59}$$

2.7 .4 Inverted Population: maser emission

In thermal equilibrium the Boltzmann relation is such that

$$\frac{N_u\,g_l}{N_l\,g_u} = \exp\left(\frac{-h\,\nu}{k\,T}\right) < 1 \tag{2.60}$$

$$\frac{N_l}{g_l} > \frac{N_u}{g_u} \tag{2.61}$$

Even when the material is out of thermal equilibrium, this relation is usually satisfied. When, however, it is possible to populate enough particles in the upper state by e.g. radiative pumping, than it may occur that we have an inversion in the population (see Fig. 2.11) and

$$\frac{N_l}{g_l} < \frac{N_u}{g_u} \tag{2.62}$$

In this case, equation 2.55 makes that the extinction coefficient, corrected for stimulated emission is negative (!) and at the given frequency the radiation will increase rather then decrease: we have a laser (light amplification by stimulated emission radiation). In many astrophysical sources, this occurs in masering molecules which are pumped by IR photons. These are masers (microwave amplification by stimulated emission radiation). Well known masering molecules are SiO, H_2O and OH. Masers can be very efficient e.g. a negative optical depth of say 50 gives an amplification of $5\ 10^{21}$....

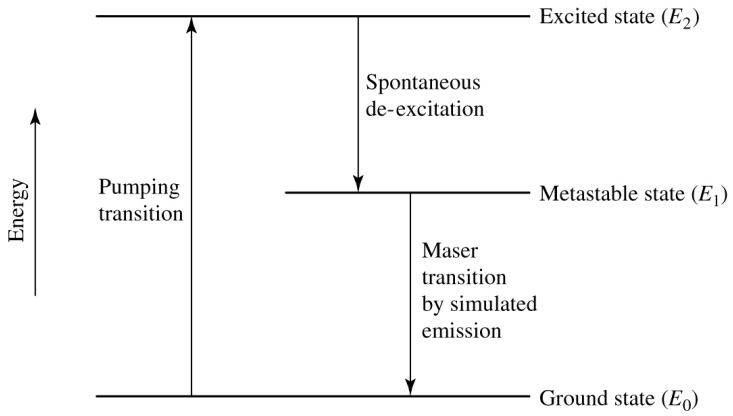

Figure 2.11: Maser emission can occur when population inversion occurs thanks to radiative pumping. *Fig. taken from Carroll & Ostlie (1996)*

2.8 Broadening of Spectral Lines

Different effects will contribute to the broadening profiles introduced in previous sections and in this section we quantise those.

We touched upon the subject of line broadening by only considering natural broadening which occurs due to the uncertainty principle of Heisenberg and the associated uncertainties in the energy levels. Often, however, the natural broadening is a minor effect. While we will not develop a rigorous theory of broadening of spectral lines here, we will focus on several aspects of the broadening theory. The final profile will be a convolution of the different profile functions.

2.8 .1 Microscopic velocities in (L)TE

This thermal broadening is caused by the microscopic velocity distribution of the matter elements in the gas phase.

In thermal equilibrium, the gas particles will have their velocity distribution which can be described by the Maxwell-Boltzmann distribution. For every component in the velocity vector we can write the number of particles of mass m with a velocity along the x axis inbetween v_x and $v_x + dv_x$:

$$\frac{n(v_x)}{N}\mathrm{d}v_x = \left(\frac{m}{2\pi kT}\right)^{1/2} \mathrm{e}^{-(1/2)mv_x^2/kT}\mathrm{d}v_x \tag{2.63}$$

with N the total number of particles with mass m per unit volume. The other symbols have their usual meaning.

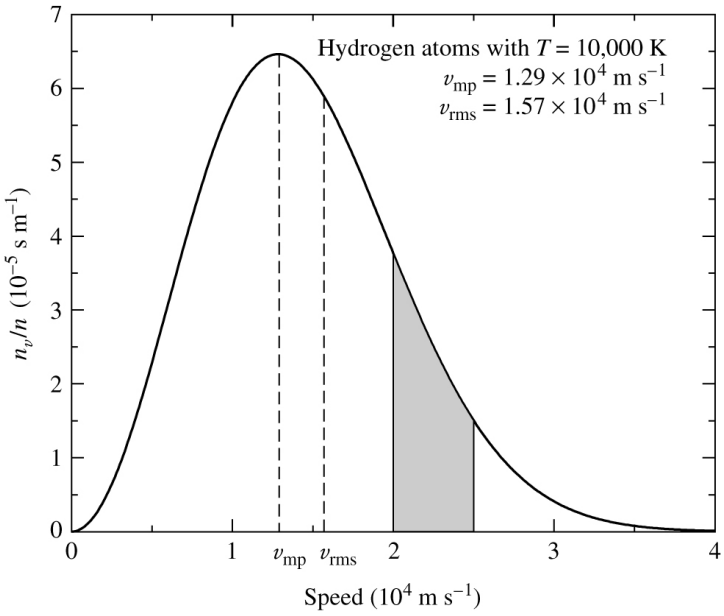

Figure 2.12: The velocity distribution in TE of hydrogen atoms of temperature 10000K. The most probable (v_mp) and mean (v_{rms}) velocity is indicated on the distribution. *Fig. taken from Carroll & Ostlie (1996)*

The number of particles of mass m that have a velocity amplitude between v and $v + dv$ is:

$$\frac{n(v)}{N}\mathrm{d}v = \left(\frac{m}{2\pi kT}\right)^{3/2} 4\pi v^2 \mathrm{e}^{-(1/2)mv^2/kT}\mathrm{d}v\,. \tag{2.64}$$

The distribution is a Gauss distribution (see Fig. 2.12). The maximum in the distribution is the most probable velocity $v_mp = \sqrt{2kT/m}$, while the mean velocity is $< v >= v_{rms} = \sqrt{3kT/m}$.

The Maxwell-Boltzmann distribution has a high velocity tail which declines at

$$\text{tail} \approx e^{-mv^2/2kT} \tag{2.65}$$

This thermal velocity will also give rise to a line-broadening because of the Doppler effect: atoms/ions with a given velocity will absorb/emit at a slightly

different frequency then the ones at rest because of the Doppler frequency shift. The microscopic distribution of those velocities will cause a smearing of the line-profile as net effect.

The change in frequency is:

$$\nu - \nu_0 = \frac{\nu_0 \, v_z}{c} \tag{2.66}$$

with z the radial component so along the line-of-sight towards the observer. Assuming we can describe the distribution of velocities as being thermal, we can use eq 2.63 to transform the radial velocity in frequency units:

$$v_z = \frac{c\,(\nu - \nu_0)}{\nu_0} \tag{2.67}$$

$$dv_z = \frac{c\,d\nu}{\nu_0} \tag{2.68}$$

The strength of the emission in the frequency range ν and $\nu + d\nu$ will be proportional to

$$\exp\left[-\frac{m\,c^2\,(\nu - \nu_0)^2}{2\,\nu_0^2\,k\,T}\right] d\nu \tag{2.69}$$

The associated normalised profile function is:

$$\varphi(\nu - \nu_0) = \frac{1}{\Delta\nu_D\,\sqrt{\pi}}\, e^{(\nu-\nu_0)^2/(\Delta\nu_D)^2} \tag{2.70}$$

with the definition of the Doppler width $\Delta\nu_D$ as:

$$\Delta\nu_D = \frac{\nu_0}{c}\sqrt{\frac{2\,k\,T}{m}} \tag{2.71}$$

When only velocity broadening is taken into account we can use the profile to state that the cross section at the line centre (the equation 2.50) will become:

$$\alpha_\nu^{\text{rad. excitation}} = \frac{h\nu_0}{4\pi}\, N_l\, B_{lu}\, \varphi(\nu - \nu_0) = \frac{1}{\Delta\nu_D\,\sqrt{\pi}}\frac{h\nu_0}{4\pi}\, N_l\, B_{lu} \tag{2.72}$$

2.8 .2 Microturbulent velocity

Often lines of stellar photospheres are broader in their Doppler profile than what we would expect from the thermal broadening alone. Turbulent motion, adds to the thermal velocity component.

The term *micro-turbulent velocity* was initially introduced by Struve to indicate the turbulent velocities which act on a length-scale smaller than the line-forming region in the stellar atmospheres.

Assuming that these velocity fields are indeed small compared to the line-forming layers in the atmosphere, we get an extra broadening in the profile function:

$$\Delta\nu = \frac{\nu_{lu}}{c}\sqrt{\xi^2_{thermal} + \xi^2_{micro}} \tag{2.73}$$

With the thermal velocity

$$\xi_{thermal} = \left(\frac{2kT}{m}\right)^{1/2} = 12.895\left(\frac{T}{10^4 A}\right)^{1/2} \ \mathrm{km\,s^{-1}} \tag{2.74}$$

with A the atomic weight in amu

2.8 .3 Pressure broadening

Pressure broadening is connected to slight energy-level disturbance due to the Coulomb interaction induced by collisions. Pressure broadening is dependent of particle which collides with the most dominant effect coming from electrons.

$$\Delta\nu = \frac{C_n}{R^n} \tag{2.75}$$

with C_n the interaction constant and R the minimal distance of the collider

1. n=2 Linear Starck effect
2. n=3 Resonance broadening (only for H important)
3. n=4 Quadratic Starck effect
4. n=6 Van Der Waals forces

The lowest-order broadening is called the Linear Starck effect and it is only relevant for H. It is very efficient and it relates to the fact that the energy levels of H are degenerate for the l quantum number. The collisional broadening of H by protons or electrons will have a strong effect on the profile which is very well detected in stellar spectra: the H-profiles are much broader than profiles of bound-bound transitions of heavier elements (except for He II). The profile function of H-lines is called a Holtzmark profile.

In the impact approximation (not developed here), the pressure broadening results in a Lorentz profile (broadening is $2/\tau$) :

$$\mathcal{P}(\omega) = \int_0^\infty \mathrm{d}T \, \frac{1}{\tau} \, \mathrm{e}^{-T/\tau} \frac{1}{(\omega_{lu} - \omega)^2} \left(2 - \mathrm{e}^{-i(\omega_{lu}-\omega)T} - \mathrm{e}^{i(\omega_{lu}-\omega)T}\right) \tag{2.76}$$

$$= \frac{1}{(\omega_{lu} - \omega)^2 + (1/\tau)^2} \, . \tag{2.77}$$

τ is the mean time between two collisions.

2.9 Voigt Profile

The main intrinsic broadening effects are summarised:

1. Natural broadening : Lorentz profile
2. Doppler broadening, including microturbulence : Gauss profile
3. Pressure broadening : Lorentz profile (except for H)

The associated cross section profile will be a convolution of the different profiles:

$$\sigma_\nu^l = \left[\frac{\sqrt{\pi} e^2}{m_e c} \frac{f}{\Delta\nu_D} \mathrm{e}^{-(\Delta\nu/\Delta\nu_D)^2} \right] * \left[\frac{\gamma/4\pi^2}{(\nu - \nu_0)^2 + (\gamma/4\pi)^2} \right] \tag{2.78}$$

$$= \frac{\sqrt{\pi} e^2}{m_e c} \frac{f}{\Delta\nu_D} \int_{-\infty}^{\infty} \frac{(\gamma/4\pi^2) \, \mathrm{e}^{-(\Delta\nu/\Delta\nu_D)^2}}{(\nu - \nu_0)^2 + (\gamma/4\pi)^2} \, \mathrm{d}\nu \tag{2.79}$$

$$= \frac{\sqrt{\pi} e^2}{m_e c} \frac{f}{\Delta\nu_D} H(a, v) \tag{2.80}$$

And by changing to velocity instead of frequency we get the *Voigt* Profile:

$$H(a,v) \equiv \frac{a}{\pi}\int_{-\infty}^{\infty}\frac{\mathrm{e}^{-y^2}}{(v-y)^2+a^2}\mathrm{d}y \tag{2.81}$$

$$y \equiv \frac{\xi}{\xi_0} = \frac{\xi}{c}\frac{\nu_0}{\Delta\nu_D} = \frac{\xi}{c}\frac{\lambda_0}{\Delta\lambda_D} \tag{2.82}$$

$$v \equiv \frac{\nu-\nu_0}{\Delta\nu_D} = \frac{\lambda-\lambda_0}{\Delta\lambda_D} \tag{2.83}$$

$$a \equiv \frac{\gamma}{4\pi\Delta\nu_D} = \frac{\lambda^2}{4\pi c}\frac{\gamma}{\Delta\lambda_D} \tag{2.84}$$

$$f \equiv f_{lu}, \text{ the oscillatorstrength.} \tag{2.85}$$

So v is the velocity (associated with the frequency difference to the line-centre) in units of Doppler width. The a factor is the ratio between the Lorentz broadening factor, to the Doppler width.

The Voigt profile is not normalised and has an integral of $\sqrt{\pi}$ in v-units

The normalised b-b extinction profile is:

$$\varphi(\nu-\nu_0) = \frac{H(a,v)}{\sqrt{\pi}\Delta\nu_D}\,. \tag{2.86}$$

A rather crude approximation gives ($a \ll 1$):

$$H(a,v) \approx e^{-v^2} + \frac{a}{\sqrt{\pi}v^2} \tag{2.87}$$

In the line-centre the Gauss component dominates. In the wings, the damping profile. This is illustrated in Fig 2.13.

In this chapter we focussed on the description of bound-bound transitions and their relation with the radiation field. In the next chapters we discuss which lines will be observable under which thermodynamic conditions.

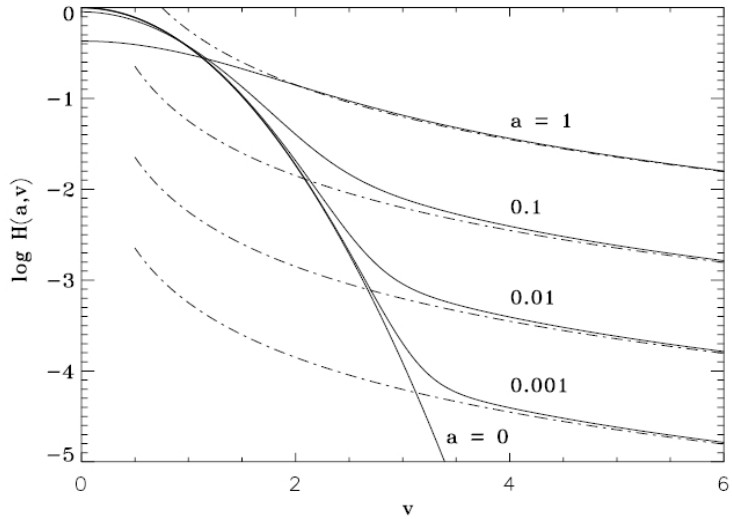

Figure 2.13: Wings of the Voigt profile. The dashed-dotted lines is the $a/\sqrt{\pi}v^2$ approximation

2.10 Problems

1. For a gas of neutral hydrogen. Compute the temperature for which there will be an equal number of atoms with the electron in the ground state, as there are atoms in the first excited state. The degeneracy of the H electron is $g_n = 2n^2$ with n the principal quantum number. Can you relate this temperature to the observational constraint that the Balmer lines appear strongest for A stars (say near 9000K) ?

2. Compute the average density of the Sun (mass and radius are listed in the appendix), Sirius (2.3 $M_\odot$, 1.6 $R_\odot$) and Betelguese (10 $M_\odot$; 1000 $R_\odot$).

3. A supernova remnant has an angular diameter of 4.3 arcmin and a measured flux of 100 Mega-Hz of 1.6×10^{-19} in units of $erg\,cm^{-2}\,s^{-1}\,Hz^{-1}$. Assume the emission is thermal.

   - Compute the brightness temperature
   - If the angular diameter were smaller, would the brightness temperature increase or decrease ?
   - At what frequency will this object's radiation be maximal assuming the emission is as a blackbody ?

- Can you say something on the actual true temperature of the object ?

4. The Einstein coefficient of the CO rotational line 1-0 at 2.6mm wavelength (115 GHertz) is $6\times10^{-8}\,\mathrm{s}^{-1}$. The cross-section of the line center is equal to:

$$\sigma_{line\,center} = \frac{\lambda^2}{8\,\pi}\,\frac{A}{\Delta\,\nu} \tag{2.88}$$

with $\Delta\,\nu$ the Doppler width in frequency units.

Assume now there is a molecular cloud with a temperature of 20K; a H_2 particle density of $10^4\,\mathrm{cm}^{-3}$ and a typical CO particle density of 10^{-4} with respect to H_2.

How big needs a cloud to be, to become optically thick ? A typical molecular cloud is between 1 and 100 pc.

Chapter 3

Transitions of H

3.1 Introduction

Hydrogen is, by virtue of its very high abundance, one of the most important elements to study the physical interactions between radiation and matter. In this chapter we focus on the most important astrophysical probes of H and discuss the different bound-bound transitions of Hydrogen which are relevant for astrophysics.

Hydrogen appears in different forms which include H,H^+, H^-,H_2,H_2^+,H_3, H_3^+, but also heavy hydrogen, deuterium (D), and the associated molecules D_2HD are important elements in astrophysics. The amount of deuterium which was made during the Big-Bang and its associated nucleosynthesis, is an important constraint on any hot Big-Bang model.

In Fig. 3.1, the energy scheme of H is shown. Any atom with a single electron orbiting a nucleus of charge Z is hydrogen-like and is basically a two-particle problem. The Hamiltonian is written as:

$$\mathbf{H} = -\frac{\hbar^2}{2\,\mu}\,\nabla^2 \;-\; \frac{Z\,e^2}{4\,\pi\,\epsilon_0\,r} \tag{3.1}$$

In atomic units:

$$\mathbf{H} = -\frac{1}{2\,\mu}\,\nabla^2 \;-\; \frac{Z}{r} \tag{3.2}$$

The Hamiltonian includes the kinetic energy operator for the electron and the potential energy term which describes the Coulomb attraction between the nucleus and the electron.

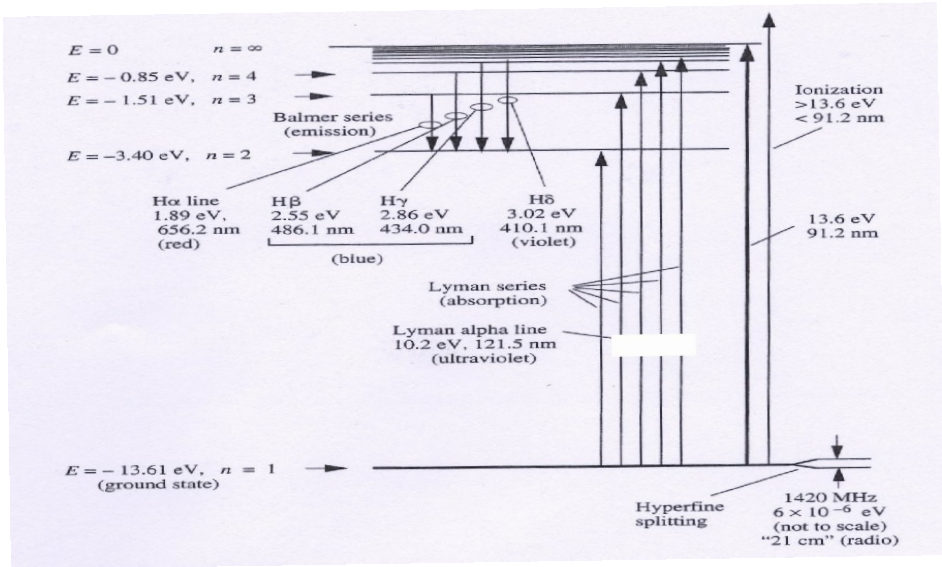

Figure 3.1: Bound-bound transition for neutral Hydrogen. *Fig. taken from Tennyson (2007)*

The masses involved are the one of an electron (m_e) and the mass of the nucleus (M). The reduced mass is defined as:

$$\mu = \frac{m_1\, m_2}{m_1 + m_2} \tag{3.3}$$

Or for a H-like atom:

$$\mu = \frac{m_e\, M}{M + m_e} \tag{3.4}$$

with M the nuclear mass. The reduced mass is very similar to m_e.

The atomic unit system is scaled to the dimensions of the atoms and includes:

1. unit of mass is the electron mass
2. unit of charge is the electron charge
3. unit of length is the Bohr radius
4. Planck's constant is divided by 2π
5. $4\,\pi\,\epsilon_0 = 1$

6. Atomic unit of energy is the Hartree

The atomic unit of energy is known as the Hartree and is given by:

$$1E_h = 2R_\infty = 27.2113661eV = 4.3597482 \times 10^{-18}J \tag{3.5}$$

The R_∞ corresponds to a system of infinite nuclear mass:

$$\frac{1}{\lambda} = \frac{1}{hc}\left(E_{n_1} - E_{n_2}\right) = R_H\left(\frac{1}{n_1^2} - \frac{1}{n_2^2}\right) \tag{3.6}$$

$$R_H = \frac{\mu}{m_e}R_\infty = \left(\frac{M_H}{M_H + m_e}\right)R_\infty \tag{3.7}$$

$$R_\infty = 109737.31 \text{ cm}^{-1} \tag{3.8}$$

$$R_H = 109677.581 \text{ cm}^{-1} \tag{3.9}$$

The energy levels are therefore easy to compute and will give rise to the typical H-series (Lyman, Balmer, Paschen etc.), Fig 3.1.

The state of the gas over its ionisation and excitation levels, will depend on the balance between collisional excitations and radiative excitations. The concept of critical density was introduced to express the balance between both processes:

The ratio between the timescale of radiative de-excitation or collisional is:

$$n_c = \frac{\sum_{i<j} A_{ji}}{\sum_{i\neq j} q_{ji}} \tag{3.10}$$

q_{ij} is the rate of collisional de-population. Often only 1 to a couple of dominant processes are taken into account in this calculations.

In many environments (ISM, intergalactic space, circumstellar matter), only the electrons are thermalised (T_e)

3.2 Solutions of the Schrödinger equation

The analytical solution in polar coordinates can be written as:

$$\chi(r,\theta,\phi) = R_{nl}(r)\,Y_{lm}(\theta,\phi) \tag{3.11}$$

1. Radial solutions : Laguerre polynomials
2. Angular solutions: spherical harmonics

In Fig 3.2 the radial part and the probability distribution of the lowest radial solutions is shown. In Fig 3.3 wave functions are shown for the angular motions in terms of the spherical harmonics.

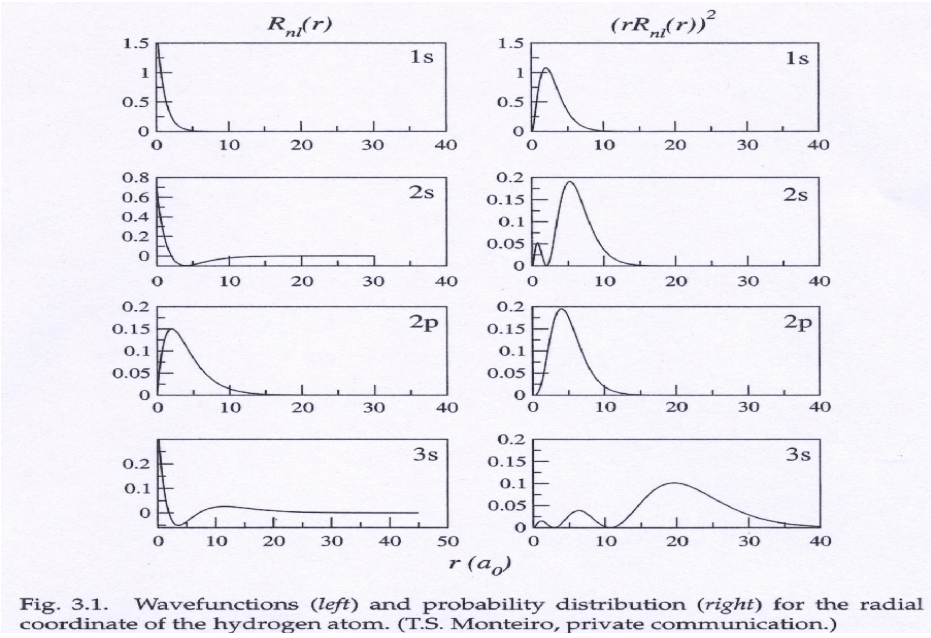

Figure 3.2: Wave functions and probability functions for the radial coordinate and this for the lowest radial solutions. *Fig. taken from Tennyson (2007)*

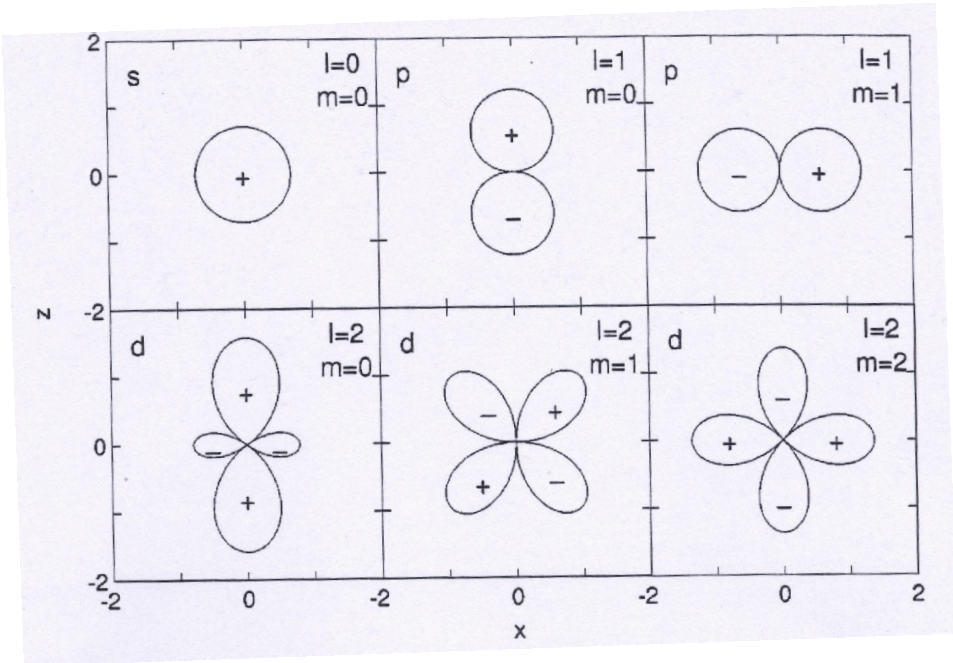

Figure 3.3: Wave functions in terms of the spherical harmonics. What is given is the absolute value of the spherical harmonic at a distance from the origin for each angle. The - and + give the sign of the wavefunction in each region. *Fig. taken from Tennyson (2007)*

3.3 Energy Levels and Quantum Numbers

The energy levels for bound states are given by the solutions of the Schrödinger equation and are given by:

$$E_n = \frac{\mu\, Z^2\, e^4}{8\, h^2\, \epsilon_0^2} \frac{1}{n^2} = -R\frac{Z^2}{n^2} \tag{3.12}$$

- n: principal quantum number (q.n.)
- l: electron angular momentum $\hbar\,[l(l+1)]^{1/2}$ (l can take 0,1,2,...,n-1
- m: magnetic q.n. m$\hbar$ is the projection of the electron angular momentum vector along the z-axis of the system. (2l+1) values -l,-l+1...l-1,l
- s: electron spin. A single electron has spin 1/2

Table 3.1: Orbital Angular momentum nomination rules

0	1	2	3	4	5	6	...
s	p	d	f	g	h	i	...

- s_z: projection of the spin angular momentum (2s+1) values so for a single electron: -1/2 and +1/2

The standard nomenclature is to denote each state with its nl value. The ground state is given as 1s, the first excited state as 2s etc. If there is no external field, the energy is only dependent on the principle quantum number n.

Any nl combination is 2(2l+1)-fold degenerate when there is no external field. The wavelengths of the transitions are given by the Rydberg formula:

$$\frac{h\,c}{\lambda} = \frac{-13.6\,\mathrm{eV}}{n_u^2} + \frac{13.6\,\mathrm{eV}}{n_l^2} \tag{3.13}$$

$$\frac{12398.4..\,\mathrm{eV\,\AA}}{\lambda} = -13.6\,\mathrm{eV}\left(\frac{1}{3^2} - \frac{1}{2^2}\right) \tag{3.14}$$

This gives 6563.9 Å for the H-alpha line.

The Balmer jump is another defining feature in stellar spectra and this occurs at:

$$\lambda\ (\mathrm{\AA}\,) \approx \frac{12400}{\mathrm{E\ (eV)}} \tag{3.15}$$

Some imporant bb-transitions of Hydrogen and the associated atomic data is given in Fig. 3.4.

Hydrogen is one of the few cases where the exact values of the oscillatorstrengths of b-b transitions are known. The exact values are given by:

$$f(l,u) = \frac{1}{3l^2}\left(\frac{1}{l^2} - \frac{1}{u^2}\right)\left[\sum_{k=1}^{l-1} k\,\sigma^2(l,k;u,k-1) + \sum_{k=0}^{l-1}(k+1)\,\sigma^2(l,k;u,k+1)\right] \tag{3.16}$$

Wavelength in Å

Series	l	u=2	3	4	5	6	7	8
Ly	1	1215.67	1025.72	972.54	949.74	937.80	930.75	926.23
H	2		6562.80	4861.32	4340.46	4101.73	3970.07	3889.05
P	3			18751.0	12818.1	10938.1	10049.4	9545.98
Br	4				40512.0	26252.0	21655.0	19445.6
Pf	5					74578	46525	37395
Hu	6						123680	75005

Oscillator strength

Series	l	u=2	3	4	5	6	7	8
Ly	1	0.4162	0.07910	0.02899	0.01394	0.007799	0.004814	0.003183
H	2		0.6407	0.1193	0.04467	0.02209	0.01270	0.008036
P	3			0.8421	0.1506	0.05584	0.02768	0.01604
Br	4				1.038	0.1793	0.06549	0.03230
Pf	5					1.231	0.2069	0.07448
Hu	6						1.424	0.2340

Einsteincoefficient A_{ul} in $\sec^{-1}$

Series	l	u=2	3	4	5	6	7	8
Ly	1	$4.699\,10^8$	$5.575\,10^7$	$1.278\,10^7$	$4.125\,10^6$	$1.644\,10^6$	$7.568\,10^5$	$3.869\,10^5$
H	2		$4.410\,10^7$	$8.419\,10^6$	$2.530\,10^6$	$9.732\,10^5$	$4.389\,10^5$	$2.215\,10^5$
P	3			$8.986\,10^6$	$2.201\,10^6$	$7.783\,10^5$	$3.358\,10^5$	$1.651\,10^5$
Br	4				$2.699\,10^6$	$7.711\,10^5$	$3.041\,10^5$	$1.424\,10^5$
Pf	5					$1.025\,10^6$	$3.253\,10^5$	$1.388\,10^5$
Hu	6						$4.561\,10^5$	$1.561\,10^5$

Figure 3.4: The wavelengths λ_{lu}, the oscillatorstrengths (f_{lu}) and Einsteincoefficients (A_{lu}) of some important bb transitions of Hydrogen.

with the normal nomenclature of l being main quantumnumber of the lower level and u the one of the higher level. The σ^2 are given by:

$$\sigma^2(l,k;u,k') = \left(\int_0^\infty dr\, r^3\, R_{lk}(r)\, R_{uk'}(r)\right)^2 \tag{3.17}$$

A useful approximation for the oscillatorstrength was proposed by Kramer and the $f(l,u)$ value can be approximated by:

$$f_K(l,u) = \frac{32}{3\pi\sqrt{3}}(\frac{1}{l^2} - \frac{1}{u^2})^{-3}\frac{1}{u^3 l^5} \tag{3.18}$$

The difference between the exact value and the Kramer formula is given by the Gaunt factor. In the case of H, the Gaunt factor is of order unity since the approximation is good.

$$f(l,u) = g_I(l,u) f_K(l,u) \tag{3.19}$$

A page to refresh the concepts of atomic structure can be found here.

The most efficient line is undoubteldy the Lyman α line (see Fig.3.4). Since neutral Hydrogen in the ISM is almost completely in the ground state, the line is very opaque, even at the densities of the ISM. We can detect the line, providing that the Ly-alpha photons are shifted to wavelengths where the ISM is less opaque. This is showns in the spectrum of a quasar with high redshift in Fig 3.5 and Fig. 3.6. In the line-of-sight towards the quaser, the ISM clouds with a less high redshift will be visible by discrete Ly$_\alpha$ lines. This is called the 'Lyman alpha forrest'

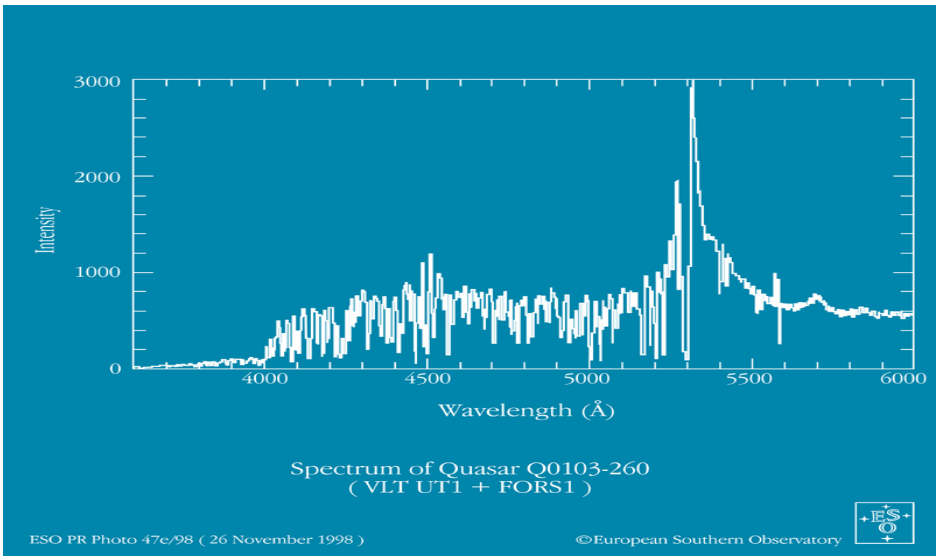

Figure 3.5: The Spectrum of a Quasar at high redshift. The strong line is the Ly$_\alpha$ line of the quasar. The forrest of lines in the blue part of the spectrum come from Ly$_\alpha$ absorptions by ism clouds in the line-of-sight towards the quasar. Fig. Courtesy by ESO

The discrete levels at high excitation are non populated in stellar atmospheres (see Problems at the end of the chapter). In circumstellar/interstellar/intergalactic gas, the density is so low that also higher levels will show transitions at recombination cascades. As we have seen in Chapter 2, the thermal excitation of these high levels will not yield a significant population. These high levels will only be populated by recombination of an electron and a proton. Recombination is not an efficient process (the densities in H[II] regions are low), but the lines can be detected in the radio (see Fig. 3.7). The naming of recombination lines is according to the following rules:

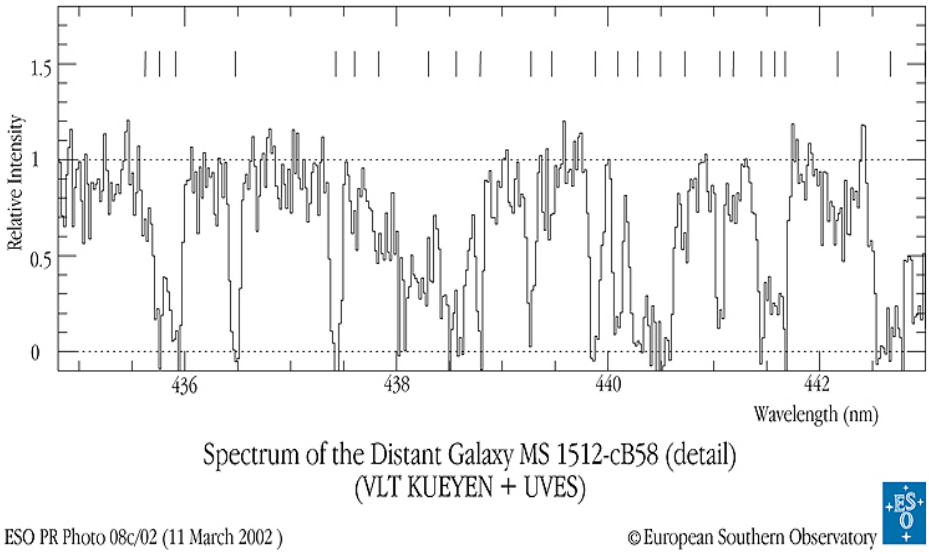

Figure 3.6: Spectral details of the Ly$_\alpha$ forrest of lines.

1. Transitions n $\leftarrow$ n+1 : Hnα
2. Transitions n $\leftarrow$ n+2 : Hnβ

Very high levels have been observed, up to H766α where the size of this atom approaches 0.1mm... Radio recombination can lead to a population inversion and in very dense H[II] regions, H can maser, but the most efficient masers are from molecules like OH, SiO, H_2O.

Since recombination of heavier elements pupulate very high levels, these levels can be considered Hydrogen-like because the core including the bound electrons can be considered as a point-like. The energy levels can be computed like (see Fig 3.8):

$$E_n = -\frac{R_\infty}{n^2}\frac{M}{M+m_e} \tag{3.20}$$

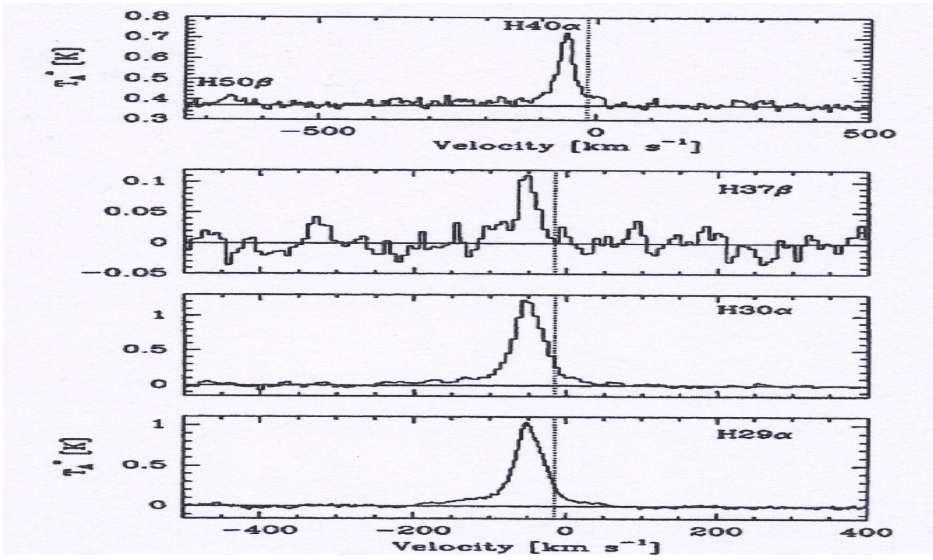

Figure 3.7: High level radio recombination transitions in the spectrum of η Car.

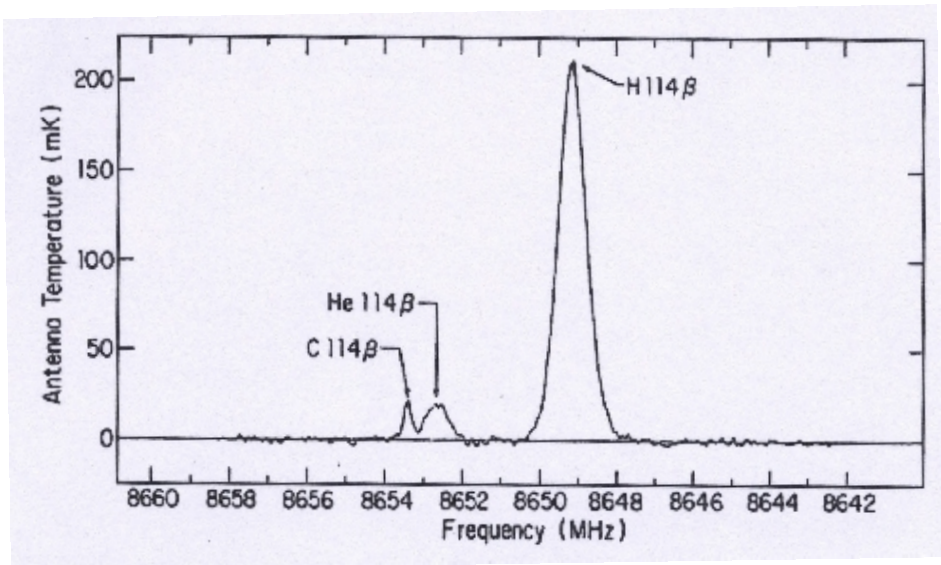

Figure 3.8: Radio recombination lines of H, He and C observed in the gaseous nebula W3 *Fig. taken from Tennyson (2007)*

3.4 Angular Momentum Coupling

One-electron atoms have several sources of angular momentum

1. Electron orbital angular momentum l
2. Electron spin angular momentum s
3. Nuclear spin angular momentum i

The couplings between the momenta are ordered following the strength of the coupling. The nuclear spin, arises from the spin coupling of the various nucleons (protons, neutrons both have intrinsic spin 1/2). For atomic spectra, the total spin of the nucleus is represented by the quantum number i. A nice summery of H-like (and more complex) possible transitions can be found HERE.

For H, the usual coupling scheme is to combine l and s to give the total electron angular momentum j. The quantum numbers add vector-wise.

Combination of electron orbital and spin coupling. In vector addition, the total electron angular moment is usually written as:

$$\vec{j} = \vec{l} + \vec{s} \tag{3.21}$$

Combination of total electron angular moment and nuclear spin this is:

$$\vec{f} = \vec{j} + \vec{i} \tag{3.22}$$

The vector addition $\vec{c} = \vec{a} + \vec{b}$ follows the rules that the range of c is:

$$c = |a - b|, |a - b| + 1, ..., a + b \tag{3.23}$$

3.4.1 Fine Structure Lines of H

The fine-structure lines of H appear when the relativistic effects couple electron orbital angular momentum and electron spin to give rise to fine structure in the energy level. See Fig. 3.9) and Fig. 3.10 for an example. The Lamb shift is due to a quantum electrodynamical effect which makes the splitting of the energy level significant.

3.4.2 Hyper Fine Structure line of H

The nuclear spin for H is i = 1/2. Coupling between the nuclear spin and the total electron angular momentum gives:

$$f = j \pm \frac{1}{2} \tag{3.24}$$

Configuration	l	s	j	H atom	Term	Level
ns	0	$\frac{1}{2}$	$\frac{1}{2}$	$ns_{\frac{1}{2}}$	$n\,^2S$	$n\,^2S_{\frac{1}{2}}$
np	1	$\frac{1}{2}$	$\frac{1}{2}, \frac{3}{2}$	$np_{\frac{1}{2}}, np_{\frac{3}{2}}$	$n\,^2P^o$	$n\,^2P^o_{\frac{1}{2}}, n\,^2P^o_{\frac{3}{2}}$
nd	2	$\frac{1}{2}$	$\frac{3}{2}, \frac{5}{2}$	$nd_{\frac{3}{2}}, nd_{\frac{5}{2}}$	$n\,^2D$	$n\,^2D_{\frac{3}{2}}, n\,^2D_{\frac{5}{2}}$
nf	3	$\frac{1}{2}$	$\frac{5}{2}, \frac{7}{2}$	$nf_{\frac{5}{2}}, nf_{\frac{7}{2}}$	$n\,^2F^o$	$n\,^2F^o_{\frac{5}{2}}, n\,^2F^o_{\frac{7}{2}}$

Figure 3.9: Fine Structure levels in the hydrogen atom. Splitting of the nl orbitals due to the finestructure for level l=0,1,2,3. The different quantumnumbers are given as well as the general spectroscopic notation of terms and levels. *Fig. taken from Tennyson (2007)*

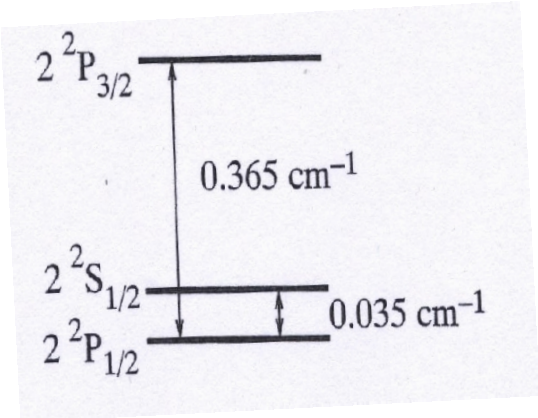

Figure 3.10: Example of Fine-Structure coupling effects on the level splitting. The splitting in the n=2 level of atomic H is shown. The larger splitting is the fine structure and the smaller the Lamb shift.

The ground state of H is

$$^2S_{1/2} \tag{3.25}$$

So nuclear spin coupling can split the state in two having f=0 or 1. This is at 6 10^{-5} eV which is the famous 21cm line. This line is very important in Galactic

(dynamical) studies (see course on the Milkey Way Galaxy).

1. Very good velocity tracer (e.g. Galactic structure)
2. Its intensity gives the number of atoms. The Einsteincoefficient is 2.9 10^{-15} s^{-1} which is a life-time of 10 million years...it is always optically thin
3. The profile can be used to probe the temperature of the gas
4. The Zeeman splitting can be used to measure the magnetic field strength

3.5 Transition Rules

The transition probablities are govened by the quantum-mechanical selection rules and for H this reduces to:

- Δn : any
- Δl : $\pm$ 1
- Δs : 0 (for H this is always the case)
- Δj : 0, $\pm$ 1
- Δm_j : 0, $\pm$ 1

To illustrate the effect we show the Balmer H_α substructure. The transition is from n=2 to 3 but by the Δl : $\pm$ 1 selection rule, not all transitions between sub-levels are allowed. 2s-3p; 2p-3s;2p-3d are allowed (e.g. 2s-3s is forbidden). The Fine-structure selection rules are illustrated in Fig 3.11.

3.5 .1 Two-Photon process

At low densities, the life-time of a given excited state is given by its radiative decay :

$$\tau = \left(\sum_j A_{ij} \right)^{-1} \tag{3.26}$$

So excited states which decay only by weak line emission, will be long-lived while the reverse is true for excited levels decaying via strong transitions.

$$
\begin{aligned}
2s_{\frac{1}{2}} - 3p_{\frac{1}{2}} &\quad \text{is allowed;} \\
- 3p_{\frac{3}{2}} &\quad \text{is allowed;} \\
2p_{\frac{1}{2}} - 3d_{\frac{5}{2}} &\quad \text{is not allowed;} \\
- 3s_{\frac{1}{2}} &\quad \text{is allowed;} \\
- 3d_{\frac{3}{2}} &\quad \text{is allowed;} \\
2p_{\frac{3}{2}} - 3s_{\frac{1}{2}} &\quad \text{is allowed;} \\
- 3d_{\frac{3}{2}} &\quad \text{is allowed;} \\
- 3d_{\frac{5}{2}} &\quad \text{is allowed .}
\end{aligned}
$$

Figure 3.11: The sub-levels which are related to the Balmer H_α transition. *Fig. taken from Tennyson (2007)*

Table 3.2: Lifetimes τ for decay by spontaneous emission for low-lying excited states of H

level	2s	2p	3s	3p	3d
τ	0.14	1.6×10^{-9}	1.6×10^{-7}	5.4×10^{-9}	2.3×10^{-7}

The metastable state 2s is so long-lived because the 2s-1s is strongly forbidden. It will decay by an inefficient process of two photon-decay in which the sum of the photons must be the excitation energy difference between two levels (E(2s) - E(1s)) but the photons themselves can take every energy inbetween. The photons will appear as continuous emission radiation. The process has an Einstein coefficient of 7 s^{-1}. This process, inefficient it may be, is responsible for a significant portion of the continuum energy observed from HII regions.

3.6 H-like atoms

Also HeII has only one bound electron and the energy states are easy to compute. The reduced mass will determine the Rydberg constant appropriate for this atom.

$$\frac{1}{\lambda} = Ry_{He} \left[\frac{1}{\left(\frac{n_1}{2}\right)^2} - \frac{1}{\left(\frac{n_2}{2}\right)^2} \right] \tag{3.27}$$

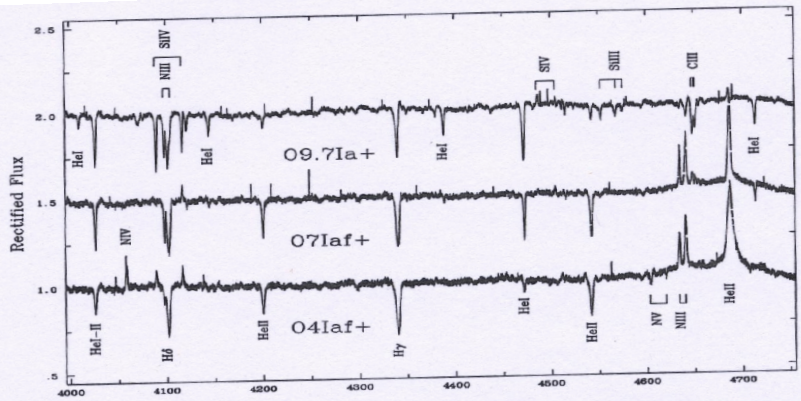

Fig. 5.1. Spectra of early (O4 star HDE 269698), mid (O7 star AzV 232) and late (O9 star Sk-66°169) type O-supergiant stars showing the sensitivity of the subtypes to the ratio of He I 4471 Å to He II 4542 Å absorptions. The spectra were recorded using the Very Large Telescope (VLT) by P.A. Crowther *et al.* [see *Astrophys. J.* **579**, 774 (2002)]. (P.A. Crowther, private communication.)

3.7 Problems

1. H-alpha occurs at 15237 cm^{-1}. What is the transition for Deuterium ?

   In stellar interiors, deuterium is destroyed and there are no known nuclear processes other than the Big-Bang nucleosynthesis (Fig. 3.12) which can produce deuterium. The Deuterium abundance is very hard to get, but it yields important constraints on the hot Big-Bang nucleosynthesis models.

2. The Bohr radius:

$$r_n = \frac{n^2}{Z}\, a_0 \tag{3.28}$$

   For the Sun, N is about 10^{17} cm^{-3}. What is the highest H-atom n-level you would expect ?

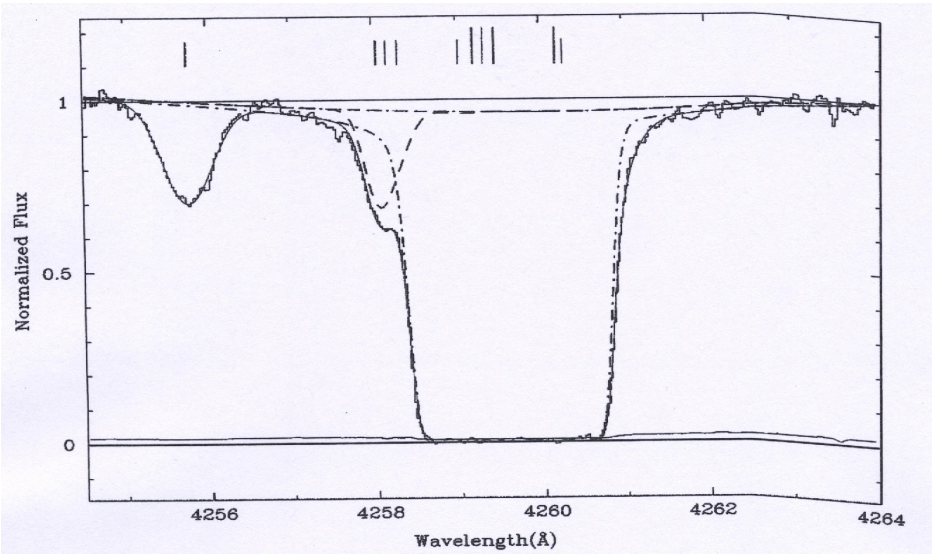

Figure 3.12: A spectrum of a high redshift quasar. The spectral tracer for the deuterium Lyman alpha line is given on the more energetic wing of the strongly saturated redshifted Lyman$_\alpha$ line. Fig. from ESO

Chapter 4

Lines of more complex systems

In this chapter we reiterate some basic concepts in atomic physics and the focus is on relevant concepts in the interpretation of astronomical spectral data. A good web-based synopsis is given here. The transition rules between the different electron configurations of complex atoms is also given and the astronomical nomination explained.

An atom with N electrons and a nuclear charge Z will have the non-relativistic Schrödinger equation :

$$\left[\sum_{i=1}^{N}\left(-\frac{\hbar^2}{2m_e}\nabla_i^2-\frac{Z\,e^2}{4\,\pi\,\epsilon_0\,r_i}\right)+\sum_{i=1}^{N-1}\sum_{j=i+1}^{N}\frac{e^2}{4\,\pi\,\epsilon_o\mid\vec{r_i}-\vec{r_j}\mid}-E\right] \tag{4.1}$$

$$\times\psi(\vec{r_1},\vec{r_2},...\vec{r_N})=0 \tag{4.2}$$

where r_i is the coordinate of the i-th electron with the origin in the nucleus. The first part is the kinetic energy operator for the motion of each electron and the Coulomb attraction between the electron and the nucleus. The second summation contains the electron-electron Coulomb repulsion term. The Coulomb repulsion between pairs make that the equation is not solvable analytically. That's why an atom with two or more valence electrons is *complex*.

In the Central Field approximation, it is assumed that each electron moves in its own angle-independent central potential V_i. The total energy of the system is the sum of the single electron energies and the Schrödinger equation 4.2 separates into N single electron equations. The motion of the electron simplifies to:

$$\left[-\frac{\hbar^2}{2\,m_e}\nabla_i^2+V_i(r_i)\right]\phi_i(\vec{r_i})=e_i\phi_i(\vec{r_i}) \tag{4.3}$$

with solutions in radial and angular functions:

$$\phi_i(\vec{r_i}) = R_{n_i,l_i}\ Y_{l_i,m_i}(\theta_i, \phi_i) \tag{4.4}$$

It is standard to use the same quantum numbers as for the hydrogen orbitals n,l and m. The angular behaviour given by l and m are the same, but the radial component is not.

4.1 Indistinguishable Particles

A system with two identical particles (electron, protons, neutrons...) with wave functions Ψ. The probability function of two indistinguishable particles should obey:

$$|\Psi(1,2)|^2 = |\Psi(2,1)|^2 \tag{4.5}$$

The symmetric solution:

$$\Psi(1,2) = \Psi(2,1) \tag{4.6}$$

and the anti-symmetric solution:

$$\Psi(1,2) = -\Psi(2,1) \tag{4.7}$$

Pauli (1900-1958) postulated that *wavefunctions are antisymmetric with respect to interchange of identical fermions.* Fermions are particles with half-integer spin such as electrons, protons or neutrons. This leads to one of the fundamentals of atomic physics with the exclusion principle often summarised as: *No two electrons can occupy the same spin-orbital.*

This accounts for key ingredients in atomic structure, shell electron structure and all nucleons. It also provides the degeneracy pressure which avoids gravitational collapse of compact objects like White Dwarfs and Neutron stars.

The degeneracy with respect to the atomic number l, which is present for hydrogen, is lifted and in the absence of an external field, an energy level is dependent on n and l. The degeneracy is 2 (2l+1) so any nl orbital can hold 2(2l+1) electrons.

An atomic configuration is given by the distribution of the electrons amongst the orbitals and the ground state is the state of lowest energy. C has six electrons

Atom		Z	Configuration			
hydrogen	H	1	1s			
helium	He	2	$1s^2$			
lithium	Li	3	K	2s		
beryllium	Be	4	K	$2s^2$		
boron	B	5	K	$2s^2 2p$		
carbon	C	6	K	$2s^2 2p^2$		
nitrogen	N	7	K	$2s^2 2p^3$		
oxygen	O	8	K	$2s^2 2p^4$		
fluorine	F	9	K	$2s^2 2p^5$		
neon	Ne	10	K	$2s^2 2p^6$		
sodium	Na	11	K	L	3s	
magnesium	Mg	12	K	L	$3s^2$	
aluminium	Al	13	K	L	$3s^2 3p$	
silicon	Si	14	K	L	$3s^2 3p^2$	
phosphorus	P	15	K	L	$3s^2 3p^3$	
sulphur	S	16	K	L	$3s^2 3p^4$	
chlorine	Cl	17	K	L	$3s^2 3p^5$	
argon	Ar	18	K	L	$3s^2 3p^6$	
potassium	K	19	K	L	$3s^2 3p^6$	4s
calcium	Ca	20	K	L	$3s^2 3p^6$	$4s^2$

Figure 4.1: The atomic configuration of the first 20 elements in the periodic table
Fig. taken from Tennyson (2007)

and the ground state is $1s^2 2s^2 2p^2$. The superscript gives the number of electrons in that orbital. Neon has a closed shell electron distribution and the ground state is given by: $1s^2 2s^2 2p^6$ (see Fig. 4.1).

Ions which have the same number of electrons are isoelectronic series. These ions have the same ground-state configuration and hence similar chemical properties. Fe XVII (16 times ionised Fe) is called neon-like iron.

4.2 Russell-Saunders Coupling scheme

Complex atoms contain more than one electron and thus they have several sources of angular momentum. Ignoring nuclear spin effects, the total angular momentum (spin, orbital) is called J. The convention in the nomenclature is that capital letters are used for the many electron momenta and lower case letters are used for single electron momenta.

In the Russell-Saunders coupling scheme the orbital and spin angular momenta of the electrons are added (vector wise) to give the total angular moment:

- $L = \sum_i l_i$
- $S = \sum_i s_i$
- $J = L + S$

Closed shells have both $L = 0$ and $S = 0$. The *term* is given is a standard notation:

$$^{2S+1}L^{(o)} \tag{4.8}$$

with following nomination rules:

- S = 0 : a singlet
- S = $\frac{1}{2}$: a doublet
- S= 1 : a triplet
- L = 0 : an S state
- L = 1 : an P state
- L = 2 : an D state...
- superscript o means : odd parity

To illustrate the nomination rule we take O III with the configuration $1s^2\,2s^2\,2p\,3d$. 2p : l_1 = 1 and s_1 = 1/2, 3d is l_2 = 2 and s_2 = 1/2 This gives as possible vector additions: L = 1,2,3 and S = 0,1 (see also Fig. 4.2):

Each state of an atom or ion is characterised by a unique combination of L, S and J dubbed a *level*.

In the spectroscopic notation, a *term* is a configuration with a specific value of L and S. A state with S=0 is a singlet, a state with S=1 is a triplet. The value of the total orbital angular momentum L is given as S,P,D, F which is L=0,1,2,3... respectively.

	L	S	J	Level
$\underline{J}=\underline{L}+\underline{S}\Rightarrow$	1	0	1	$^1P^o_1$
	1	1	0,1,2	$^3P^o_0, ^3P^o_1, ^3P^o_2$
	2	0	2	$^1D^o_2$
	2	1	1,2,3	$^3D^o_1, ^3D^o_2, ^3D^o_3$
	3	0	3	$^1F^o_3$
	3	1	2,3,4	$^3F^o_2, ^3F^o_3, ^3F^o_4$.

Figure 4.2: All possible states of O III in the $1s^2\,2s^2\,2p\,3d$ configuration. *Fig. taken from Tennyson (2007)*

The *terms* have different energies. Every term will be split into different levels according to the J-values (relativistic effects)

$$^{2S+1}L_J^{(o)} \tag{4.9}$$

For each level characterised with a particular value of J, there are 2J+1 sub-levels and are called *states*. When an external field is present, the *Zeeman effect* will split the level of a particular value of J into these 2J+1 sub-levels with different energy.

4.2.1 Hund's rules

The Hund's rules are related to the energy levels and their order of appearance in the L-S coupling scheme.

1. For a given configuration, the term with maximal spin multiplicity lies lowest in energy

2. For a given configuration and spin multiplicity, the term with the largest value of L lies lowest in energy

3. For atoms with less than half-filled shells, the level with the lowest value of J lies lowest in energy

4. For atoms with more than half-filled shells, the level with the highest value of J lies lowest in energy.

As an example consider the first excited configuration of He (1s2s): this has L=0 and both a S=0,1 are possible. The ^{3}S term ($^3S_1$ level) is lower in energy than the ^{1}S term ($^1S_0$ level).

The Sodium D lines are intrinsically very strong and even at very low spectral resolution, they provide an important spectral signature to allow spectral type determination on the basis of low resolution data.

The transitions are within the terms:

$$^2P^o_{\frac{1}{2},\frac{3}{2}} \rightarrow^2 S_{\frac{1}{2}} \tag{4.10}$$

and the Sodium D lines (doublet) are:

$$D_2\ 5890\text{Å}\ 3p - 3s\ ^2P_{\frac{3}{2}} -^2 S_{\frac{1}{2}} \tag{4.11}$$

$$D_1\ 5896\text{Å}\ 3p - 3s\ ^2P_{\frac{1}{2}} -^2 S_{\frac{1}{2}} \tag{4.12}$$

4.2 .2 Parity and the Laporte Rule

The parity of a wave function is determined by how a wave function behaves upon inversion Odd parity gives negative but identical wavefunctions upon inversion

$$(-1)^{l_1+l_2+l_3+l_4..+l_N} \tag{4.13}$$

As an example: the O III configuration $1s^2\,2s^2\,2p\,3d$ is odd since (-1)$^{1+2}$ is negative.

The parity is important since it leads to an important dipole selection rule which is the rule *Laporte* which states that *all electric dipole (strongest transitions) transitions connect states of opposite parity*.

4.3 Selection Rules

Strong transitions are driven by electric dipoles which obey both rigorous rules which should always be valid and propensity rules, which, when violated, lead to much weaker (forbidden) transitions. The selection rules are summarised in Fig 4.3.

The associated Einstein coefficients are in the range:

	Electric dipole	Electric quadrupole	Magnetic dipole
1.	$\Delta J = 0, \pm 1$ Not $J = 0 - 0$	$\Delta J = 0, \pm 1, \pm 2$ Not $J = 0 - 0, \frac{1}{2} - \frac{1}{2}, 0 - 1$	$\Delta J = 0, \pm 1$ Not $J = 0 - 0$
2.	$\Delta M_J = 0, \pm 1$	$\Delta M_J = 0, \pm 1, \pm 2$	$\Delta M_J = 0, \pm 1$
3.	Parity changes	Parity unchanged	Parity unchanged
4.	$\Delta S = 0$	$\Delta S = 0$	$\Delta S = 0$
5.	One electron jumps Δn any $\Delta l = \pm 1$	One or no electron jumps Δn any $\Delta l = 0, \pm 2$	No electron jumps $\Delta n = 0$ $\Delta l = 0$
6.	$\Delta L = 0, \pm 1$ Not $L = 0 - 0$	$\Delta L = 0, \pm 1, \pm 2$ Not $L = 0 - 0, 0 - 1$	$\Delta L = 0$

Figure 4.3: Selection rules for atomic spectra. Rule 1,2 and 3 must always be obeyed. For electric dipole transitions, intercombination lines violate rule 4 and forbidden lines violate rule 5 and/or 6. Electric quadrupole and magnetic dipole transitions are also described as forbidden. *Fig. taken from Tennyson (2007)*

1. Electric dipoles : typically 10^8 s^{-1}
2. Magnetic dipoles: typically 10^3 s^{-1}
3. Electric Quadrupoles: typically 1 s^{-1}

Photons do not change spin. ($\Delta S = 0$). For high Z atoms or ions, relativistic effects can induce weak spin changing transitions. These are called *intercombination lines* and are indicated with an open]. An example is:

$$CIII]\ 2s^2\,{}^1S - 2s2p\ {}^3P^o \ \text{ at } \ 1908.7\text{Å} \tag{4.14}$$

This is an interesting transition because the 2s2p ${}^3P^o$ state is metastable which means that it cannot decay along allowed radiative transitions. The above transi-

tion determines the lifetime of the state. It is interesting to note that the $^3P^o$ term splits into three levels: $^3P^o_0$,$^3P^o_1$,$^3P^o_2$. The intercombination line at 1908.7 Å is the $^1S_0$-$^3P^o_1$ line with an Einstein coefficient of 114 s^{-1}. The transition $^1S_0$-$^3P^o_2$ (1906.7 Å) is completely forbidden by dipole selection rules (ΔJ = 2). It only occurs via a very weak magnet quadrupole transition. This line is 10^5 times smaller than the weak 1908.7 Å line and has an A value of 0.0052 s^{-1}. The J=0-0 line is not observed.

Electric dipole transitions which violate the propensity rules 5 and/or 6 are called *forbidden*. An example is given by

$$[CIII]\ 2s^2\ {}^1S_0 - 2p3s\ {}^1P^o_2\ \ at\ \ 322.7\text{Å} \tag{4.15}$$

The *Grotrian* diagrams give the energy levels of the atom with the different levels and indicate possible allowed transitions. The intercombination and forbidden lines are also given. Examples are given in Fig. 4.4, 4.5.

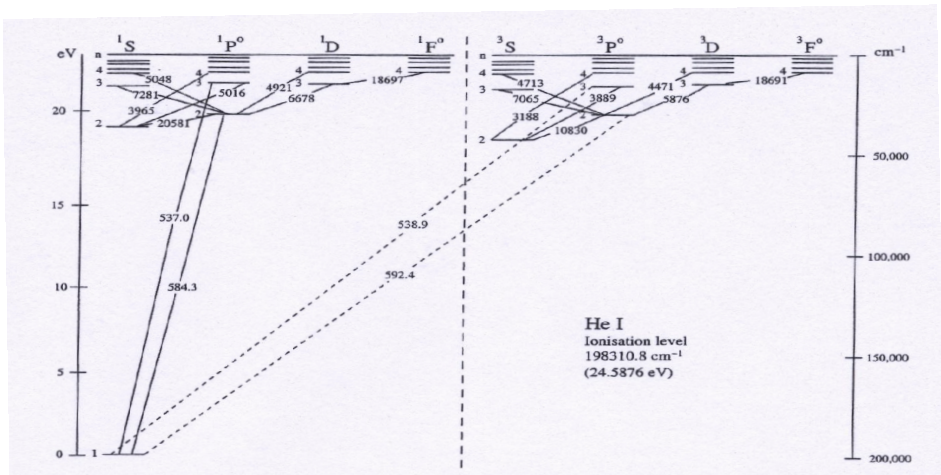

Fig. 5.2. Grotrian diagram for He I. The running numbers denote the principal quantum number of the active electron. The left-hand side of the figure is for 'para' singlet helium and the right-hand side is for 'ortho' triplet helium.

Figure 4.4: Grotrian diagram of He I

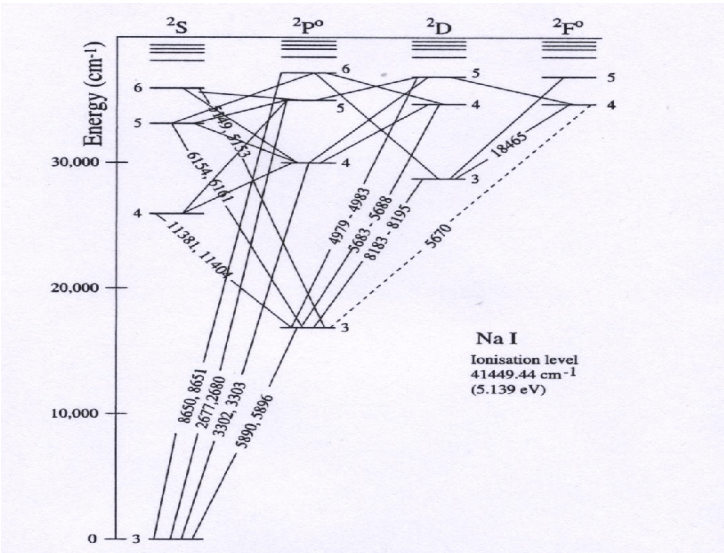

Figure 4.5: Grotrian diagram of He I

4.4 Nebular spectra

States decaying only via forbidden lines live for a long time and are called *metastable*. Forbidden lines are difficult to study in the lab since collisional-free conditions are needed and only occur at very low densities.

Forbidden lines are important in hot, low density regions (e.g. H II regions, Planetary Nebulae (PNe), solar corona, Earth's aurora) and those lines may form a very important way to cool. In Fig 4.6 a typical spectrum of a PNe. The transitions are weak and have low optical depth but nonetheless can be the dominant lines under certain special conditions.

Lines observed in Nebulae can come from different processes which involve:

1. *Electron collisions.* Thermal in origin, populate low-lying excited states

2. *Recombination.* cascade of emissions by recombination of an ion and an electron. They can populate highly-excited states which are inaccessible for collisional excitation.

3. *Optical pumping (resonance-fluorescence).* Rather specific line-emission. It requires detailed physics of the system being observed.

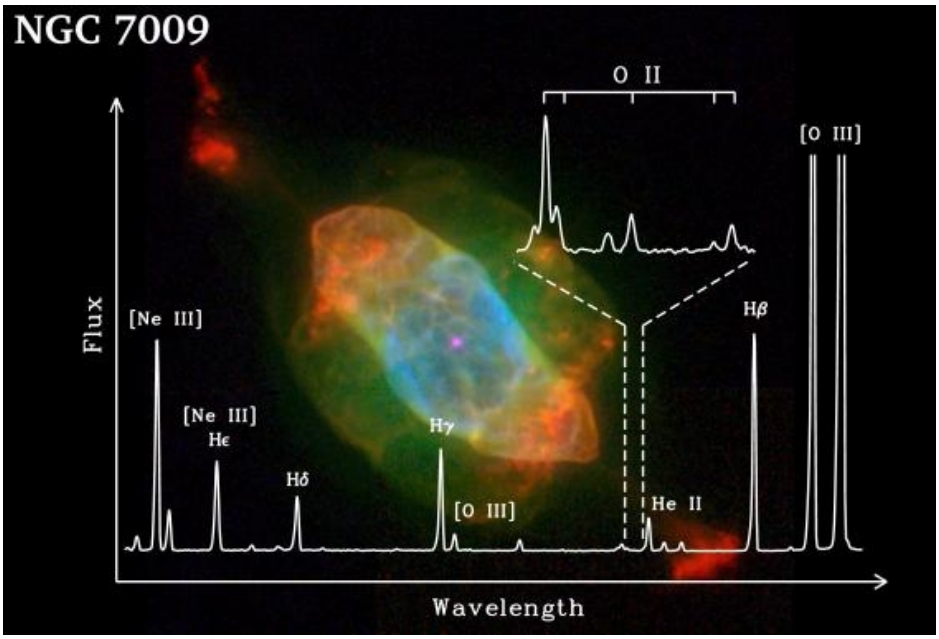

Figure 4.6: A typical spectrum of a Planetary Nebula, in this case NGC 7009

4.4 .1 Electron collisions

The lines observed in Nebulae which are thermal in origin can be forbidden lines when the metastable levels are excited by electron collisions.

The most famous are certainly the [OIII] lines which are:

$$5006.84\,\text{Å}\ [OIII]\ 1s^2 2s^2 2p^2\ {}^1D_2 -^3 P_2 \tag{4.16}$$
$$4958.91\,\text{Å}\ [OIII]\ 1s^2 2s^2 2p^2\ {}^1D_2 -^3 P_1 \tag{4.17}$$

They are strongly forbidden for electric dipoles by the Laporte rule and occur only as very weak magnetic dipole transitions. They have Einstein coefficients of 1.8×10^{-10} and 6.2×10^{-11} respectively. The excited terms associated with the ground state configuration are populated with electron collisions. ${}^1S$ term is higher in energy.

$$4363.2\text{Å}\ [OIII] 1s^2 2s^2 2p^2\ {}^1S_0 -^1 D_2 \tag{4.18}$$

The emission rate from ^{1}D relative to ^{1}S depends directly on the electron temperature because the levels involved are collisionally excited. The higher the T_e,

the stronger the $\lambda 4363$ line since the ^1S will be more populated. This is because the forbidden lines have similar lifetimes. Maps tracing the electron temperature can be obtained by adding and dividing calibrated images taken with filters on the specific lines.:

$$[OIII](\lambda 4959 + \lambda 5007)/\lambda 4363 \tag{4.19}$$

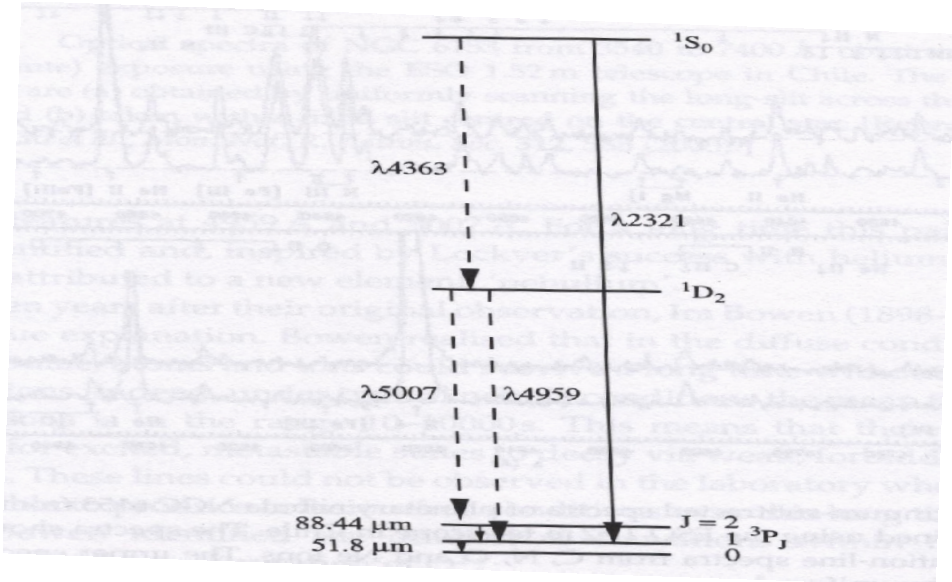

Figure 4.7: The levels involved in the nebular [OIII] lines.

In the infrared, fine-structure lines of [OIII] can be observed. Those lines are transitions in the $2p^2$ ground state (see Fig. 4.7). They are weak magnetic dipole transitions and are detected by far-IR spectrographs mounted in ESA satellite ISO:

$$51.8\ \mu m\ [OIII]:\ 2p^2\ {}^3P_1 -^3 P_2 \tag{4.20}$$
$$88.4\ \mu m\ [OIII]:\ 2p^2\ {}^3P_0 -^3 P_1 \tag{4.21}$$
$$\tag{4.22}$$

In Fig. 4.8 we show 2D images of PNe which are taken through special narrow band filters which samples only one line. The false colours have physical meaning because (red,green,blue) is mostly used for the ([N II], [O III], He II) images.

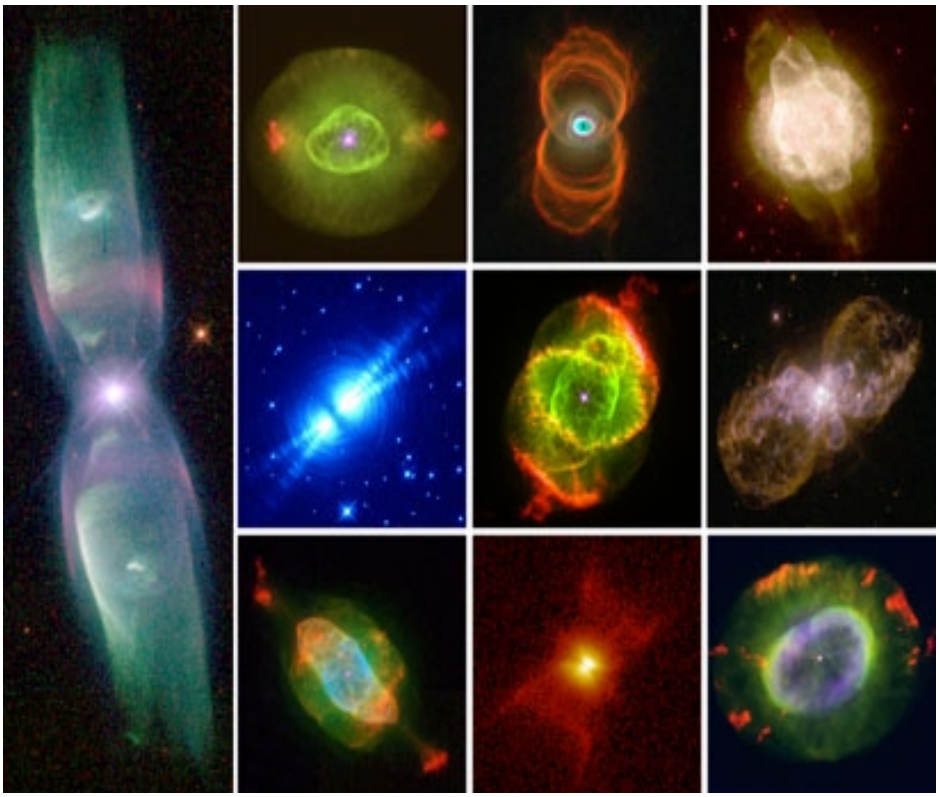

Figure 4.8: With special narrow band filters, tuned to sample the most important diagnostic lines, a good 2D map of the line-emission is shown in those colour coded images. Fig. from Bruce Balick at this web page

4.4 .2 Bowen (1898-1973) lines: Resonance-Fluorescence

In PNe spectra many allowed transitions are detected from O III (see Fig. 4.4 .2) which come from energy levels which are too high in energy to be populated by electron collisions for typical electron temperatures in PNe. There is a whole series of these lines in the UV inbetween 310 and 380 nm. The transitions are electric dipole transitions which are allowed. It was Bowen (1898-1973) who realised that the population of the $^3P_2^0$ level was not thermal but the excitation can happen thanks to an accidental resonance : The Ly$_\alpha$ of He II lines has very similar energy than the excitation energy of the O III level. The $^3P^0$ level will cascade down to make what is known as the Bowen lines (see Fig. 4.9).

This process is called Resonance-Fluorescence and the process involves pumping of the excited level by, in this case, an accidental energy match between transitions of different species. The He II Lyman$_\alpha$ line is a recombination line in hotter

nebulae so there is a large supply of those photons.

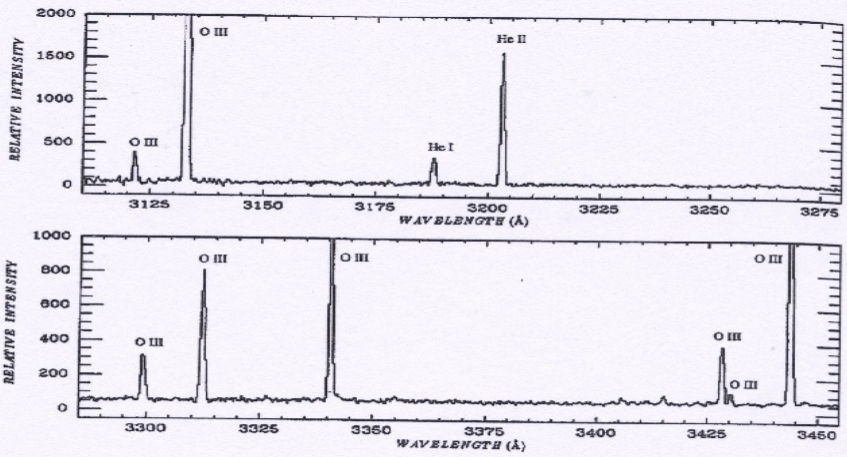

Fig. 7.5. O III emission lines excited by the Bowen mechanism from planetary nebula NGC 3242, recorded using the Isaac Newton Telescope at La Palma. [Adapted from X.-W. Liu and J. Danziger, *Mon. Not. R. Astron. Soc.* **261**, 465 (1993).]

Another example which is relevant in astronomical spectra is the match between the recombination line Ly_β of hydrogen at 1025.72 Å which can pump the transition:

$$1025.77\,\text{Å OI } 2p^4\ {}^3P_2 - 2p^3({}^4S^0)\ 3d\,{}^3D^0 \tag{4.23}$$

The fine structure splitting is small in this case so all three ${}^3D^0$ lines will be populated.

Whether the Bowen mechanism for [OIII] can operate or not, depends on the presence of pumping photons. In colder [HII] regions those allowed [OIII] lines will not be observed by the lack of Ly_α He II photons.

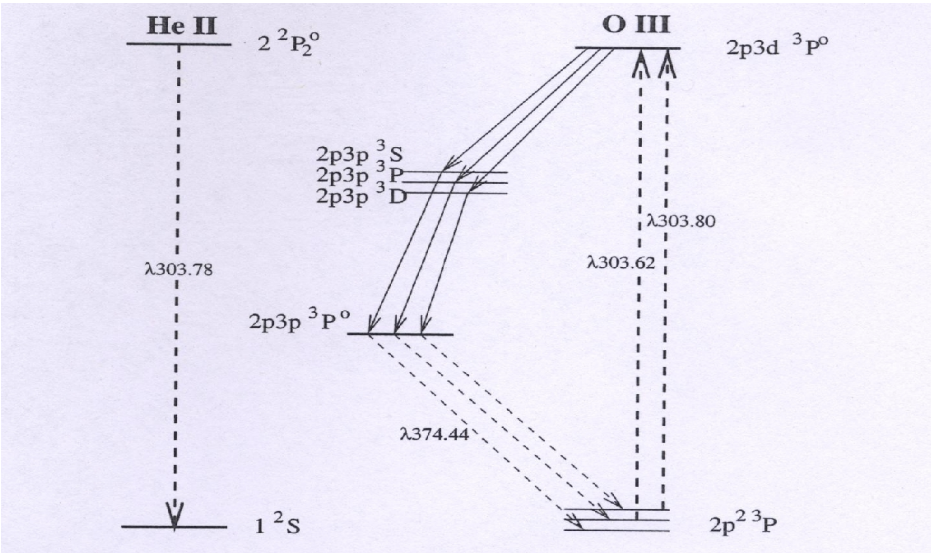

Figure 4.9:

4.5 Molecules

In colder stars (check e.g. the late spectral types at UVESPROP) we can detect that the optical spectrum is dominated by molecular bands, but it was with the advent of radio astronomy, that the molecular astrophysics boasted. The search and study of molecules in the interstellar, circumstellar media as well as in atmospheres led to the discovery of about 120 molecules.

In the following the limit is mainly on diatomic molecules. Polyatomic molecules all dissociated at about 4000K while some diatomic molecules can survive up to about 8000K. In Table 4.1 we list the dissociation energies of some of the most important molecules. H_2 is the most abundant molecule in space but it is hard to detect. Also CO is very abundant. It has a very strong binding and will form at high temperature. For stellar photospheres it is the C/O ratio which will determine which molecules can form in the extended photosphere or circumstellar medium: an excess of O will make that oxides can form, while for excess C, carbon based molecules will form in abundance.

Molecular spectroscopy is far more complicated because there is no single charge centre about which the electrons move. The wavefunctions are less symmetric and harder to compute. Also the nuclei themselves move and the vibrational and rotational motions give rise to discrete spectra.

In first approximation, the energy of a molecule can be represented by:

Table 4.1: Dissociation energy in eV.

	CN	HCN	C_2	C_2H	C_2H_2	CH
D_0	7.76	13.085	6.21	12.069	16.776	3.465
	CH_4	NH	NO	CO	H_2O	OH
D_0	17.021	3.47	6.497	11.092	9.512	4.392
	SiO	TiO	VO	ZrO	YO	LaO
D_0	8.233	6.87	6.437	7.89	7.413	8.23

$$E = E_e + E_v + E_r. \tag{4.24}$$

- E_e: electronic energy
- E_v: vibrational energy
- E_r: rotational energy

With $E_e > E_v > E_r$. The molecular spectra will be divided into:

- Pure rotational transition: transition within the same electronic and vibrational state (radio)
- ro-vibrational transition: transition between two vibrational levels of the same electronic state. The possible rotational transitions make this a 'band' (IR)
- electronic spectrum: transition between two ro-vibrational states of different electronic states of the molecule (UV-Visible).

Homo-nuclear molecules like H_2 and C_2 have no strong pure rotational nor pure vibrational transitions.

4.5 .1 Nomenclature

Traditionally a transition from the electronic state A to B, which includes a vibrational transition ν'' to ν' as well as a rotational transition J′ to J′ is given by :

$$B(\nu', J') \leftarrow A(\nu'', J'') \tag{4.25}$$

The convention is that the $'$ are for the upper state, the $''$ for the lower state. The quantum states in electronic transitions are depicted:

$$\begin{aligned} \Lambda = 0 &= \Sigma \\ = 1 &= \Pi \\ = 2 &= \Delta \end{aligned} \tag{4.26}$$

The labeling of the electronic states is based on the symmetry of the molecule and for diatomic molecules only two separate symmetry cases need to be considered: the homonuclear and heteronuclear diatomics. Abundant examples of the former are H_2 O_2 and CO,CH,CN of the latter.

The electronic spin is normally not very well coupled and the sum of the spins is depicted S (paired electrons in closed shells make no contribution to S). The spin multiplicity 2S+1 is often given as a left superscript.

For diatomic molecules, the total orbital angular momentum L is strongly coupled to the nuclear axis and the components (given by Γ) are taken along the nuclear axis. Electronic states are labelled by the Greek equivalent to the Latin letter.

The symmetry of the electronic wavefunctions of diatomics which contribute to the electronic selection rules and which are reflected into the nomenclature. For homonuclear diatomics, we can consider the behaviour of the wavefunction upon swapping the nuclei. Electronic states which are positive with respect to this interchange are known as *gerade* or simply g, the *ungerade* u. The g/u label is given as a trailing subscript. The ground state of H_2 is $^1\Sigma_g^+$. Another symmetry is the reflection of the wavefunction through any mirror plane containing the nuclei. This parity behaviour is denoted by a trailing superscript. The nomenclature becomes quite heavy when the electronic state is preceeded by a lettre :

- X labels the ground electronic state
- A,B,C,... labels states of same spin multiplicity as the ground state

- a,b,c,... labels states of different spin multiplicity to the ground state.

In the literature, the extra labeling is not always strictly applied and quite some confusing persists in the nomenclature because of historic reasons.

4.5 .2 Born-Oppenheimer approximation

In the Born-Oppenheimer approximation, it is assumed that the the wavefunctions for the motions of electrons can be separated from the wavefunctions for the motions of the nuclei. This is a reasonable approach since the electrons are much lighter than the nuclei which make that they move much faster. Typical values for $m_e/M_{molecule}$ is 10^{-4} - 10^{-5}. For any motion of the nuclei, the electrons will relax instantly. For any position of the nuclei, the wavefunctions of the electrons are considered separately. The electronic energy associated with each of these electronic wavefunctions will yield the energy curves in which are given typically the energy of the electronic wavefunction, in function of the bondlength.

If a is the typical molecular size, the momentum of an electron is of the order of $\hbar$/a and the electronic energy states have typical spacings of :

$$E_{elect} \sim \frac{\hbar^2}{m_e a^2} \tag{4.27}$$

For typical molecular sizes ($\sim 10^{-8}$ cm) this is a few eV.

For stable molecules: intranuclear potential has a minimum and vibrations around this minimum can be described as a harmonic oscillator (see below). The potential takes the form :

$$\frac{1}{2} M_{molecule}\, \omega^2 \zeta^2 \tag{4.28}$$

With ζ the displacement form the equilibrium position

$$E_{veb} \sim \hbar\omega \sim \left(\frac{m_e}{M_{molecule}}\right)^{1/2} E_{electron} \tag{4.29}$$

ω is the frequency of the vibration and we assumed that ζ is in the order of a. The vibrational energies are typically tenths or hundreds of an eV, so in the IR.

To estimate typical rotational energy levels, we can assume the molecule rotates as a rigid rotator. The moment of inertia I is then in the order of $M\, a^2$ with

M the total mass of the molecule. If the angular momentum of this motion is $l\,\hbar$ (l=0,1,2,3) the energy of rotation is (see also below):

$$E_{rot} \sim \frac{\hbar^2\, l(l+1)}{2\, I} \tag{4.30}$$

With I the moment of inertia ($I \sim M_{molecule} a^2$). Which means

$$E_{rot} \sim (\frac{m_e}{M_{molecule}})\, E_{elect} \tag{4.31}$$

This is in the far-IR or radio wavelength-regime.

4.5 .3 Schrödinger equation

The Schrödinger equation for diatomic molecules with nucleus A of mass M_A and nucleus B of mass M_B is given by:

$$\left(-\frac{\hbar^2}{2M_A}\Sigma_A^2 \; - \; \frac{\hbar^2}{2M_B}\Sigma_B^2 - \frac{\hbar^2}{2m_e}\Sigma_i^2 \; + \; V_e \; - \; E \right) \Psi(R_A, R_B, r_i) = 0 \tag{4.32}$$

The first terms are the kinetic energy operators for the motion of nuclei A and B respectively, the third term gives the kinetic energy operator for the electrons. The potential V_e is determined by the various Coulomb interactions within the molecule. Within the Born-Oppenheimer approximation, the wavefunctions are split into an electronic and nuclear term. For every internuclear distance, the electronic wavefunction needs to be solved and the internal motions.

The effective mass of the problem is the reduced mass, which differs significantly from the mass of one of the components :

$$\mu = \frac{M_A\, M_B}{M_A + M_B} \tag{4.33}$$

The effect on the energy levels of change in the reduced mass is significant and molecules are very well suited to trace isotopic ratios because the isotopic shift is significant.

We can reduce the Schrödinger equation when the translational motion is ignored, the equation is given with respect to the centre of mass and we rewrite in polar coordinates:

$$\left[\frac{\hbar^2}{2\mu}\Sigma^2 + V(R) - E\right]\psi_n(\mathbf{R}) = 0 \tag{4.34}$$

with **R**(R,θ,ϕ) a vector given the internuclear separation R and the orientation (θ,ϕ) of the molecular axis relative to a reference axis.

Vibrational motion and rotational motion cannot be separated rigorously but in a good first approximation we get:

$$\psi_n(\mathbf{R}) = \psi_{vib.}(R)\ \psi_{rot}(\theta,\phi) \tag{4.35}$$

Solutions of the rotational part without the potential are given by spherical harmonics:

$$\Psi_r(\theta,\phi) = Y_{J,M_J}(\theta,\phi) \tag{4.36}$$

with the rotation energy given by:

$$E_r = \frac{\hbar^2}{2\,\mu\,R^2}\,J(J+1) \tag{4.37}$$

in which the rotational angular momentum quantum number J takes integer values, and the projection of J onto the molecular axis is denoted by M_J. There are 2J+1 possible values of M_J.

When we assume a rigid rotator, R is fixed at some value R_0, independent of the rotation. The moment of inertia (in general this is I = $\sum_i m_i\,r_i^2$ the sum over the different nuclei multiplied with the square of the distance towards the axes of rotation) is for a rigid rotator equal to: $I_0 = \mu\,R_0^2$. The rotational energy is:

$$E_r = \frac{\hbar^2}{2I_0}J(J=1) = B_0 J(J+1) \tag{4.38}$$

B_0 is known as the rotational constant. In practice, however, molecules are no rigid rotators and at high rotational rates, the nuclei will drift apart. A rotational spectrum of a molecule will be needed to determine the rotational constant. In the R-coordinate this is:

$$\left[-\frac{\hbar^2}{2\mu}\frac{d^2}{dR^2} + V(R) - E_v\right]\psi_v(R) \tag{4.39}$$

The radial part of the Schrödinger equation contains the potential which is not only dependent on R and has no algebraic solution. For low vibrational levels, V(R) can be approximated by a parabola with minimum R_e: V(R) = 1/2 k $(R-R_e)^2$. The vibrational part of the Schrödinger equation is then reduced to an harmonic oscillator.

The energy levels are given by:

$$E_v = \hbar\omega(v + 1/2) \tag{4.40}$$

$$\omega = \left(\frac{k}{\mu}\right)^{1/2} \tag{4.41}$$

with v the vibrational quantum number. Also here, the reduced mass is important for studies of molecules with different isotopic composition. In molecular spectroscopy it is custom (unfortunately) to give $\hbar\omega$ in cm^{-1}... In this approximation, the vibrational levels are equidistant ! In Fig 4.10 the vibrational levels and the potential is given for a more realistic potential.

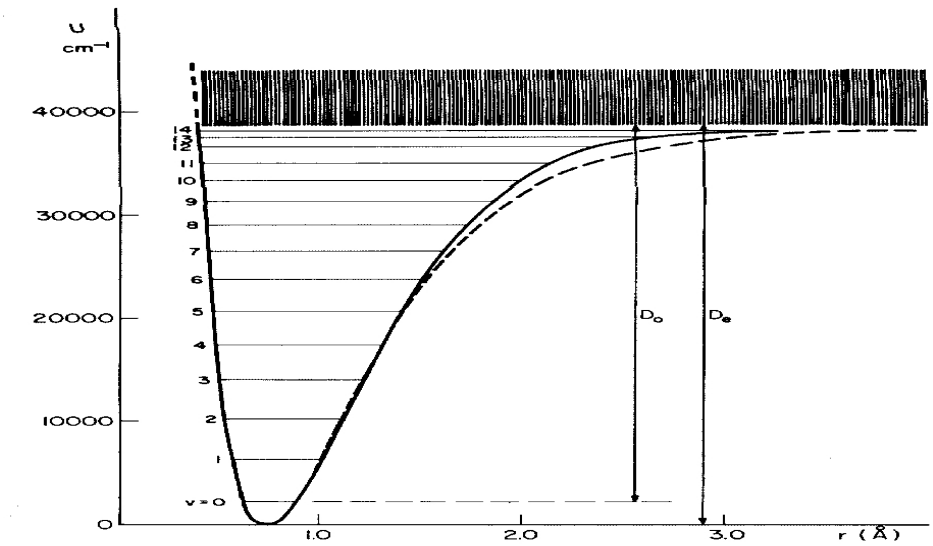

Figure 4.10: The vibrational levels and the potential curve with a more realistic shape than in the text, where a parabola was used. The levels are no longer equidistant at high vibrational states. This curve is from H_2 in the ground electronic state.

4.5 .4 Tri-atomic molecules

For molecules with more atoms the modes of vibration increase in complexity. For N atoms, we need 3N-6 coordinates to indicate the relative positions in a stationary, non-rotating molecule. This is depicted in Fig 4.11, where different vibrational modes are illustrated.

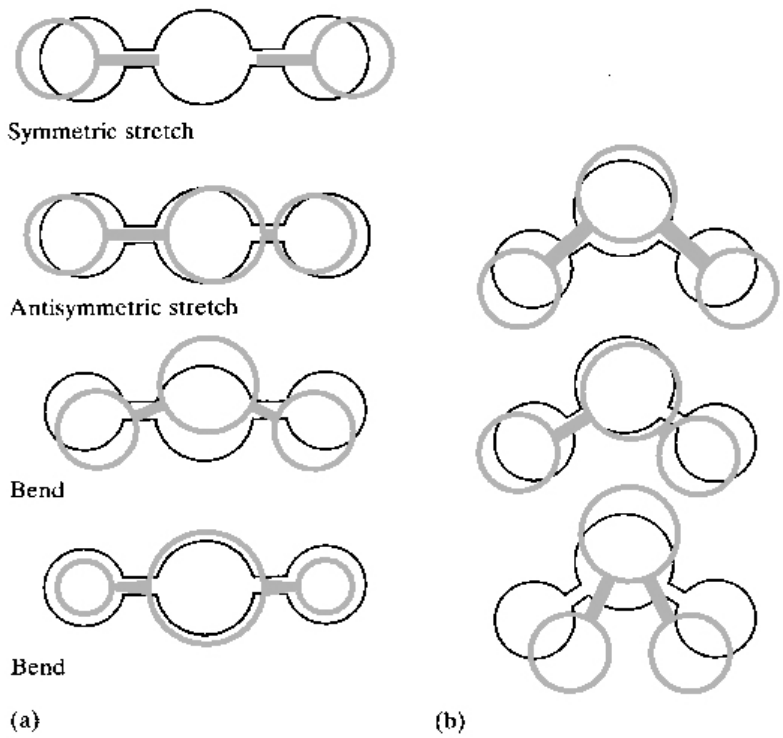

Figure 4.11: The vibrational modes of a linear tri-atomic molecule (left) and of a angular triatomic molecule.

4.6 Molecular spectroscopy

In Fig. 4.12 we illustrate the different transitions of a molecule and in this section we touch upon the transition probabilities of the different modes.

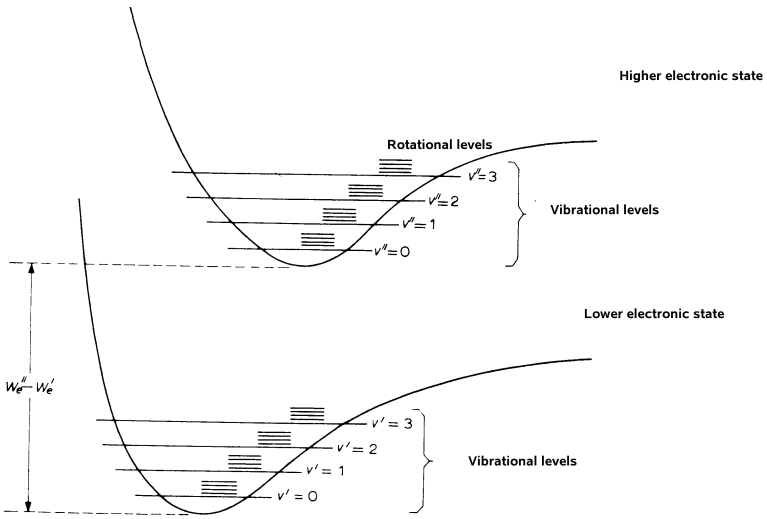

Figure 4.12: Illustration of the different transitions of a molecule.

4.6 .1 Pure rotational lines

Within the rigid rotation model (see Equation 4.38), it is straightforward to obtain the energy of the rotational transition:

$$\Delta E_{rot} = B_0 \left[J'(J'+1) - J''(J''+1) \right] \tag{4.42}$$

So the rotational spacings trace the molecular rotation constant. For diatomic molecules in the Σ symmetry electronic states, the selection rule is:

$$\Delta J = \pm 1 \tag{4.43}$$

which means that a rigid rotator leads directly to a very regular pure rotational spectrum with equally spaced transitions ($\Delta E_{rot} = 2B_0 J'$). A transition from J′ →J″ is a 1-0 emission at $2B_0$, the reverse yields an absorption.

The selection rules for pure rotational lines can be summarised:

1. d different from 0: permanent dipole moment of a molecule

$$d = Z_1\, e\, r_1 + Z_2\, e\, r_2 + d_e \tag{4.44}$$

2. $\Delta\, J$ = +/- 1

d_e is the electronic component. The first selection rule states that a molecule needs to have an asymmetric charge distribution in order to have a dipole allowed rotational spectrum. Heteronuclear diatomics do have a permanent dipole, homonuclear do not have one. This means that molecules like H_2, N_2 C_2 do not have a dipole-allowed rotational spectrum... Those molecules will cool therefore quite difficult.

In Fig 4.13 the pure rotational spectrum of $^{12}C^{16}O$ is shown including the isotopic shift. CO is a very abundant molecule because of the high abundance of its components but also because it has a very high binding energy (see Table 4.1). The most abundant molecule is H_2, but this is more difficult to observe in cold regions because of the lack of a strong rotational spectrum. A commonly used number density ratio between both is n(CO) = 10^{-4}n(H_2).

The strength of the isotopic effect for CO can be estimated since the rotational constant for a rigid rotator is given by:

$$B_0 = \frac{\hbar^2}{2\mu r_o^2} \tag{4.45}$$

$$\mu = \frac{M_C\, M_O}{M_C + M_O} \tag{4.46}$$

Assuming that the bond length r_o remains unchanged, a replacement of ^{12}C by ^{13}C will lead to an increase in reduced mass and hence a decrease in the rotational constant. This leads to a significant frequency shift which can be resolved easily.

In Fig. 4.14 the rich molecular diagnostics of pure rotational transitions is illustrated using the Orion giant molecular cloud. This rich potential is for the moment only harvested from the ground within the atmospheric windows. This will change when the instrument HIFI will become operational. HIFI is one of the instruments on board of the ESA satellite Herschel to be launched in 2008.

4.6 .2 Ro-Vibrational transitions

Ro-vibrational transitions within one electronic state are illustrated in Fig. 4.15. Within the harmonic oscillator approximation, the electric dipole selection rule is:

$$\Delta v = \pm 1 \tag{4.47}$$

which leads directly to (Equation 4.41) $\Delta E_v = \hbar\omega$.

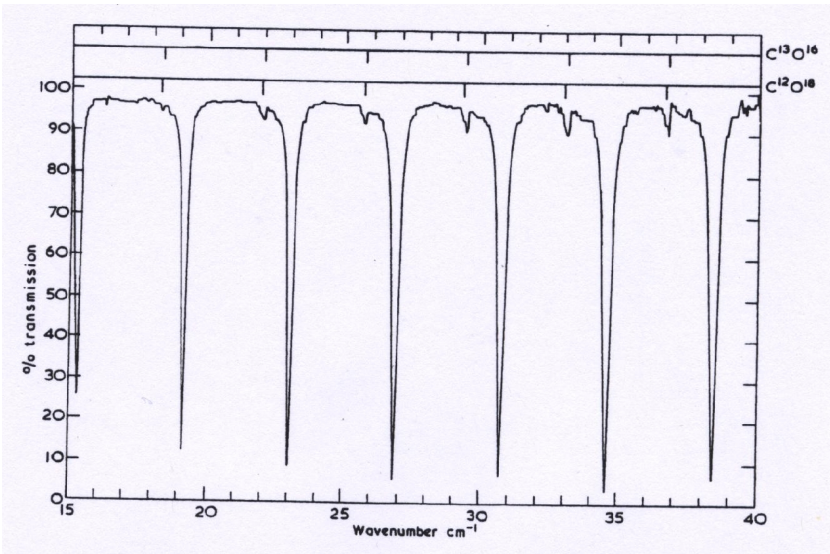

Figure 4.13: Lab spectrum of the rotational levels of CO and the associated isotopic shifts for two different isotopic settings. $^{12}C^{16}O$ is dominant in terrestrial abundances. *Fig. taken from Tennyson (2007)*

For anharmonic molecules, different changes in Δv are allowed but these are much weaker. Vibrational transitions with a change in v by more than one quantum number are called *overtones*. A vibrational transition, is usually also associated with a rotational transition as well and the selection rules for those are:

The selection rule $\Delta J = \pm 1$ with J′ the upper state and J″ the lower we get:

- $\Delta J = J' - J'' = +1$ ('R branch'):

$$\Delta E_R = \hbar\omega + J'(J'+1)B_1 - J''(J''+1)B_0 \cong \hbar\omega + 2B(J''+1) \quad (4.48)$$

- $\Delta J = J' - J'' = -1$ ('P branch'):

$$\Delta E_P = \hbar\omega + J'(J'+1)B_1 - J''(J''+1)B_0 \cong \hbar\omega - 2BJ'' \quad (4.49)$$

When the rotational constants of both states are similar, the P branch will be at lower energy than the bandhead while the R branch will be at higher energy.

If the ground state of the molecule is a Π-state ($\Lambda = 1$), both $\Delta J = 0$ and $\Delta J = \pm 1$ transitions are allowed. $\Delta J = 0$ gives a 'Q branch' with

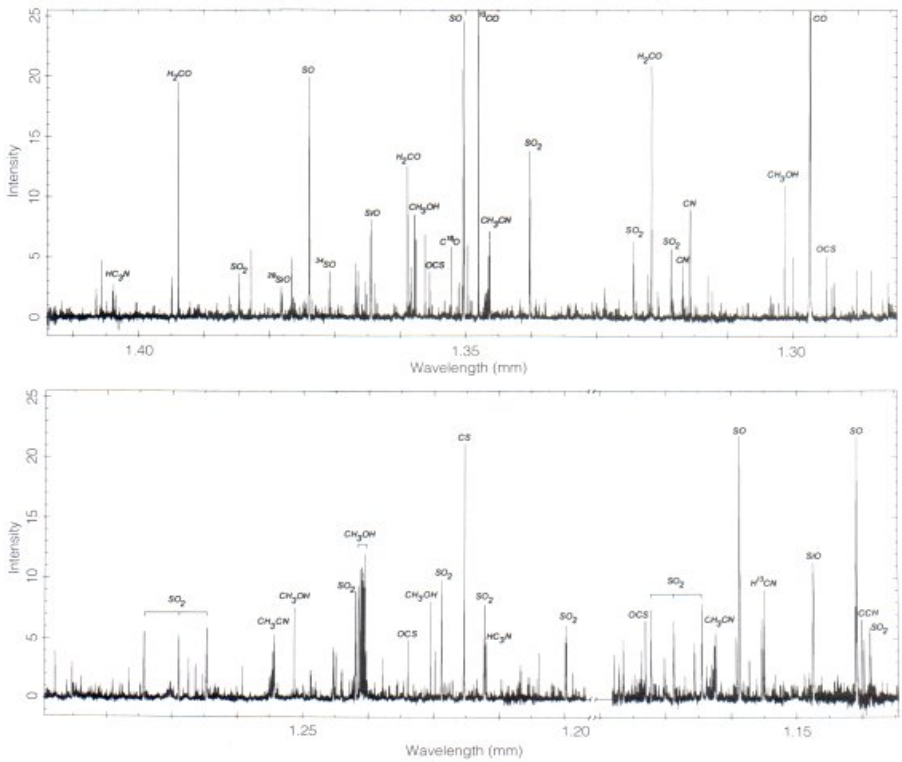

Figure 4.14: A millimeter-wavelength spectrum of the core of the Orion giant molecular cloud, made at the Owens Valley Radio Observatory. The spectrum covers a small interval in the atmospheric window at 1.3 mm. Over 800 spectral features are seen! This type of data is needed to understand the chemistry of cold and dense interstellar regions. Fig. from `http://loke.as.arizona.edu/ ckulesa/research/overview.html`.

$$\Delta E_P = \hbar\omega + J'(J'+1)B_1 - J''(J''+1)B_0 = \hbar\omega J''(J''+1)(B_1 - B_0) \quad (4.50)$$

The different Q band lines will not have a big difference in energy spacing and they will cluster together. In Fig. 4.16 we illustrate the spectral lines of AlH including the different P,R and Q branches.

Fig. 4.16 and 4.17 illustrations are given of ro-vibrational bands of two molecules.

For homonuclear molecules, the dipole moment is 0 for all internuclear separations and also here, vibrational transitions are dipole forbidden. Symmetric

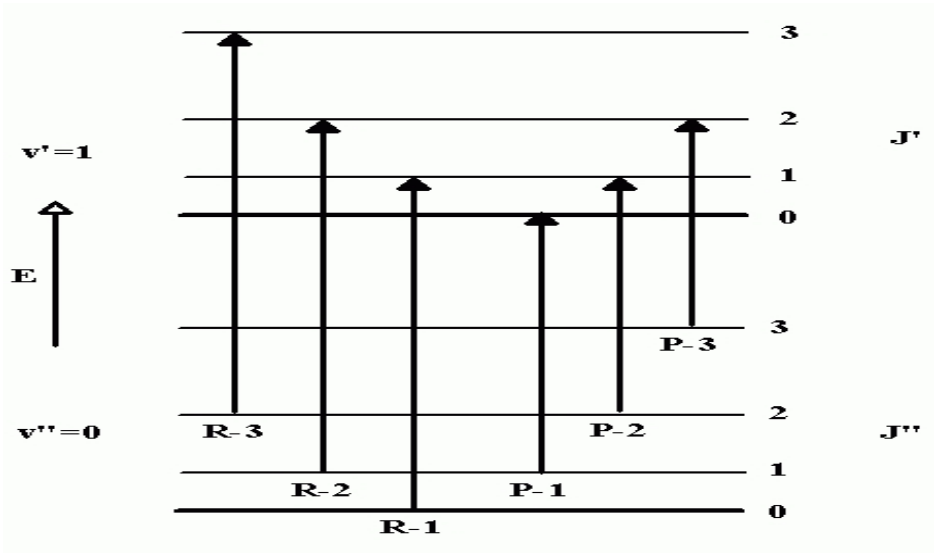

Figure 4.15: Illustration of ro-vibrational transitions in a molecule.

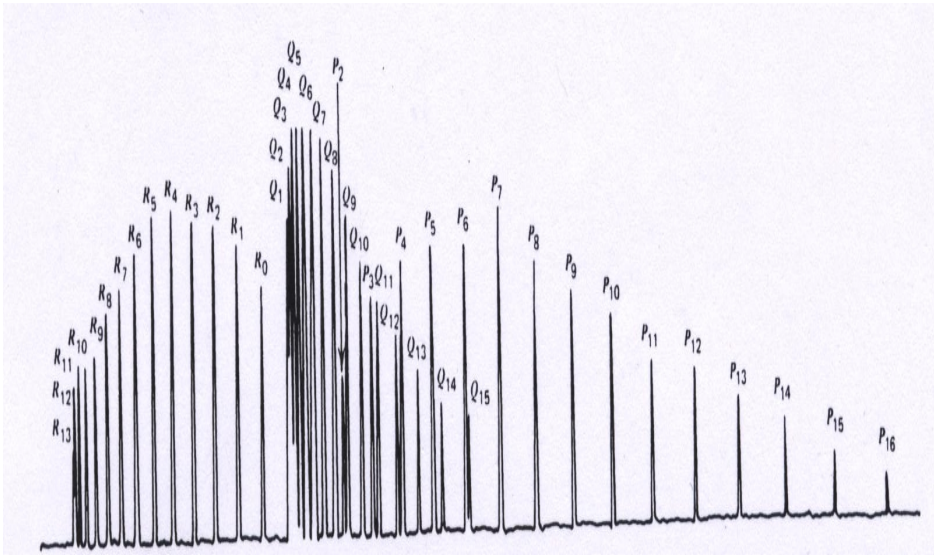

Figure 4.16: The spectral lines observed in the lab of the the molecule AlH. The P,Q and R branches are labeled. y-units are arbitrary. *Fig. taken from Tennyson (2007)*

polyatomic linear molecules like CO_2 does not have a dipole moment in its equilibrium geometry, but any distortion will give an instantaneous dipole moment.

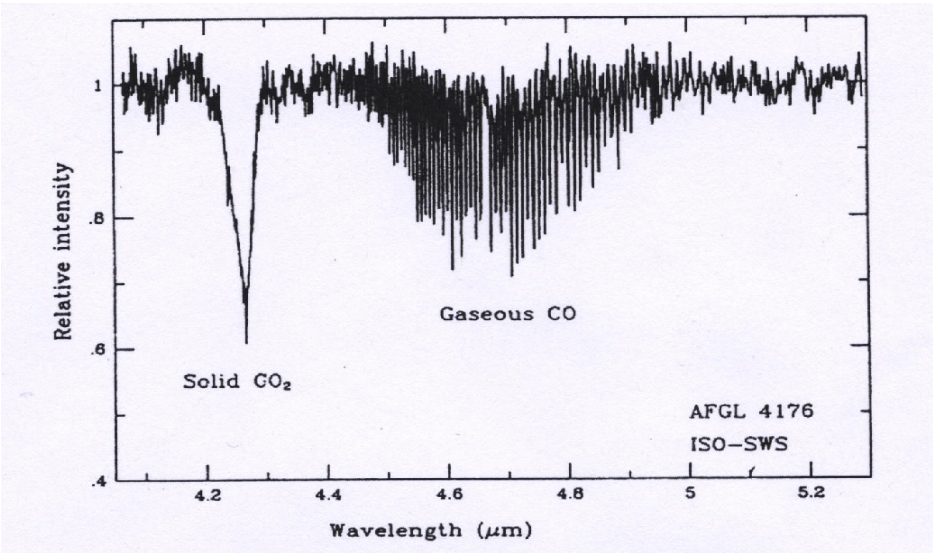

Figure 4.17: The spectrum observed towards the young massive stellar object AFGL 4176. The strong but structureless band is due to solid CO_2, while the characteristic ro-vibrational P and R-branch structure of the CO molecule is due to the presence of warm CO gas in the line-of-sight. Fig. from "The molecular astrophysics of Stars and Galaxies, E.F. Van Dishoeck, Clarendon Press, Oxford, 1998.

Some CO_2 vibrational transitions are dipole-allowed and are quite strong. It is these vibrational transitions which account for a significant part of the greenhouse effect.

4.7 Problems

1. What is the ground state configuration, term and level of the Be atom ? One of the outer electrons is excited to the 3d orbital. What terms and levels can this configuration have ?

Chapter 5

The Strength of Spectral Lines

5.1 Introduction

Fig. 5.1 shows a small piece of a high spectral resolution spectrum of the star HD 56126. This star is of spectral type F5Iab and one of the proto-typical Galactic carbon rich post-Asymptotic Giant Branch (AGB) stars. The star has a high luminosity of several thousands of solar luminosities and is now in a rather rapid transition between its evolution from the AGB towards the Planetary Nebula (PN) region in the HR-diagram.

The figure shows a very small spectral region including Paschen 12 line of Hydrogen (well recognisable by its profile in which the linear Starck effect is dominating the wings) and a Mg I line of 8809.8 Å. The array of narrow absorption lines are the R, P and Q band of the C_2 molecule in the Phillips system $A^1\Pi_u - X^1\Sigma_g^+$ (2,0). The whole detected band is the (2,0) vibrational band of the $A^1\Pi_u - X^1\Sigma_g^+$ electronic transition. The individual lines are different rotational components of this transition.

You can clearly see that different broadening factors of the line profiles indicate a different origin of the lines. While the Paschen and Mg line are photospheric, the C_2 features come from the colder circumstellar material which is seen in the line-of-sight towards the photosphere of the object. The figure is taken from Bakker et al., 1996, A&A 310, 893. The velocity difference between the photospheric lines and the circumstellar molecular absorption lines of - 8.5 km/s can be interpreted as the outflow velocity of the circumstellar material. Not only C_2 is found, also other circumstellar lines are detected in the high quality optical spectrum of this object (see Fig. 5.2).

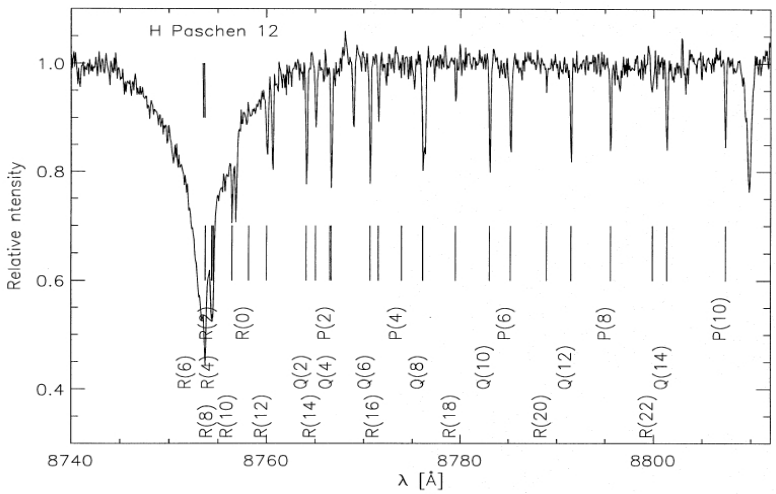

Fig. 1. The Phillips (2,0) band in the spectrum of HD 56126. The C_2 transitions are recognized by the narrow absorption profiles (not resolved). The photospheric absorption line at 8809.8 Å is the MgI(7) transition.

Figure 5.1: A high signal-to-noise and high-resolution spectrum of the post-AGB star HD 56126 (SpT F5Iab). The narrow lines is the Phillips band of C_2. Fig. from Bakker et al., 1996.

By intuition, it is clear that there must be a relation between the *equivalent width* and the *column density*. This relation is, however, not straightforward and dependent on optical depth effects induced by e.g. temperature gradients, density gradients, etc.

In the optical thin approximation, there is a direct relation between the measured equivalent width and the column density. This relation is given by:

$$N_{v''J''} = 1.13 \times 10^{17} \frac{W_\lambda^{J'J''}}{f_{J'J''}\ \lambda^2_{J'J''}} \tag{5.1}$$

with

- column density in cm^{-2}
- equivalent width in mÅ
- wavelength in Å
- $f_{J'J''}$ is the oscillator strength

Table 3. Identified molecular bands in the optical spectrum of HD 56126

Molecule	System	Band		Wavelength range [Å]	
C_2	Phillips	$A^1\Pi_u - X^1\Sigma_g^+$	(1,0)	10137	10213
C_2	Phillips	$A^1\Pi_u - X^1\Sigma_g^+$	(2,0)	8753	8913
C_2	Phillips	$A^1\Pi_u - X^1\Sigma_g^+$	(3,0)	7717	7809
C_2	Swan	$d^3\Pi_g - a^3\Pi_u$	(0,0)	5100	5166
C_2	Swan	$d^3\Pi_g - a^3\Pi_u$	(1,0)	4710	4740
CN	Red system	$A^2\Pi - X^2\Sigma^+$	(1,0)	9142	9202
CN	Red system	$A^2\Pi - X^2\Sigma^+$	(2,0)	7874	7918
CN	Red system	$A^2\Pi - X^2\Sigma^+$	(3,0)	6927	6954
CN	Red system	$A^2\Pi - X^2\Sigma^+$	(4,0)	6190	6225

Figure 5.2: The optical and red circumstellar bands measured in the spectrum of HD 56126

To prove this relation we reduce the complexity of the radiative transfer through the photospheric and circumstellar material by assuming the stellar photosphere can be reproduced by a black-body radiator with a temperature similar to the effective temperature of the central object (HD 56126 in this case). This photosphere is seen through a isothermal cold layer of circumstellar material in which the molecular species reside. The radiative transfer equation (1.63) is then reduced to:

$$I_\lambda = I_{\lambda,ster}\, e^{-\tau_\lambda} + B_\lambda(T_{laag})\,(1 - e^{-\tau_\lambda})$$

To get the equivalent width this becomes:

$$\begin{aligned}
\frac{I_{\lambda,ster} - I_\lambda}{I_{\lambda,ster}} &= \frac{I_{\lambda,ster} - I_{\lambda,ster}\, e^{-\tau_\lambda} - B_\lambda(T_{laag})\,(1 - e^{-\tau_\lambda})}{I_{\lambda,ster}} \\
&= \frac{I_{\lambda,ster} - B_\lambda(T_{laag})}{I_{\lambda,ster}}\left(1 - e^{-\tau_\lambda}\right) \\
\frac{I_{\lambda,ster} - I_\lambda}{I_{\lambda,ster}} &= \left(1 - e^{-\tau_\lambda}\right)
\end{aligned}$$

Since the layer is optically thin ($\tau \ << 1$) we can write $e^{-\tau_\lambda} \approx 1 - \tau_\lambda$ so that the equation becomes:

$$W_\lambda = \int_\lambda (1 - e^{-\tau_\lambda})\ d\lambda = \int_\lambda \tau_\lambda\ d\lambda$$

The question is, under these assumptions, reduced to the question of how we can determine the optical depth. We therefore take the cross-section per particle and by multiplying this

$$\begin{aligned}
\sigma_\lambda^l &= \frac{\pi e^2}{m_e c}\frac{\lambda^2}{c}\frac{f_{lu}}{\sqrt{\pi}\Delta\lambda_D}\ H(a,v) \\
\tau_\lambda &= \sigma_\lambda^l\ N_i \\
\tau_\lambda &= N_i \frac{\sqrt{\pi} e^2}{m_e c}\frac{\lambda^2}{c}\ \frac{f}{\Delta\lambda_D}\ H(a,v)
\end{aligned}$$

For small lines, the Voigt profile can be reduced to the Gauss component only and the integral of the simplified profile becomes $\sqrt{\pi}\Delta\lambda_D$:

$$W_\lambda = \frac{\pi\, e^2}{m_e c}\frac{\lambda^2}{c} N_i f$$

Using the physical constants we get:

$$W_\lambda = \frac{N\ f\ \lambda^2}{1.13 \times 10^{20}}$$

with W_λ and λ in Å. It is clear that this simplified approach cannot be used in all circumstances and a more elaborate radiative transfer should be performed.

For the units in this expression we used the classical "electron radius" (electrostatic potential energy of a charge e in a sphere with electron radius = the energy in rest of the electron):

$$\frac{e^2}{m\, c^2} = 2.818\, 10^{-13} cm$$

Using SI units this is (ϵ_o = permittivity of the vacuum) :

$$\text{“electronradius”} = \frac{e^2}{4\,\pi\,\epsilon_0 m_e\, c^2}$$

5.1 .1 Rotational Diagrams

The energy (in LTE) of a rotation level is:

$$\frac{E_{J''}}{k} = \frac{B_e\, hc}{k}\, J''(J''+1) \quad [K] \tag{5.2}$$

$$Q_r = \sum_{J''}^{\infty} (2J''+1)\, e^{\frac{-E_{J''}}{k\,T_{rot}}} \tag{5.3}$$

with

- Be is the rotational constant
- Q_R the partition function
- k, h, c the normal physical constants
- 2J"+1 is the degeneracy of the level J"

When we assume now a Boltzmann distribution over the different rotational levels within a given vibrational and electronic system, we can write:

$$N_{v'',J''} = \frac{N_{Bolz}}{Qr}\,(2J''+1)\,\exp^{\frac{-E_{J''}}{k\,T_{rot}}} \tag{5.4}$$

The first term is quantized using the equivalent width of the different rotationally spit transitions. The total column density of this line as well as the rotational temperature can be determined using a rotation diagram (see Figs. 5.3, 5.4). In this diagram, the natural logarithm of the specific column density ($N_{v'',J''}$) divided by the levels degeneracy is plotted against the rotational energy of the level under consideration (E''_J/k). The inverse of the slope is then the rotational temperature and crossing at zeroth energy is related to the column density of the material.

In the Figs 5.3, 5.4 we see that the levels at low energies do not match very well the Bolzmann distribution (which is shown as the linear slope in the figures). This is also an effect from the requirements that, in order to use the Equation 5.1 to transfer the observable (equivalent width) to the physical relevant information (column density) you have to assume an optically thin medium, also in the lines. At low rotational energies, so at higher specific column densities ($N_{v'',J''}$), this may not be valid. The rotational diagrams should therefore concentrate on the

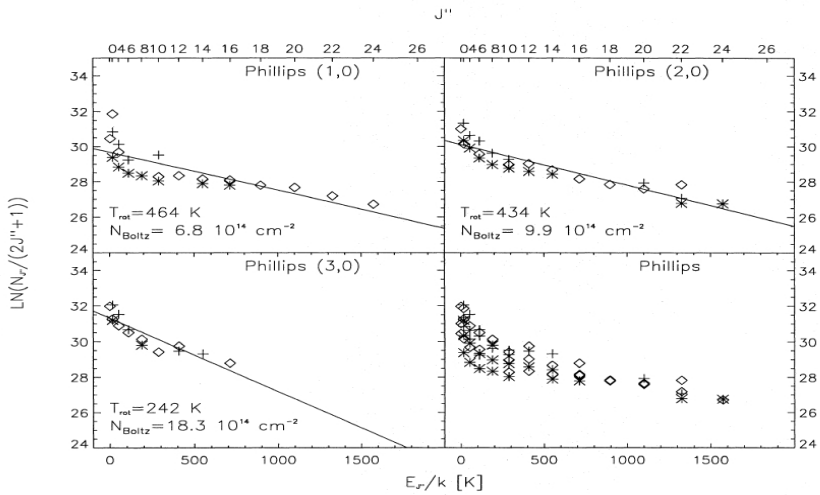

Fig. 5. Rotational diagram of the Phillips (1,0), (2,0), and (3,0) bands. The P, Q, and R branch lines are denoted by a plus, asterisk, and square respectively. Only the weakest rotational band (3,0) is optically thin and gives an almost linear relation in the rotational diagram.

Figure 5.3: Rotational diagrams for C_2 measured in the spectrum of HD$\tilde{5}$6126

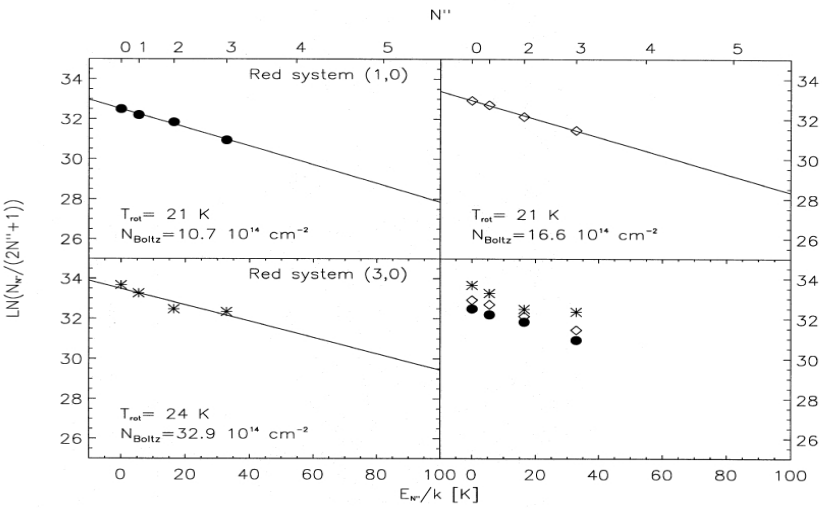

Fig. 6. Rotational diagram of the Red system of CN.

Figure 5.4: Rotational diagrams for CN measured in the spectrum of HD$\tilde{5}$6126

higher rotational levels, despite the fact that those lines are weak and a very good S/N spectrum is needed.

It is left to the reader to determine why the CN molecule in its rotational transitions is much cooler than C_2.

5.2 Curve of Growth in an isothermal slab

The Curve of Growth gives the relation between the equivalent width and the number of ions (molecules) in the correct excited state to determine the b-b transition. This is intimately related to the behavior of the Voigt profile.

The relation between the abundance of the element and the cross section is given by:

The Voigt profile gives:

$$\sigma_\nu = \frac{\pi e^2}{m_e c} f_{lu} \frac{1}{\sqrt{\pi}} \frac{1}{\Delta\nu_D} H(a,v)\,, \tag{5.5}$$

Per unit pathlength, per unit wavelengthbin and including the stimulated emission gives:

$$\alpha_\lambda^l = \frac{\sqrt{\pi} e^2}{m_e c} \frac{\lambda^2}{c} \frac{n_l^{\mathrm{LTE}}}{N_{\mathrm{el}}} N_{\mathrm{H}} A_{\mathrm{el}}\; f_{lu} \frac{H(a,v)}{\Delta\lambda_D} \left[1 - \mathrm{e}^{-hc/\lambda kT}\right]\,, \tag{5.6}$$

With n_{LTE} the number of particles in the correct ionisation and excitation state, N_{el} the total number of the given species.

A_{el} is the abundance of that element (with respect to H).

The maximal value in the line centre is about: H(a,v=0) $\approx$ 1-a with a<1. In most of the astrophysical situations, a is inbetween *10^{-3} and 10^{-1}*.

The centre of a line is dominated by the Gauss profile, the wings are dominated by the Pressure broadening (Lorentz profile). For small values of a, the profile is well described by a Gaussian core and a Lorentz profile for the wings:

$$H(a,v) \approx exp(-v^2) + \frac{a}{\sqrt{\pi}\, v^2} \tag{5.7}$$

Examples: when a $\sim 10^{-2}$; the Doppler core and Lorentz-wing transition is around v=2.7 when H(a,v) equals 10^{-3}. So quite far into the profile (see Fig. 5.5).

It is only for very strong lines that the profile is independent on the Doppler width:

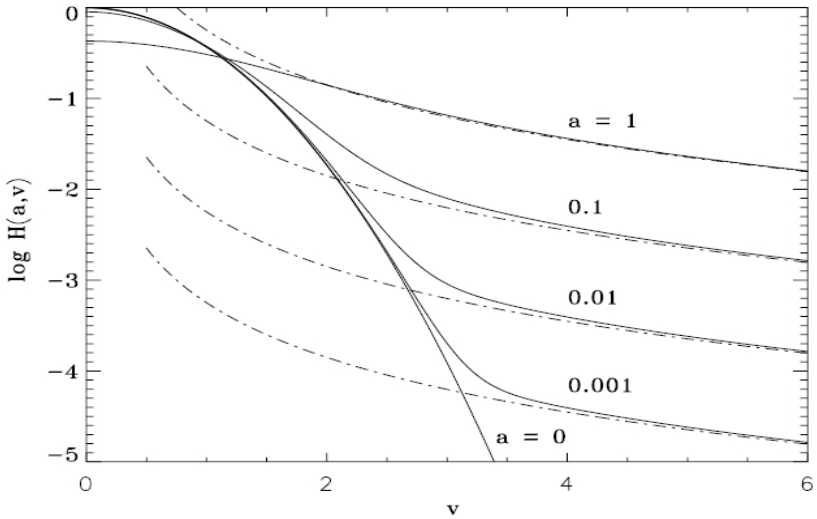

Figure 5.5: The Voigt profile for different values of the a-parameter. The dashed-dotted lines is the $a/\sqrt{\pi}v^2$ approximation.

$$\varphi(\nu - \nu_0) \sim \tag{5.8}$$

$$\frac{1}{\sqrt{\pi}\,\Delta\,\nu_D}\,\frac{a}{\sqrt{\pi}\,v^2} = \tag{5.9}$$

$$\frac{1}{\sqrt{\pi}\,\Delta\,\nu_D}\,\frac{\gamma}{4\,\pi\,\Delta\nu_D}\,\frac{\Delta\nu_D^2}{\sqrt{\pi}\,\Delta\nu^2} = \tag{5.10}$$

$$\frac{\gamma}{4\,\pi^2\,\Delta\nu^2} \tag{5.11}$$

So only very strong lines are independent on the Doppler-velocity ! Doppler broadening is often dominant.

In Fig. 5.6 the line profile changes are given

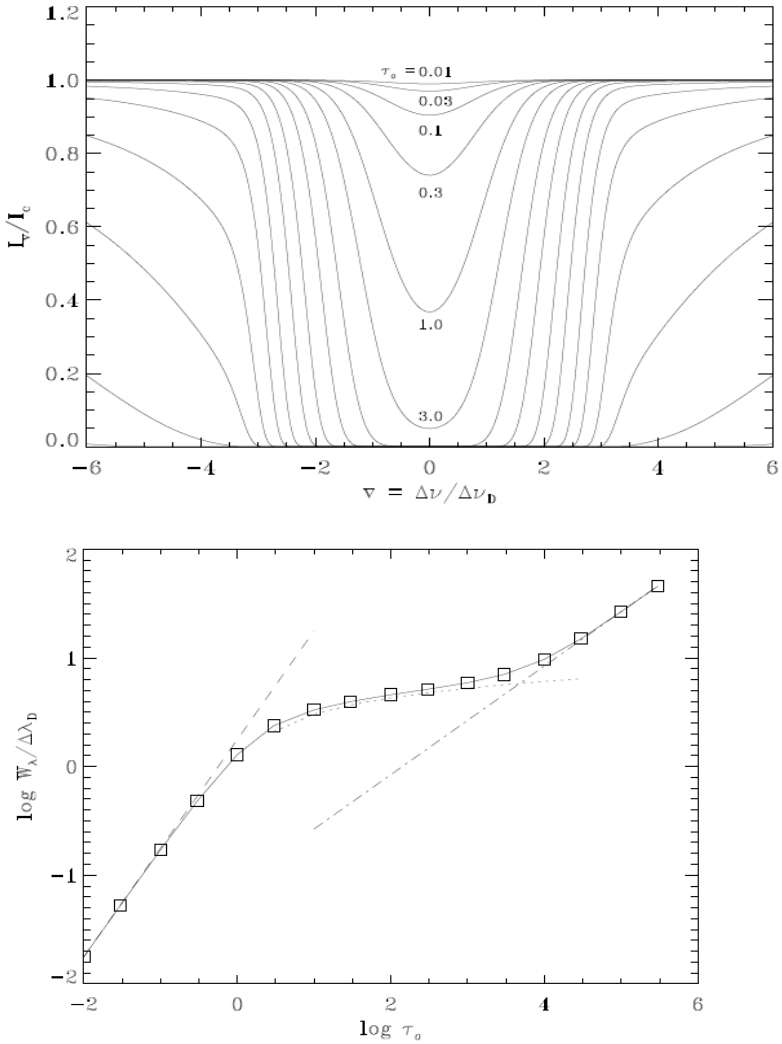

Figure 5.6: In the upper panel we show the line profile change for increasing line strength. When the wings become important contributors to the total line strength, the line becomes saturated. In the lower panel the associated curve-of-growth

5.3 Two layer atmosphere model in LTE

Assume a simple two-layer atmosphere model. The deeper layer has brightness temperature T_b; the line-forming layer has a lower temperature T_L.

$$I_\lambda = B_\lambda(T_b)e^{-\tau_\lambda} + B_\lambda(T_L)\left[1 - e^{-\tau_\lambda}\right] \tag{5.12}$$

with τ_λ the optical thickness of the spectral line. Without stimulated emission, this becomes:

$$\alpha_\lambda = \sigma_{lu}(\lambda)\, n_l = \frac{\pi\, e^2}{m_e c}\frac{\lambda^2}{c}\, f_{lu}\frac{1}{\sqrt{\pi}\,\Delta\lambda_D}\, n_l\, H(a,v) \tag{5.13}$$

The Column Density in the line-of-sight:

$$N_l = \int n_l(s)ds \tag{5.14}$$

Or in optical thickness this becomes:

$$\tau_\lambda = \sigma_{lu}\, N_l = \frac{\pi\, e^2}{m_e c}\frac{\lambda^2}{c}\, f_{lu}\frac{1}{\sqrt{\pi}\,\Delta\lambda_D}\, N_l\, H(a,v) \tag{5.15}$$

$$= \frac{\tau_0}{H(a,0)}\, H(a,v) \approx \tau_0\, H(a,v) \tag{5.16}$$

With τ_0, the optical thickness in the line center. In the last part we used the a $\ll$ 1 (and thus H(a,0) $\approx$ 1-a) approximation.

The expression of the equivalent width then becomes:

$$d_\lambda = 1 - \frac{I_\lambda}{I_\lambda^c} = \frac{B_\lambda(T_b) - B_\lambda(T_L)}{B_\lambda(T_b)}(1 - e^{\tau_\lambda}) \equiv d_\lambda^{max}(1 - e^{\tau_\lambda}) \tag{5.17}$$

with d the relative depth of the line profile.

So, the integrated relative depth over the whole profile is:

$$W_\lambda = d_\lambda^{max}\int_{line}(1 - e^{\tau_\lambda}) \tag{5.18}$$

5.3 .1 Weak lines

For weak lines we have $\tau_\lambda \ll 1$. Moreover, the Voigt-profile can be reduced to the $exp(-(\Delta\lambda/\Delta\lambda_D)^2)$ with integral $\sqrt{\pi}\Delta\lambda_D$.

$$W_\lambda \approx d_\lambda^{max}\, \tau_0\, \sqrt{\pi} \Delta\lambda_D = \frac{\pi\, e^2}{m_e c} \frac{\lambda^2}{c}\, f_{lu}\, d_\lambda^{max}\, N_l \tag{5.19}$$

So there is a *linear* relation between the equivalent width and the increased column density.

5.3.2 Saturated lines

Saturation (for $\tau_0 > 1$) makes that the intensity at the line centre approaches $B_\lambda(T_L)$ which corresponds to d_λ^{max}.

The equivalent width still increased but less linear with τ_0.

$$W_\lambda = d_{\lambda^{max}}\, Q_\lambda\, \Delta\lambda_D \tag{5.20}$$

the $Q(\tau_0)$ values can be estimated and a good representation is that:

$$Q(\tau_0) = 2\sqrt{\ln \tau_0} \tag{5.21}$$

From about τ_0 3 onwards, the curve of growth has a *logarithmic regime*.

5.3.3 Very Strong Lines

Very strong lines $\tau_0 \gg 1$ can no longer deepen their core, but the wings of the profile will become stronger.

$$H(a, v) \approx \frac{a}{\sqrt{\pi} v^2} = \frac{a}{\sqrt{\pi}} (\Delta\lambda_D / \Delta\lambda)^2 \sim \frac{1}{\Delta\lambda^2} \tag{5.22}$$

There is no exponential decay in the wings.

$$\tau_\lambda = \tau_0\, \frac{a}{\sqrt{\pi}\, v^2} = \tau_0\, \frac{a}{\sqrt{\pi}} \frac{\Delta\lambda_D^2}{\Delta\lambda^2} \tag{5.23}$$

The equivalent width becomes ($u^2 = 1/\tau_\lambda$):

$$W_\lambda \approx d_\lambda^{max} \Delta\lambda_D \sqrt{\tau_0 \frac{a}{\sqrt{\pi}}} \int_{line} (1 - e^{-1/u^2}) du \tag{5.24}$$

$$= d_\lambda^{max} \Delta\lambda_D \sqrt{\tau_0\, a} 2\pi^{1/4} \tag{5.25}$$

In which the standard integral is used:

$$\int_{-\infty}^{+\infty} (1 - e^{-1/x^2}) dx = 2\sqrt{\pi} \tag{5.26}$$

5.4 The Curve of Growth following the approach of Milne & Eddington

The previous was a very crude approximation of an atmosphere: just two isothermal layers, one colder (with the line-formation) and an underlying hotter layer.

A more sophisticated approach was developed by Milne and Eddington and assumes

- The source function is linear in continuum optical depth
- LTE
- The profile function and the ratio between line and continuum extinction coefficient is INdependent of optical depth in the atmosphere

The results are very similar (replace τ_0 by the line-to-cont opacity ratio) to the curve-of-growth behaviour, but they do give a very good physical insight into the behaviour of spectral lines in general and to the line strength in particular.

It is important to make a devision between line absorption and line scattering. Absorption occurs when the photon is used to excite a given level but de-excitation occurs by collisions. The photon is destroyed and mainly thermalised. The source function for pure absorption in LTE is a black body (B_λ, B_ν). For scattering, the photon de-excitation is by a radiative process which creates a very similar photon than the one which was used to excite the electron. The release of photons is basically isotropic. For pure coherent scattering, the photons which enter the bundle come from a similar process at adjacent bundles of different orientation. The source function for scattering is then the mean intensity (J_λ,J_ν) which gives the mean number of photons per solid angle.

We differentiate the extinction coefficient in a pure absorption component and a pure scattering component.

$$\alpha_\nu^l = \alpha_\nu^a + \alpha_\nu^s \,, \tag{5.27}$$

The *absorption parameter* gives which fraction of the photons are destroyed:

$$\epsilon_\nu = \frac{\alpha_\nu^a}{\alpha_\nu^a + \alpha_\nu^s} \,. \tag{5.28}$$

The *scattering parameter*, $\rho_\nu = 1 - \epsilon_\nu$, is given by:

$$\rho_\nu = \frac{\alpha_\nu^s}{\alpha_\nu^a + \alpha_\nu^s} \,, \tag{5.29}$$

We use subscript l for the line and c for the continuum.

The transfer equation becomes than somewhat more complicated:

$$\cos\theta \, \frac{\partial \, I_\nu}{\partial \, z} = (\alpha_c^a + \alpha_c^s + \alpha_l) \, I_\nu - \alpha_c^a \, B_\nu - \alpha_c^s \, J_\nu - \epsilon_l \, \alpha_l \, B_\nu - (1 - \epsilon_l) \, \alpha_l \, J_\nu \,. \tag{5.30}$$

So we differentiate between line and continuum extinction.

The total optical depth for a given geometry becomes:

$$\tau_\nu = \int_0^z \mathrm{d}z \, (\alpha_c^a + \alpha_c^s + \alpha_l) \tag{5.31}$$

The *optical depth of the continuum* gives:

$$\tau_c = \int_0^z \mathrm{d}z \, (\alpha_c^a + \alpha_c^s) \,. \tag{5.32}$$

The *line contrast*:

$$\beta_\nu = \frac{\alpha_l}{\alpha_c} = \frac{\alpha_l}{\alpha_c^a + \alpha_c^s} \tag{5.33}$$

Assume now the line-contrast to be independent of the optical depth, the optical depth becomes:

$$\begin{aligned}
\tau_\nu &= \int_0^z \mathrm{d}z\,(\alpha_c^a + \alpha_c^s + \alpha_l) && (5.34)\\
&= \tau_c + \int_0^z \alpha_l\,\mathrm{d}z && (5.35)\\
&= \tau_c + \int_0^z \frac{\alpha_l}{\alpha_c^a + \alpha_c^s}\,(\alpha_c^a + \alpha_c^s)\;\mathrm{d}z && (5.36)\\
&= \tau_c + \beta_\nu \int_0^z (\alpha_c^a + \alpha_c^s)\;\mathrm{d}z && (5.37)\\
&= \tau_c + \beta_\nu\,\tau_c && (5.38)
\end{aligned}$$

When defining:

$$\zeta_\nu = \frac{(1-\rho_c) + \epsilon_l\,\beta_\nu}{1+\beta_\nu} \tag{5.39}$$

The transfer equation becomes the *Milne-Eddington equation*:

$$\cos\theta\,\frac{\partial\,I_\nu}{\partial\,\tau_\nu} = I_\nu - \zeta_\nu\,B_\nu - (1-\zeta_\nu)\,J_\nu\,. \tag{5.40}$$

5.4.1 Curve of Growth

$$W_\nu = \int_{\mathrm{line}} d\nu\,A_\nu = \frac{c}{\lambda^2}\,W_\lambda \tag{5.41}$$

The line contrast R_ν gives:

$$A_\nu = 1 - R_\nu = 1 - \frac{\mathcal{F}_\nu}{\mathcal{F}_c}\,. \tag{5.42}$$

Assume now pure absorption in LTE ($S_\nu = B_\nu(T)$).

$$B_\nu(T(\tau)) = B_0 + B_1\,\tau_c \tag{5.43}$$

The flux at the surface is given by:

$$\mathcal{F}_\nu(\tau_\nu = 0) = 2\,\pi \int_0^\infty dt_\nu\,S(t_\nu)\,E_2(|t_\nu|)\,, \tag{5.44}$$

To solve the equation, assume:

- Milne-Eddington approach by assuming the line-contrast $\beta_\nu \equiv \alpha_\nu^l/\alpha_\nu^c = \kappa_\nu^l/\kappa_\nu^c$ to be **independent** of the depth in the atmosphere.
- we write $dt_\nu = (1 + \beta_\nu)\, d\tau_c$ so in function of the optical depth of the continuum.

$$\mathcal{F}_\nu(\tau_\nu = 0) = 2\,\pi \int_0^\infty \mathrm{d}\tau_c\,(1+\beta_\nu)\,(B_0 + B_1\,\tau_c)\,E_2[(1+\beta_\nu)\,\tau_c] = B_0 + \frac{2}{3}\,\frac{B_1}{1\,+\,\beta_\nu}\,, \tag{5.45}$$

The flux in the continuum becomes :

$$\mathcal{F}_c = B_0 \,+\, \frac{2}{3}\,B_1 \tag{5.46}$$

The flux contrast becomes:

$$A_\nu = 1 - \frac{\mathcal{F}_\nu}{\mathcal{F}_c} = \frac{\beta_\nu}{1\,+\,\beta_\nu}\,\frac{1}{1\,+\,\frac{3B_0}{2B_1}} = A_0\,\frac{\beta_\nu}{1\,+\,\beta_\nu}\,, \tag{5.47}$$

With A_0 the depression for very strong lines ($\beta_\nu \gg 1$) :

$$A_0 = \frac{1}{1 + \frac{3B_0}{2B_1}}\,. \tag{5.48}$$

The absorption coefficient per unit length gives:

$$\alpha(\nu) = \left(\frac{\pi\,e^2}{mc}\right)\,f\,\underbrace{\frac{n_{\mathrm{el}}^{\mathrm{LTE}}}{N_{\mathrm{ion}}}}_{\text{Boltz-mann}}\,\underbrace{\frac{N_{\mathrm{ion}}}{N_{\mathrm{el}}}}_{\text{Saha}}\,N_{\mathrm{H}}\,A_{\mathrm{el}}\,\frac{1}{\sqrt{\pi}}\,\frac{1}{\Delta\nu_D}\,H(a, v(\nu))\,, \tag{5.49}$$

with:

$$\beta_\nu = \frac{\alpha_\nu^l}{\alpha_\nu^c} = \beta_0\,H(a, v) \tag{5.50}$$

and

$$\beta_0 = \left(\frac{\sqrt{\pi}\,e^2}{mc}\right)\,f\,\frac{n_{\mathrm{el}}^{\mathrm{LTE}}}{N_{\mathrm{ion}}}\,\frac{N_{\mathrm{ion}}}{N_{\mathrm{el}}}\,N_{\mathrm{H}}\,A_{\mathrm{el}}\,\frac{1}{\Delta\nu_D}\,\frac{1}{\alpha_\nu^c} \tag{5.51}$$

This β_0 is the line contrast in the line centre.

The equivalent width W_ν is given by:

$$W_\nu = \int_{\text{line}} d\nu\, A_\nu = 2\, A_0\, \Delta\, \nu_D \int_{\text{halve lijn}} dv\, \frac{\beta(v)}{1\, +\, \beta(v)}\,. \tag{5.52}$$

the integration is over half the line. The differentiation between weak, saturated and strong lines are equivalent to the different regimes of the Voigt profile.

5.4 .1.1 Weak Lines

For **weak lines** the Doppler core will dominate $\beta(v) = \beta_0\, e^{-v^2}$.

$$W_\nu = 2\, A_0\, \Delta\nu_D\, \beta_0 \int_{\text{halve lijn}} dv\, e^{-v^2}\, (1 - \beta_0\, e^{-v^2} + \beta_0^2\, e^{-2v^2} - ...) \tag{5.53}$$

or

$$W_\nu = 2\, A_0\, \Delta\nu_D\, \beta_0\, \frac{\sqrt{\pi}}{2}\, (1 - \frac{\beta_0}{\sqrt{2}} + \frac{\beta_0^2}{\sqrt{3}} - ...) \tag{5.54}$$

For weak lines we have $W_\nu\ \sim$ the abundance. This is the linear part of the curve of growth.

5.4 .1.2 Saturated lines

For **strong, saturated lines** with still a dominant Doppler core, the solution becomes :

$$W_\nu = 2\, A_0\, \Delta\nu_D\, \sqrt{\ln \beta_0}\, [1 - \frac{\pi^2}{24\, (\ln \beta_0)^2} - ...] \tag{5.55}$$

The equivalent width is only weakly dependent on β_0. This is the **flat part** of the curve-of-growth. These lines are NO good abundance indicator...

5.4 .1.3 Very strong lines

Very strong lines have important and even dominant Lorentz wings. The Voigt profile reduces to $H(a, v) = a/(\sqrt{\pi}\, v^2)$

$$\begin{aligned} W_\nu &= 2\,A_0\,\Delta\nu_D \int_{\text{halve lijn}} dv\,(1 + \frac{\sqrt{\pi}\,v^2}{a\beta_0})^{-1} \\ &= A_0\,\Delta\nu_D\,(\pi\,a\,\beta_0)^{1/2}\,. \end{aligned}$$

So in the *damping* part of the curve of growth, W_ν varies according to the square root of β_0.

5.4.2 Theoretical Curve of Growth

The curve-of-growth gives the functional relation between $\log(W_\nu/\Delta\nu_D)$ and $\log\,\beta_0$

$$\beta_0 = (\frac{\sqrt{\pi}\,e^2}{mc})\,f\,\frac{n_{\text{el}}^{\text{LTE}}}{N_{\text{ion}}}\frac{N_{\text{ion}}}{N_{\text{el}}}\,N_{\text{H}}\,A_{\text{el}}\,\frac{1}{\Delta\nu_D}\,\frac{1}{\alpha_\nu^c} \tag{5.56}$$

In LTE, the solutions of the Boltzmann and Saha equations yield $\frac{n_{\text{el}}^{\text{LTE}}}{N_{\text{ion}}}$ and $\frac{N_{\text{ion}}}{N_{\text{el}}}$.

Different lines of the same ion, will have a different β_0 value, because they have different oscillator strengths, different n_{el} but also different Doppler widths (because they occur at different frequencies). The different parts are separated into:

$$\log\beta_0 = \log\,(gf\lambda) - \theta\chi + C \tag{5.57}$$

In which C is dependent of: the abundance, the velocity, the continuum extinction coefficient and the Saha population factor.

With the temperature given by:

$$\theta = \frac{\log\,\text{e}}{k_{\text{in eV per Kelvin}}}\,\frac{1}{T_{\text{exc}}} = \frac{5040}{T_{\text{exc}}} \tag{5.58}$$

Note that:

$$\frac{W_\nu}{\Delta\nu_D} = \frac{W_\lambda c}{\lambda^2}\,\frac{c}{\xi\,\nu} = \frac{W_\lambda}{\lambda}\,\frac{c}{\xi}\,, \tag{5.59}$$

The Curve-Of-Growth of a given ion is also dependent on the Doppler width and on the damping parameter. This is illustrated in Fig 5.7. A noticeable difference is the Doppler width, which includes both the thermal velocity as well

as the micro-turbulent velocity. For a stronger microscopic Doppler broadening, the saturation level is delayed in equivalent width since the broader intrinsic line profile makes that the frequency width of the radiation field which can excite the level is larger.

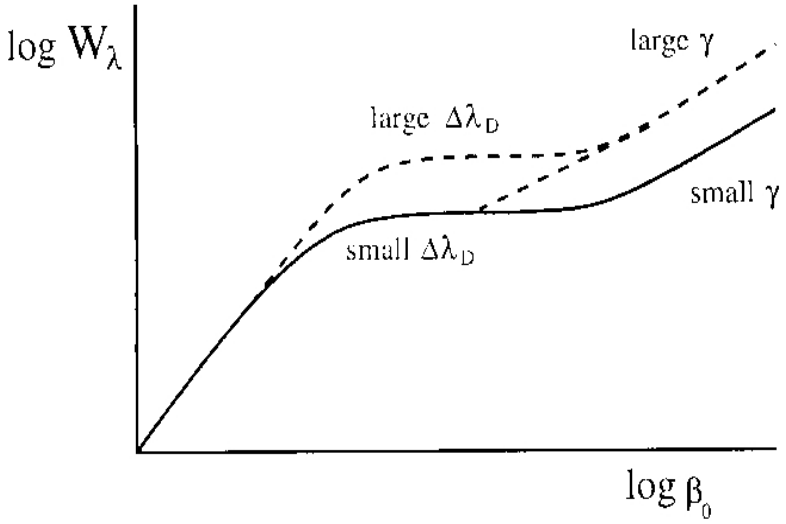

Figure 5.7: The behaviour of the curve of growth for different Doppler-widths and different damping constants. For a larger Doppler width, the saturation point is delayed in equivalent width

5.4.3 Observable Curve of Growth

The Doppler width nor the excitation temperature are known so the theoretical curve-of-growth is not an observable. The empirical curve-of-growth will give: $\log(W_\lambda/\lambda)$ in function of $\log(gf\lambda)$. The devision of λ is meant to compensate Doppler related phenomena (since $\Delta\lambda = \lambda\,\xi\,/c$):

$$W_\nu = 2\,A_0\,\Delta\nu_D\,\beta_0\,\frac{\sqrt{\pi}}{2} \tag{5.60}$$

$$\beta_0 = (\frac{\sqrt{\pi}\,e^2}{mc})\,f\,\frac{n_{\rm el}^{\rm LTE}}{N_{\rm ion}}\frac{N_{\rm ion}}{N_{\rm el}}\,N_{\rm H}\,A_{\rm el}\,\frac{1}{\Delta\nu_D}\,\frac{1}{\alpha_\nu^c} \tag{5.61}$$

We get:

$$\log\left(\frac{W_\lambda}{\lambda}\right) = \log\left(\frac{\pi e^2}{m_e c^2}\frac{1}{U}\frac{N_{\rm ion}}{N_{\rm el}}\,N_{\rm H}\,A_0\right) + \log\left(gf\lambda\right) - \theta\,\chi + \log(A_{\rm el}) - \log(\alpha_\nu^c) \tag{5.62}$$

The left part of the equation is a direct observable. The right-hand-side contains the Saha term, the abundance, the oscillator strength, the excitation temperature and the continuum opacity. The latter is negative : can you explain why ?

Different lines of the same multiplet (=coming from the same level in the energy scheme of the ion) are used, the equation only differs in the oscillator strength while the other parameters (abundance, cont. extinction coefficient, A_0, Saha population factor) all are the same. In Fig. 5.8 we show two empirical curve-of-growths for the Ti I multiplets with respectively 0.03 and the series at 0.03, 0.82, 1.44 and 1.99 eV are shown.

In Fig 5.8 is illustrated that there is a horizontal shift in both curves. From equation 5.62 we can see that the shift is related to the $\theta\,\chi$: by shifting in the horizontal direction, the different curves of the different multiplets and minimising the difference, the offset is directly related to the θ and the excitation temperature can be determined ($\theta = 5040/T_{exc}$). This is given in Fig. 5.9). For the different Ti I multiplets of the solar optical spectrum, this is illustrated in Fig. 5.10.

Once the excitation temperature is known, the Saha and Boltzmann equations can be solved so that we can compare $\log(W_\nu/\Delta\nu_D) = \log\left(\frac{W_\lambda}{\lambda}\frac{c}{\lambda}\frac{1}{\Delta\nu_D}\right)$ with the curve showing $\log(\beta_0) = \log\left(gf\lambda\right) - \theta\chi + C$, with $C = \log\left(\frac{\sqrt{\pi}e^2}{m_e c}\frac{1}{U}\frac{N_{\rm ion}}{N_{\rm el}}N_{\rm H}A_{\rm el}\frac{1}{\xi\alpha_\nu^c}\right)$. The vertical shift gives $\Delta\nu_D$ and therefore ξ. When the Dopplerwidth is large, the profiles are intrinsically broad and saturation will occur at larger equivalenth width. The Doppler width was found to be significantly larger that only the thermal microscopic velocity can account for. The microturbulent velocity was defined as the additional velocity field which acts on microscopic scales.

From the horizontal shift, as well as the specific shape of the curve-of-growth, the constant C can be estimated. The only unknown now in this term is the abundance of the element.

A curve-of-growth analysis gives a good physical insight in what the important physical parameters are, which determine the relation between equivalent width observable and the abundance.

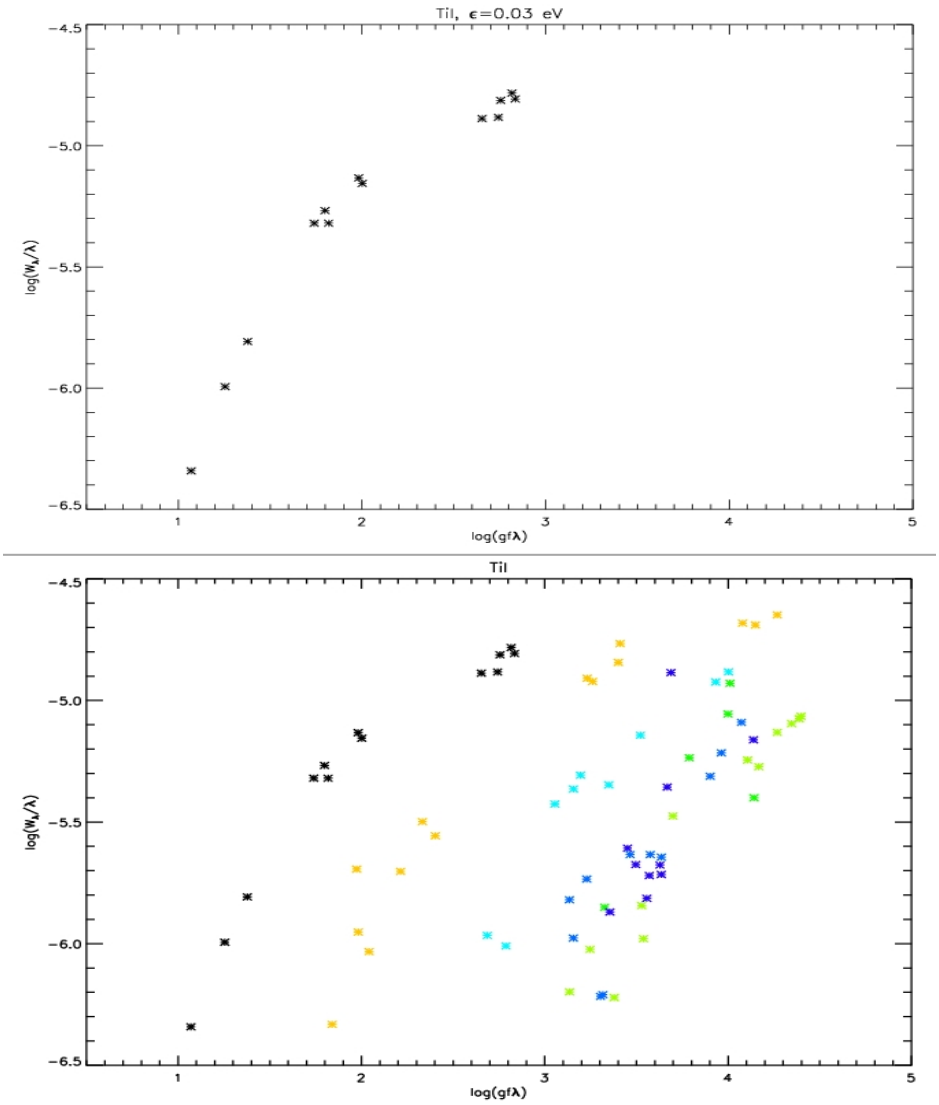

Figure 5.8: Curve of Growths of the Ti I multiplet as observed in the Sun. The specific multiplet with excitation level at 0.03 eV is shown (upper part). Different multiplets in different colour-codes (0.03, 0.82, 1.44 and 1.99 eV) are shown in the lower level.

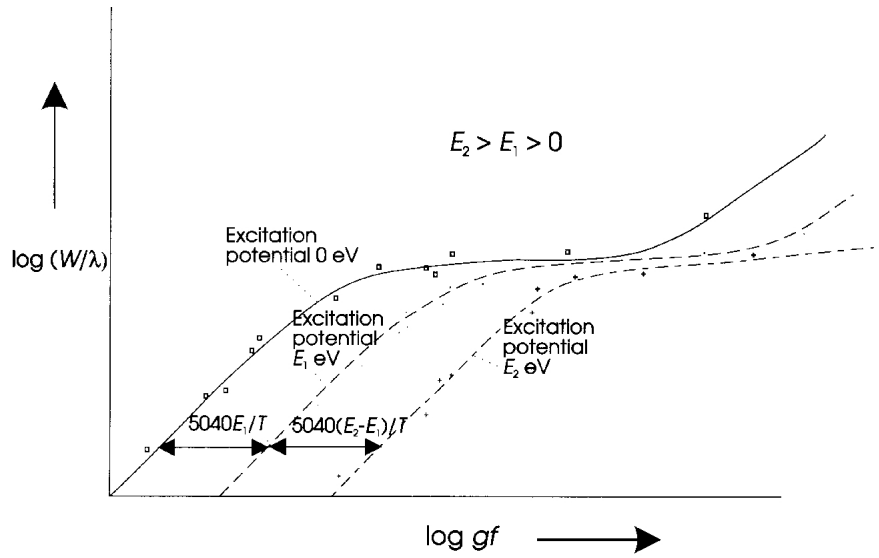

Figure 5.9: Determination of the Excitation Temperature using different multiplets of the same ion.

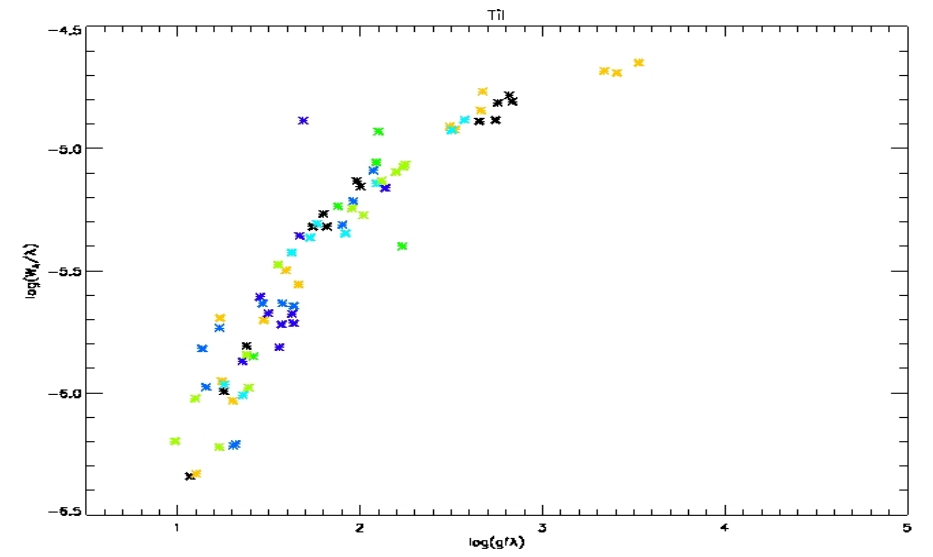

Figure 5.10: The curves-of-growth of the different Ti I multiplets (see Fig. 5.8) corrected for the excitation temperature. The different colours represent different multiplets. The data is from the Sun.

5.5 Abundance Determinations

In LTE computations to determine the abundance of a given species in a stellar photosphere, the distribution over the different excitation and ionsiation stages is determined by the local application of the equilibrium equations (Saha and Boltzmann equations). The equivalent width is then computed by integrating over the stellar atmosphere and the curve-of-growth is now rarely used. For hotter stars (as well as for (super)giants), the LTE approach is too coarse since non-LTE effects are too important. LTE computations are commonly used for giants and stars of intermediate spectral type, providing only weak lines are used which are formed deep in the stellar photosphere. Stellar photosphere model codes themselves are gaining complexity and spherical models (for (super)giants), Non-LTE models and multidimensional models are now standard in use or in development. In the course 'Stellar atmospheres' this will be highlighted further.

To compute LTE abundances, several free software packages are available and the most commonly used are the suite of programs and model atmospheres developed by Prof. Kurucz at Harvard and the more recent grids computed with more up-to-date atomic data Nemo2003. MOOG, developed by Prof. C. Sneden is often used for Giant (RGB-giants) as well as somewhat hotter stars. The program includes a spectral synthesis procedure (Fig 5.11) which allows detailed matching of an observed spectral range. To allow for a spectrum synthesis, the macroscopic broadening function should be quantified as well. Another widely used package is from Prof. R.O. Gray et al. and is called Spectrum. This package allows for detailed modelling of sythetic spectra of stars with low to intermediate temperatures.

The codes for hotter stars should include appropriate stellar atmospheres and a widely used package to compute appropriate model atmospheres is TLusty, with its model spectrum synthesis code Synspec.This list is by no means complete but it does give a flavour on what is available (and widely used) already.

Whenever the molecular opacities become important and certainly when those become so dominant that they will form a pseudo-continuum, the model atmospheres should include a detailed molecular opacity computation. The detailed abundances of the CNO and Fe-peak elements (the latter are the main electron donors for colder stars) will play an important role in the model structure and the number of parameters describing those models increase significantly. Up-to-date models for colders stars are computed in the MARC project and more details can be found here.

An important aspect in the error budget of the abundance determinations of (stellar) spectra are the atomic data. The wavelengths and excitation and ionisa-

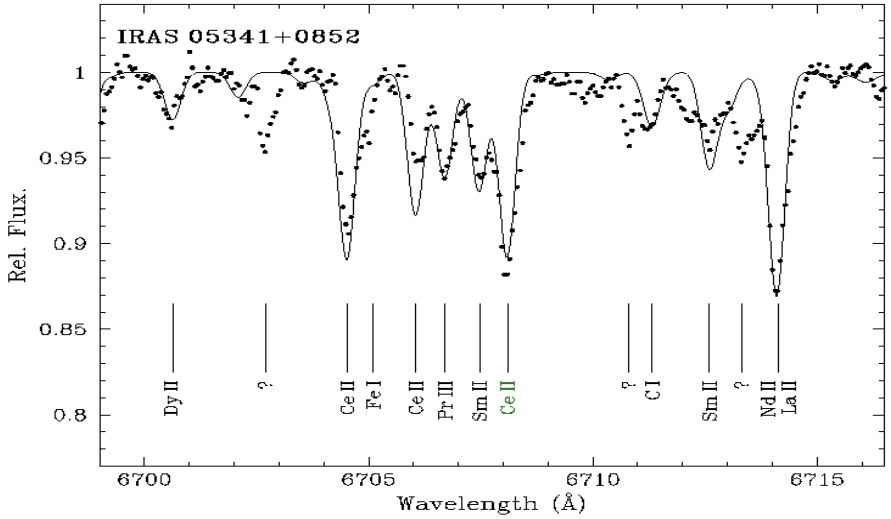

Figure 5.11: An example of a spectral synthesis: to match the observed spectrum (dots) the model (full line) should not only contain the correct abundances, also the total broadening function of the b-b profiles should be known

tion potentials are often (but not always !) known to high accuracy, but this is not the case for the oscillator strengths. In many examples of the literature on abundance determinations, the number of lines used in the analysis is limited to those lines for which accurate oscillator strengths are available. Good web-based data-bases are available and a widely used is kept in Vienna (Vienna Atomic Line Database) with acronym **VALD**. And at the website of the National Institute of Standards and Technology **NIST**. A useful tool in the VALD page is that it allows for a fast and easy determination of the expected strength of a given line for any model atmosphere of your choice. The database of photospheric lines taken into account by Prof. Kurucz to compute the total opacity can be queried from here. A broader database with allowed, intercombination and forbidden atomic transitions is assembled by Dr. Peter Van Hoof and this can be queried from here. For colder objects where molecular opacities are important a very useful compendium is given by Dr. Leen Decin and an overview can be found on her web-page here. For line identification, a usefule website is the one by Dr. A. Lobel in which a detailed account is given on spectral features deteced in some bright objects. This link will forward you to SpectroWeb.

The basis of any detailed atmospheric (abundance) study of a given star, is a high signal-to-noise spectrum of high spectral resolution. Thanks to the specific wavelength dependent opacity, any bound-bound transition of a given chemical

species, which occurs in the line-forming region of the stellar atmosphere, is a very good probe to the abundance of this element. This is illustrated in Fig. 5.12 where three spectra are shown of stars with very similar atmospheric parameters, but different abundances of trace elements : in this case the s-process elements which are synthesised by the slow neutron capture process.

One line of a specific ionisation stage and excitation level is in principle enough to determine the abundance of the element but since the Boltzmann and Saha factors can be large, they will be important factors in Equation 5.62 . As many weak lines with accurate oscillator strength should be use and the most accurate abundances will come from the most dominant ionisation stage. These will be less dependent on temperature effects.

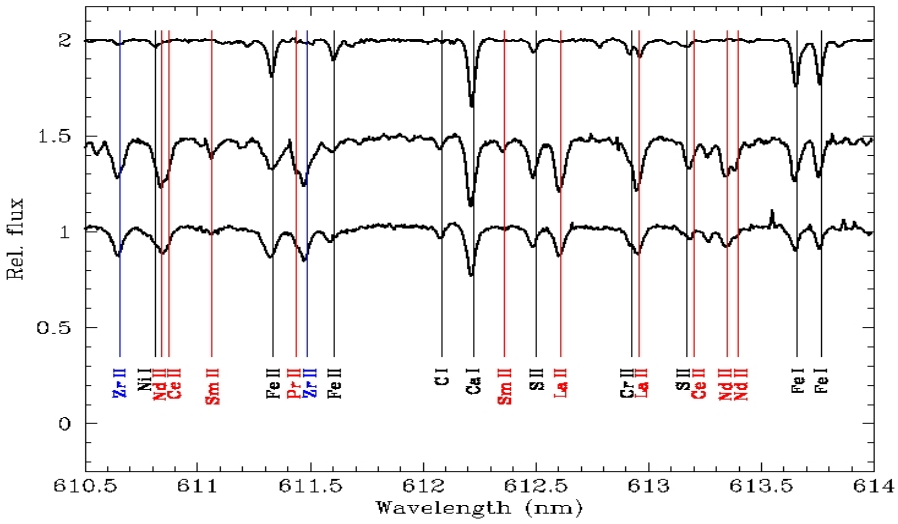

Figure 5.12: A figure illustrating the rich potential of high resolution spectroscopic data of high quality to detect trace elements in the photospheres of stars. Normalised spectra of three stars are shown with a small offset to ease comparison. All three spectra are brought to the same Doppler velocity. The identification of the different lines is given below. The elements marked in red and blue are heavy elements which are very rare in a solar composition (see the solar abundances in chapter 2)

5.5.1 Spectroscopic determination of the stellar atmosphere parameters

The basic parameters of a stellar photosphere are the effective temperature (T_{eff}), the surface gravity ($\log g$), the overall chemical composition and the micro-turbulent velocity. The overall chemical composition is often scaled to the Solar composition pattern e.g.: if the metallicity is ten times less than solar, all initial abundances will have a [el/H] = -1.0. Quantifying the temperature and the gravity of a stellar photosphere is therefore a primordial step and many techniques have been developed to constrain both.

An excitation analysis will compare the strength of lines of very different excitation levels of a given ion, with the strength expected for a given model atmosphere. The reason is that Equation 5.62 contains the Boltzmann factor which is temperature dependent: for a higher temperature, we expect a higher overall excitation distribution of the ions. By obtaining abundances based on lines of a given ion but with very different excitation potentials, we can constrain the temperature of the star by requiring that the abundance needs to be independent of the excitation potential. This is illustrated in Fig. 5.13.

This is excitation analysis, model atmospheres are used with a different temperature. The best estimate for the stellar temperature is obtained by requiring that there is no trend in the obtained abundances for lines of the same ion but with a wide range of excitation potentials. In practice, the most suitable element for this analysis are the different ions of Fe: an abundant element with a very rich spectrum for intermediate spectral type stars. For hotter stars, with much less lines in the optical, this excitation analysis is made difficult due to the lack of lines.

Once a good temperature estimate is obtained, the Saha ionisation factor is used to constrain the surface gravity: the gravity estimate is obtained again by the requirement that the obtained abundances from lines of a given element but of a different ion should be the same. This analysis can only be performed if the spectrum does indeed contain enough spectral lines of the same element but of a different ionisation stage.

The micro-turbulent velocity is a more difficult parameter since it unites all possible velocity fields other than the thermal velocity which act on a microscopic scale. Quantifying the micro-turbulent velocity is performed by using Fig. 5.7 and tracing the start of the saturation level. Using lines of the same ion but of different strength, we can require that stronger lines, which are near the saturation limit, do yield the same abundance as very weak lines. Abundances based on very weak lines, on the linear part of the curve-of-growth, are quite independent on micro-turbulent velocity. This is illustrated in Fig 5.14 where the obtained abundances

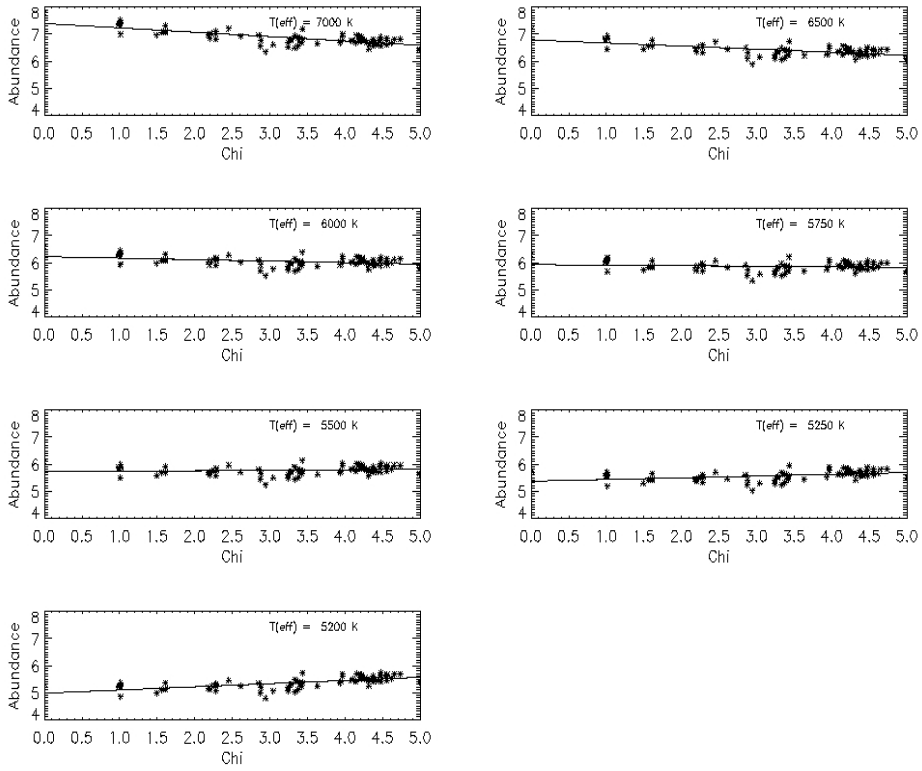

Figure 5.13: The determination of the temperature of AC Her, using the excitation analysis of the Fe I lines.

are given using a range of micro-turbulent velocity parameters. Typical values are somewhat dependent on the spectral type of the star but range from 1-10 km/s.

It is good to remember that absolute abundance determinations are still quite uncertain (e.g. see also the recent changed in even the Solar abundances) , certainly if they are based on a 1D, LTE analysis of the spectra. The most reliable abundances are based on weak lines of the most dominant levels of the element. On top of that, the lines should have reliable oscillator strengths. Given all the constraints and the uncertainties, relative abundances which quantify the difference in abundances of stars with very similar spectral types are much more reliable than any absolute determination (Fig. 5.15).

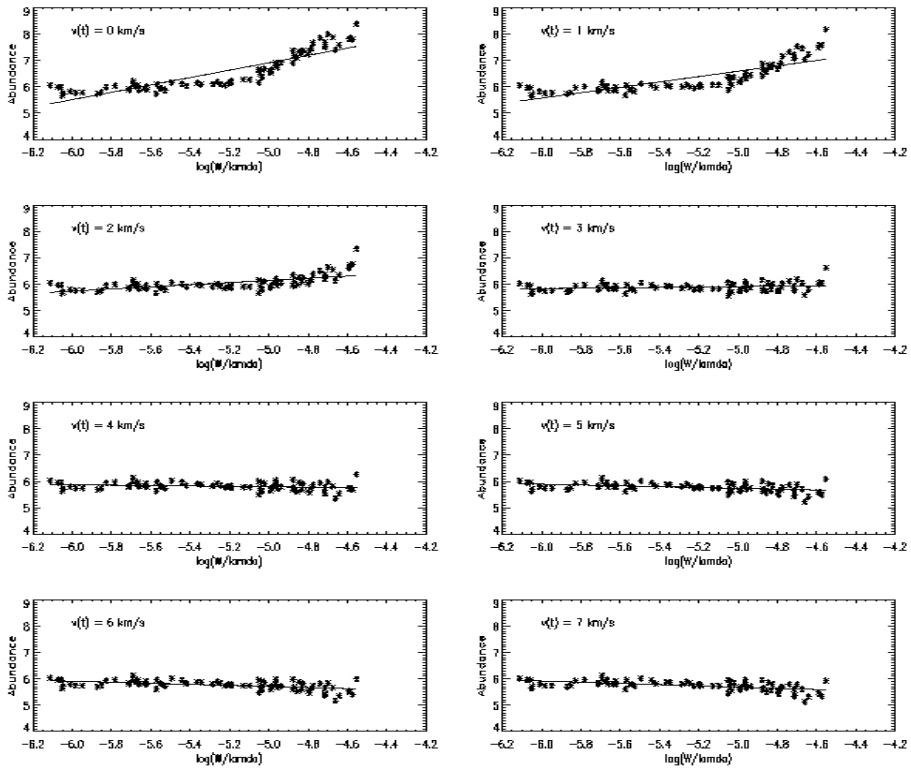

Figure 5.14: The micro-turbulent velocity determination using the Fe I lines as observed in the star AC Her.

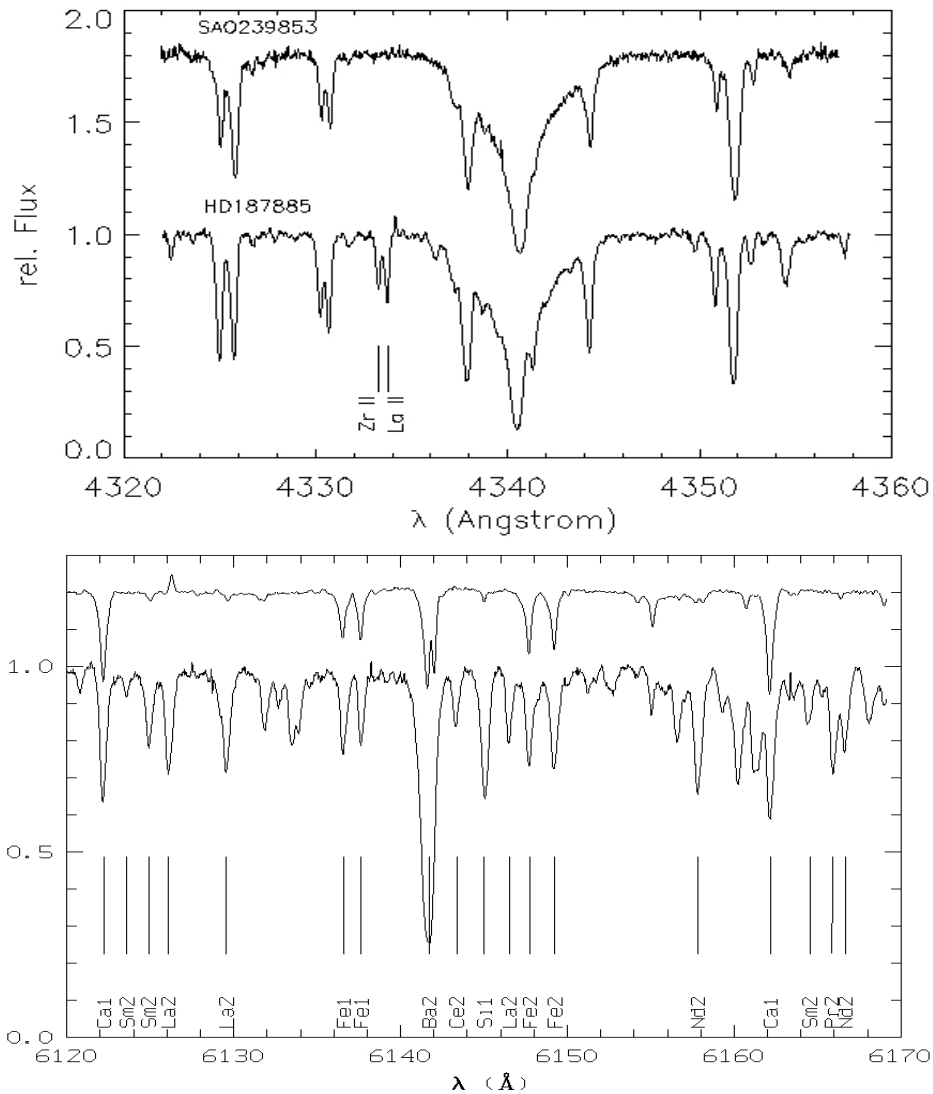

Figure 5.15: Both panels show sample spectra of stars with very similar spectral type. The relative abundances are much more reliable than the absolute values.

Chapter 6

Continuum processes

Contrary to bound-bound transitions, continuum processes will yield extinction and emission coefficients which affect the interaction with the radiation field in a broad spectral band. The continuum processes can involve bound electrons, but they are also relevant in the radiative continuum interactions with free particles (electrons, heavier charged particles, neutral particles).

We differentiate between bound-free, free-free processes as well as scattering processes on free or bound electrons. In this chapter we begin with refreshing some basics of the classical theory of electromagnetic radiation. We develop this in the context of an accelerating electron due to the coulomb interaction with a proton and we come to an expression for the free-free radiation of an optically thin, completely ionised gas cloud of hydrogen. In the next section, the cross-sections of scattering processes are given. The cross-sections of the dominant bound-free processes are given in the next section and we elaborate a bit more on the dominant continuum process in the Solar atmosphere: the H^- opacity source (bound-free and free-free). We end the chapter by evaluation the continuum processes in stellar atmospheres.

6.1 Classical Theory

In the classical description of electromagnetic interaction with particles it is the Electric field $\mathbf{E}(\mathbf{r},t)$ and the Magnetic field $\mathbf{B}(\mathbf{r},t)$ which will interact with the charges. The charges will oscillate and the accelerated charges produce on their turn electromagnetic fields and thus they will radiate energy.

Electromagnetic waves carry energy and the rate at which the energy flows through a unit surface area perpendicular to the direction of the wave propagation,

is the *Poynting vector*. The magnitude of the Poynting vector is the power per unit area (SI units: Watt/m^2):

In the classical approach, the extinction coefficient associated with the interaction is related to the net flux decrease of the incoming electromagnetic field.

The field equations give the relation between Electric field, the Magnetic field and the charges and currents they influence.

The Lorentz force on a particle with charge q with a velocity **v**:

$$\mathbf{F} = q\left(\mathbf{E} + \frac{\mathbf{v}}{c} \times \mathbf{B}\right) \tag{6.1}$$

and the rate of work performed by the fields on the particle is (**v.(v** $\times$ **B)** = 0):

$$\mathbf{v}.\mathbf{F} = q\mathbf{v}.\mathbf{E} \tag{6.2}$$

which is for non relativistic particles:

$$q\mathbf{v}.\mathbf{E} = \frac{d}{dt}\left(\frac{1}{2}\, m\, \mathbf{v}^2\right) \tag{6.3}$$

The total force on a volume with many charges (j = current density; ρ is charge density):

$$\mathbf{f} = \rho\,\mathbf{E} + \frac{1}{c}\,\mathbf{j} \times \mathbf{B} \tag{6.4}$$

where ρ is the charge density and **j** the current density:

$$\rho = \lim_{\Delta V \to 0} \frac{1}{\Delta V} \sum_i q_i \tag{6.5}$$

$$\mathbf{j} = \lim_{\Delta V \to 0} \frac{1}{\Delta V} \sum_i q_i \mathbf{v_i} \tag{6.6}$$

If we work per unit volume, the rate of work done by the fields is then (Equation 6.2):

$$\frac{1}{\Delta V} \sum_i q_i \mathbf{v_i}.\mathbf{E} = \mathbf{j}.\mathbf{E} \tag{6.7}$$

This is also the rate of change of mechanical energy (see Equation 6.3).

$$\frac{dU_{mech}}{dt} = \mathbf{j}.\mathbf{E} \tag{6.8}$$

The Maxwell equations relate the electric field, the magnetic field and the charge and current densities. In differential form they read:

1. Law of Gauss for the electric field :

$$\nabla \cdot \mathbf{E} = \frac{\rho}{\epsilon_0}$$

2. Law of Faraday (induction):

$$\nabla \times \mathbf{E} = -\frac{\partial \mathbf{B}}{\partial t}$$

3. Law of Gauss for the magnetic field:

$$\nabla \cdot \mathbf{B} = 0$$

4. Law of Maxwell:

$$\nabla \times \mathbf{B} = \frac{\mathbf{j}}{\epsilon_0\, c^2} + \frac{1}{c^2}\frac{\partial \mathbf{E}}{\partial t}$$

$\mathbf{E}$	:	the electric field,
$\mathbf{B}$	:	the magnetic field,
ϵ_0	:	the permittivity of the vacuüm,
$\mathbf{j}$	:	the current density,
ρ	:	the charge density.

With ϵ_0 the permittivity of the vacuum (a physical constant connecting mechanical quantities to units of electrical charge) and μ_0 the magnetic permeability or magnetic constant. Remember that $\epsilon_0 \nu_0 c^2 = 1$. Often the relations are expressed Gaussian units, ($\epsilon_0 = 1, \mu_0 = 1$).

In Gaussian units, the Maxwell equations read:

1. Law of Gauss for the electric field :

$$\nabla \cdot \mathbf{D} = 4\pi\rho \tag{6.9}$$

2. Law of Faraday (induction):

$$\nabla \times \mathbf{E} = -\frac{1}{c}\frac{\partial \mathbf{B}}{\partial t} \tag{6.10}$$

3. Law of Gauss for the magnetic field:

$$\nabla \cdot \mathbf{B} = 0 \tag{6.11}$$

4. Law of Maxwell:

$$\nabla \times \mathbf{H} = \frac{4\pi}{c}\mathbf{j} + \frac{1}{c}\frac{\partial \mathbf{E}}{\partial t} \tag{6.12}$$

With $D = \epsilon_0 E$ and $B = \mu_0 H$.

6.1.1 Poynting's Theorem

The conservation of charge is found by taking the $\nabla.$ of the Maxwell law and using the law of Gauss we get:

$$\nabla.\mathbf{j} + \frac{\partial \rho}{\partial t} = 0 \tag{6.13}$$

which expresses the conservation of charge for a volume element.

Conservation of energy is expressed as:

$$\frac{\partial u}{\partial t} = -\nabla \cdot \mathbf{S} - \mathbf{E} \cdot \mathbf{j}, \tag{6.14}$$

with

u : the energy density of the fields
$\mathbf{S}$: the energy flux

When we consider the energy density and energy flux of the electromagnetic radiation we use the Maxwell equation to isolate $\mathbf{j}.\mathbf{E}$:

$$\begin{aligned}
\frac{\partial u}{\partial t} &= -\nabla \cdot \mathbf{S} - \mathbf{E} \cdot \left[\epsilon_0\, c^2\, \nabla \times \mathbf{B} - \epsilon_0 \frac{\partial \mathbf{E}}{\partial t}\right] \\
&= -\nabla \cdot \mathbf{S} + \epsilon_0\, \mathbf{E} \cdot \frac{\partial \mathbf{E}}{\partial t} + \epsilon_0\, c^2\, [\nabla \cdot (\mathbf{E} \times \mathbf{B}) - \mathbf{B} \cdot (\nabla \times \mathbf{E})] \\
&= -\nabla \cdot \mathbf{S} + \epsilon_0\, \mathbf{E} \cdot \frac{\partial \mathbf{E}}{\partial t} + \epsilon_0\, c^2\, \nabla \cdot (\mathbf{E} \times \mathbf{B}) + \epsilon_0\, c^2\, \mathbf{B} \cdot \frac{\partial \mathbf{B}}{\partial t}
\end{aligned} \tag{6.15}$$

using the identity known from calculus:

$$\nabla \cdot (\mathbf{E} \times \mathbf{B}) = -\mathbf{E} \cdot (\nabla \times \mathbf{B}) + \mathbf{B} \cdot (\nabla \times \mathbf{E}) \,. \tag{6.16}$$

The energy density is given by:

$$u = \frac{\epsilon_0}{2}\mathbf{E} \cdot \mathbf{E} + \frac{\epsilon_0\, c^2}{2}\mathbf{B} \cdot \mathbf{B} \tag{6.17}$$

and the energy flux is given by the Poynting vector:

$$\mathbf{S} = \epsilon_0\, c^2\, (\mathbf{E} \times \mathbf{B}) \,. \tag{6.18}$$

The Poynting theorem expresses that the rate of change of mechanical energy ($\mathbf{j}.\mathbf{E}$) per unit volume, plus the rate of change of field energy ($\partial u/\partial t$) per unit volume equals minus the divergence of the field energy flux.

Poynting vector is the flux of energy of a EM wave perpendicular to the direction through a unit surface (units: Watt/m^2). If we multiply the Poynting vector with the total surface area, we compute the total power.

6.2 Free-Free radiation or thermal bremsstrahlung

In a hot plasma of ionised atoms, the free electrons will interact with the ions by the Coulomb force. The electrons will get accelerated and hence will emit photons. In this section we deduce the volume emissivity (power emitted per unit volume per unit frequency at frequency ν):$j_\nu(\nu)$. We will assume the plasma to be optically thin so all created photons will leave the plasma cloud. An example are H II regions which are ionised by neighbouring hot stars but also in cluster of galaxies, hot plasma exist. These are even heated to x-ray temperatures.

Such plasma will exist when the electrons are energetically so that collisions between electrons and protons will not result in recombination: the plasma will remain ionised. For a mono-atomic gas in thermal equilibrium the average translational kinetic energy is:

$$\frac{3}{2}\, k\, T = (\frac{1}{2}\, m\, v^2)_{average} \tag{6.19}$$

The fraction of atoms ionised is *the degree of ionisation.* At low densities, collisional excitation is low and a hydrogen plasma becomes almost totally ionised at temperature as low as $\sim$ 3000 K ! In stellar atmospheres, with much higher densities, the full ionisation of hydrogen only occurs at much higher temperatures.

In a H-plasma, the average kinetic temperature of ions and electrons is the same. The electrons will therefore move about 40 times faster that the protons. We consider the protons (of heavier ions) to be at rest.

In the development we assume that the total energy loss of an electron, integrated over the total collision, is only *a small part of the total kinetic energy.*

In general, collisions are quantum phenomena: the electromagnetic force itself is an exchange of virtual photons of which few escape and become observable. For slowly moving particles and relatively near collisions, the number of virtual photons is large and the classical approach is appropriate. We therefore assume the collisions are at non-relativistic speeds. The classical approach developed in this section also requires that the accelerated electrons emit photons with energies significantly less than their own kinetic energy. Under these assumptions, quantum effects can be neglected.

The development to come to the volume emissivity of an optically thin plasma will yield a continuum spectrum without spectral lines. In general, however, HII regions are rich in spectral signatures and they show.:

- Free-free emission
- Transitions at closely spaced very high levels at radio wavelengths
- Recombination lines in the optical-radio
- X-rays coming from spectral lines of heavy elements

In what follows we develop the expression for an optically thin monoatomic plasma cloud. The reader is referred to Bradt (2008) for a more detailed exposure of the whole development. We come to the expression of the volume emissivity in several steps:

- what will a single electron-ion collision emit (Larmor's formula)
- the ν of the emitted radiation in terms of electron speed and impact parameter
- the power of the emitted radiation at ν into $d\nu$ by all electrons at different speeds that collide with a single proton

- the emitted power at ν into $d\nu$ from all collisions in a unit volume (volume emissivity $j_\nu(\nu, T)$) in units Watt m^{-3} Hz^{-1}
- The integrated volume emissivity j (integral over ν)
- The specific intensity $I(\nu, T)$ in terms of line-of-sight thickness of the plasma

6.2.1 Free-free radiation of a single electron-ion collision

In Fig 6.1 the single accelerated positive charge is depicted with an acceleration of $\vec{a}$ at an earlier time $t' = t - r/c$. The instantaneous pattern of the electric field lines of a moving charge q is isotropic when the charge q is moving in straight lines at a constant speed v (v$\ll$). When there is an acceleration, the field lines become distorted and at large distances the field consists of transverse electric and magnetic field vectors.

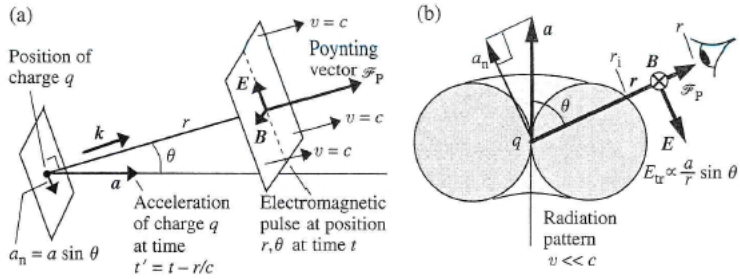

Figure 6.1: Electric and Magnetic vectors at position r,θ at time t coming from a acceleration $\vec{a}$ of a positive charge at earlier time. The propagation vector $\vec{k} = 2\pi/\lambda\,\hat{k}$ *Fig. taken from Bradt (2008)*

The propagating electric vector $\mathbf{E}$, lines in a plane defined by the acceleration vector $\mathbf{a}$ and the propagation vector $\mathbf{k}$. The $\mathbf{E}$ vector is proportional to the projection of $\mathbf{a}$ onto the line of sight (a_n) and is opposite to it, when the charge is positive and in the same direction when the charge is negative. The amplitude is also proportional to the charge q and varies with the distance 1/r.

The magnitude of the transverse electric field in vacuum is (q a/r) sinθ. In SI units this becomes:

$$\mathbf{E}(\mathbf{r}, t) = \frac{q\, a(t')\, \sin\theta}{4\,\pi\,\varepsilon_0\, c^2\, r}\hat{\mathbf{n}} \tag{6.20}$$

$$= \frac{q}{4\,\pi\,\varepsilon_0\, c^2\, r}(\mathbf{a} \times \hat{\mathbf{k}}) \times \hat{\mathbf{k}} \tag{6.21}$$

with ε_0 the permittivity of the vacuum. Together with the permeability of free space μ_0 they relate to

$$c^2 = \frac{1}{\mu_0 \varepsilon_0} \tag{6.22}$$

The angular dependency is also depicted in Fig. 6.1 which gives the dipole radiation pattern.

At a given point in space and at a given time t the energy flux (Watt/m^2) carried by the electromagnetic radiation is given by the Poynting vector, which becomes here:

$$\mathbf{S_p} = \frac{\mathbf{E} \times \mathbf{B}}{\mu_0} \tag{6.23}$$

In the case of a dipole of previous figure (**B** and **E** perpendicular to each other) this becomes:

$$S_p = \varepsilon_0 \, c\mathbf{E}.\mathbf{E} = \varepsilon_0 \, cE_{tr}^2 \tag{6.24}$$

The magnitude of the Poynting vector is then:

$$S_p(r, \theta, t) = \frac{q^2 \, \sin^2 \theta \; a^2(t')}{(4\,\pi)^2 \, \varepsilon_0 \, c^3 \, r^2} \tag{6.25}$$

The natural 1/r^2 relation is clear and and maximal power is measured at θ = 90^0.

6.2.1.1 Larmor's formula

The total power, radiated by the electron into *all* direction is obtained by summing over the whole spherical surface at distance r from the charge:

$$P(t) = \int_{\theta=0}^{\pi} \int_{phi=0}^{2\pi} S_p(r, \theta, t) \, r^2 \, \sin\theta d\phi \, d\theta \tag{6.26}$$

After integration this becomes Larmor's formula:

$$P(t) = \frac{1}{6\,\pi\,\varepsilon_0} \frac{q^2 \, a^2(t)}{c^3} \tag{6.27}$$

This is the total power crossing a sphere at radius r at time t in terms of a earlier acceleration at time t'. The unit is just Watt. The power is independent of distance r because the same power is radiated at a large r at a later time. P(t) is the power radiated instantaneously by an electron.

6.2 .1.2 Energy radiated in the event

The acceleration will depend on the strength of the Coulomb force between two charges during the collision:

$$\mathbf{F} = \frac{q_1\, q_2}{4\,\pi\,\varepsilon_0\, r^2}\,\hat{r} \tag{6.28}$$

The acceleration of an electron (-e) of mass m and ion charge Ze is :

$$\mathbf{a} = \frac{\mathbf{F}}{m} = -\frac{1}{4\,\pi\,\varepsilon_0}\,\frac{Z\,e^2}{r^2\,m}\hat{r} \tag{6.29}$$

In Fig 6.2 we illustrate the impact approach in the description of a collision.

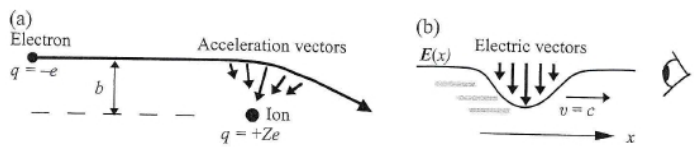

Figure 6.2: The impact parameter and the approximate duration of the collision. *Fig. taken from Bradt (2008)*

The projected distance of closed approach is given by the impact parameter b. The collision is at low energies so the deflection is only marginal. The impact parameter is different from collision to collision. Here we consider the ion to be just a point source. The acceleration is maximal at closest approach and there it can be written as:

$$a_{max} \approx \frac{1}{4\,\pi\,\varepsilon_0}\,\frac{Z\,e^2}{b^2\,m} \tag{6.30}$$

The collision time depends not only on the impact parameter, but also on the velocity v of the charge. The total collision time may be approximated by:

$$\tau_b \approx \frac{b}{v} \tag{6.31}$$

In this approximation, we assume that the collision takes τ_b seconds and that the distance traveled during the collision is b.

The total energy emitted is the integration over the duration of the collision. This becomes:

$$Q(b,v) = \int_{-\infty}^{\infty} P(t)dt = \frac{1}{6\,\pi\,\varepsilon_0}\,\frac{e^2}{c^3}\int_{-\infty}^{\infty} a^2(t)\,dt \tag{6.32}$$

Approximate (constant at maximum acceleration during collision and zero before and after this period) this is :

$$Q(b,v) \approx \frac{1}{6\,\pi\,\varepsilon_0}\,\frac{e^2}{c^3} a_{max}^2(t)\,\tau_b \tag{6.33}$$

This becomes (when we include the approximate collision duration to be b/v):

$$Q(b,v) \approx \frac{1}{(4\,\pi\,\varepsilon_0)^3}\,\frac{2}{3}\,\frac{Z^2\,e^6}{c^3\,m^2\,b^3\,v} \tag{6.34}$$

This is the total energy, radiated by a single electron of speed v as it passes an ion of charge Ze. The unit is Joule/collision. The energy loss increases strongly with decreasing impact parameter b. The velocity before and after the collision is very similar as only a small part of the initial kinetic energy is transformed to radiation. For faster electrons, the radiation energy Q is *smaller* as the duration of the collision is short.

6.2 .2 ν of the emitted radiation

The radiation of a single event, consists of a single pulse of downward pointing **E** vectors running towards the observer. The frequency of the radiation derives directly from the duration of the central portion of the pulse as inferred from an observer at rest. ($\tau_b \approx b/v$) The pulse of a negative accelerating particle (electron) will be observed at at angular frequency ($2\pi\nu$).:

$$\omega_{tb} \approx \frac{1}{\tau_b} = \frac{v}{b} \tag{6.35}$$

The characteristic frequency of the radiation of a single collision is thus:

$$\nu = \frac{\omega_{tb}}{2\pi} \approx \frac{v}{2\pi\, b} \tag{6.36}$$

So there is a direct relation between the impact parameter and the frequency of the radiation : the smaller the impact parameter, the higher the frequency. Or after the derivative:

$$db = \frac{-v}{2\pi\nu^2}\, d\nu \tag{6.37}$$

This is the relation between the intervals of the impact parameter b and the frequency $d\nu$.

6.2 .3 Many thermal electrons and a single ion

6.2 .3.1 single speed electrons

To address the question of what radiation will be observed when we deal with a single ion in a sea of thermal electrons, we assume first that the electrons have the same velocity vector (see Fig. 6.3). So we consider the electron come from a parallel beam and have speed v.

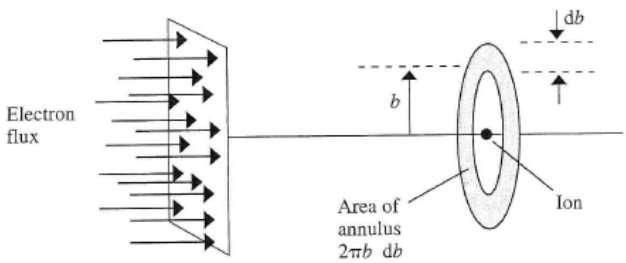

Figure 6.3: When a flux of electrons is approaching an ion. *Fig. taken from Bradt (2008)*

The number of electrons crossing an annulus of db at impact parameter b depends on the electron density n_e and the electron flux $n_e\, v$ (electrons m^{-2} s^{-1}). The energy radiated by all these electrons per unit time is given by:

$$P_b(b,v)db = Q(b,v)\, n_e\, v\, 2\pi\, b\, db \tag{6.38}$$

The unit here is watt/ion in db at b so per unit impact parameter. This is the power per ion, per unit impact-parameter interval. This can converted per unit frequency interval $P_b(\nu,v)$:

$$P_b(b,v)db = -P_\nu(\nu,v),\, d\nu \tag{6.39}$$

This becomes (replacing db/dν):

$$P_\nu(\nu,v) = Q(b,v)\, n_e\, v\, 2\pi\, b \frac{v}{2\pi\, \nu^2} \tag{6.40}$$

The power emitted by a single ion from the cloud of electrons at speed v:

$$P_\nu(\nu,v)\, d\nu \approx \frac{1}{(4\,\pi\,\varepsilon_0)^3}\, \frac{8\,\pi^2}{3}\, n_e\, \frac{Z^2\, e^6}{c^3\, m^2\, v} d\nu \tag{6.41}$$

The unit is watt/ion in dν at ν. We see that this is *independent* of frequency... There are more collisions at larger b but they will emit lower frequency photons. This is approximate and at a more rigorous development will yield a frequency dependence. This exact classical formalism differs only from this formula by the inclusion of a ν-dependence *Gaunt* factor which is of order unity. The characteristic kinetic energy $\sim\ k\,T$ must be substantially less than the rest energy (mc^2). The temperature of the plasma must be $\ll\ 6 \times 10^9\ K$.

The maximal frequency is determined by the total kinetic energy of the electron (where the formula is not correct):

$$\nu_{max} = \frac{m\, v^2}{2\, h} \tag{6.42}$$

This is the cut-off frequency above which the radiated power drops to zero.

6.2 .3.2 electrons at many speeds

The probability of an electron having a speed v in the interval dv is

$$P(\mathbf{v}) = (\frac{m}{2\,\pi\, k\, T})^{2/3} \exp\,(-\frac{m\, v^2}{2\, k\, T}) \tag{6.43}$$

This is the probability of a vector velocity **v** per unit 3-D velocity space. When you consider the speed v, the probability of an electron having a speed v (irrespective of the vector direction)

$$P(v)\,dv = P(\mathbf{v})\,4\pi\,v^2\,dv \tag{6.44}$$

So integral over all speeds. The power summed over all speeds is an integral over these speeds:

$$< P(\nu)_{ion} >_{speed} = \int_{v_{min}}^{\infty} P_\nu(\nu, v), P(\mathbf{v})\,4\pi\,v^2\,dv \tag{6.45}$$

This is the power of radiation emitted at frequency ν (per bandwidth) form a single ion in a sea of electrons with Maxwell-Boltzmann distribution of speeds. The lower limit of the integral is the smallest velocity an electron can have and still emit a photon of energy $h\nu$. An electron can of course not give up more energy than it had and for a fixed frequency this speed limit is:

$$v_{min} = \sqrt{(\frac{2h\nu}{m})} \tag{6.46}$$

6.2 .4 Volume emissivity

When there is a density of ions n_i and a density of electrons n_e with a Maxwell-Boltzmann distribution of speeds, the volume emissivity per frequency bin $j_\nu(\nu)\,d\nu$ has units Watt/m^3 in dν at ν.

$$j_\nu(\nu)\,d\nu =< P(\nu)_{ion} >_{speed}\; n_i\,d\nu \tag{6.47}$$

or this becomes:

$$j_\nu(\nu)\,d\nu = n_i \left[\int_{v_{min}}^{\infty} P_\nu(\nu, v), P(\mathbf{v})\,4\pi\,v^2\,dv\right] d\nu \tag{6.48}$$

After substitution and including the QM correction factor (Gaunt factor), the corrected expression reads:

$$j_\nu(\nu)\,d\nu = g(\nu, T, Z)\,\frac{1}{(4\,\pi\,\varepsilon_0)^3}\,\frac{32}{3}\,(\frac{2}{3}\frac{\pi^3}{m^3\,k})^{1/2}\,\frac{Z^2\,e^6}{c^3}\,n_e\,n_i\frac{e^{-h\nu/kT}}{T^{1/2}}\,d\nu \tag{6.49}$$

Or with all proportionality constants represented by C_1:

$$j_\nu(\nu)\, d\nu = C_1\, g(\nu, T, Z)\, Z^2\, n_e\, n_i\, \frac{e^{-h\nu/kT}}{T^{1/2}}\, d\nu \tag{6.50}$$

With $C_1 = 6.8 \times 10^{-51}$ J m^3 K$^{1/2}$.

The frequency dependence is given in Fig 6.4 in a log-log scale At low frequencies, the exponential approaches unity and the emissivity becomes flat. The frequency dependent Gaunt factor is only measurable at many decades in frequency but gives a slight rise at lower frequencies.

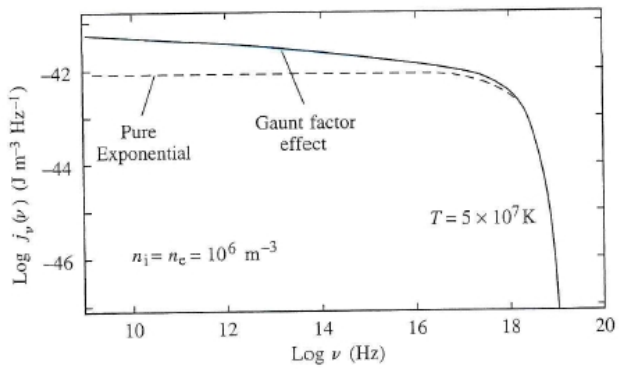

Figure 6.4: Frequency dependence of the volume emmisivity of free-free radiation coming from electron-ion collisions. *Fig. taken from Bradt (2008)*

In Fig 6.5, several representations of the volume emissivity is given at two different temperatures. The exponential term causes a rapid decrease of flux at higher cut-off frequencies for a higher temperature. At low frequencies, the $T^{-1/2}$ ter governs the slope when the other variables are held fixed. So at low frequencies, the lower temperature plasma has a higher flux than the higher temperature plasma.

Most of the power, however occurs at frequencies near the cut-off (the volume emissivity is per bandwidth).

6.2.5 Integrated volume emissivity

The integration of the volume emissivity over the frequencies give the total power:

$$j(T) = \int_0^\infty j_\nu\, d\nu = C_2\, \bar{g}(T, Z),\ Z^2\, n_e\, n_i\, T^{1/2} \tag{6.51}$$

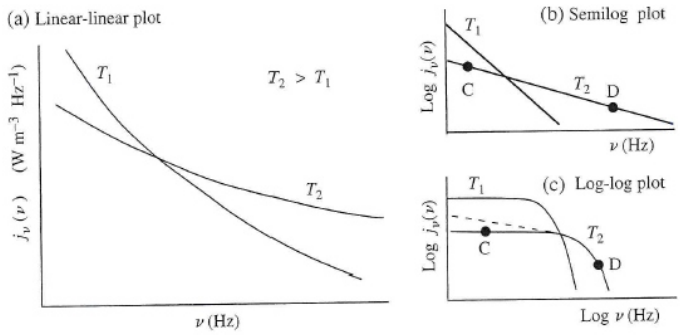

Figure 6.5: The volume emissivity at two different temperatures. At low frequencies, the volume emissivity is higher at lower temperatures...

with C_2 = 1.44$\times 10^{-40}$ W m^3 K$^{-1/2}$

The $\bar{g}$ is the frequency averaged Gaunt factor which can range between 1.1 and 1.5. The total power increases with temperature for fixed densities.

The total luminosity of a cloud is than the integration over the volume. For a Hydrogen plasma this is:

$$L(T) = C_2\, \bar{g}(T)\, T^{1/2} \int_{volume} n_e^2 dV \tag{6.52}$$

6.2.6 Specific Intensity

The specific intensity $I(\nu, T)$ has units of Watt/m^2/Hz-1/sr^{-1} and it is the quantity we measure for resolved plasma clouds.

The product of the angular spatial extend, is the measured energy flux detected at frequency ν in the bandwidth dν. $I(\theta, \phi, \nu, T)\, d\nu\, d\Omega$ gives the measured flux at frequency ν in the bandwidth $d\nu$ in the increment solid angle $d\Omega = \sin\theta d\theta\, d\phi$.

In general, the specific intensity of a cloud of thickness Λ is:

$$I(\nu, T) = \int_0^\Lambda \frac{j_\nu(r, \nu, T)}{4\pi} = \frac{j_\nu(\nu, T)_{av}}{4\pi}\, \Lambda \tag{6.53}$$

for a isothermal cloud with only fully ionised hydrogen this becomes:

$$I_\nu(\nu, T) = \frac{C_1}{4\pi}\, g(\nu, T, Z)\, \frac{e^{-h\nu/kT}}{T^{1/2}} \int_0^\Lambda n_e^2 dr \tag{6.54}$$

or with a average electron density this is:

$$I_\nu(\nu, T) = \frac{C_1}{4\pi}\, g(\nu, T, Z)\, \frac{e^{-h\nu/kT}}{T^{1/2}} n_{e,av}^2\, \Lambda \tag{6.55}$$

We call the square of the average electron density times the line-of-sight thickness the *Emission Measure* (EM).

For a given hydrogen cloud, the intensity is determined by only two unknowns: the temperature and the EM. Two measurements at different frequencies would yield a good estimate of the two unknowns. The frequency at which the function has dropped to e^{-1} of its low frequency intercept, gives T as $h\nu = kT$. With this value of the temperature, any measurement of the specific intensity gives the EM without knowledge of the distance to the cloud ! A direct measurement of the specific intensity is only possible when the cloud is resolved !

6.2 .7 Free-Free extinction

The free-free process (or *bremsstrahlung* process) involves an interaction between an electron and an ion such that the electron interacts with the Coulomb field of the ion and will emit or absorb a photon to loose or gain energy. The process is an interchange between kinetic energy and radiative energy. The electron will remain free in this process. The nomenclature is such that e.g. FeI ff denotes the interaction between a electron and a Fe II ion ! Free-free emission is also called.

In TE, the source fuction of this process is the Plancks function $B_\nu(T)$. Also outside TE this is the case whenever the velocity distribution of the particles follow the Maxellian velocity distribution. Free-free extinction is a collisional process.

Following equation 6.49 and the source function defined by the Plancks function we get:

$$\alpha_\nu^{\rm ff} \propto Z^2\, N_{\rm ion}\, T^{-1/2}\, \nu^{-3}\,. \tag{6.56}$$

We see that for higher temperatures, the absorption coefficient will be lower (with a similar electron density): the higher the velocities, the lower the chance of an interaction. Hydrogen free-free is an important opacity source when there are protons an free electrons (so in stellar interiors and in O-star photospheres).

In the Wien part of the EM spectrum ($h\nu/kT \gg 1$) the correction for stimulated emission can be omitted an we get a ν^{-3} dependency. In the Rayleigh-Jeans area ($h\nu/kT \ll 1$), the slope is less steep and we get a (ν^{-2}) dependency.

6.3 The Dipole approximation

As used in previous section: an electromagnetic field will interact with a charged particle and we assume this particle to move at a non-relativistic speed. The fields will interact with the particles making them to accelerate. Hence they produce electromagnetic fields on their turn.

The total energy emission from a single accelerated charge q at a velocity v is given by the Larmor's formula.

$$P = \int \mathbf{S}.dA = \frac{1}{6\pi\epsilon_0 c^3}\ddot{p}^2 = \frac{q^2\,\dot{v}^2}{6\pi\epsilon_0 c^3} \tag{6.57}$$

The power emitted is proportional to the square of the charge and the square of the acceleration.

Often confusion is generated in the literature by the unit conventions:

$$e^2 = \frac{q^2}{4\pi\epsilon_0} \quad \text{in SI} - \text{units} \tag{6.58}$$

or

$$q = \pm e \quad \text{in cgs} - \text{units.} \tag{6.59}$$

In cgs units (which do often appear in the literature) the Larmor's formula reads:

$$P = \frac{e^2\dot{v}^2}{6\pi\epsilon_0 c^3}\,, \text{ and} \tag{6.60}$$

$$P = \frac{2e^2\dot{v}^2}{3c^3} \tag{6.61}$$

in SI-units.

Assume now that the dipole oscillates with circular frequency ω,

$$z = z_0\, cos\,\omega\, t\,, \tag{6.62}$$

The mean intensity radiated by the electromagnetic wave is given by taking the mean:

$$< P >= \frac{e^2\omega^4 z_0^2}{12\pi\epsilon_0 c^3} \text{ and} \tag{6.63}$$

$$< P >= \frac{e^2 \omega^4 z_0^2}{3c^3} \tag{6.64}$$

in the appropriate units. The spectrum is directly related to the frequency.

6.4 Scattering processes

Scattering processes involve a double process in which the particle will absorb energy from the fields and re-emits this energy with very similar characteristics. The process can be isotropic (same spatial redistribution) but also anisotropic. Coherent scattering is monochromatic scattering and net effect is that the photon just changes direction. In frequency redistribution processes, there may be a small shift in frequency: e.g. for bound-bound scattering, there may be a redistribution over the line profile. We can have scattering processes on free electrons, but also on bound electrons.

6.4.1 Thomson scattering

For low-energy free electrons, the scattering on free electrons is non-relativistic ($h\nu \ll m_e c^2$) and the scattering is coherent (also dubbed "elastic scattering").

Assume a electromagnetic wave with frequency ω which runs along the x-direction. The interaction with the free electron is described such that the electron will oscillate with the wave undamped. The electric field associated with the wave points in the z-direction and can be written as:

$$\mathbf{E} = E_0 \, cos(kz - \omega t) \, \mathbf{e}_z \tag{6.65}$$

A charge q is accelerated by the wave which yields:

$$m \, \ddot{\mathbf{r}} = q\mathbf{E} \tag{6.66}$$

so we can write:

$$\ddot{p} = q \, \ddot{z} = \frac{q^2}{m} \, E_0 \, cos(kz - \omega t) \tag{6.67}$$

and

$$< \ddot{p}^2 >= \left(\frac{q^2}{m}\right)^2 < E^2 >= \frac{1}{2}\left(\frac{q^2}{m}\right)^2 E_0^2 \tag{6.68}$$

In SI units, the energy radiated by the moving charge is:

$$P \equiv < P >= \frac{1}{6\pi\epsilon_0 c^3}\frac{1}{2}\left(\frac{q^2}{m}\right)^2 E_0^2 = \frac{4\pi}{3}\frac{\epsilon_0 e^4}{m^2 c^3} E_0^2 \tag{6.69}$$

The energy density of the incoming field can be expressed as (see Equation 6.17).

$$u = \frac{\epsilon_0}{2}\mathbf{E}\cdot\mathbf{E} + \frac{\epsilon_0 c^2}{2}\mathbf{B}\cdot\mathbf{B} = \epsilon_0\,\mathbf{E}\cdot\mathbf{E} \tag{6.70}$$

and

$$< u >= \frac{\epsilon_0\, E_0^2}{2}\,. \tag{6.71}$$

The energy of the wave per unit time and per unit surface area perpendicular to the running direction is given by $P_0 =< u > \; c$.

The ratio between the emitted and incoming radiation is given by:

$$\sigma \equiv \frac{P}{P_0} = \frac{8\pi}{3}\left(\frac{e^2}{mc^2}\right)^2 \tag{6.72}$$

which is the amount of absorption of energy. σ has units of cm^2 and is the cross-section. For free electrons this cross-section is quantified as:

$$\sigma_e = 6.65\,10^{-25}\,\mathrm{cm}^2. \tag{6.73}$$

This cross section is frequency INdependent so irrespective of the frequency of the incoming radiation, the cross section is the same. Such a process is called a *grey* process.

This effect has a strong impact in stellar interiors. A back-of-the-envelope calculation learns us that if we take the mean density of the Sun (1 g/cm^3) and we assume that about $1/2000$ are electrons. The mass of an electron is 10^{-27} g. So per cm^3 there are about $5\,10^{23}$ electrons. Every electron fills about $2\,10^{-24}$ cm cube. The mean-free-path of a photon for electron scattering can be estimated as

$(2\,10^{-24})/(6.65\,10^{-25})$ cm, which is... 3 cm !. In the atmosphere, the density is lower so the mean-free-path will be significantly larger (fortunately).

The cross section had a m^{-2} dependency so scattering on free ions and even protons will be much less important.

6.4 .2 Rayleigh scattering

When an electromagnetic wave interacts with an atom, the bound electrons will also get distorted. Those atoms will send electromagnetic radiation on their turn with the same frequency as in incoming wave. Since the incoming and outgoing wave has the same frequency, it is a scattering process. Classical electromagnetism does not give a good description of spectral signatures of bound systems, however. In the classical approach, the damped harmonic oscillator is used to describe the process and the resonance frequency is unique to the given transition.

$$\ddot{z} + \gamma\,\dot{z} + \omega_0^2\,z = 0\,, \tag{6.74}$$

with γ the damping constant.

The incoming electromagnetic wave with frequency ω will induce a forced oscillation of the electron with mass m_e:

$$\ddot{z} + \gamma\,\dot{z} + \omega_0^2\,z = \frac{q\,E_0}{m_e} e^{i\omega\,t}\,, \tag{6.75}$$

A solution in the form $z = z_0\,e^{i\omega t}$ gives:

$$\ddot{z} = \frac{q\,E_0}{m}\frac{-\omega^2}{(\omega_0^2 - \omega^2) + i\,\gamma\,\omega} e^{i\,\omega\,t} \tag{6.76}$$

such that:

$$< \ddot{z}^2 >= \frac{q^2 E_0^2}{2m^2}\frac{\omega^4}{(\omega_0^2 - \omega^2)^2 + \gamma^2\,\omega^2}\,. \tag{6.77}$$

Adapting equation 6.69, we get for the energy radiated by the oscillator (in SI-units):

$$P = \frac{4\pi}{3}\frac{\epsilon_0\,e^4\,E_0^2}{m^2\,c^3}\frac{\omega^4}{(\omega_0^2 - \omega^2)^2 + \gamma^2\,\omega^2} \tag{6.78}$$

the cross section becomes:

$$\sigma = \frac{8\pi}{3}\frac{e^4\omega^4}{m^2c^4}\frac{1}{(\omega_0^2-\omega^2)^2+\gamma^2\,\omega^2}\,. \tag{6.79}$$

This is a Lorentz profile. The quantummechnical correction is given by the oscillator strength which is a multiplication factor in the cross-section given above which gives the classical expression. When the damping constant is small with respect to the frequency ω if the EM-wave ($\gamma \ll \omega$) and the eigenfrequency of the bound electron in an atom is large ($\omega \ll \omega_0$), we can approximate the cross section as:

$$\sigma(\omega) \propto \omega^4 \propto \lambda^{-4}\,. \tag{6.80}$$

Under these conditions we call the scattering *Rayleigh-scattering*. In the limit of no damping and $\omega_0 = 0$ we will find the cross section of electron scattering. This classical description is good as long as the frequency of the incoming radiation is different enough from the resonance frequency.

The total cross section for small damping constants is found by integrating all possible frequencies ($\nu = \omega/2\pi$)

$$\sigma_{tot} = \int_0^\infty d\nu\,\sigma(\omega) = \frac{\pi\,e^2}{m\,c} = 0.02654\,\mathrm{cm}^2\,. \tag{6.81}$$

Raileighscattering is much weaker than electron scattering and will only have a significant contribution when there are trace amounts of free electrons. The ratio of the cross sections are:

$$\frac{\sigma_{rayl.}(\omega)}{\sigma_{Thom.}} \sim f_{lu}\,(\frac{\omega}{\omega_{lu}})^4 \ll 1. \tag{6.82}$$

A low number of free electrons is found in stars of G and K spectral type and colder. The contribution of Rayleigh scattering will increase at lower metallicities for these stars because the iron peak elements are the main electron donors in those atmospheres: the H^- opacity (see later section) will be lower in metal poor stars. For colder objects like M stars, Rayleigh scattering on H_2 will become important.

6.5 Bound-Free processes

In a bound-free process, part of the energy in the process is used to ionise the atom or ion and liberate an electron from a bound state. The total energy available

in the process, either from a photon or from a collision, needs to be in excess of the ionisation potential of the valence bound electron. The energy excess will be transformed into kinetic energy of the particles. Similar to the bound-bound processes we differentiate between:

1. photo-ionisation (E_{photon} = $E_{ionsiation}$+$E_{e^-,kinetic}$)
2. spontaneous photo-recombination
3. induced photon-ionisation
4. collisional ionisation ($E_{collision}$ = $E_{ionsiation}$+$E_{e^-,kinetic}$)
5. collisional recombination (three body collision)

The latter process needs three particles and is rather rare.

6.5 .1 Photo-Ionisation

Given the very high abundance of H (and the high ionisation potential of He) it is the bound-free process of H which can be a dominant absorption process in stellar photospheres.

The energy of a free electron is not quantised and will depend on its velocity. The photon energy involved in the process will be $h\nu = -E_n + (1/2)mv^2$ with E_n the ionisation energy. The free electron can be seen as a particle with an imaginary quantum number $u = i\kappa_u$:

$$T = E_{\text{kin}} = \frac{1}{2}mv^2 = \frac{\Re}{\kappa_u^2} = \frac{-\Re}{(i\kappa_u)^2} \,. \tag{6.83}$$

The oscillator strength of the bound-free process is then (see Equation 3.18 of Kramer):

$$f_{n_l\kappa_u} = \frac{32}{3\pi\sqrt{3}}(\frac{1}{n_l^2} + \frac{1}{\kappa_u^2})^{-3}\frac{1}{n_l^5\kappa_u^3}g_{II}(n_l,\kappa_u)\,, \tag{6.84}$$

With g_{II} the Gaunt factor of the bound-free process. The cross section σ_ν^{bf} for absorption in the frequency interval [ν,ν+$\Delta\nu$] is found by considering the number of transitions in this interval $\Delta\kappa_u$ times the cross section for every transition:

$$\sigma_\nu^{\rm bf}\Delta\nu = (\frac{\pi e^2}{mc}) f_{n_l\kappa_u}\frac{\Delta\kappa_u}{\Delta\nu}\Delta\nu\,. \tag{6.85}$$

The related energy is given by:

$$h\nu = \frac{\Re}{\kappa_u^2} + \frac{\Re}{n_l^2} \tag{6.86}$$

so we find an expression for the $\frac{d\kappa_u}{d\nu}$ term:

$$\frac{-2\Re}{\kappa_u^3}\frac{d\kappa_u}{d\nu} = h\,, \tag{6.87}$$

The cross-section can then be written as:

$$\sigma_\nu^{\rm bf} = \frac{\pi e^2}{mc}\frac{32}{3\pi\sqrt{3}}\frac{1}{n_l^5\kappa_u^3}\frac{1}{(h\nu/\Re)^3}\frac{h\kappa_u^3}{2\Re}g_{II}(n,\kappa_u) = \frac{64\pi^4 m e^{10}}{3\sqrt{3}\,c\,h^6}\frac{1}{n_l^5\nu^3}g_{II}(n,\nu)\,. \tag{6.88}$$

With g_{II} the bound-free Gaunt factor. Near the ionisation limit this is ~ 1 (see Fig. 6.6).

The energy (frequency) limit above which the bound-free process can take place, depends on the ionisation potential (hν = $\mathcal{R}$/n^2) and the frequency limit is $\nu_0(n,Z)$ = ($\mathcal{R}$Z^2/(h n^2)). For H the energy scheme is simple and for the different ionisation levels we get when inluding isolating n from the above equation and including this in equation 6.88 :

$$\sigma_\nu^{\rm bf}(\nu_n,n) = 7.91\times 10^{-18}\frac{n}{Z^2}g_{II}(\nu_n,n)\left(\frac{\nu_o}{\nu}\right)^3 \tag{6.89}$$

With respect to electron scattering, the b-f process is intrinsically about 10^7 times more efficient.

Inbetween the different ionisation breaks (coming from the different excitation levels), the extinction has a slope of ν^3 so the fall off at higher energies is quite steep. The frequency band inbetween the Paschen ionisation and Balmer ionisation is called the Paschen continuum because those photons can ionise from the Paschen excited level, but not from the Balmer excited level.

For stellar spectra, the effect of the b-f H extinction is very much dependent on how many H is in the different excited states. The maximal effect for visible photons is observed in A stars.

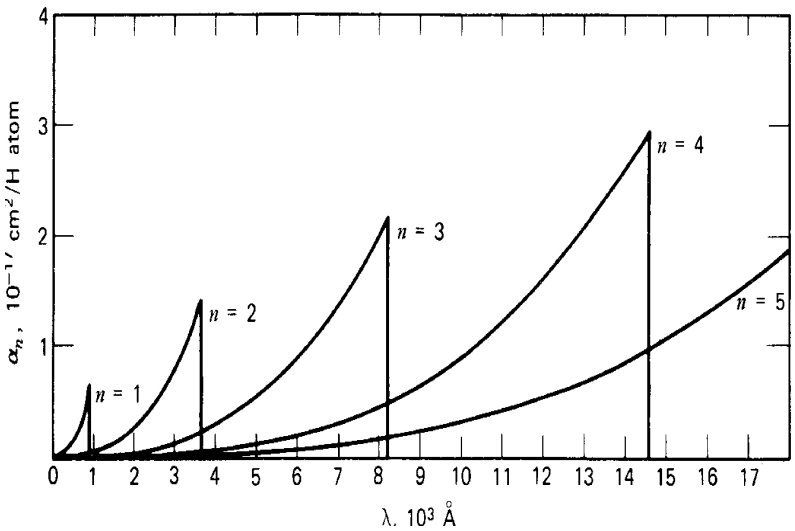

Figure 6.6: The Bound-Free cross-section of H per particle. The cross-section increases with n but the reaction rate is dependent on the number of atoms in the correct state as well as the number of photons available.

Also in the cold ISM, the hydrogen b-f is a very important process. Under ISM conditions all neutral H will be in the ground state and despite the fact that the density is low, the extinction coefficient of neutral H in the ground state for the bound-free process is so strong, that the ISM is very opaque for UV-radiation with $\lambda < 91.2$ nm. At higher energies the transparency of the ISM becomes better, since the cross-section falls off of like ν^3. Other elements are much less abundant but do play a role in the propagation of radiation through the ISM. The total extinction coefficient will be modulated by the abundances of the given element and we can normalise this to the effective cross-section per H-atom.

$$\sigma_{eff} = \sigma_H + \sum_i \sigma_i \, a_i \tag{6.90}$$

with σ_i the cross section for element i and a_i the number abundance relative to hydrogen. The total attenuation by the ISM gas component is then computed by multiplying with the column density of H. Complex atoms with more valence electrons will have a more complex behaviour in the cross-sections and these will have to be determined experimentally.

Radio astronomers can determine the amount of hydrogen in different parts of the Galaxy by detecting the 1420 MHz emission and using a kinematical model,

and the Doppler shift in a given line-of-sight, the intensity of the radiation can be used to constrain the density and location of the hydrogen clouds. In Fig 6.7 the effective cross section per H-atom is given in a log-log scale. The strong H-peak is at 13.6 eV and the slope is $\sim$ to -3. The ionisation edges of other elements are given as well but owing to their small abundances, they are less prominent. The dashed lines indicate the e^{-1} attenuation by the bound-free extinction for several line-of-sights : Proxima Centaurus is the nearest star next to the sun, and the Centre of our Galaxy is given as well. A nominal value for the number density of H in the plane of the Galaxy is $n \approx 0.5 \times 10^6$ m^{-3}.

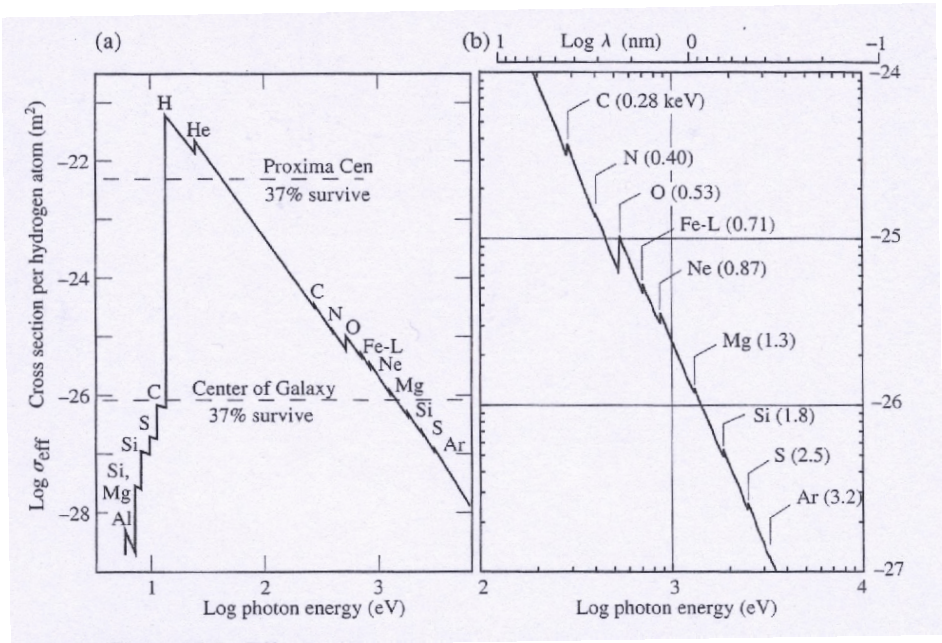

Figure 6.7: The effective cross-section per H-atom in units of m^2 for the bound-free process in the ISM. The dominant contributer is H with a very high extinction peak at 13.6 eV. The cross-section falls of after the peak with a slope of $\sim$ -3. Ionisation edges of other atoms are shown as well. The left panel is blown-up on the right. *Data taken from Bradt (2004)*

In photo-ionisation, the radiation field properties will determine the photon density of those photons which are energetic enough to ionise. So the b-f rate will depend on the properties of the radiation field and the state (excitation-ionisation) of the atoms. The number of photons available with a frequency $\nu \geq \nu_0$ is found by integrating $4\pi J_\nu / h\nu$ over the correct wavelength range. The number of photo-ionisations for particles n_i with ionisation potential proportional to ν_0 is then (per sec and per cm^2):

$$n_i\, R_{i,bf} = n_i 4\pi \int_{\nu_0}^{\infty} \sigma_{i,bf}(\nu) \frac{J_\nu}{h\,\nu}\, d\nu \tag{6.91}$$

6.5 .2 Spontaneous recombination

For spontaneous recombination, an electron will be captured by a ion in state κ and a photon will be emitted.

The number of spontaneous recombinations can be computed in TE assuming detailed balance between photon-ionisation and spontaneous recombination. With $J_\nu = B_\nu$ we get :

$$n_\kappa^{LTE}\, R_{\kappa i} = n_i^{LTE}\, R_{i\kappa} = n_i^{LTE}\, 4\pi \int_{\nu_0}^{\infty} \sigma_{i,\kappa}(\nu) \frac{B_\nu}{h\,\nu}\, d\nu \tag{6.92}$$

and together with the induced recombination this becomes:

$$n_\kappa^{LTE}\, R_{\kappa i} = n_\kappa^{LTE}\, R_{\kappa i}^{spon} + n_\kappa^{LTE}\, R_{\kappa i}^{stim} \tag{6.93}$$

The number of spontaneous recombinations in a given radiation field becomes:

$$n_\kappa^{LTE}\, R_{\kappa i}^{spon} = n_i^{LTE} 4\pi \left[\int_{\nu_0}^{\infty} \sigma_{i,\kappa}(\nu) \frac{B_\nu}{h\,\nu} \left(1 - e^{-h\nu/kT}\right) d\nu \right] \tag{6.94}$$

with the inclusion of the Planck's curve this becomes:

$$n_\kappa^{LTE}\, R_{\kappa i}^{spon} = n_i^{LTE} 4\pi \int_{\nu_0}^{\infty} \frac{\sigma_{i,\kappa}}{h\nu} \frac{2h\nu^3}{c^2}\, e^{-h\nu/kT} d\nu \tag{6.95}$$

Spontaneous recombination will depend on the number of free electrons. Even if LTE does not apply but the electrons do follow a Maxwell velocity distribution the process per ion will still follow the same rate. Only will the number density in this environment be different than in LTE conditions.

We can write:

$$n_\kappa\, R_{\kappa i}^{spon} = n_\kappa \left(\frac{n_i}{n_\kappa}\right)^{LTE} 4\pi \int_{\nu_0}^{\infty} \frac{\sigma_{i,\kappa}}{h\nu} \frac{2h\nu^3}{c^2}\, e^{-h\nu/kT} d\nu \tag{6.96}$$

With $\left(\frac{n_i}{n_\kappa}\right)^{LTE}$ the TE number density fractions of the ion with the bound electron n_i and the ion which is ionised one electron higher (n_κ). If we now include the Saha-Boltzmann equation into this relation and we incorporate the integral and the Saha-Boltzmann equation into one term we get:

$$n_\kappa \, R^{spon}_{\kappa,i} = n_\kappa \, n_e \; \alpha^{RR}_{i,\kappa}(T) \tag{6.97}$$

The $\sigma^{rr}_{i,\kappa}(T)$ is the recombination coefficient in cm^3, the recombination towards i. At higher T, when the electrons move faster, it will be harder to recombine. We also see that the reaction rate is dependent on the number density in electrons and in element in the κ ionisation stage.

6.5 .3 Induced photo-recombination

The same reasoning as in previous subsection (Equation 6.94) leads to the quantisation of the number of induced (stimulated) recombinations per cm^3 in TE:

$$n^{LTE}_\kappa \, R^{stim}_{\kappa i} = n^{LTE}_i 4\pi \left[\int_{\nu_0}^{\infty} \sigma_{i,\kappa}(\nu) \frac{B_\nu}{h\,\nu} \, e^{-h\nu/kT} \, d\nu \right] \tag{6.98}$$

In general application, we have to rescale this to non-LTE conditions so the number densities can be affected as well as the radiation field:

$$n_\kappa \, R^{stim}_{\kappa i} = n_\kappa \left(\frac{n_i}{n_\kappa}\right)^{LTE} 4\pi \left[\int_{\nu_0}^{\infty} \sigma_{i,\kappa}(\nu) \frac{J_\nu}{h\,\nu} \, e^{-h\nu/kT} \, d\nu \right] \tag{6.99}$$

Combining the spontaneous and induced formulae for the total number of photo-recombinations per second and per cm^3 gives:

$$n_\kappa \, R_{\kappa i} = n_\kappa \left(\frac{n_i}{n_\kappa}\right)^{LTE} 4\pi \int_{\nu_0}^{\infty} \frac{\sigma_{i,\kappa}(\nu)}{h\nu} \left[\frac{2h\nu^3}{c^2} + J_\nu \right] e^{-h\nu/kT} d\nu \tag{6.100}$$

6.5 .4 Collisional Ionisation

The rate of collisional ionisation depends on the energy of the colliding particle. The energy limit above which a ionisation can take place, is now no longer expressed in frequency (ν_0) but in velocity (v_0). The energy is $E_0 = \frac{1}{2}\, m\, v_0^2 = h\nu_0$.

Electron collisions will be most frequent and using the collisional coefficients we get:

$$n_i\, C_{i\kappa} = n_i\, n_e \int_{v_0}^{\infty} \sigma_{i,\kappa}(v)\ f(v)\ v\ dv \equiv n_i\, n_e\, q_{i,\kappa}(T) \tag{6.101}$$

f(v) is the velocity distribution, $\sigma_{i,\kappa}$ the collisional cross section, v the velocity. Approximation formulae have been computed by Van Regemorter which relates to the efficiency in function of thermodynamic quantities:

$$q_{i,\kappa}(T) \approx 2.7\zeta \left(\frac{E_0}{kT}\right)^{-2} T^{-3/2} e^{-E_0/kT} \tag{6.102}$$

with ζ the number of electrons in the outer electron shell.

6.5 .5 Collisional Recombination

This is a collisional process with three particles. In LTE we get detailed balance:

$$n_i^{LTE} C_{i,\kappa} = n_\kappa^{LTE} C_{\kappa,i} \tag{6.103}$$

the number of collisional recombinations is :

$$n_\kappa C_{\kappa,i} = n_\kappa \left(\frac{n_i}{n_\kappa}\right)^{LTE} C_{i,\kappa} = n_\kappa\, n_e^2\, \phi(T)\, q_{i,\kappa}(T) \tag{6.104}$$

were we used the Saha-Boltzmann relation (and its temperature part in the ϕ function). The dependency of n_e^2 shows that it is a three particle interaction. Collisional recombination is much less temperature sensitive than collisional ionisation because the exponential term does not appear. Because of the low energy transitions, recombination will occur to high excitation levels, after which the bound electron can (and will) cascade down to lower levels.

6.6 Special Case: H^- extinction

H is strongly dipolar and can sustain easily a supplementary electron. The H^- has just one stable state with a small binding energy of 0.745 eV. The ionisation limit is at around $\lambda \approx 1650$ nm. The main important reactions are the bound-free and free-free process:

$$\mathrm{H}^- + h\nu \rightleftharpoons \mathrm{H} + e(v) \tag{6.105}$$

with $h\nu - 0.754\mathrm{eV} = 1/2m_e v_e^2$ and

$$\mathrm{H} + e(v) + h\nu \rightleftharpoons \mathrm{H} + e(v') \tag{6.106}$$

with $1/2m_e v_e'^2 = h\nu + 1/2m_e v_e^2$

The cross sections are rather difficult to compute because the wavefunctions are quite complex. We illustrate the cross section in Fig. 6.8. The bound-free continuum does not have a sharp edge and is very smooth with a maximum at 860 nm and a decreasing strength both red and blue wards. The new increase after 1.65 μm is due to the free-free contribution.

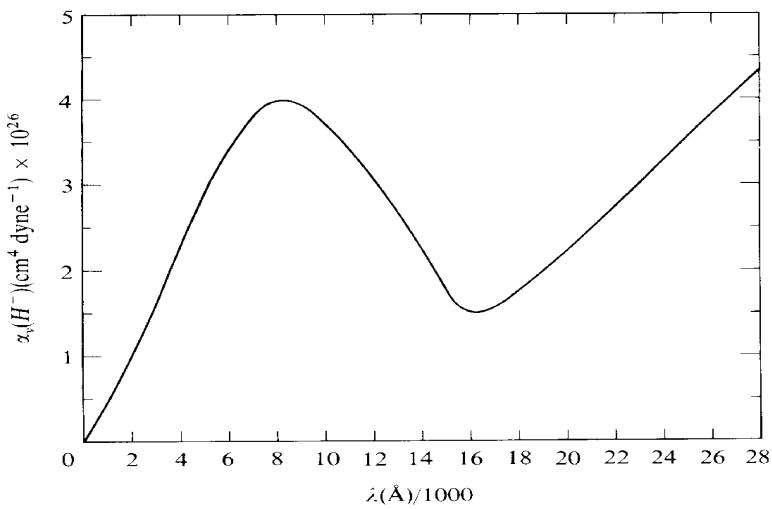

Figure 6.8: The cross section of the H^- opacity in function of wavelength. The slope at low energies are from the free-free contribution, the bound-free contribution is not sharp-edged but maximal at 860 nm

6.7 Dominant continuum process in the Sun

To trace the dominant continuum process in the Sun, we can use the solar limb darkening (Fig. 6.10) as measured at different wavelengths. As the sun is well

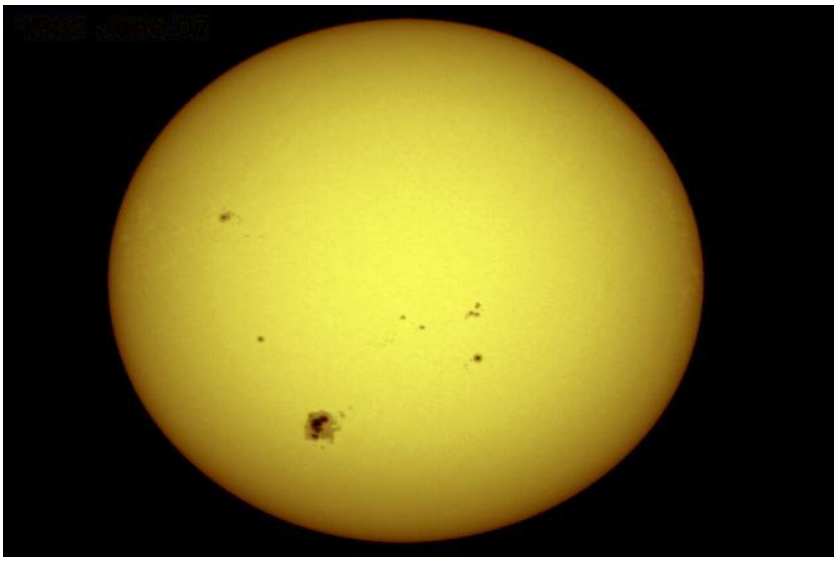

Figure 6.9: Solar limb darkening is clearly seen.

resolved, we trace the θ dependency of the intensity distribution at the surface of the sun.

In the Eddington-Barbier relation (see equation 1.73) the surface intensity at a given θ is related to the source function by following relation:

$$S_\lambda(\tau_\lambda) = \sum_i a_{\lambda,i}\tau_\lambda^i \tag{6.107}$$

$$I_\lambda(0,\theta) = \sum_i a_{\lambda,i}\, i!\ \cos^i\ \theta \tag{6.108}$$

And by measuring the solar limb darkening for a given wavelength and given $\cos\theta$, we trace the source function at the monochromatic optical depth $\tau_\nu = \cos\theta$. Using only up to the quadratic term we get for 5010 Å:

$$\frac{I_\lambda(0,\theta)}{I_\lambda(0,0)} = a_0 + a_1\cos\theta + 2a_2\cos^2\theta \tag{6.109}$$

The quantisation of the solar limb darkening is: Measured at 5010 Å: $I_\lambda(0,0) = 4.03\,10^6\,\mathrm{erg\,cm^{-2}s^{-1}\,\text{Å}^{-1}}$, and for the ease of computation we put the bandwidth on $\Delta\lambda = 1cm$. $I_\lambda(0,0) = 4.03\,10^{14}\,\mathrm{erg\,cm^{-2}s^{-1}\,cm^{-1}}$:

The associated monochromatic source function is then:

$$S_\lambda(\tau_\lambda = 0.5) = 2.66826\ 10^{14} \quad erg\, cm^{-2} s^{-1}\, cm^{-1} \tag{6.110}$$

When we assume LTE, the source function is the Planck function and we can connect a unique temperature to the monochromatic source function of a given optical depth: $S_\lambda(\tau_\lambda) = B_\lambda(T)$.

With the values given above this is for 5010 Å: T(τ_λ= 0.5) = 5792 Kelvin.

$$B_\lambda(T(\tau_\lambda)) = \frac{2\,h\,c^2}{\lambda^5}\,\frac{1}{e^{hc/\lambda\,kT} - 1} \tag{6.111}$$

The quantisation of the solar limb darkening at different wavelengths is given in Table 6.1.

Table 6.1: The Solar limb darkening coefficients for several wavelengths as well as the intensity of the centre of the solar disc

λ (Å)	a_0	a_1	$2a_2$	$I_\lambda(0,0)$ erg cm^{-2}s^{-1} cm^{-1}
3737	0.1435	0.9481	−0.0920	42.0 10^{13}
4260	0.1754	0.9740	−0.1525	44.9 10^{13}
5010	0.2593	0.8724	−0.1336	40.3 10^{13}
6990	0.4128	0.7525	−0.1761	25.0 10^{13}
8660	0.5141	0.6497	−0.1657	15.5 10^{13}
12250	0.5969	0.5667	−0.1646	7.7 10^{13}
16550	0.6894	0.4563	−0.1472	3.6 10^{13}
20970	0.7249	0.4100	−0.1360	1.6 10^{13}

Using the solar limb-darkening we can reconstruct the behaviour of the monochromatic source function in function of monochromatic optical depth and therefore also the temperature. When doing this for several discrete wavelengths we have a T(τ_λ) relation for several wavelengths. As a given geometrical depth has a fixed temperature we can associate for the same temperature different wavelength dependent optical depths and hence different monochromatic extinction coefficients: $\tau_{\lambda,1} = \kappa_{\lambda,1}$ t ; $\tau_{\lambda,2} = \kappa_{\lambda,2}$ t etc..

By doing so we can reconstitute the wavelength dependent extinction coefficient. This is depicted in Fig. 6.10.

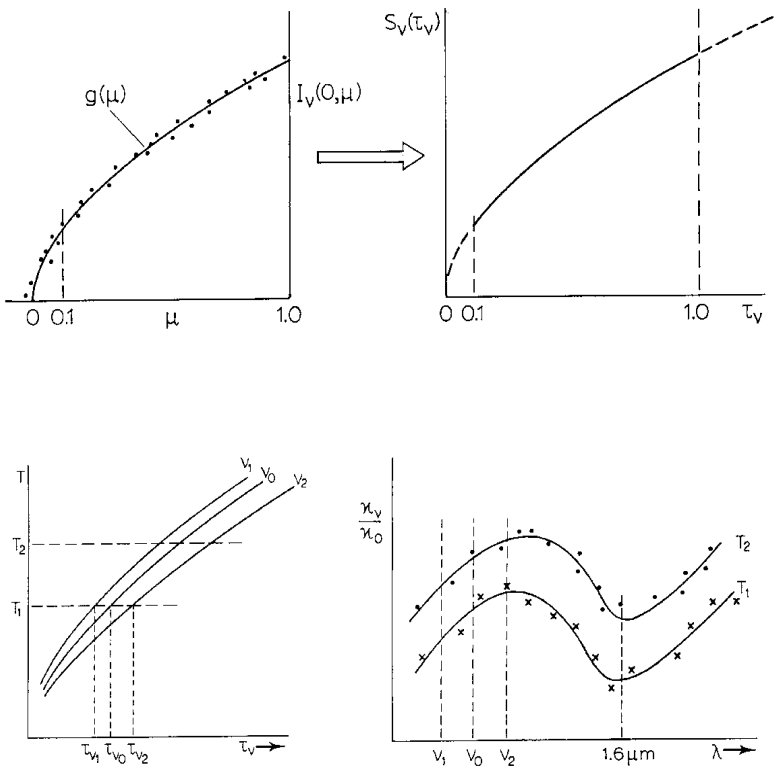

Figure 6.10: The reconstruction of the wavelength dependency of the monochromatic extinction coefficient from the Solar Limb darkening. Fig. from Gray (2002)

6.8 Notions of high-energy processes

The Crab nebula (Fig. 6.11) is a good object to illustrate the emission of high-energy processes. The nebula is resolved and what we observe now, is a supernova remnant. The supernova event from 1054 CE itself was described by Arab, Chinese and Japanese astronomers.

The spectrum of the source extends all the way from the radio to the gamma-ray band (Fig. 6.12). Moreover, the nebula is very energetic with an overall luminosity of about 10^5 $L_\odot$. The optical radiation from the nebula includes filaments that exhibit hydrogen Balmer emission spectral lines, forbidden nebular lines indicating a temperature of $\sim 10^4$ K. The blue emission is quite featureless.

The origin of this intense bluish luminosity remained a mystery in astrophysics for many years. The nebula was discovered in 1731 and also Charles Messier

observed the diffuse nebula (1758). The Crab nebula is even the first entry in the Messier catalogue (M1) of diffuse objects.

In 1953, the Russian scientist Shklovsky postulated that the emission of the Crab could have a similar physical origin as synchrotron radiation which was, at that time, recently discovered with electron accelerators. He suggested to look at the polarisation of the emission, because synchrotron radiation is highly polarised. This was indeed observed a year later in 1954. The process of the radiation was discovered, but not the source. It was only in 1969 when the central rapidly spinning neutron star (the Crab pulsar) was detected. The rotation period is only 0.0333 sec which means that the central object rotates about 30 times per second. It was found to be the central engine for the emission currently observed in the Crab nebula.

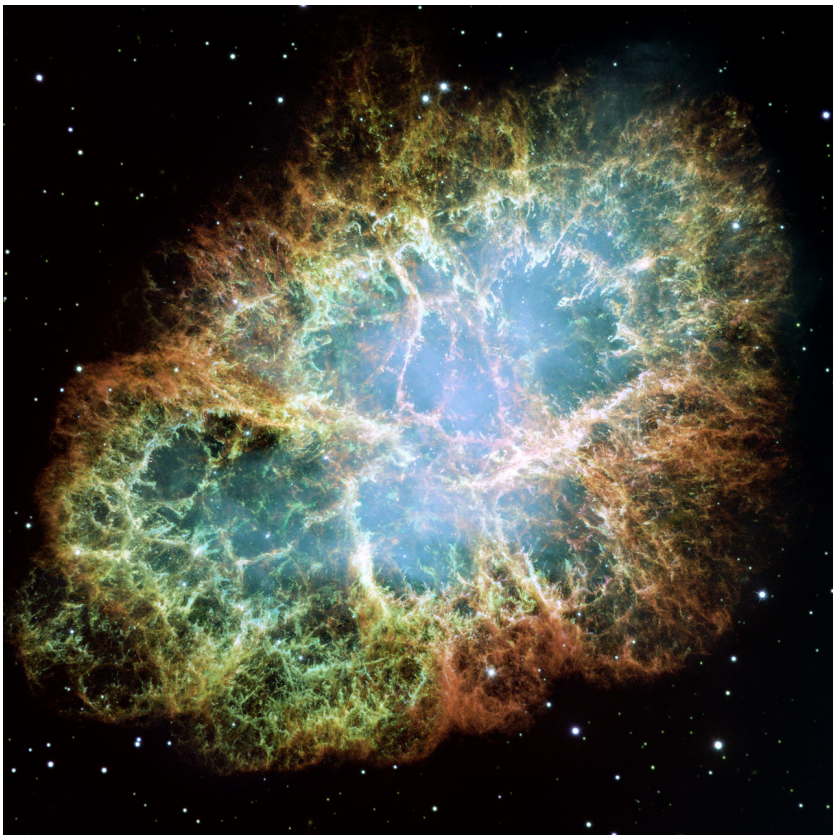

Figure 6.11: The SN remnant imaged by the HST. The blue central emission is coming from synchrotron emission. The image is a mosaic of 24 deep pointings of the HST WFPC2 camera. A digital high-resolution version can be found here

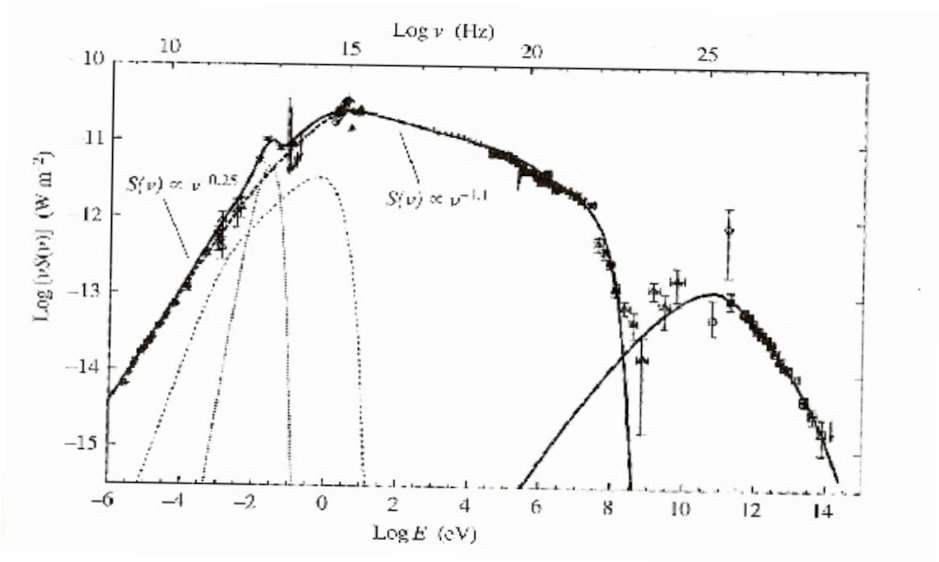

Figure 6.12: SED of the Crab nebula. The plot shows ν_ν in function of the frequency (top) or energy (bottom) of the detected photons. Note that the emission covers over 19 decades (!) of frequency down to the gamma-ray domain (TeV). The polarisation measurements as well as the spectral slope indicates that most energy to about 100 MeV is coming from synchrotron radiation. The solid line is a fit through the data of a synchrotron self-Compton (SCC) model for a magnetic field of 16 nT. The narrow and broader dashed lines show the contribution from millimeter synchrotron and from nebular dust respectively. The distinct peak at TeV energies is attributed to synchrotron photons that have been up-scattered via inverse Compton scattering. *Fig. taken from Bradt (2004).*

6.8 .1 Synchrotron emission

The basis of the free-free emission is that accelerating electrons will emit photons. The reason for the acceleration can be the Coulomb interaction (like in the case of free-free interactions) but it can also be due to the trapping of electrons in magnetic field lines.

The magnetic force on a moving charge q will be (in cgs units): $(q/c\ \mathbf{v} \times \mathbf{B})$ The component of the electron's velocity perpendicular to the field-lines produces a circular orbit around the field-line, while the velocity component perpendicular to it, will be not affected. As the electron follows curved field lines, it will be accelerated and emit electromagnetic radiation. In a non-relativistic situation, the electron is freely orbiting in a static magnetic field **B** and the frequency would be the cyclotron circular frequency ω_B = qB/m.

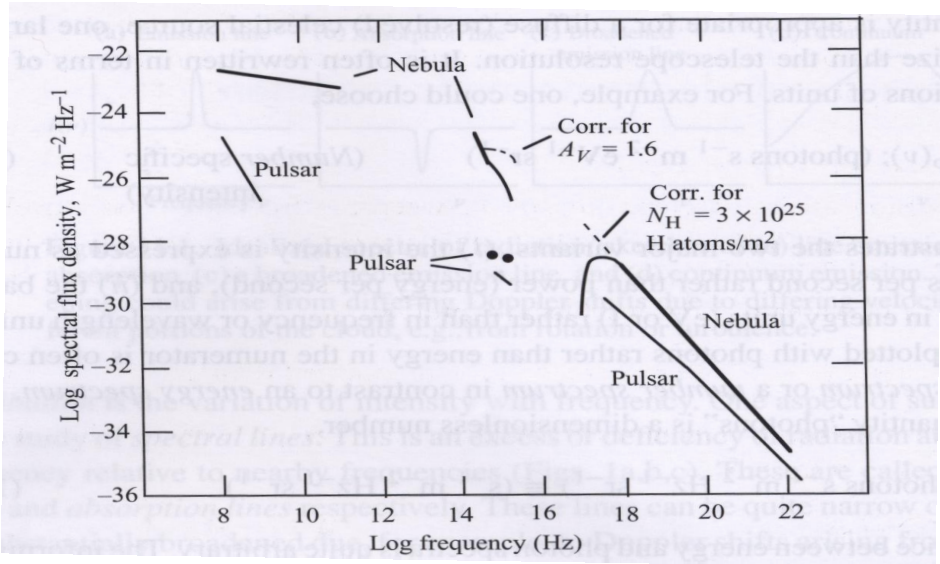

Figure 6.13: The spectral behaviour of the emission of different components of the Crab pulsars and Crab nebula, depicted in a log-log scale. The dashed line is the correction of the data for ISM extinction. The straight lines are typical for synchrotron emission. the time-average pulsar fluxes are shown as lines. Typical peak fluxes are shown by two frequencies. *Fig. taken from Bradt (2004)*

When very high energy (relativistic) electrons spiral in magnetic field-lines, the charges are relativistic and the radiation will be very intense and beamed. This is called *synchrotron emission*, when the circular motion is mainly around the field-lines, and *curvature emission* when the motion is primarily along the field-lines (e.g. along strongly curved field-lines). In both cases, the radiation is strongly polarised in the plane of circular motion in the case of synchrotron emission and in the plane of the curving magnetic field line for curvature radiation. The continuous emission is dependent on the electron speed and field characteristics and is very different from a black-body spectrum. This type of radiation is called 'non-thermal'.

The first detection of synchrotron radiation was from visual observations of electrons circulating an electron accelerator. When not on relativistic speeds the electrons will emit with a power which follows the classical Larmor's formula. This is as intense in the direction of the motion as opposite to it. At the radio frequency of 10 GHz, the degree of polarisiation is as a whole about 5%.

At relativistic speeds, the radiation is beamed and the beaming opening angle is dependent on the Lorentz factor (γ). For relativistic speeds, the angular cyclotron circular frequency of the observed radiation scales as:

$$\omega_{syn} \sim \gamma^2 \, \omega_B \tag{6.112}$$

In the Crab nebula the magnetic field strength is found to be B $\sim 5 \times 10^{-8}$ Tesla. The cyclotron frequency is (m the electron mass) :

$$\nu_B = \frac{e\,B}{2\,\pi\,m} = 1.4 \times 10^3 Hz \tag{6.113}$$

The radiation of the Crab nebula is in the optical band, however, which is typical of say 5 $\times 10^{14}$ Hz. This means that the Lorentz factor is :

$$\gamma \sim \sqrt{(\frac{\nu_s yn}{\nu_B})} = \sqrt{\frac{4 \times 10^{14}}{1.4 \times 10^3}} = 6.0 \times 10^5 \tag{6.114}$$

This means that the electrons exceed their rest energy (mc^2 = 0.5 MeV) by a factor of about 600 000... The electrons in the Crab nebula must be extremely relativistic.

By radiating, the electron lose energy and the energy loss can be used to determine the lifetime of these electrons by dividing the total energy of the electron by the energy loss per second. It turns out that at optical wavelengths, the electron lifetime in the Crab nebula is about 109 years, for X-ray wavelengths ($\sim$ 4.1 keV) its is only 2.4 years and in the gamma domain ($\sim$ 40 MeV) it is 0.024 years (9 days). The high energy radiation is coming from electrons with very small lifetimes, which means that these cannot be connected any longer to the SN explosion from 1054 AC. This puzzle was solved when Radio Pulsars were discovered. The one in the Crab is spinning at 30 Hz !. The power source for the synchrotron radiation is the rotational energy of this neutron star.

The emitted spectrum of synchrotron radiation has a typical power-law behaviour

$$I = K \; \nu^{\alpha} \tag{6.115}$$

with K a constant.

In a log-log plot this becomes a line (see Fig 6.13):

$$\log I = \log K + \alpha \log \nu \tag{6.116}$$

6.8 .2 Compton Scattering

Thomson scattering is a low energy process on low-energy free electrons. The photon energy is much smaller than the rest energy of an electron : $h\nu \ll m_e c^2$.

When the photon energy is very large and approaching $h\nu \sim m_e\, c^2$ (511 keV) the probability of scattering from free electrons decreases fast.

The high energy tail of Thomson is Compton scattering.

The photon will transfer momentum and energy to the electron.

The energy of the scattered photon will depend on the scattering angle. The variation can be calculated by considering energy and momentum in a relativistic calculation. It is only relevant for high-energies and we show in Fig 6.14 the high energy tail of the cross-sections for different processes.

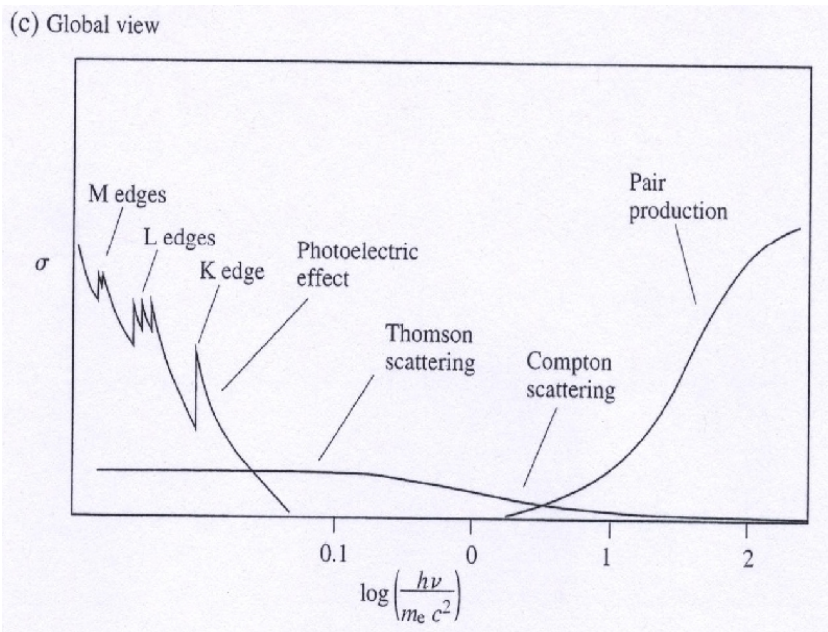

Figure 6.14: High energy cross section for different processes. *Fig. taken from Bradt (2004)*

γ rays at very high energies ($> 10^{14}$ eV) will interact with CMB photons and produce:

$$\gamma_\gamma + \gamma_{CMB} = e^- + e^+ \tag{6.117}$$

This is called pair production.

The inverse Compton effect, in which high energy electron interact with lower energy photons such as to increase the photon-energy. It is an important process in high-energy astrophysics. In the relativistic case, where the relativistic electrons with Lorentz factor γ, will increase the photon energy by a factor that scales with γ^2. In astrophysical jets, X-ray photons can be propelled up to extreme gamma-ray energies in the TeV electron domain. This inverse Compton effect is called 'Comptonisation'. The effect is also seen in the SED of the Crab nebula (Fig. 6.12), where the peak in the gamma domain is due to the comptonisation of synchrotron photons.

Another observation of this effect relates to the Comptonisation of low-energy photons of the background radiation (CMB). Very hot plasmas are detected in cluster of Galaxies. The strong gravitational pull of this cluster matter squeezes the gas and heats it to about 100 million degrees, making it only detectable in X-rays. The two X-ray observatories orbiting today are XMM (ESA) and Chandra (NASA) and here some X-ray observations of clusters for Galaxies are shown.

By the inverse Compton scattering: the CMB photons are scattered and in this process they will be gaining energy. The typical CMB black-body curve will be distorted to higher energies 6.15. This application of the inverse compton scattering is called the Sunyaev-Zeldovich effect.

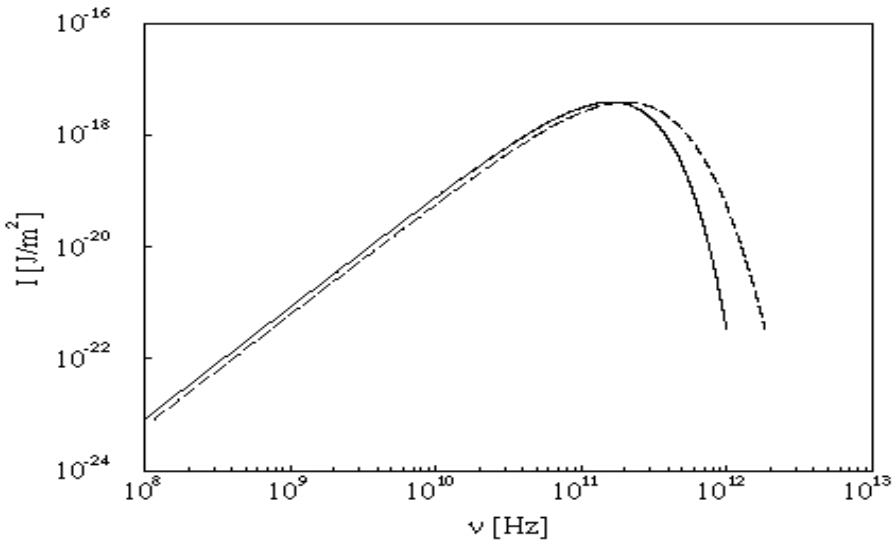

Figure 6.15: The black-body spectrum of the CMB in the direction of a cluster of Galaxies with respect to one in an undisturbed line-of-sight. The inverse Compton scattering effect by high energetic electrons in the very hot inter-cluster plasma disturbs the CMB photons to higher energies. This effect is known as the Sunyaev-Zeldovich effect

6.9 Evaluation

The study of the interaction between matter and radiation includes a detailed study of the microphysics. This involves the quantisation of the different cross-sections, the number densities of the different contributing particles as well as the quantisation of the energy density and spectral characteristics of the radiation field.

In Fig 6.16 we focus on stellar photospheres and illustrate for different spectral types, the main continuum opacity sources in the photospheres. The Y-axis gives the continuum extinction coefficient (in units of 10^{26} cm^2) per neutral H-atom (excited following the Boltzmann equation) and normalised to electron pressure. The latter is done because H^- scales with the electron pressure. The linear extinction coefficient can be found from this graph by $10^{-26}\,\kappa_0(\nu)\,N_0\,p_e\,cm^{-1}$. In units of κ_0 (the value and nomenclature of the graph) the extinction by Thomson scattering is $10^{26}\sigma_T\,n_e/N_0\,p_e$.

The top figure shows a star somewhat hotter than the sun. The H^- opacity is clearly the dominant process in the continuum opacity. The bound-free process from the Balmer continuum is significantly more prominent than in the Paschen continuum due to the higher population factor.

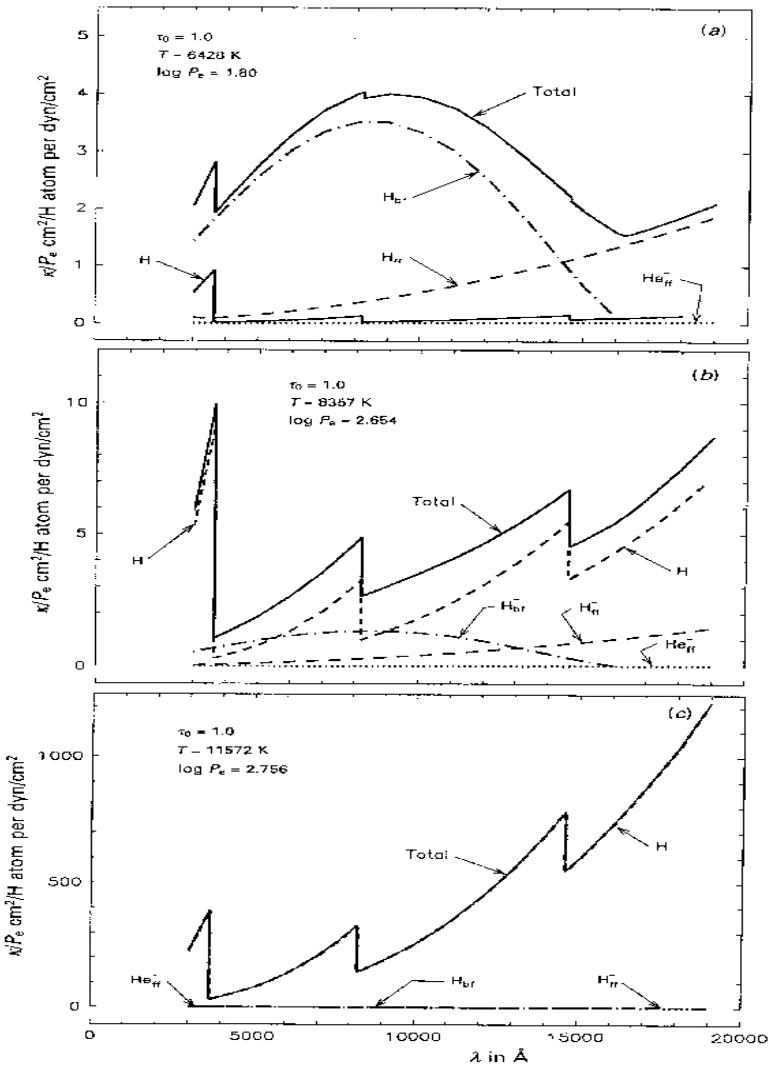

Figure 6.16: The major continuum opacity sources in the photospheres of stars of different spectral type. For the Sun and solar analogues the main contributor in the optical-nearIR is H^- opacity. Fig. from Gray (1992)

For a A dwarf (seen in the middle panel), the major opacity source is the hydrogen bound-free and free-free processes. With increasing wavelength, the relative contribution of the free-free extinction becomes more prominent due to the λ^3 dependency (equation 6.56). The contribution of H^- has diminished strongly with respect to the upper plot.

The lower diagram gives the continuum processes of a late B-dwarf. H^- has no

longer a significant contribution and it is the H free-free opacity which dominates the near-IR and in the optical, the H bound-free.

6.10 Concluding Remarks

The quantified study of the electromagnetic radiation of celestial objects calls for both a detailed understanding of both microphysics and macrophysics. The interpretation of data includes reflection on:

- is the object seen in emission or absorption and why ?
- is the object optically thin or thick ?
- from where comes the observed radiation ?
- what is the state of the gas (excitation, ionisation, velocity distribution)
- which processes are likely relevant for the object ?
- does scattering have an important contribution in the observed radiation ?
- is the radiation thermal or not and why ?
- ....

This course is meant to introduce the basic concepts of radiative processes and radiative transfer in astronomical conditions.

Appendix A

Astronomical and Physical constants.

Table A.1: Overview physical constants. A useful link can be found here

Name	symbol	SI	cgs
Velocity of light	c	2.99792458×10^{8} m s^{-1}	$2.99792458 \times 10^{10}$ cm s^{-1}
Planck constant	h	6.62620×10^{-34} J s	6.62620×10^{-27} erg s
	h		4.13566×10^{-15} eV s
Bolzmann constant	k	1.380662×10^{-23} J K^{-1}	1.380662×10^{-16} erg K^{-1}
	k		8.617385 x 10-5 eV/K
Stefan-Bolzmann constant	σ	5.66956×10^{-8} W m^{-2} K^{-4}	5.66956×10^{-5} erg cm^{-2} s^{-1} K^{-4}
Gravitation constant	G	6.673×10^{-11} N m^{2} kg^{-2}	6.673×10^{-8} dyn cm^{2} g^{-2}
electron charge	e	1.602176×10^{-19} C	
electron mass	m_e	9.109382×10^{-31} kg	9.109382×10^{-28} g
		0.511 MeV	
proton mass	m_p	1.672622×10^{-27} kg	1.672622×10^{-24} g
		938.272 MeV	
neutron mass	m_n	1.674927×10^{-27} kg	1.674927×10^{-24} g
		939.565 MeV	
Avogadro number	N_0	6.0221367×10^{23} mol$^{-}1$	6.0221367×10^{23} mol$^{-}1$
Universal gas constant	R	8.31441 J mol^{-1} K^{-1}	
Coulomb constant	K	8.98755×10^{9} N m^{2} kg^{-2}	
Rydberg constant for ^{1}H	R	1.09677583×10^{7} m^{-1}	1.09677583×10^{5} cm$^{-}1$
Relative permeability of vacuum	μ_0	$4\pi \times 10^{-7}$ N A^{-2}	
Relative permittivity of vacuum	ϵ_0	$8.85418782 \times 10^{-12}$ s^{4} A^{2} m^{-3} kg^{-1}	

Table A.2: Astronomical constants and typical numbers.

Quanity	Value	Unit
Solar mass	$1.9891 \times 10^{+30}$	kg
Solar irradiance	$1.365 \times 10^{+3}$	$\mathrm{W\,m^{-2}}$
Solar luminosity	$3.839 \times 10^{+26}$	W
Solar radius	$6.95508 \times 10^{+8}$	m
Solar effective temperature	5777	K
Solar absolute bolometric magnitude	4.74	magn
Solar apparent bolometric magnitude	-26.83	magn
Solar apparent ultraviolet magnitude (U)	-25.91	magn
Solar apparent blue magnitude (B)	-26.10	magn
Solar apparent visual magnitude (V)	-26.75	magn
Solar bolometric correction (BC)	-0.08	magn
Earth mass	$5.9736 \times 10^{+24}$	kg
Earth radius (equatorial)	$6.378136 \times 10^{+6}$	m
Astronomical unit (AU)	$1.4959787066 \times 10^{+11}$	m
Light year (ly, Julian)	$9.460730472 \times 10^{+15}$	m
Parsec (pc)	$2.06264806 \times 10^{+5}$	AU
	3.0856776×10^{16}	m
	3.2615638	light year (Julian)
Sidereal day	$8.61640905309 \times 10^{+4}$	s
Solar day	$8.6400 \times 10^{+4}$	s
Sidereal year	$3.15581450 \times 10^{+7}$	s
	$3.65256308 \times 10^{+2}$	d
Tropical year	$3.155692519 \times 10^{+7}$	s
	$3.652421897 \times 10^{+2}$	d
Julian year	$3.1557600 \times 10^{+7}$	s
	$3.6525 \times 10^{+2}$	d
Gregorian year	$3.1556952 \times 10^{+7}$	s
	$3.652425 \times 10^{+2}$	d

Table A.3: SI to cgs Unit Conversions. Many (older) astronomical literature is in cgs units. This table helps to compute the conversions. One of the many web-conversion tools can be found here

Quantity	SI Unit	cgs Unit	Conversion Factor (SI to cgs)
Distance	meter (m)	centimeter(cm)	10^{-2}
Mass	kilogram (kg)	gram (g)	10^{-3}
Time	second (s)	second (s)	1
Current	ampere (A)	esu s^{-1}	3.335640952 10^{-10}
Charge	coulomb (C; A s)	esu	3.335640952 10^{-10}
Velocity	m s^{-1}	cm s^{-1}	10^{-2}
Acceleration	m s^{-2}	cm s^{-2}	10^{-2}
Linear momentum	kg m s^{-1}	g cm s^{-1}	10^{-5}
Angular momentum	kg m^2 s^{-1}	g cm^2 s^{-1}	10^{-7}
Force	newton (N; kg m s^{-2})	dyne (g cm s^{-2})	10^{-5}
Energy (work)	joule (J; N m)	erg (dyne cm)	10^{-7}
Power (luminosity)	watt (W; J s^{-1})	erg s^{-1}	10^{-7}
Pressure	pascal (Pa; N m^{-2})	dyne cm^{-2}	10^{-1}
Mass density	kg m^{-3}	g cm^{-3}	10^{+3}
Charge density	C m^{-3}	esu cm^{-3}	3.335640952 10^{-4}
Current density	A m^{-2}	esu s^{-1} cm^{-2}	3.335640952 10^{-6}
Electric potential	volt (V; J C^{-1})	statvolt (erg esu^{-1})	2.997924580 10^{+2}
Electric field	V m^{-1}	statvolt (cm^{-1})	2.99792458 10^{+4}
Magnetic field	tesla (T; N A^{-1} m^{-1})	gauss (G; dyne esu^{-1})	10^{-4}
Magnetic flux	weber (Wb; T m^2)	G cm^2	10^{-8}

Table A.4: Often used quantities and relations.

Quantity	Misc. Unit	Conversion
Wavelength	Angstrom Å	10^{-10} m
Wavelength	nanometer (nm)	10^{-9} m
Spectral flux density	Jansky (Jy)	10^{-26} W m^{-2} Hz^{-1}
energy	eV	$1.602\,10^{-19}$ J
1eV	associated wavelength	$1.23963 \times 10^{-4}\,\mathrm{cm}$
	associated wavenumber	$8.0671 \times 10^{3}\,\mathrm{cm}^{-1}$
	associated frequency	$2.41838 \times 10^{14}\,\mathrm{Hz}$
	associated energy	$1.60184 \times 10^{-19}\,\mathrm{J}$
	associated energy	$1.60184 \times 10^{-12}\,\mathrm{erg}$
	associated temperature	$1.16059 \times 10^{4}\,\mathrm{K}$

Appendix B

Stellar properties in function of Spectral Type

Table B.1: Typical characteristics of stars in function of their Spectral Type. *Data taken from Carroll & Ostlie (1996)* .

Main-Sequence Stars (Luminosity Class V)									
Spectral Type	T_e (K)	$L/L_\odot$	$R/R_\odot$	$M/M_\odot$	M_{bol}	BC	M_V	U-B	B-V
O5	42000	499000	13.4	60	-9.51	-4.40	-5.1	-1.19	-0.33
O6	39500	324000	12.2	37	-9.04	-3.93	-5.1	-1.17	-0.33
O7	37500	216000	11.0		-8.60	-3.68	-4.9	-1.15	-0.32
O8	35800	147000	10.0	23	-8.18	-3.54	-4.6	-1.14	-0.32
B0	30000	32500	6.7	17.5	-6.54	-3.16	-3.4	-1.08	-0.30
B1	25400	9950	5.2		-5.26	-2.70	-2.6	-0.95	-0.26
B2	20900	2920	4.1		-3.92	-2.35	-1.6	-0.84	-0.24
B3	18800	1580	3.8	7.6	-3.26	-1.94	-1.3	-0.71	-0.20
B5	15200	480	3.2	5.9	-1.96	-1.46	-0.5	-0.58	-0.17
B6	13700	272	2.9		-1.35	-1.21	-0.1	-0.50	-0.15
B7	12500	160	2.7		-0.77	-1.02	+0.3	-0.43	-0.13
B8	11400	96.7	2.5	3.8	-0.22	-0.80	+0.6	-0.34	-0.11
B9	10500	60.7	2.3		+0.28	-0.51	+0.8	-0.20	-0.07
A0	9800	39.4	2.2	2.9	+0.75	-0.30	+1.1	-0.02	-0.02
A1	9400	30.3	2.1		+1.04	-0.23	+1.3	+0.02	+0.01
A2	9020	23.6	2.0		+1.31	-0.20	+1.5	+0.05	+0.05
A5	8190	12.3	1.8	2.0	+2.02	-0.15	+2.2	+0.10	+0.15
A8	7600	7.13	1.5		+2.61	-0.10	+2.7	+0.09	+0.25
F0	7300	5.21	1.4	1.6	+2.95	-0.09	+3.0	+0.03	+0.30
F2	7050	3.89	1.3		+3.27	-0.11	+3.4	+0.00	+0.35
F5	6650	2.56	1.2	1.4	+3.72	-0.14	+3.9	-0.02	+0.44
F8	6250	1.68	1.1		+4.18	-0.16	+4.3	+0.02	+0.52
G0	5940	1.25	1.06	1.05	+4.50	-0.18	+4.7	+0.06	+0.58
G2	5790	1.07	1.03		+4.66	-0.20	+4.9	+0.12	+0.63
Sun	5777	1.00	1.00	1.00	+4.74	-0.08	+4.82	+0.195	+0.650
G8	5310	0.656	0.96		+5.20	-0.40	+5.6	+0.30	+0.74
K0	5150	0.552	0.93	0.79	+5.39	-0.31	+5.7	+0.45	+0.81
K1	4990	0.461	0.91		+5.58	-0.37	+6.0	+0.54	+0.86
K3	4690	0.318	0.86		+5.98	-0.50	+6.5	+0.80	+0.96
K4	4540	0.263	0.83		+6.19	-0.55	+6.7		+1.05
K5	4410	0.216	0.80	0.67	+6.40	-0.72	+7.1	+0.98	+1.15
K7	4150	0.145	0.74		+6.84	-1.01	+7.8	+1.21	+1.33
M0	3840	0.077	0.63	0.51	+7.52	-1.38	+8.9	+1.22	+1.40
M1	3660	0.050	0.56		+7.99	-1.62	+9.6	+1.21	+1.46
M2	3520	0.032	0.48	0.40	+8.47	-1.89	+10.4	+1.18	+1.49
M3	3400	0.020	0.41		+8.97	-2.15	+11.1	+1.16	+1.51
M4	3290	0.013	0.35		+9.49	-2.38	+11.9	+1.15	+1.54
M5	3170	0.0076	0.29	0.21	+10.1	-2.73	+12.8	+1.24	+1.64
M6	3030	0.0044	0.24		+10.6	-3.21	+13.8	+1.32	+1.73
M7	2860	0.0025	0.20		+11.3	-3.46	+14.7	+1.40	+1.80

Table B.2: Typical characteristics of stars in function of their Spectral Type. *Data taken from Carroll & Ostlie (1996)* .

Giant Stars (Luminosity Class III)									
Spectral Type	T_e (K)	$L/L_\odot$	$R/R_\odot$	$M/M_\odot$	M_{bol}	BC	M_V	U-B	B-V
O5	39400	741000	18.5		-9.94	-4.05	-5.9	-1.18	-0.32
O6	37800	519000	16.8		-9.55	-3.80	-5.7	-1.17	-0.32
O7	36500	375000	15.4		-9.20	-3.58	-5.6	-1.14	-0.32
O8	35000	277000	14.3		-8.87	-3.39	-5.5	-1.13	-0.31
B0	29200	84700	11.4	20	-7.58	-2.88	-4.7	-1.08	-0.29
B1	24500	32200	10.0		-6.53	-2.43	-4.1	-0.97	-0.26
B2	20200	11100	8.6		-5.38	-2.02	-3.4	-0.91	-0.24
B3	18300	6400	8.0		-4.78	-1.60	-3.2	-0.74	-0.20
B5	15100	2080	6.7	7	-3.56	-1.30	-2.3	-0.58	-0.17
B6	13800	1200	6.1		-2.96	-1.13	-1.8	-0.51	-0.15
B7	12700	710	5.5		-2.38	-0.97	-1.4	-0.44	-0.13
B8	11700	425	5.0		-1.83	-0.82	-1.0	-0.37	-0.11
B9	10900	263	4.5		-1.31	-0.71	-0.6	-0.20	-0.07
A0	10200	169	4.1	4	-0.83	-0.42	-0.4	-0.07	-0.03
A1	9820	129	3.9		-0.53	-0.29	-0.2	+0.07	+0.01
A2	9460	100	3.7		-0.26	-0.20	-0.1	+0.06	+0.05
A5	8550	52	3.3		+0.44	-0.14	+0.6	+0.11	+0.15
A8	7830	33	3.1		+0.95	-0.10	+1.0	+0.10	+0.25
F0	7400	27	3.2		+1.17	-0.11	+1.3	+0.08	+0.30
F2	7000	24	3.3		+1.31	-0.11	+1.4	+0.08	+0.35
F5	6410	22	3.8		+1.37	-0.14	+1.5	+0.09	+0.43
G0	5470	29	6.0	1.0	+1.10	-0.20	+1.3	+0.21	+0.65
G2	5300	31	6.7		+1.00	-0.27	+1.3	+0.39	+0.77
G8	4800	44	9.6		+0.63	-0.42	+1.0	+0.70	+0.94
K0	4660	50	10.9	1.1	+0.48	-0.50	+1.0	+0.84	+1.00
K1	4510	58	12.5		+0.32	-0.55	+0.9	+1.01	+1.07
K3	4260	79	16.4		-0.01	-0.76	+0.8	+1.39	+1.27
K4	4150	93	18.7		-0.18	-0.94	+0.8		+1.38
K5	4050	110	21.4	1.2	-0.36	-1.02	+0.7	+1.81	+1.50
K7	3870	154	27.6		-0.73	-1.17	+0.4	+1.83	+1.53
M0	3690	256	39.3	1.2	-1.28	-1.25	+0.0	+1.87	+1.56
M1	3600	355	48.6		-1.64	-1.44	-0.2	+1.88	+1.58
M2	3540	483	58.5	1.3	-1.97	-1.62	-0.4	+1.89	+1.60
M3	3480	643	69.7		-2.28	-1.87	-0.4	+1.88	+1.61
M4	3440	841	82.0		-2.57	-2.22	-0.4	+1.73	+1.62
M5	3380	1100	96.7		-2.86	-2.48	-0.4	+1.58	+1.63
M6	3330	1470	116		-3.18	-2.73	-0.4	+1.16	+1.52

Table B.3: Typical characteristics of stars in function of their Spectral Type. *Data taken from Carroll & Ostlie (1996)* .

Supergiant Stars (Luminosity Class Approximately Iab)									
Spectral Type	T_e (K)	$L/L_\odot$	$R/R_\odot$	$M/M_\odot$	M_{bol}	BC	M_V	U-B	B-V
O5	40900	1140000	21.2	70	-10.40	-3.87	-6.5	-1.17	-0.31
O6	38500	998000	22.4	40	-10.26	-3.74	-6.5	-1.16	-0.31
O7	36200	877000	23.8		-10.12	-3.48	-6.6	-1.14	-0.31
O8	34000	769000	25.3	28	-9.98	-3.35	-6.6	-1.13	-0.29
B0	26200	429000	31.7	25	-9.34	-2.49	-6.9	-1.06	-0.23
B1	21400	261000	37.3		-8.80	-1.87	-6.9	-1.00	-0.19
B2	17600	157000	42.8		-8.25	-1.58	-6.7	-0.94	-0.17
B3	16000	123000	45.8		-7.99	-1.26	-6.7	-0.83	-0.13
B5	13600	79100	51.1	20	-7.51	-0.95	-6.6	-0.72	-0.10
B6	12600	65200	53.8		-7.30	-0.88	-6.4	-0.69	-0.08
B7	11800	54800	56.4		-7.11	-0.78	-6.3	-0.64	-0.05
B8	11100	47200	58.9		-6.95	-0.66	-6.3	-0.56	-0.03
B9	10500	41600	61.8		-6.81	-0.52	-6.3	-0.50	-0.02
A0	9980	37500	64.9	16	-6.70	-0.41	-6.3	-0.38	-0.01
A1	9660	35400	67.3		-6.63	-0.32	-6.3	-0.29	+0.02
A2	9380	33700	69.7		-6.58	-0.28	-6.3	-0.25	+0.03
A5	8610	30500	78.6	13	-6.47	-0.13	-6.3	-0.07	+0.09
A8	7910	29100	91.1		-6.42	-0.03	-6.4	+0.11	+0.14
F0	7460	28800	102	12	-6.41	-0.01	-6.4	+0.15	+0.17
F2	7030	28700	114		-6.41	0.00	-6.4	+0.18	+0.23
F5	6370	29100	140	10	-6.42	-0.03	-6.4	+0.27	+0.32
F8	5750	29700	174		-6.44	-0.09	-6.4	+0.41	+0.56
G0	5370	30300	202	10	-6.47	-0.15	-6.3	+0.52	+0.76
G2	5190	30800	218		-6.48	-0.21	-6.3	+0.63	+0.87
G8	4700	32400	272		-6.54	-0.42	-6.1	+1.07	+1.15
K0	4550	33100	293	13	-6.56	-0.50	-6.1	+1.17	+1.24
K1	4430	34000	314		-6.59	-0.56	-6.0	+1.28	+1.30
K3	4190	36100	362		-6.66	-0.75	-5.9	+1.60	+1.46
K4	4090	37500	386		-6.70	-0.90	-5.8		+1.53
K5	3990	39200	415	13	-6.74	-1.01	-5.7	+1.80	+1.60
K7	3830	43200	473		-6.85	-1.20	-5.6	+1.84	+1.63
M0	3620	51900	579	13	-7.05	-1.29	-5.8	+1.90	+1.67
M1	3490	60300	672		-7.21	-1.38	-5.8	+1.90	+1.69
M2	3370	72100	791	19	-7.41	-1.62	-5.8	+1.95	+1.71
M3	3210	89500	967		-7.64	-2.13	-5.5	+1.95	+1.69
M4	3060	117000	1220		-7.93	-2.75	-5.2	+2.00	+1.76
M5	2880	165000	1640	24	-8.31	-3.47	-4.8	+1.60	+1.80
M6	2710	264000	2340		-8.82	-3.90	-4.9		

Appendix C

Literature: Books

The books listed here can give you a good support and offer recommended background reading for the courses on *Observational Techniques in Astronomy* and *Radiative processes in Astronomy*.

Table C.1: Books for backgroundreading and support of the courses

Title	Authors	Year	Comments	Publisher
			Observational Astrophysics	
Observational Astronomy	Scott Birney D., Gonzalez G., Oesper D.	2006	Good book to familiarise yourself with Observational Astrophysics	Cambridge
Introduction to Astronomical Photometry	Budding E., Demircan	2007	Introductory book focused on photometry and its application on stellar phenomena	Cambridge
Astronomical Photometry : A Guide	Sterken Chr., Manfroid J.	1992	Good book on photometric observations (Photomultipliers, CCD) and the reduction techniques	Kluwer
Astronomical Polarimetry	Tinbergen J.	1996	Introduction to polarimetric observations. Covers a wide range of wavelenghtregimes	Cambridge
Observing the Universe	Norton A.J.	2004	Very general book on observational astronomy. Basic.	The Open University
Astronomical Spectroscopy	Tennyson	2007	Useful handbook for a spectroscopist	Imperial College Press
Tools of Radio Astronomy	Rohlfs K., Wilson T.L.	2003	Good textbook on radio astronomy, rather technical (antenna's, receivers etc.) but with quite some chapters on astrophysical results	A&A library
Astronomy Methods	Bradt H.,	2005	Well written book on *a physical approach to astronomical observations.*	Cambridge
Astrophysics Processes	Bradt H.,	2008	Well written book on *a broad range of physical processes related to astronomical phenomena.*	Cambridge
An introduction to Optical Stellar Interferometry	Labeyrie A., Lipson S.G., Nisenson P.,	2006	Very appropriate title.	Cambridge

Table C.2: Books for backgroundreading and support of the courses

Title	Authors	Year	Comments	Publisher
			Radiative processes in Astronomy and Astrophysics	
The observation and analysis of stellar photospheres	D.F.Gray	1992	Good book which focusses on stellar photosphere. Some chapters cover instrumentation issues (including Fourier analysis)	Cambridge
Interpreting Astronomical Spectra	D. Emerson	1997	Good well written book which covers not only stellar atmospheres, also ISM, photo-ionisation, AGNs etc.	Wiley
Radiative processes in Astrophysics	Rybicki G.B., Lightman A.P.	1979	An older but well written but concise classic on radiative processes. In cgs. Unfortunately expensive...	Wiley
Astrophysics of Gaseous Nebulae and Active Galactic Nuclei	Osterbrock D.E.	1989	An older work but classic to anybody working on Gaseous Nebulae	University Science Book
			General recommended literature Astronomy and Astrophysics	
Introduction to Modern Astrophysics	Carroll B.W. Ostlie D.A.	1996	Good book which gives a wide overview of Astrophysics from the Solar System, over stellar evolution to Galactic structure. If you were to buy one book, take this one (a renewed edition is available)	Addison Wesley Longman
The elements	Cox P.A.	1989	A book on the elements, their origin, abundances and distribution on Earth. Intersection between astronomy and geophysics	Oxford

List of Figures

1.1 A sample of spectra of main sequence stars spanning the spectral range from O to M. The spectral window covers the UV up to the near-IR. 4

1.2 A sample of spectra of main sequence stars spanning the spectral range from O to M. The spectral zoom is around the Balmer-γ transition of Hydrogen. 5

1.3 A spectral detail of several stars with very similar temperatures and gravities. Only in this case is the difference in strength of a spectral line, directly related to a difference in the abundance of the carrier. High-resolution spectra are very powerful to quantify trace elements: e.g. for every Pr atom in the sun, there are 2×10^{11} particles of H. 6

1.4 A spectral detail of the telluric contamination. This band is mainly due to O_2 absorptions in the earth atmosphere. 6

1.5 The period table of chemical elements known as the table of Mendeljev. 7

1.6 The abundance pattern of the solar photosphere. Note the strong general decline of the abundance in function of atomic mass, but with a few significant exceptions: the Fe-peak elements make up a local maximum. This is directly related to the stability of these nuclei, with ^{56}Fe, the most stable of all nuclei (See Fig. 1.7). Note as well that O is more abundant than C thanks to the vigorous O-production of massive stars. The odd-even effect is very well detected and is the result of the nuclear stability of odd versus even nucleon numbers. Some elements do not have a stable isotope (e.g. Tc). *Fig. from Cox (1998)* 9

1.7 The binding energy per nucleon (E_b/A) as a function of the mass number A. *Fig. taken from Carroll & Ostlie (1996)* 10

1.8 The abundance pattern of the whole earth. Compared to the sun, the most apparent difference is that the volatile elements (like H and He) are lacking. The main abundance trend is also determined by the chemical properties of the species. Note that only 4 elements have an abundance of more than 10% Fe, O, Mg and Si and together they make up some 90% of the total mass of the earth. S, Ni, Ca and Al occur with more than 1 %. All other elements together constitute only about 1%.*Fig. from Cox (1989)* 11

1.9 The solid angle Ω is the angular area on a sphere (gray area on the figure). The units is in "steradians" (square radians) or sr. Integration over a total sphere yields a total solid angle of 4π steradians. *Fig. from Bradt (2004)* 14

1.10 The solid angle of your device (eye, optical telescope, X-ray telescope etc.) and the solid angle of the source will determine whether the object is unresolved or resolved. *Fig. taken from Carroll & Ostlie (1996)* 15

1.11 The specific intensity. *Fig. taken from Carroll & Ostlie (1996)* . . 16

1.12 The sphere has uniform brightness B and is seen in point P at a distance of r. *Fig. from Rybicki & Lightmann (1979)* 19

1.13 The orientation vectors to describe the optical thickness of a material. *Fig. taken from Carroll & Ostlie (1996)* 24

1.14 This figure illustrates the solution of the transfer equation assuming a homogeneous spectral slab, with a source function which includes a spectral line.*Fig. from Rutten (2000).* 27

1.15 This figure illustrates the difference between a plane-parallel approximation and a spherical case. In the latter case, a ray will intersect with different layers at another angle from the radial direction. In the plane-parallel approximation, the ray intersects with all the different layers at the same angle θ. *Fig. from Gray (1992)* 28

1.16 This figure illustrates the solution of the transfer equation to determine the outcoming radiation in function of the viewing angle θ. The left panel shows the evaluation of the integral $S_\nu \exp(-\tau_\nu)$ and the relative contribution of the different layers at different optical depth. The panel on the right, shows the limb-darkening: under a given angle θ on the normal, the layer which contribute most, is at shallower optical depth when θ becomes larger. *Fig. from Rutten (2000)* 30

1.17 This figure illustrates the limb darkening. Only the sun is close enough, so that the measured limbdarkening gives a direct probe on how the source function behaves in function of optical depth. *Fig. from Rutten (2000)* 31

1.18 The Black-Body spectrum (B_λ) for different temperatures. For hot resp. cool stars, the peak of the energy distribution falls outside the visible range. *Fig. taken from Carroll & Ostlie (1996)* 32

1.19 Illustration of the geometry of a pin-hole camera. *Fig. from Rybicki & Lightmann (1979)* 39

1.20 The Hubble ultra deep field press release image. 41

2.1 Normalised spectra of a G2 V star. The upper panel shows the strong Ca II doubled known as the Fraunhofer H and K lines. The lower panel shows the Hydrogen Balmer H_α line. 44

2.2 Electron transitions inbetween two bound electron states. *Fig. from Rutten (2000)* 46

2.3 The ionisation fraction of Fe in function of the temperature. The density is kept constant. 49

2.4 Bound-bound transition for hydrogen. *Fig. from Bradt (2005)* . . 51

2.5 The exponential in the ionisation law of Saha, makes that the ionisation fraction (here the one of H is shown) is a steep function of temperature. *Fig. taken from Carroll & Ostlie (1996)* 54

2.6 The fraction of H atoms with electrons in the Balmer level to the total number of H particles. *Fig. taken from Carroll & Ostlie (1996)* 55

2.7 The relative strengths of lines coming from a given ion in function of the effective temperature of the central star. *Fig. taken from Carroll & Ostlie (1996)* 56

2.8 The ionisation potentials (eV) of the different ions. The ionisation will determine which lines of which atom-ion will be visible in the spectrum of a star. 57

2.9 The colour-colour diagram with the Black-Body slope and the position of Main Sequence stars. *Fig. taken from Carroll & Ostlie (1996)* 58

2.10 The number of discrete Balmer lines in the spectrum is a tracer of the local density. Compare the spectrum of this post-AGB star HR 4049 (supergiant of 7000K) to the spectra of similar stars in "UVESPOP" 59

2.11 Maser emission can occur when population inversion occurs thanks to radiative pumping. *Fig. taken from Carroll & Ostlie (1996)* . . 68

2.12 The velocity distribution in TE of hydrogen atoms of temperature 10000K. The most probable (v_mp) and mean (v_{rms}) velocity is indicated on the distribution. *Fig. taken from Carroll & Ostlie (1996)* 69

2.13 Wings of the Voigt profile. The dashed-dotted lines is the $a/\sqrt{\pi}v^2$ approximation 74

3.1 Bound-bound transition for neutral Hydrogen. *Fig. taken from Tennyson (2007)* 78

3.2 Wave functions and probability functions for the radial coordinate and this for the lowest radial solutions. *Fig. taken from Tennyson (2007)* 80

3.3 Wave functions in terms of the spherical harmonics. What is given is the absolute value of the spherical harmonic at a distance from the origin for each angle. The - and + give the sign of the wave-function in each region. *Fig. taken from Tennyson (2007)* 81

3.4 The wavelengths λ_{lu}, the oscillatorstrengths (f_{lu}) and Einsteinco-efficients (A_{lu}) of some important bb transitions of Hydrogen. . . 83

3.5 The Spectrum of a Quasar at high redshift. The strong line is the Ly_α line of the quasar. The forrest of lines in the blue part of the spectrum come from Ly_α absorptions by ism clouds in the line-of-sight towards the quasar. Fig. Courtesy by ESO 84

3.6 Spectral details of the Ly_α forrest of lines. 85

3.7 High level radio recombination transitions in the spectrum of η Car. 86

3.8 Radio recombination lines of H, He and C observed in the gaseous nebula W3 *Fig. taken from Tennyson (2007)* 86

3.9 Fine Structure levels in the hydrogen atom. Splitting of the nl orbitals due to the finestructure for level l=0,1,2,3. The different quantumnumbers are given as well as the general spectroscopic notation of terms and levels. *Fig. taken from Tennyson (2007)* . . 88

3.10 Example of Fine-Structure coupling effects on the level splitting. The splitting in the n=2 level of atomic H is shown. The larger splitting is the fine structure and the smaller the Lamb shift. . . . 88

3.11 The sub-levels which are related to the Balmer H_α transition. *Fig. taken from Tennyson (2007)* 90

3.12 A spectrum of a high redshift quasar. The spectral tracer for the deuterium Lyman alpha line is given on the more energetic wing of the strongly saturated redshifted Lyman_α line. Fig. from ESO . 92

4.1 The atomic configuration of the first 20 elements in the periodic table *Fig. taken from Tennyson (2007)* 95

4.2 All possible states of O III in the $1s^2\,2s^2\,2p\,3d$ configuration. *Fig. taken from Tennyson (2007)* 97

4.3 Selection rules for atomic spectra. Rule 1,2 and 3 must always be obeyed. For electric dipole transitions, intercombination lines violate rule 4 and forbidden lines violate rule 5 and/or 6. Electric quadrupole and magnetic dipole transitions are also described as forbidden. *Fig. taken from Tennyson (2007)* 99

4.4 Grotrian diagram of He I 100

4.5 Grotrian diagram of He I 101

4.6 A typical spectrum of a Planetary Nebula, in this case NGC 7009 102

4.7 The levels involved in the nebular [OIII] lines. 103

4.8 With special narrow band filters, tuned to sample the most important diagnostic lines, a good 2D map of the line-emission is shown in those colour coded images. Fig. from Bruce Balick at this web page 104

4.9 106

4.10 The vibrational levels and the potential curve with a more realistic shape than in the text, where a parabola was used. The levels are no longer equidistant at high vibrational states. This curve is from H_2 in the ground electronic state. 112

4.11 The vibrational modes of a linear tri-atomic molecule (left) and of a angular triatomic molecule. 113

4.12 Illustration of the different transitions of a molecule. 114

4.13 Lab spectrum of the rotational levels of CO and the associated isotopic shifts for two different isotopic settings. $^{12}C^{16}O$ is dominant in terrestrial abundances. *Fig. taken from Tennyson (2007)* 116

4.14 A millimeter-wavelength spectrum of the core of the Orion giant molecular cloud, made at the Owens Valley Radio Observatory. The spectrum covers a small interval in the atmospheric window at 1.3 mm. Over 800 spectral features are seen! This type of data is needed to understand the chemistry of cold and dense interstellar regions. Fig. from `http://loke.as.arizona.edu/ ckulesa/research/ov` 117

4.15 Illustration of ro-vibrational transitions in a molecule. 118

4.16 The spectral lines observed in the lab of the the molecule AlH. The P,Q and R branches are labeled. y-units are arbitrary. *Fig. taken from Tennyson (2007)* 118

4.17 The spectrum observed towards the young massive stellar object AFGL 4176. The strong but structureless band is due to solid CO_2, while the characteristic ro-vibrational P and R-branch structure of the CO molecule is due to the presence of warm CO gas in the line-of-sight. Fig. from "The molecular astrophysics of Stars and Galaxies, E.F. Van Dishoeck, Clarendon Press, Oxford, 1998. 119

5.1 A high signal-to-noise and high-resolution spectrum of the post-AGB star HD 56126 (SpT F5Iab). The narrow lines is the Phillips band of C_2. Fig. from Bakker et al., 1996. 122

5.2 The optical and red circumstellar bands measured in the spectrum of HD 56126 123

5.3 Rotational diagrams for C_2 measured in the spectrum of HD$\tilde{5}$6126 126

5.4 Rotational diagrams for CN measured in the spectrum of HD$\tilde{5}$6126 126

5.5 The Voigt profile for different values of the a-parameter. The dashed-dotted lines is the $a/\sqrt{\pi}v^2$ approximation. 128

5.6 In the upper panel we show the line profile change for increasing line strength. When the wings become important contributors to the total line strength, the line becomes saturated. In the lower panel the associated curve-of-growth 129

5.7 The behaviour of the curve of growth for different Doppler-widths and different damping constants. For a larger Doppler width, the saturation point is delayed in equivalent width 138

5.8 Curve of Growths of the Ti I multiplet as observed in the Sun. The specific multiplet with excitation level at 0.03 eV is shown (upper part). Different multiplets in different colour-codes (0.03, 0.82, 1.44 and 1.99 eV) are shown in the lower level. 140

5.9 Determination of the Excitation Temperature using different multiplets of the same ion. 141

5.10 The curves-of-growth of the different Ti I multiplets (see Fig. 5.8) corrected for the excitation temperature. The different colours represent different multiplets. The data is from the Sun. 141

5.11 An example of a spectral synthesis: to match the observed spectrum (dots) the model (full line) should not only contain the correct abundances, also the total broadening function of the b-b profiles should be known 143

5.12 A figure illustrating the rich potential of high resolution spectroscopic data of high quality to detect trace elements in the photospheres of stars. Normalised spectra of three stars are shown with a small offset to ease comparison. All three spectra are brought to the same Doppler velocity. The identification of the different lines is given below. The elements marked in red and blue are heavy elements which are very rare in a solar composition (see the solar abundances in chapter 2) 144

5.13 The determination of the temperature of AC Her, using the excitation analysis of the Fe I lines. 146

5.14 The micro-turbulent velocity determination using the Fe I lines as observed in the star AC Her. 147

5.15 Both panels show sample spectra of stars with very similar spectral type. The relative abundances are much more reliable than the absolute values. 148

6.1 Electric and Magnetic vectors at position r,θ at time t coming from a acceleration $\vec{a}$ of a positive charge at earlier time. The propagation vector $\vec{k} = 2\pi/\lambda\,\hat{k}$ *Fig. taken from Bradt (2008)* 155

6.2 The impact parameter and the approximate duration of the collision. *Fig. taken from Bradt (2008)* 157

6.3 When a flux of electrons is approaching an ion. *Fig. taken from Bradt (2008)* 159

6.4 Frequency dependence of the volume emmisivity of free-free radiation coming from electron-ion collisions. *Fig. taken from Bradt (2008)* 162

6.5 The volume emissivity at two different temperatures. At low frequencies, the volume emissivity is higher at lower temperatures... 163

6.6 The Bound-Free cross-section of H per particle. The cross-section increases with n but the reaction rate is dependent on the number of atoms in the correct state as well as the number of photons available. 172

6.7 The effective cross-section per H-atom in units of m^2 for the bound-free process in the ISM. The dominant contributer is H with a very high extinction peak at 13.6 eV. The cross-section falls of after the peak with a slope of $\sim$ -3. Ionisation edges of other atoms are shown as well. The left panel is blown-up on the right. *Data taken from Bradt (2004)* 173

6.8 The cross section of the H^- opacity in function of wavelength. The slope at low energies are from the free-free contribution, the bound-free contribution is not sharp-edged but maximal at 860 nm 177

6.9 Solar limb darkening is clearly seen. 178

6.10 The reconstruction of the wavelength dependency of the monochromatic extinction coefficient from the Solar Limb darkening. Fig. from Gray (2002) 180

6.11 The SN remnant imaged by the HST. The blue central emission is coming from synchrotron emission. The image is a mosaic of 24 deep pointings of the HST WFPC2 camera. A digital high-resolution version can be found here 181

6.12 SED of the Crab nebula. The plot shows ν_ν in function of the frequency (top) or energy (bottom) of the detected photons. Note that the emission covers over 19 decades (!) of frequency down to the gamma-ray domain (TeV). The polarisation measurements as well as the spectral slope indicates that most energy to about 100 MeV is coming from synchrotron radiation. The solid line is a fit through the data of a synchrotron self-Compton (SCC) model for a magnetic field of 16 nT. The narrow and broader dashed lines show the contribution from millimeter synchrotron and from nebular dust respectively. The distinct peak at TeV energies is attributed to synchrotron photons that have been up-scattered via inverse Compton scattering. *Fig. taken from Bradt (2004).* 182

6.13 The spectral behaviour of the emission of different components of the Crab pulsars and Crab nebula, depicted in a log-log scale. The dashed line is the correction of the data for ISM extinction. The straight lines are typical for synchrotron emission. the time-average pulsar fluxes are shown as lines. Typical peak fluxes are shown by two frequencies. *Fig. taken from Bradt (2004)* 183

6.14 High energy cross section for different processes. *Fig. taken from Bradt (2004)* 185

6.15 The black-body spectrum of the CMB in the direction of a cluster of Galaxies with respect to one in an undisturbed line-of-sight. The inverse Compton scattering effect by high energetic electrons in the very hot inter-cluster plasma disturbs the CMB photons to higher energies. This effect is known as the Sunyaev-Zeldovich effect 187

6.16 The major continuum opacity sources in the photospheres of stars of different spectral type. For the Sun and solar analogues the main contributor in the optical-nearIR is H^- opacity. Fig. from Gray (1992) 188

List of Tables

1.1 The Solar photospheric abundances up to Ni as given in Asplund et al., 2005, ASPC 336, 25. A is the proton number, ATW the atomic weight, both abundance by number as by mass are given. 12

1.2 The estimated solar photospheric abundances based on different tracers and different models. It is remarkable to note that the abundance of key elements like C, N are still a matter of debate. For a detailed review the interested reader is referred to Asplund, M., 2005, ARA&A 43, 481-530 13

1.3 The recent history in the estimated solar photospheric abundances. The older values are from Anders & Grevesse, 1989, Geochimica et Cosmochimica Acta, Vol. 53,, the recent ones from Asplund et al., 2005, ASPC 336, 25. 13

1.4 The Riemann ζ-functions and their numerical value for different z values. 34

2.1 The classification of stellar spectra was originally 1-dimensional. It turned out later that the main discrimination parameter was the Effective Temperature 59

2.2 The Einstein coefficients for transitions between u and l states. . . 61

2.3 From A_{ul} to the associated emission coefficient 65

3.1 Orbital Angular momentum nomination rules 82

3.2 Lifetimes τ for decay by spontaneous emission for low-lying excited states of H 90

4.1 Dissociation energy in eV. 107

6.1 The Solar limb darkening coefficients for several wavelengths as well as the intensity of the centre of the solar disc 179

A.1 Overview physical constants. A useful link can be found here . . . 191

A.2 Astronomical constants and typical numbers. 192

A.3 SI to cgs Unit Conversions. Many (older) astronomical literature is in cgs units. This table helps to compute the conversions. One of the many web-conversion tools can be found here 193

A.4 Often used quantities and relations. 194

B.1 Typical characteristics of stars in function of their Spectral Type. *Data taken from Carroll & Ostlie (1996)* 196

B.2 Typical characteristics of stars in function of their Spectral Type. *Data taken from Carroll & Ostlie (1996)* 197

B.3 Typical characteristics of stars in function of their Spectral Type. *Data taken from Carroll & Ostlie (1996)* 198

C.1 Books for backgroundreading and support of the courses 200

C.2 Books for backgroundreading and support of the courses 201